SAPIENZA
UNIVERSITÀ DI ROMA

The New Hadron Spectroscopy

Scuola di Dottorato in Scienze Astronomiche, Chimiche, Fisiche e Matematiche Vito Volterra

Dottorato di Ricerca in Fisica – XXIV Ciclo

Candidate

Chiara Sabelli

ID number 696815

Thesis Advisor

Prof. Antonio Davide Polosa

A thesis submitted in partial fulfillment of the requirements
for the degree of Doctor of Philosophy in Physics

December 2011

Thesis defended on 14 February 2012
in front of a Board of Examiners composed by:

Prof. Giovanni Ridolfi (chairman)

Prof. Antonio Davide Polosa

Prof. Mauro Dell'Orso

Chiara Sabelli. *The New Hadron Spectroscopy.*
Ph.D. thesis. Sapienza – University of Rome

EMAIL: chiara.sabelli@gmail.com

"One rarely gets the feeling of the true nature of the scientific development, in which the element of farce is as great as the element of triumph."
David J. Gross [1]

Contents

Introduction

One of the open problems in particle physics is the understanding of strong interactions in the low energy region, where the theory is non perturbative. This would not be merely a mathematical achievement, but rather the solution to an old conceptual problem: which are the fundamental structures of nature? In other words: how do quarks and gluons arrange themselves to produce the particles we observe in the final states of high energy collisions?

Quantum Chromo Dynamics (QCD) is the quantum field theoretical description of strong interactions, a non abelian gauge theory with gauge group SU(3). The charge associated to this group is the color charge, and the fundamental fields, the quarks and the gluons, are colored objects: $q \in \mathbf{3}_c$ and $g \in \mathbf{8}_c$. The dynamics of the interaction is contained in the Lagrangian density of the theory, which implies on the one hand *asymptotic freedom* and on the other hand *confinement*. These two aspects are associated with the behavior of the running coupling constant α_s. The high energy region belongs to the perturbative regime of the theory and is widely explored at hadronic colliders. At lower energies instead the theory is strongly coupled and thus low energy processes, such as the production and decay of hadrons, are inherently non perturbative. Confinement can thus be seen as the phenomenological manifestation of the strong coupling regime: quarks and gluons cannot be observed as free particles, but only trapped inside hadrons.

This is the reason why it took almost fifteen years to firmly establish the existence of quarks and gluons. The three lightest quarks, u, d, s, were first introduced to explain the observed flavor pattern of the growing number of hadronic resonances, discovered in the first collider experiments, but the confirmation of their dynamical nature came after Deep Inelastic Scattering results and the discovery of asymptotic freedom.

The discovery of heavy quarks, the *charm* quark in 1974, which existence was predicted by the GIM mechanism, and soon after of the *bottom* quark, offered the unique possibility to make solid theoretical predictions on the spectrum of $c\bar{c}$ and $b\bar{b}$ states, usually named *charmonium* and *bottomonium*. This is due to asymptotic freedom and in particular to the accidental value of $\Lambda_{\mathrm{QCD}} \sim 200$ MeV, the scale at which strong interactions enter the non perturbative regime. Since the mass of the charm and the bottom happens to be much larger than Λ_{QCD} ($m_c \sim 1.5$ GeV and $m_b \sim 4.7$ GeV), a non relativistic treatment of $c\bar{c}$ and $b\bar{b}$ interactions is allowed. Theoretical predictions on masses, decay widths and production rates of heavy quarkonia below the open-charm ($D\bar{D}$) and open-bottom ($B\bar{B}$) thresholds have been computed and strikingly confirmed by experimental data.

Nevertheless during the search for orbitally and radially excited $c\bar{c}$ and $b\bar{b}$, we

came across a number of resonances which cannot be straightforwardly identified with higher heavy quarkonium states and therefore were classified as *exotic mesons*, usually called XYZ. The XYZ decay into final states containing a pair of D/B mesons and/or charmonium/bottomonium plus light mesons. Hints on the existence of exotics came first in the light sector: the scalars σ f_0 and a_0 are an example. Nevertheless their classification as non standard mesons is much more challenging than in the heavy quarkonium sector, where theoretical predictions for ordinary states are available.

There is no doubt about the fact that crossing the open-charm and open-bottom thresholds spoils the reliability of those predictions: the $c\bar{c} \to c\bar{u} + \bar{c}u$ process is inherently relativistic, since it involves the creation of a light quark pair from the vacuum. At any rate one expects the prediction on the masses to be more affected by corrections, than those on decay and production rates. Thus to definitely classify mesons as exotics, more than one single property for each particle must be taken into account.

The first of the XYZ particles to be discovered was the $X(3872)$ in 2003, initially thought to be a $J^{PC} = 1^{++}$ state. Its identification with the first radial excitation of a P-wave charmonium was soon excluded, not only because the predicted mass did not match the experimental one, but especially because the radiative decay to $J/\psi\,\gamma$ was observed much less copiously than what expected.

After the $X(3872)$ more and more similar resonances have been discovered at electron-positron and proton-antiproton colliders. Now we know about the existence of nearly twenty XYZ states. The first results from the LHC, a proton-proton collider, starts to appear in these days.

A variety of theoretical interpretations on the nature of XYZ mesons has been proposed during the years. Among the most investigated possibilities there are *meson-meson molecules*, *tetraquarks*, *hybrids*, *glueballs* and *hadrocharmonium*.

Two mesons can form a bound state through the exchange of light mesons, such as π or η. As first proposed by Tornqvist [8], relativistic potential models can be used to predict the existence or otherwise of meson molecules in some spin-isospin configuration. In particular in 1994 he predicted [9] the existence of a $D^0\bar{D}^{0*}$ bound state nearly at threshold with $J^P = 1^+$ and $I = 0$. When in 2003 the $X(3872)$ was discovered it seemed to be the perfect candidate. Nevertheless the decay and production dynamics of such a state appears quite challenging to study. Such a loosely bound molecule is an extremely extended state, much larger than ordinary hadrons. An estimate of its spatial size can be obtained from the binding energy $a \sim 1/\sqrt{2\mu E_B} \sim 8$ fm. The decay into hidden-charm states must proceed through the rearrangement of c and $\bar{c}$ which on average are 8 fm apart from each other. This rearrangement must be driven by strong interactions, which are notoriously short-distance interactions. Not to talk about the production mechanism, which must proceed through the production of a pair of nearly collinear D mesons. Many other molecular candidates have been identified among the XYZ, but none of them is supported by a study of the interacting potential. Their identification relies basically on the fact that the mass of the exotic state matches the sum of the constituent masses. A detailed study of the dynamical properties should be used as a table test.

Tetraquarks with hidden charm or bottom are $[Qq][\bar{Q}\bar{q}]$ states ($Q = c, b$ and $q = u, d, s$) in which the color is saturated among all the four constituents. They are

expected to be of ~ 1 fm size, like ordinary hadrons, and they are usually described as diquark-antidiquark bound states, the diquark being a quark-quark bound state which is likely to be stable due to color interactions. Their distinctive feature would be the prominency of the baryon-antibaryon decay mode, if allowed by kinematics. The rearrangement of quarks into final states containing $Q\bar{Q}$ states plus light mesons happens here at short distances. Nevertheless the very existence of tetraquarks implies the appearance of charged states, *e.g.* $[Qu][\bar{Q}\bar{d}]$, which was initially claimed by Belle but never confirmed by BaBar. Beside charged resonances, a large number of tetraquark states arises when considering the flavor multiplicity of the light quarks $q = u, d, s$. Constituent quark models or sum rules allow to make predictions on this rich spectrum, but most of the expected states are not observed in experiments. This represents the main drawback to the tetraquark picture.

Hybrids and glueballs include the gluons as active degrees of freedom, being $q\bar{q}g$ or gg bound states respectively. Their spectrum has been studied mainly on the lattice. Distinctive decay patterns are predicted, and some of them require additional experimental investigation in order to establish the hybrid nature of some of the XYZ states.

Finally hadrocharmonium has been recently proposed to explain a specific class of resonances among the XYZ. It envisages the possibility that a charmonium or bottomonium state gets stuck inside light hadronic matter.

The theoretical interpretation of these resonances based on a phenomenological approach is the subject of this thesis.

In the first part of our work we focused on multiquark states, either molecules or tetraquarks.

As for tetraquarks, our considerations originated from the observation of a vector resonance decaying prominently into baryon-antibaryon ($\Lambda_c^+\Lambda_c^-$), as a tetraquark is expected to do. We have developed a string model to describe orbitally excited diquark-antidiquark bound states, since a relative P-wave is required to obtain odd parity. Exploiting the similarity of the color interactions between diquark and antidiquark to that between quark and antiquark, we have first tested this model on the standard charmonium and bottomonium states, also including relativistic corrections. This string model has then been used to compute the spectrum of orbitally excited tetraquarks. We also tried to give tentative selection rules on the existence of the predicted states, based mainly on the fact that some of them could be too broad to be observable.

As for molecules, we considered the case of $X(3872)$, focusing on the prompt production mechanism in $p\bar{p}$ collisions. Due to its extremely small binding energy, in order for the $X(3872)$ to be created, a $D^0\bar{D}^{0*}$ pair nearly collinear (with relative three-momentum not exceeding ~ 35 MeV) needs to be produced in a high energy $p\bar{p}$ collision. Using standard Monte Carlo event generators, we computed the theoretical prompt production cross section at the Tevatron and compared it to the experimental results by CDF.

From these analyses, and from the many other present in the literature, one realizes that the experimental picture is fragmentary and incomplete. Many final states have not been even searched, and for many others data analysis is still to be performed. For this reason, in the second part of our work we focused instead on indirect searches of XYZ, in order to answer the question: how many XYZ

do really exist besides those we have already discovered? We have thus considered processes in which the XYZ resonances act as intermediate states, and could in this way play a role in some phenomena which are of general interest.

First we studied the J/ψ suppression in ultra relativistic heavy ion collisions. This long lasting evidence has been indicated as one of the most compelling signal for the formation of Quark Gluon Plasma (QGP). Nevertheless many authors suggested that J/ψ production suppression could be due to the dissociation processes occurring inside the hot hadronic gas which is formed in place or after QGP. $X(3872)$, which is the only exotic decaying both into open-charm mesons and into J/ψ plus light mesons, could play a role in this dissociation process. Without making any assumption on the nature of $X(3872)$, we quantified its contribution to the J/ψ suppression.

Finally we considered the J/ψ inclusive production in B-decays. The J/ψ decay momentum spectrum has been of difficult interpretation since a long time. A discrepancy between data and theory showed up in the low energy part of the spectrum, where the contribution from non resonant multi-body final states is expected to be dominant. However also processes mediated by XYZ mesons are expected to peak in that momentum region. Indeed some of the exotics are produced in B-decays and decay into final states containing a J/ψ. We have thus computed the distribution associated to the decays $B \to \mathcal{X}\mathcal{K} \to J/\psi + \text{light hadrons}$, where $\mathcal{X}$ and $\mathcal{K}$ are XYZ and kaons respectively. Furthermore we updated the analysis on the two-body modes, including recent experimental data, and reconsidered the non resonant multi-body contribution in the framework of non relativistic QCD. Summing up all these three components, we obtained a new comparison between theory and data.

This thesis is organized as follows:

- Chapter 1 contains an introduction on the birth of the quark model, how light quarks were introduced and then accepted, and a review on heavy quarkonium, their discovery and their description in a non-relativistic approach.

- In Chapter 2 we present the experimental state of the art about XYZ mesons, giving then a summary of the main theoretical models proposed to explain their nature. For each of these models we list the candidates among the XYZ.

- Chapter 3 is devoted to tetraquarks. After enumerating some of the evidences which favor the existence of tetraquarks in the form of diquark-antidiquark bound states, we discuss the constituent quark model which is used to compute spectra and show the results.

  In Section 3.3 the description of our original work begins with the introduction of a string model to describe P-wave diquark-antidiquark bound states. We test this model on standard charmonium and bottomonium spectra, including spin-orbit and tensor interactions. Then we exploit our string model to interpret the 1^{--} resonances $Y(4350)$ and $Y(4630)/Y(4660)$ as two P-wave tetraquarks, taking into account both the possible J^{PC} quantum numbers assignments (1^{++} and 2^{-+}) for the $X(3872)$, which serves as an input to our calculations. Indeed a recent experimental analysis claimed that $X(3872)$ is more likely a 2^{-+} state.

- In Chapter 4 we focus on the $X(3872)$, studying its decay and production mechanisms in both the 1^{++} and 2^{-+} hypotheses. In Section 4.1 we compute the strong couplings of $X(3872)$ without making any assumptions on its internal structure, but simply relying on Lorentz invariance. These couplings will be used in the last chapter in the study of J/ψ suppression in heavy ion collisions. In Section 4.2 we deal with the problem of prompt production cross section. In the molecular hypothesis, which is valid only if $J^{PC} = 1^{++}$, we use Monte Carlo event generators to obtain a theoretical prediction of the cross section and compare the result with the CDF measurements. In the case of 2^{-+} quantum numbers the molecular hypothesis is ruled out, and the charmonium option comes back into play. We thus exploit a previous study on the production of D-wave charmonia in hadronic collisions to estimate the cross section of a 1^1D_2 charmonium with mass 3872 MeV.

- Chapter 5 contains the two studies we mentioned above about indirect searches. Section 5.1 contains our results about the role of $X(3872)$ in the J/ψ suppression in heavy ion collisions. We sum this contribution to the non-resonant one, computed in previous works, in order to make a comparison with the recent data from RHIC. In Section 5.2 we consider the problem of the inclusive production of J/ψ in B-decays, including for the first time the XYZ contribution.

Chapter 1

From light to heavy quarks

In this chapter we aim at giving an overview about the quark model description of the standard hadrons. Quarks were indeed introduced at the dawn of the collider experiments era, to explain the rich spectrum of baryons and mesons observed. Afterwards Deep Inelastic Scattering experiments established their existence, and furthermore provided evidence for the gluons. Quarks and gluons were finally accepted as dynamical entities when asymptotic freedom was discovered. We will describe these three phases in Section 1.1.

For almost ten years only three quarks, relatively light, were needed to the interpret experimental data. Nevertheless in 1974 a fourth quark, the *charm*, much heavier than the first three, was discovered. Its existence had been previously predicted to explain some weak interactions data through the GIM mechanism. The discovery of the *charm* quark and later on also of the *bottom* one, opened a completely new spectroscopy. Indeed charm and anti-charm bound states as well as bottom anti-bottom ones, offer the unique possibility in QCD to make reliable theoretical predictions, essentially because strong interactions are described by an asymptotically free quantum field theory. Section 1.2 is thus devoted to heavy quarkonium.

This introduction should serve as a guide to approach the completely new spectroscopy we are facing today and which is the main subject of this thesis.

1.1 Quark model

When studying hadrons the objects one deals with are *quarks* and *gluons*, the fundamental particles involved in the strong interactions. We start recalling the history of quarks and gluons, *i.e.* how the theory of strong interactions in the form of a SU(3) non-Abelian quantum field theory was discovered and accepted.

The discovery and acceptance of quarks proceeds through a long history of experimental evidences and theoretical revolutions. Indeed they were first introduced independently by Gell Mann and Zweig [10] to explain the growing number of hadronic resonances which were observed since the 1950s, when the first accelerator machines were ideated and constructed. At that time these objects were regarded as mere mathematical devices, nobody believing in their effective dynamical nature. (Section 1.1.1).

The evidence for their existence came only when, striking the proton with high energy electron beams, a scaling properties was observed. Feynman [11] proposed the parton model to explain this feature of experimental data, describing the proton as made from more elementary particles, called generically *partons*. (Section 1.1.2)

Nevertheless quarks and gluons were not asymptotic states, since nobody was able to observe free quarks produced in accelerators experiments, regardless how high was the energy involved in the collisions. The discovery by 't Hooft and Veltman that a SU(N) gauge theory is renormalizable [12, 13] rehabilitated quantum field theory (QFT) and prepared the path for asymptotic freedom. In order to explain the scaling behavior observed in experimental data in terms of a QFT, it was required an asymptotically free QFT.

While weak and electromagnetic interactions were perfectly codified in terms of a gauge theory with gauge group $SU(2) \otimes U(1)$, strong interactions seemed for a long time to elude this kind of description. At the beginning, before quarks and gluons were introduced, it was not clear which were the fundamental fields of the theory. Moreover the intensity of the interactions between hadrons was such that any perturbative computation appeared completely meaningless. The disillusion toward quantum field theory, at least for strong interactions, led to the formulation of alternative descriptions, such as the bootstrap hypothesis and the S-matrix theory.

Asymptotic freedom implied the existence of a weak coupled regime of the theory, the one explored by the Deep Inelastic Scattering experiments, and of a strong coupled one, which in principle could explain the phenomenon of confinement, *i.e.* why free quarks cannot be observed. The final word came when two groups independently, Gross and Wilczek on the one hand [14] and Politzer on the other [15], performed the computation of the β function of an SU(3) gauge theory showing that if the matter fields, spin 1/2 quarks, were limited to 16 flavors the β function has negative sign, which in turn implies that the coupling constant decreases as the energy grows. (Section 1.1.3).

A review on the history of QCD can be found in [1].

1.1.1 Symmetry and hadron spectroscopy

In physics symmetries manifest themselves through conserved quantities or through the appearance of degenerate multiplets. In hadronic physics the degeneracy of the neutron-proton doublet led to introduce a symmetry of the strong interactions with respect to an SU(2) group, associated to a new quantum number, called the *isotopic spin* or *isospin*. Neutron and proton differ only in the electric charge and indeed their slight mass difference is due to electromagnetic interactions

$$\begin{aligned} m_p &= (938.272013 \pm 0.000023)\ \text{MeV}, \\ m_n &= (939.565346 \pm 0.000023)\ \text{MeV}. \end{aligned} \tag{1.1}$$

The isospin symmetry leads to the appearance of other multiplets as the (π^+, π^-, π^0) one

$$\begin{aligned} m_{\pi^\pm} &= (139.57018 \pm 0.00035)\ \text{MeV}, \\ m_{\pi^0} &= (134.9766 \pm 0.0006)\ \text{MeV}. \end{aligned} \tag{1.2}$$

Until the 1950s there were very few particles known besides the proton, the neutron and the pions, and thus they were identified as fundamental point like particles. The neutron and the proton were assigned to the fundamental representation of $SU(2)$, while the three pions to the three-dimensional one. However in the 1950s the first accelerator machines started their run and a multitude of new hadrons were produced in high energy collisions.

It seemed unnatural to interpret all the newly discovered particles as fundamental ones. Furthermore it was noticed that some of these particles were produced in pair and decayed much more slowly back into ordinary particles.

It was realized that a lot of the properties of this new class of particles could be understood if an additional quantum number were introduced, called *strangeness* S, conserved by strong and electromagnetic interactions but not by weak interactions.

It was possible to identify a series of almost mass degenerate multiplets assigning to them a specific value of three quantum numbers, conserved by strong interactions: (i) I_3: the third component of the $SU(2)$ isospin; (ii) S: the strangeness; (iii) B: the baryon number ($B = 1$ for *baryons* and $B = 0$ for *mesons*).

The lightest strange particles are the pseudo-scalar K-mesons, an isospin doublet with $S = 1$

$$\begin{aligned} K^+ \qquad & \text{with } \ I_3 = 1/2 \\ K^0 \qquad & \text{with } \ I_3 = -1/2 \end{aligned}$$

and their antiparticles with $S = -1$

$$\begin{aligned} \bar{K}^0 \qquad & \text{with } \ I_3 = 1/2 \\ K^- \qquad & \text{with } \ I_3 = -1/2, \end{aligned}$$

all having $B = 0$. There are also strange baryons, $B = 1$ and $S = -1$ which come into an isospin triplet

$$\begin{aligned} \Sigma^+ \qquad & \text{with } \ I_3 = 1 \\ \Sigma^0 \qquad & \text{with } \ I_3 = 0 \\ \Sigma^- \qquad & \text{with } \ I_3 = -1 \end{aligned}$$

and an isosinglet

$$\Lambda \qquad \text{with } \ I_3 = 0.$$

Finally with $S = -2$ comes the isodoublet

$$\begin{aligned} \Xi^0 \qquad & \text{with } \ I_3 = 1/2 \\ \Xi^- \qquad & \text{with } \ I_3 = -1/2. \end{aligned}$$

Defining the hypercharge Y as

$$Y = B + S, \tag{1.3}$$

one realizes that all of these particles satisfy the empiric relation

$$Q = I_3 + \frac{Y}{2}, \tag{1.4}$$

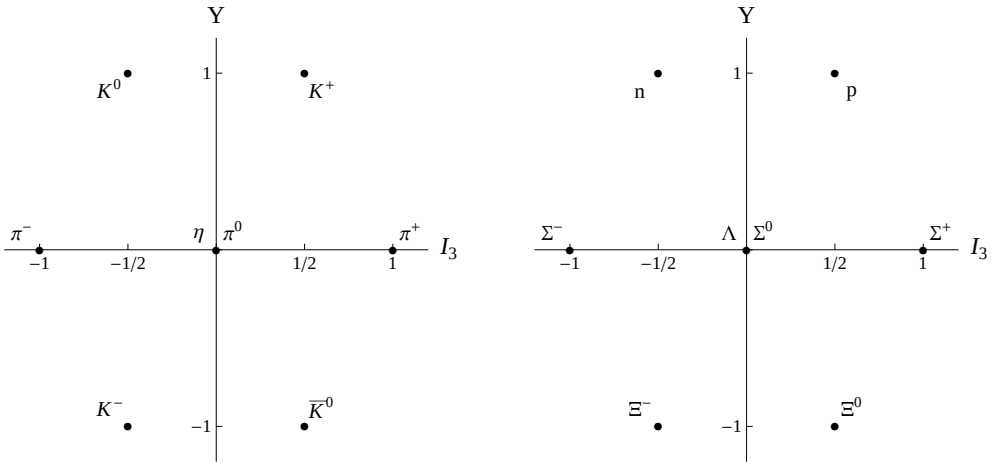

(a) Mesons **(b)** Baryons

Figure 1.1. I_3-Y diagram of baryons and mesons.

where Q is the electric charge in unit of the proton charge. Now if we plot Y versus I_3 we realize that the lightest hadrons are organized in octets, Fig. 1.1a for mesons and Fig. 1.1b for baryons. In 1964 Gell-Mann and Zweig [10] independently proposed to explain the observed pattern of hadrons as the result of the compositions of three elementary objects, called *quarks*, assigned to the the fundamental representation of $SU(3)$ and named *up*, *down* and *strange*

$$\mathbf{3} = \begin{pmatrix} u \\ d \\ s \end{pmatrix}, \tag{1.5}$$

This means that they transform as

$$\mathbf{3} \to \exp\left(\frac{i}{2}\boldsymbol{\alpha}\cdot\boldsymbol{\lambda}\right)\mathbf{3}, \tag{1.6}$$

where $\boldsymbol{\alpha}$ are some parameters, and $\boldsymbol{\lambda}$ are the $SU(3)$ generators in the $\mathbf{3}$ representation, *i.e.* the eight Gell-Mann matrices

$$\begin{aligned}
\lambda_1 &= \begin{pmatrix} 0 & 1 & 0 \\ 1 & 0 & 0 \\ 0 & 0 & 0 \end{pmatrix} \qquad \lambda_2 = \begin{pmatrix} 0 & -i & 0 \\ i & 0 & 0 \\ 0 & 0 & 0 \end{pmatrix} \qquad \lambda_3 = \begin{pmatrix} 1 & 0 & 0 \\ 0 & -1 & 0 \\ 0 & 0 & 0 \end{pmatrix} \\
\lambda_4 &= \begin{pmatrix} 0 & 0 & 1 \\ 0 & 0 & 0 \\ 1 & 0 & 0 \end{pmatrix} \qquad \lambda_5 = \begin{pmatrix} 0 & 0 & -i \\ 0 & 0 & 0 \\ -i & 0 & 0 \end{pmatrix} \\
\lambda_6 &= \begin{pmatrix} 0 & 0 & 0 \\ 0 & 0 & 1 \\ 0 & 1 & 0 \end{pmatrix} \qquad \lambda_7 = \begin{pmatrix} 0 & 0 & 0 \\ 0 & 0 & -i \\ 0 & i & 0 \end{pmatrix} \\
\lambda_8 &= \frac{1}{\sqrt{3}} \begin{pmatrix} 1 & 0 & 0 \\ 0 & 1 & 0 \\ 0 & 0 & -2 \end{pmatrix}.
\end{aligned} \tag{1.7}$$

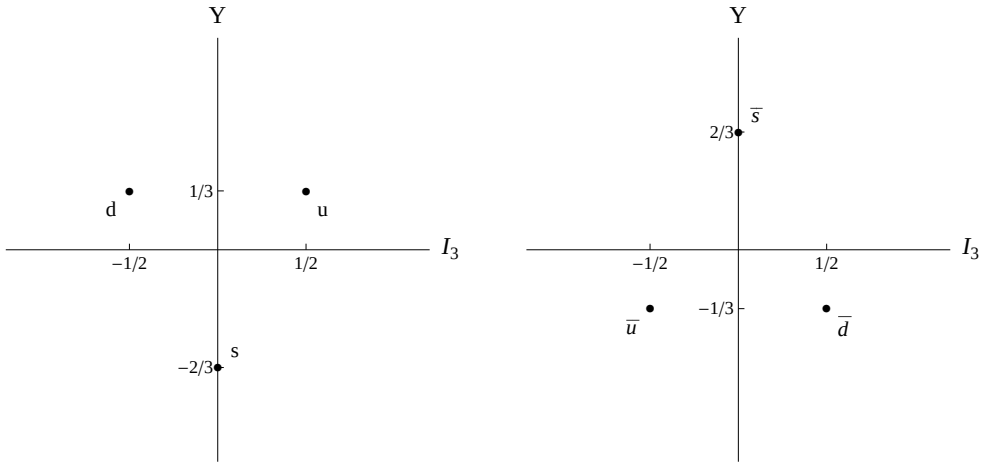

(a) Quarks **(b)** Antiquarks

Figure 1.2. I_3-Y diagram fro quarks and antiquarks.

A unitary Lie group, as the $SU(3)$ group is, can be defined through the commutation relations between pairs of generators T_R^a in a definite representation R

$$\left[T_R^a, T_R^b\right] = if^{abc}T_R^c, \tag{1.8}$$

where f^{abc} are the *structure constants* of the group. The number of generators for a $SU(N)$ group is $N^2 - 1$, thus in the case of $SU(3)$ there are eight generators. The $SU(3)$ structure constants are

$$\begin{aligned} &f_{123} = 1, \\ &f_{147} = f_{165} = f_{246} = f_{257} = f_{345} = f_{376} = \frac{1}{2}, \\ &f_{458} = f_{678} = \frac{\sqrt{3}}{2} \\ &\text{and } f_{abc} \text{ are completely antisymmteric.} \end{aligned} \tag{1.9}$$

Defining $I_3 = \lambda_3/2$ and $Y = 1/\sqrt{3}\,\lambda_8$ we find that u, d and s are placed in the $I_3 - Y$ plane as in Fig. 1.2a. Their antiparticles are showed in Fig. 1.2b.

The eightfold pattern of the lightest mesons and baryons can be understood if one assumes that baryons are made up by three quarks whereas mesons are quark antiquark bound states, assigning thus $B = 1/3$ to quarks and $B = -1/3$ to antiquarks. This implies that u and d have $S = 0$ and s has $S = -1$.

The $I_3 - Y$ diagrams in Fig. 1.1 are associated to higher dimensional representations of $SU(3)$, obtained combining the fundamental representation $\mathbf{3}$ and its conjugate, the $\bar{\mathbf{3}}$

$$\text{Mesons :} \qquad \mathbf{3} \otimes \bar{\mathbf{3}} = \mathbf{1} \oplus \mathbf{8} \tag{1.10}$$

$$\text{Baryons :} \qquad \mathbf{3} \otimes \mathbf{3} \otimes \mathbf{3} = \mathbf{1} \oplus \mathbf{8}_s \oplus \mathbf{8}_a \oplus \mathbf{10} \tag{1.11}$$

The picture became complete when the baryons belonging to the decuplet began to be discovered, starting from the Δ's, which form a 3/2 isospin multiplet. The $\mathbf{10}$ representation is depicted in Fig. 1.3.

Table 1.1. Quantum numbers of quarks.

Flavor	I_3	Y	B	S	Q
u	$+1/2$	$+1/3$	$+1/3$	0	$+2/3$
d	$-1/2$	$+1/3$	$+1/3$	0	$-1/3$
s	0	$-2/3$	$+1/3$	-1	$-1/3$

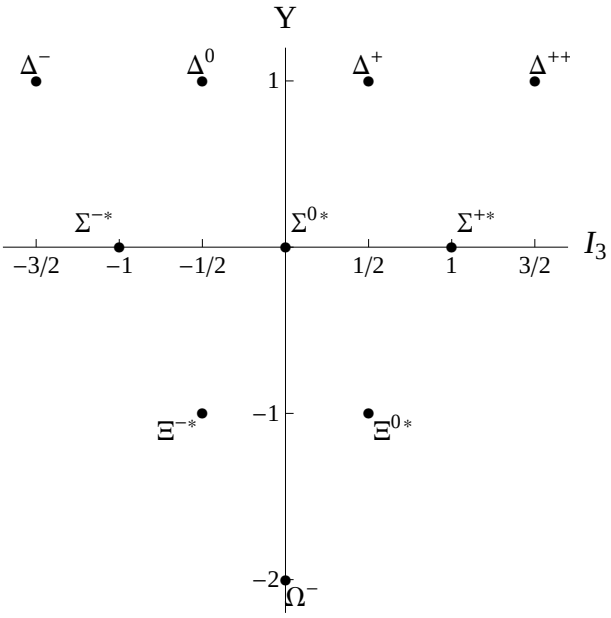

Figure 1.3. Decuplet of baryons.

The flavor content of mesons and baryons is summarized in Table 1.2.

Table 1.2. Quark content of the low-lying baryons and mesons.

MESONS				BARYONS					
1		**8**		**1**		**8**		**10**	
$u\bar{u}+d\bar{d}+s\bar{s}$	η_1	$u\bar{s}$	K^+	uds	Λ	uud	p	uud	Δ^+
		$d\bar{s}$	K^0			udd	n	udd	Δ^0
		$s\bar{u}$	K^-			uus	Σ^+	uus	Σ^{+*}
		$s\bar{d}$	$\bar{K}^0$			uds	Σ^0	uds	Σ^{0*}
		ud	π^+			dds	Σ^-	dds	Σ^{-*}
		$u\bar{u}-d\bar{d}$	π^0			uus	Ξ^0	uus	Ξ^{0*}
		$d\bar{u}$	π^-			dss	Ξ^-	dss	Ξ^{-*}
		$u\bar{u}+d\bar{d}-2s\bar{s}$	η_8			uds	Λ^0	sss	Ω^-
								uuu	Δ^{++}
								ddd	Δ^-

$SU(3)$ is not mere taxonomy. Using $SU(3)$ algebra Gell-Mann was able to derive relations between the masses of the various multiplets. For example the *Gell-Mann*

Okubo formula [10, 16]

$$2\,(m_N + m_\Xi) = 3m_\Lambda + m_\sigma, \tag{1.12}$$

is very well verified experimentally. Also, Gell-Mann was able to predict the existence of the Ω^-, which had not yet been observed when he first discussed $SU(3)$, and to give an estimate of its mass deriving the following relation between the mass spacings inside the decuplet

$$m_{\Sigma^*} - m_\Delta = m_{\Xi^*} - m_{\Sigma^*} = m_{\Omega^-} - m_{\Xi^*}. \tag{1.13}$$

At this point quarks were well-established mathematical devices, but not much more.

1.1.2 Deep Inelastic Scattering

In the 1960s the first Deep Inelastic Scattering (DIS) experiments were performed, Fig. 1.4. High energy electron beams were fired on a fixed proton target producing a scattered electron and a bunch of hadrons:

$$e^-(k)p(P) \to e^-(k')X(W). \tag{1.14}$$

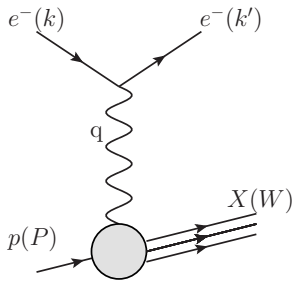

Figure 1.4. Electron scattering off a proton through the exchange of a virtual photon.

The interaction proceeds through the exchange of a space-like virtual photon $\gamma^\star(q)$ [1], $q^2 = -Q^2$. From the four momentum conservation we learn

$$\begin{aligned} &k + P = k' + W, \\ &W^2 = (q+P)^2 \xrightarrow{Q^2 >> m_p^2} -Q^2 + 2q\cdot P. \end{aligned} \tag{1.15}$$

If the scattering is *elastic* $W^2 = m_p^2 \sim 0$ then $Q^2 = 2q\cdot P$, if the scattering is *inelastic* $W^2 > 0$ so that $Q^2 < 2q\cdot P$.

The transition matrix element for this process can be written as follows

$$\mathcal{M}(ep \to eX) = -ie\,\bar{u}(k')\gamma_\mu u(k)\,\frac{-i}{q^2}\,ie\int d^4x\, e^{iqx}\,\langle X|J^\mu(x)|p\rangle, \tag{1.16}$$

[1] If the electrons are highly relativistic, $m_e << |\boldsymbol{k}|$ then $q^2 = -2|\boldsymbol{k}||\boldsymbol{k}'|(1-\cos\theta) < 0$.

where J^μ is the hadronic current coupled to the virtual photon. When computing the square of the matrix element it is convenient to introduce the tensor $\tilde{W}^{\mu\nu}$

$$\tilde{W}^{\mu\nu}(P,q) = i \int d^4x\, e^{iqx}\, \langle p(P)|T\{J^\mu(x)J^\nu(0)\}|p(P)\rangle, \tag{1.17}$$

with proton spin averaged. $\tilde{W}^{\mu\nu}$ is related to the forward Compton scattering off a proton, Fig. 1.5, through the optical theorem

$$2\Im\left(\tilde{W}^{\mu\nu}(P,q)\right) = \sum_n \int d\Pi^{(n)}\, \langle p(P)|J^\mu(-q)|X_n\rangle\langle X_n|J^\nu(q)|p(P)\rangle, \tag{1.18}$$

where $d\Pi^{(n)}$ is the n-body phase space.

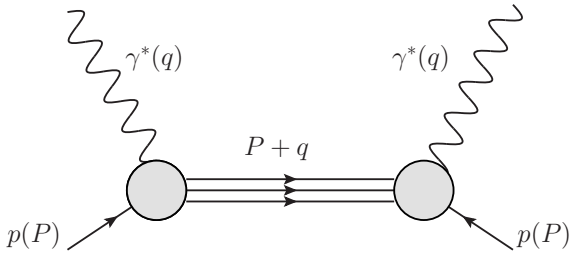

Figure 1.5. Compton scattering off a proton.

We are interested in the total deep inelastic cross section

$$d\sigma(ep\to eX) = \frac{1}{4\phi}(2\pi)^4 \sum_n \delta^{(4)}(k+P-k'-W)\overline{|\mathcal{M}(ep\to eX_n)|^2}\frac{d\boldsymbol{k'}}{(2\pi)^3 2E'}d\Phi^{(n)}, \tag{1.19}$$

where ϕ is the flux factor, $d\Phi^{(n)}$ is the n-body phase space relative to hadrons whereas k' refers to the scattered electron. The transition matrix element can be factorized into a leptonic part and a hadronic one, making use also of the result of Eq. (1.18):

$$d\sigma(ep\to eX) = \frac{1}{4\Phi}\frac{e^4}{(Q^2)^2}L^{\mu\nu}\, 2\Im\left(\tilde{W}_{\mu\nu}(P,q)\right)\frac{d\boldsymbol{k'}}{(2\pi)^3 2E'}, \tag{1.20}$$

where the leptonic tensor can be explicitly computed

$$L^{\mu\nu} = 2\left(k^\mu k'^\nu - g^{\mu\nu}k\cdot k' + k'^\mu k^\nu\right), \tag{1.21}$$

whereas the hadronic one can be built in terms of unknown structure functions exploiting the Ward identities $k^\mu\tilde{W}_{\mu\nu}=0$ and $k^\nu\tilde{W}_{\mu\nu}=0$:

$$W_{\mu\nu}(P,q) = W_1(P,q)\left(-g_{\mu\nu}+\frac{q^\mu q^\nu}{q^2}\right)+W_2(P,q)\left(P^\mu-q^\mu\frac{P\cdot q}{q^2}\right)\left(P^\nu-q^\nu\frac{P\cdot q}{q^2}\right). \tag{1.22}$$

with $\tilde{W}_{\mu\nu} = 2\pi m_p\, W_{\mu\nu}$. All our ignorance about the internal structure of the proton is contained in W_1 and W_2. In 1969 the DIS experiments at SLAC (*Stanford Linear*

Accelerator) [17] showed that it was possible to define two structure functions F_1 and F_2

$$\begin{cases} F_1(P,q) = m_p \Im(W_1(P,q)) \\ F_2(P,q) = \frac{m_p}{P\cdot q} \Im(W_2(P,q)) \end{cases} \tag{1.23}$$

that exhibited a scaling behavior, *i.e.* they did not depend on the transferred momentum Q^2, but only on the *Bjorken* x defined as

$$x = \frac{Q^2}{2q \cdot P}. \tag{1.24}$$

This feature is the footprint of the existence of partons inside the proton, which can be thought as non interacting with each other when struck by a virtual photon carrying $Q^2 >> m_p^2$. We need to compare the typical interaction time between electron and proton $\tau_{\text{DIS}} \sim 1/\sqrt{Q^2}$ with the interaction time among the constituents of the proton, the partons, which is roughly given by the inverse of the mass of the proton $\tau_{\text{partons}} \sim 1/m_p$. In the deep inelastic region of the scattering one has $Q^2 >> m_p^2$ and in turn $\tau_{\text{DIS}} << \tau_{\text{partons}}$. Thus over the time interval in which the virtual photon probes the proton structure, the partons on average do not interact with each other.

This was the main hypothesis of the parton picture proposed by Feynman [11]. He described the proton as a bunch of weakly bound partons: when the electron scatters off a proton it interacts only with one parton at a time. Each parton q_i carries a fraction of the momentum of the proton $p_i = \xi P$, where ξ can be regarded as the longitudinal momentum fraction. The transverse component of the partons momentum can be neglected. Finally one needs to introduce a probability density function for each type of parton $f_i(\xi)$, which measures the probability density of finding inside the proton a parton of type i carrying a fraction ξ of the proton momentum P.

In this scenario, showed in Fig. 1.6, the DIS cross section can be written as

$$d\sigma(e(k)p(P) \to e(k')X) = \int_0^1 \sum_i f_i(\xi)\, d\hat{\sigma}(e(k)q_i(\xi P) \to e(k')X), \tag{1.25}$$

where $d\hat{\sigma}$ is the partonic cross section and q_i the constituent parton of type i.

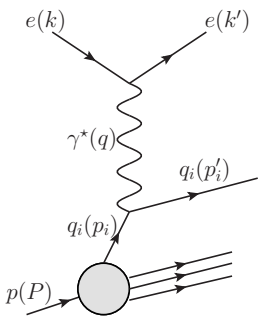

Figure 1.6. Deep Inelastic Scattering as seen in the parton model.

Since the partons are weakly bound, we can treat them as free fermions and thus we can compute explicitly the partonic matrix element

$$\overline{|\hat{\mathcal{M}}|^2} = e^4 \frac{\hat{s}^2 + \hat{u}^2}{\hat{t}^2}, \tag{1.26}$$

where $\hat{s}$, $\hat{t}$, $\hat{u}$ are the partonic Mandelstam variables. If we restore a generic charge Q_i for the partons, the partonic cross section finally reads

$$\frac{d\hat{\sigma}}{d\hat{t}} = \frac{2\pi\, Q_i^2 \alpha^2}{\hat{s}^2} \, \frac{\hat{s}^2 + (\hat{s}+\hat{t})^2}{\hat{t}^2}, \tag{1.27}$$

so that the total DIS cross section comes out to be

$$\frac{d\sigma}{dQ^2} = \int_0^1 d\xi \sum_i f_i(\xi) \frac{2\pi\, Q_i^2 \alpha^2}{Q^4} \left[1 + \left(1 - \frac{Q^2}{\xi s}\right)\right]^2. \tag{1.28}$$

Since for massless partons $\xi = x$ [2] one obtains

$$\frac{d\sigma}{dx\, dQ^2} = \sum_i f_i(x) \frac{2\pi\, Q_i^2 \alpha^2}{Q^4} \left[1 + \left(1 - \frac{Q^2}{xs}\right)\right]^2. \tag{1.29}$$

This is the result we are interested in. The parton model shows how the DIS cross section depends exclusively on the Bjorken x, a part from the standard QED factors. This feature is known as *Bjorken scaling* [18], which was largely confirmed, up to a precision of the 10%, by the DIS experiments at SLAC for $\sqrt{Q^2} > 1\text{GeV}$. The Bjorken scaling states that the proton appears the same for an electromagnetic probe, regardless of the energy with which the proton is probed, given it is much larger than the proton mass.

The observed scaling property of the two structure functions F_1 and F_2 can be understood in the framework of the parton model by computing the forward Compton scattering amplitude off a proton. Going back to Eq. (1.17) we need to substitute the matrix element between the proton with a sum of matrix elements between partons:

$$\tilde{W}^{\mu\nu}(P,q) = i \int d^4x\, e^{iqx} \int_0^1 d\xi \sum_i f_i(\xi) \frac{1}{\xi} \langle q_i(\xi P)|T\{J^\mu(x) J^\nu(0)\}|q_i(\xi P)\rangle, \tag{1.30}$$

We have two possible diagrams, Fig. 1.7, from which we can compute, using perturbation theory, $\tilde{W}^{\mu\nu}(P,q)$.

[2] Since $q^2 \leq 0$, we can find a reference frame in which $q^0 = 0$, the *Breit frame*, so that $q = (0,0,0,\sqrt{Q^2})$. Neglecting the mass of the proton, $P^2 = 0$, the proton four momentum reads

$$P = \left(\frac{\sqrt{Q^2}}{2x}, 0, 0, -\frac{\sqrt{Q^2}}{2x}\right).$$

A parton q_i carries $p_i = \xi P$, whereas the scattered parton will have four momentum

$$p_i' = q + p_i = \left(\frac{\xi}{x}\frac{\sqrt{Q^2}}{2}, 0, 0, \sqrt{Q^2}\,(1 - \frac{1}{2}\frac{\xi}{x})\right).$$

If we impose that the scattered parton is massless, $(p_i')^2 = 0$, we find $\xi = x$.

Figure 1.7. Forward Compton scattering process of a photon off a proton.

In doing this one finds the expressions of F_1 and F_2 in terms of the parton density functions $f_i(x)$:

$$\begin{cases} F_1(x) = \frac{1}{2} \sum_i f_i(x)\, Q_i^2 \\ F_2(x) = \sum_i x\, f_i(x)\, Q_i^2 \end{cases} \tag{1.31}$$

and also a relation between the two

$$F_2(x) = 2xF_1(x) \tag{1.32}$$

known as the *Callan Gross relation* [19].

Callan and Gross derived the above equation in a slight different way. Their realize that by measuring the ratio of the longitudinal and transverse DIS cross sections $R = \sigma_L/\sigma_T$, one could determine the spin of the charged constituents of the proton. In particular they discovered that if the constituents had spin zero then $\sigma_T = 0$, but if they had spin 1/2, then $\sigma_L = 0$. The experiments quickly showed that σ_L was very small.

In the scaling limit of the parton model one can show indeed that the longitudinal cross section for the scattering of a virtual photon off a proton is

$$\sigma_L(\gamma^\star p) \xrightarrow{\text{scaling limit}} \frac{4\pi\alpha^2}{Q^2} \left[F_2(x) - 2xF_1(x)\right] \tag{1.33}$$

which vanishes exactly zero in the scaling limit. The above expression allows to quantify correction to the Callan Gross relation simply measuring the longitudinal cross section, without any knowledge of the dynamics of strong interactions.

1.1.3 Asymptotic freedom and QCD

In 1971 't Hooft made his startling discovery that Yang-Mills theories are renormalizable: the infinities which materialize when going beyond the first order of perturbation theory can be reabsorbed in a finite number of measurable constants such as masses, renormalizations of fields and coupling constants. This result reintroduced non-Abelian gauge theories to the community, first of all reviving the electroweak theory of Glashow Weinberg and Salam.

As for the strong interactions it was clear by that time that the property of scaling was related to the point like behavior at short distances, as the parton model had widely proved. The quantum field theory of the strong interactions must exhibit this feature, *i.e.* its coupling constant must decrease at short distances.

The concept of running coupling constant can be understood in a more quantitative way giving a short summary on the renormalization group equations.

When computing loop diagrams one encounters infinities, since the integration over the four-momentum running in the loop is not limited. We give an example. In a scalar field theory with quartic interaction the propagator receives, at the first order in the bare coupling constant λ_0, the contribution of the diagram in Fig. 1.8.

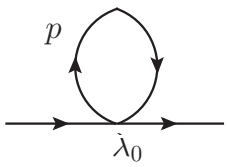

Figure 1.8. First order contribution to the propagator of a scalar field in a scalar field theory with quartic interaction. λ_0 is the bare quartic coupling.

The loop integral is

$$\lambda_0 \int \frac{d^4p}{(2\pi)^4} \frac{1}{p^2 - m_0^2}, \tag{1.34}$$

where m_0 is the bare mass of the scalar field. The above integral can be regularized introducing a dimensional cutoff Λ. Performing the Wick rotation $p_4 = ip^0$ and introducing the Euclidean norm $p_E^2 = p_4^2 + |\boldsymbol{p}|^2$, we can quantify the degree of divergence of this integral ($\sqrt{p_E^2} < \Lambda$)

$$\lambda_0 \int \frac{d^4p}{(2\pi)^4} \frac{1}{p^2 - m_0^2} = -i\lambda_0 \int \frac{p_E^3 \, dp_E \, d\Omega_4}{(2\pi)^4} \frac{1}{p_E^2 + m_0^2} \propto \Lambda^2. \tag{1.35}$$

Infinities pop up in many other Green functions: the first step is to regularize these infinities introducing a regularization parameter. The simplest way is to limit the energy of the particles in the loop, as we have done for the tadpole diagram. However this is not always allowed, if one requires that certain symmetries must be preserved. An alternative way is that of dimensional regularization, which consists in computing loop integrals in a D-dimensional space-time and then taking the limit for $D \to 4$. The tadpole diagram in dimensional regularization should be treated as follows [3]:

$$\lambda_0 \, \mu^{4-D} \int \frac{d^Dp}{(2\pi)^D} \frac{1}{p^2 - m_0^2} = -\lambda_0 \frac{\Gamma(1 - D/2)}{(2\pi)^{D/2}} \left(\frac{1}{m_0^2} \right)^{1-D/2}. \tag{1.36}$$

Now expand near $D = 4 - \epsilon$ taking into account that $\Gamma(\epsilon - 1) = -\Gamma(\epsilon)/(1 - \epsilon) \xrightarrow{\epsilon \sim 0} -(1 + \epsilon)(1/\epsilon - \gamma_E) = 1/\epsilon + 1 - \gamma_E + \mathcal{O}(\epsilon)$ and $(1/m_0^2)^{\epsilon - 1} \sim m_0^2(1 - \epsilon \ln(m_0^2))$. One obtains

$$\lambda_0 \, \mu^{4-D} \int \frac{d^Dp}{(2\pi)^D} \frac{1}{p^2 - m_0^2} = \lambda_0 m^2 \left(\frac{1}{\epsilon} + 1 - \gamma_E - \ln \left(\frac{m_0^2}{\mu^2} \right) \right) + \mathcal{O}(\epsilon). \tag{1.37}$$

Here the divergency is contained in the pole factor $1/\epsilon$.

[3] The quartic coupling λ_0 in 4 dimensions is adimensional. When generalizing to a D dimensional space-time we need to reconsider the dimensions of fields and parameters: $[\phi] = M^{D/2-1}$, $[\lambda_0] = M^{4-D}$. To make explicit the mass dimensionality of the coupling constant one usually writes $\lambda_0 \to \lambda_0 \mu^{4-D}$.

The dependence of the regularized quantities on the regularization parameter, Λ or ϵ, is eliminated by reabsorbing it into a redefinition of the mass parameter m, the coupling constant λ and the wave function renormalization factors $\sqrt{Z}$, using suitable renormalization conditions (precise definitions of m, λ and Z). For example one usually defines the renormalized mass m as the pole of the *dressed* propagator, see Fig. 1.9, the renormalization constant $\sqrt{Z}$ as its residue at the pole and the coupling constant λ as the one particle irreducible 4-point Green function divided by the 2-point Green functions associated to the external legs, see Fig. 1.10.

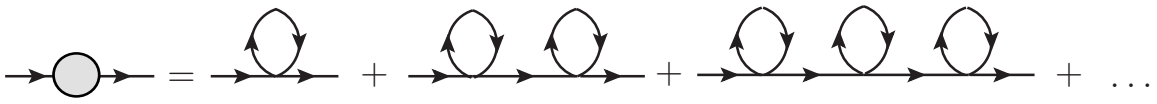

Figure 1.9. Dressed propagator in a scalar field theory with quartic interaction.

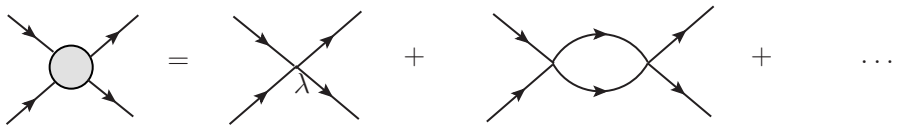

Figure 1.10. Dressed 4-point vertex in a scalar field theory with quartic interaction.

A generic regularized Green function, G_{bare}, depends on the renormalization parameter, which we will indicate generically with Λ, on the squared bare coupling constant $\alpha_0 = \lambda_0^2/4\pi$ and on the four momenta q_i of the particles involved. On the other hand the renormalized Green function, G_{ren}, depends on the renormalized coupling constant, on the renormalization point μ^2 and again on q_i. The regularized and renormalized Green functions are related by

$$G_{\text{bare}}(\Lambda, \alpha_0; p_i) = Z_G(\Lambda, \mu^2)\, G_{\text{ren}}(\mu^2, \alpha; q_i). \tag{1.38}$$

Since G_{bare} does not depend on the renormalization point μ then

$$\frac{dG_{\text{bare}}}{d\ln\mu^2} = \frac{d}{d\ln\mu^2}\left(G_{\text{ren}}\right) = 0. \tag{1.39}$$

Now recall that G_{ren} depends on μ not only directly but also trough the renormalized coupling α, so that

$$Z_G\left[\frac{\partial}{\partial\ln\mu^2} + \frac{\partial\alpha}{\partial\ln\mu^2}\frac{\partial}{\partial\alpha} + \frac{1}{Z_G}\frac{\partial Z_G}{\partial\ln\mu^2}\right] G_{\text{ren}}(\mu^2, \alpha; q_i) = 0. \tag{1.40}$$

Introducing the quantities

$$\begin{aligned} \beta(\alpha) &= \frac{\partial\alpha}{\partial\ln\mu^2} \\ \gamma_G(\alpha) &= \frac{\partial\log Z_G}{\partial\ln\mu^2}, \end{aligned} \tag{1.41}$$

we can rewrite Eq. (1.40) as

$$\left[\frac{\partial}{\partial \ln \mu^2} + \beta(\alpha)\frac{\partial}{\partial \alpha} + \gamma_G(\alpha)\right] G_{\rm ren}(\mu^2, \alpha; q_i) = 0. \tag{1.42}$$

While β does not depend on which particular Green function we are considering, *i.e.* is a property of the theory, $\gamma_G(\alpha)$ does depend on G. The above equation is known as *Callan Symanzik Equation* or *Renormalization Group Equation* (RGE).

At the time of 't Hooft discoveries it was ascertained that QED was an *infrared stable* theory, in other words the effective charge grew larger at short distances. Taking QED as a paradigmatic example, nobody could imagine a theory which behaved in the opposite way. Charge renormalization can be understood in terms of vacuum polarization. Indeed the vacuum of a relativistic quantum field theory can be thought as a medium of virtual particles. In QED the vacuum contains positron electron pairs, as shown in Fig. 1.11. When a charge e_0 is immersed in this medium it polarizes it, inducing dipoles. This medium of virtual dipoles screens the charge e_0, and the actual observable charge e will differ from e_0 as e_0/ϵ, where ϵ is the dielectric constant. Now ϵ is distance dependent and so it is e, since as the distance r from e_0 increases there is more medium that screens. Thus $e(r)$ decreases with increasing r and correspondingly increases with decreasing r. The β function is thus positive, since it is $\beta(\alpha_{\rm em}) \propto -de(r)/dr$ [4].

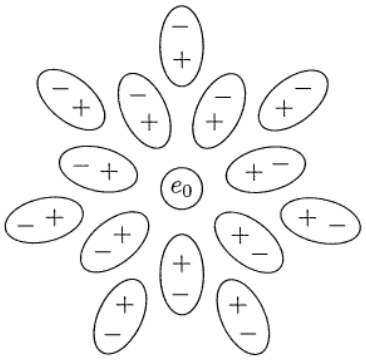

Figure 1.11. Virtual e^+e^- pairs are effectively dipoles of length $\sim 1/m_e$, which screen the bare charge of the electron.

To describe strong interactions, it was necessary to find a renormalizable quantum field theory with negative β function. After having proved that no renormalizable field theory that consisted of theories with arbitrary Yukawa, scalar or Abelian gauge interactions could be asymptotically free, Yang-Mills theories represented the only possibility.

The goal was to compute the β function of a SU(N) gauge theory with fermionic matter fields, the quarks, and spin one gauge fields, the gluons.

Applying RGE to the 3-gluon and 2-gluon Green functions, Fig. 1.12 and 1.13, and keeping only the first terms of the perturbative expansion $\beta(\alpha_s) = -b\alpha_s^2$ [5], we

[4] Recall that $r \propto 1/\mu$, thus, following Eq. (1.41) $\beta(\alpha_{\rm em}) = \frac{\partial e^2}{4\pi \partial \ln 1/r^2} = -\frac{e}{4\pi}\frac{\partial e}{\partial r}$

[5] We can compute the first term of the perturbative expansion of $\beta(\alpha_s)$ looking at the 1-loop

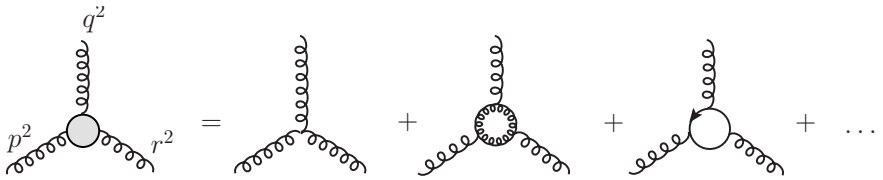

Figure 1.12. 3-point function with 3 external gluon legs.

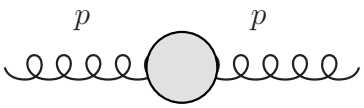

Figure 1.13. 2-point function with 2 external gluon legs.

have

$$b = 2\left(B_{3g} - \frac{3}{2}B_{2g}\right), \tag{1.43}$$

where B_{3g} and B_{2g} are the results of the 1-loop computations of the 3-gluon and 2-gluon diagrams. By direct calculation one finds

$$b = \frac{11N_c - 2n_f}{12\pi}, \tag{1.44}$$

where n_f is the number of quark flavors and N_c is the number of colors.

There are several evidences for the existence of an additional quantum number for quarks. An example is the Δ^{++}, a spin 3/2 baryon made up of three u quarks. The Δ^{++} wave function has symmetric flavor and spin parts whereas Fermi statistics requires the whole wave function to be antisymmetric. Introducing the color quantum number with three values, red/green/blue, one can build a completely antisymmetric wave function $\Delta^{++} \sim \epsilon_{ijk}u^i u^j u^k$.

A second indication for the existence of three colors comes from the ratio

$$R = \frac{\sigma(e^+e^- \to \text{hadrons})}{\sigma(e^+e^- \to \mu^+\mu^-)}. \tag{1.45}$$

Assuming that the $q\bar{q}$ pair, originated from $e^+e^- \to \gamma^\star \to q\bar{q}$, evolves into hadrons with probability equal to one, the ratio $R \sim N_C \sum_f q_f^2 n_f$, where q_f is the f-flavor electric charge. Above the $b\bar{b}$ threshold R is expected to be $\sim N_c\, 11/9$. Experiments indicates $R \sim 11/3$, Fig. 1.14 and thus $N_c = 3$.

If $N_c = 3$ then $b > 0$ as long as $n_f < 16$. How b enters the dependence of the running coupling on energy (distance), can be clarified by the evolution equation for the coupling constant α_s

$$\alpha_s(t) = \frac{\alpha_s}{1 + b\alpha_s t}, \tag{1.46}$$

where $t = \ln Q^2/\mu^2$. As the energy Q^2 grows t grows and α_s decreases.

diagrams in Fig. 1.12. They both carry 3 powers of e_{s0} so that $\partial e_s/\partial \ln \mu^2 \propto e_s^3$ and in turn $\beta(\alpha_s) = \partial\alpha_s/\partial \ln \mu^2 = (\partial\alpha_s/\partial e_s) \times (\partial e_s/\partial \ln \mu^2) \propto e_s \times e_s^3 = \alpha_s^2$.

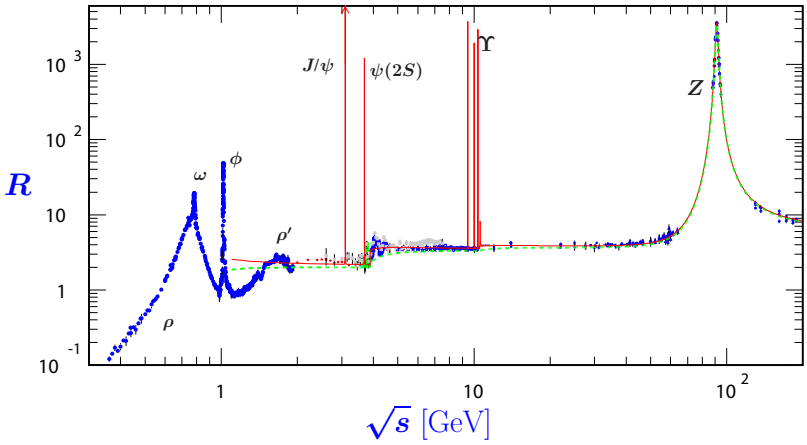

Figure 1.14. R ratio taken from [20].

On the other hand in QED at 1-loop we find $\beta(\alpha) = c\alpha^2$ leading to

$$\alpha(t) = \frac{\alpha}{1 - b\alpha t}, \tag{1.47}$$

which confirms the infrared stability of electromagnetic interaction we discussed before. Moreover from Eq. (1.47) one can learn about the existence of the so called *Landau pole* at $b\alpha t = 1$. In other words as Q^2 approaches $M^2_{\text{Planck}} = 10^{19}$ GeV $\alpha(Q^2) \to \infty$.

As the *electric* properties of vacuum allowed us to understand why QED is a quantum field theory with positive beta function, it is possible to understand why non-Abelian gauge theories are asymptotically free in a very physical fashion by considering the *magnetic* properties of the QCD vacuum [21]. As we have said before, the vacuum of a relativistic quantum field theory can be considered as a medium, which exhibits the property of relativistic invariance. The symmetry with respect to the Lorentz group implies that the magnetic permeability μ and the dielectric constant ϵ respect the relation $\epsilon\mu = 1$. The effect of the vacuum on the interaction between two charges, electric or color ones, will be that of screening if $\epsilon > 1$ and thus $\mu < 1$ or that of antiscreening if $\epsilon < 1$ thus $\mu > 1$. Now we know that the magnetic permeability is related to the magnetic susceptibility χ as: $\mu = 1 + 4\pi\chi$. On the other hand the vacuum energy of a medium in presence of an external magnetic field H is $E = -\frac{1}{2}4\pi\chi(H)H^2$. If the vacuum contains magnetic dipoles they tend to align themselves to the external magnetic field, leading to a negative energy density, so that $\chi > 0$ and $\mu > 1$. In this case the vacuum is called *paramagnetic* and is associated with antiscreening. On the other hand the *diamagnetic* case $\chi < 0$, is associated with screening. The nature of the vacuum is decided by the clouds of virtual particles with which the vacuum is filled up. While in QED only positron electron pairs populate the vacuum, in QCD also gluons, besides quarks, carry color charge and interact with each other. Since gluons are spin 1 particles, whereas quarks, like electrons, have spin 1/2, the QCD vacuum behaves as a paramagnetic medium whereas the QED one is diamagnetic. This is true as long as the number of quarks flavors is not too large. In fact the expression for the magnetic permeability

of the QCD vacuum is

$$\mu(H) \simeq 1 + \frac{(33 - 2n_F)g_s^2}{48\pi} \ln \frac{\Lambda^2}{|g_s H|}, \tag{1.48}$$

where Λ can be interpreted as the inverse of a short distances cutoff. The above expression shows that if $n_f \leq 16$ then $\mu > 1$ and we are in the antiscreening case, $\epsilon < 1$. The fact that photon, unlike the gluons, do not carry electric charge, ensures that QED is an infrared stable theory.

1.2 Heavy quarkonium

The history of strong interactions is intimately related to weak interactions. In 1970 Glashow, Iliopoulos and Maiani proposed the existence of a fourth quark [22], the *charm*, with the same quantum numbers of the *up* quark. Its mass was predicted to be between 1 and 3 GeV, to solve the problem of the different leptonic decay rates of K_L^0 and K^+ and the mass difference between K_L^0 and K_S^0 (Section 1.2.1).

The existence of a fourth quark, much heavier than u d s, was established in 1974 by the discovery of the J/ψ [23, 24],. The GIM mechanism, *i.e.* the identification of this fourth quark with the *charm*, was finally confirmed when the D-mesons were first observed in 1976 [25, 26] and their weak decays were measured. In 1977 the existence of a fifth flavor, the *bottom*, was proved by the observation of the $\Upsilon(1S)$ [23], a $b\bar{b}$ meson (Section 1.2.2). Many other excited states of *charmonium* ($c\bar{c}$), and *bottomonium* ($b\bar{b}$), have been subsequently uncovered and their properties are till today subject of research. The discoveries of charmonium and bottomonium showed the way forward to a new approach to QCD.

The dynamics of mesons made up by two heavy quarks [6], *i.e.* with a mass m_Q much larger than the typical scale at which strong interactions become non perturbative, $\Lambda_{\rm QCD} \sim 200$ MeV, can be indeed described using non relativistic quantum mechanics. The spectrum of the bound states can be computed using the Schrödinger equation with a phenomenological potential (Section 1.2.3). The non relativistic approach allows also to predict decay rates between the different radially or orbitally excitations of charmonium and bottomonium (Section 1.2.4).

The discovery of charm, beside opening a completely new kind of spectroscopy, represented a further confirmation of asymptotic freedom, which was discovered little time before J/ψ was observed for the first time.

1.2.1 The role of weak interactions

In this section we aim at giving a feeling of how important was the role of weak interactions for the discovery of the fourth quark, the *charm*. After giving a brief summary on the structure of the electroweak theory of Glashow Weinberg and Salam, we will describe how Glashow Iliopoulos and Maiani predicted the existence of a fourth quark to explain the unexpected suppression observed in the decay $K^0 \to \mu^+\mu^-$.

[6] which we will indicate collectively with Q

Electroweak Theory. Yang and Mills formulated their theories in 1954 and for a long time these remained a fascinating idea without any application. Only in 1961 Glashow [27] proposed to unify electromagnetic *and* weak interactions using a Yang-Mills theory with gauge group $SU(2)_I \otimes U(1)_Y$. The quantum numbers associated to the gauge group were named *weak isotopic spin* (I) and *weak hypercharge* (Y), in analogy with the isospin and the hypercharge introduced to describe light hadrons. This choice of the gauge group implied the existence of four gauge bosons: $W^\mu_{i=1,2,3}$ associated to the three generators of $SU(2)$ and B^μ associated to the generator of U(1).

The gauge fields Lagrangian contains the kinetic terms and the mass terms

$$\begin{aligned}\mathcal{L}_{gauge} = &-\frac{1}{4} W^\dagger_{\mu\nu} \cdot W^{\mu\nu} + M_W^2 W^\dagger_\mu W^\mu \\ &-\frac{1}{4}\left[W^3_{\mu\nu}(W^3)^{\mu\nu} + B_{\mu\nu}B^{\mu\nu}\right] \\ &+\frac{1}{2}\left[M_W^2 W^3_\mu \cdot (W^3)^\mu + M_0^2 B_\mu B^\mu + 2M_{03}^2 W^3_\mu B^\mu\right],\end{aligned} \tag{1.49}$$

where we have introduced $W_\mu = (W^2_\mu + iW^2_\mu)/\sqrt{2}$ and $W^\dagger_\mu = (W^2_\mu - iW^2_\mu)/\sqrt{2}$. Switching to the mass eigenstates Z_μ and A_μ

$$\begin{cases} Z_\mu &= \cos\theta\, W^3_\mu - \sin\theta\, B_\mu \\ A_\mu &= \sin\theta\, W^3_\mu + \cos\theta\, B_\mu, \end{cases} \tag{1.50}$$

A_μ can be identified with the photon field [7], whereas Z_μ is a new electrically neutral field with mass $M_Z^2 = M_W^2/\cos^2\theta$.

If we consider the electron with its neutrino organized as

$$l_e = \begin{pmatrix} \nu_{eL} \\ e_L \end{pmatrix}_{Y=-1} \qquad (e_R)_{Y=-2}, \tag{1.51}$$

the interaction Lagrangian in terms of A_μ and Z_μ reads

$$\mathcal{L}_{int} = -eA^\mu J^{\rm em}_\mu - \frac{g}{2\cos\theta} Z^\mu J^Z_\mu - \frac{g}{2\sqrt{2}}\left[W^\mu (J^W_\mu)^\dagger + \text{h.c.}\right], \tag{1.52}$$

where

$$\begin{aligned} J^{\rm em}_\mu &= -\left(\bar e_L \gamma_\mu e_L + \bar e_R \gamma_\mu e_R\right), \\ J^{\rm Z}_\mu &= 2(J^3_L)_\mu - 2\sin^2\theta J^{\rm em}_\mu, \\ (J^3_L)_\mu &= \bar\nu_L \gamma_\mu \nu_L - \bar e_L \gamma_\mu e_L, \\ J^W_\mu &= \bar e_L \gamma_\mu \nu_L \end{aligned} \tag{1.53}$$

and similarly for the μ and τ families. It is important to notice that the scale of the processes mediated by the charged vector boson W^μ is the same as that of neutral

[7] In order to keep the photon massless, one of the two eigenstates must vanish, so that $\det(\mathbb{M}) = 0 \Rightarrow (M^2_{03})^2 = M^2_W M^2_0$.

current ones, *i.e.* the ones mediated by the Z boson, and is determined by the Fermi constant G_F

$$\frac{G_F}{\sqrt{2}} = \frac{g^2}{8M_W^2} = \frac{e^2}{8\sin^2\theta M_W^2}. \tag{1.54}$$

The main problem of the Glashow theory was represented by the masses of the intermediate bosons in Eq. (1.49), since explicit mass terms break gauge invariance.

In 1967 Weinberg and Salam [28, 29] solved this issue, introducing a doublet of scalar fields which allowed to give mass to the gauge bosons, without breaking gauge invariance. They exploited the *Higgs mechanism* to induce a spontaneous symmetry breaking of the gauge group preserving the $U(1)$ symmetry associated to electromagnetism:

$$SU(2)_I \otimes U(1)_Y \to U(1)_{\text{em}}. \tag{1.55}$$

This pattern is obtained choosing a doublet of scalar fields with hypercharge $Y = +1$

$$\phi = \begin{pmatrix} \phi^+ \\ \phi^0 \end{pmatrix}_{Y=+1}, \tag{1.56}$$

subject to the potential

$$V(\phi) = \mu^2\phi^\dagger\phi + \lambda(\phi^\dagger\phi)^2. \tag{1.57}$$

The mass terms for the gauge fields arise from the covariant derivative of the scalar doublet once the ϕ field has acquired a non zero vacuum expectation value. In 1972 Weinberg [30] exploited the same mechanism to give mass to the matter fields, quarks and leptons, introducing Yukawa interaction terms. As for the leptons, the mass terms arise from

$$\mathcal{L}_{e\phi} = g_e\left(\bar{l}_e\phi e_R + \bar{e}_R\phi^\dagger l_e\right). \tag{1.58}$$

If we wanted to give mass to the neutrinos, considering them as standard Dirac spinors, we would include terms of this form

$$\mathcal{L}_{\nu\phi} = g_\nu\left((\bar{\nu}_e)_R l_e^a\phi^b\epsilon_{ab} + \bar{l}_e^a(\phi^\dagger)^b\epsilon_{ab}(\nu_e)_R\right), \tag{1.59}$$

with ϵ_{ab} the completely 2×2 antisymmetric tensor.

The Cabibbo Theory and the GIM Mechanism. What happens when one tries to include quarks in the Glashow-Weinberg-Salam theory? At the time the theory was formulated, only the three lightest quarks were known: *up*, *down* and *strange*. It was natural to assign the left-handed components of u and d to a weak isospin doublet, and the other fields to weak isospin singlets:

$$q_L = \begin{pmatrix} u_L \\ d_L \end{pmatrix}_{Y=1/3}, \qquad (u_R)_{Y=4/3}, \qquad (d_R)_{Y=-2/3}, \qquad (s_L)_{Y=-2/3}, \qquad (s_R)_{Y=-2/3}. \tag{1.60}$$

Mass terms arise from Yukawa interactions as in Eq. (1.58) and (1.59), leading to

$$\mathcal{L}_q^{\text{mass}} = m_u\bar{u}_R u_L + \bar{D}_L M^D D_R + \text{h.c.}, \tag{1.61}$$

where M^D is a 2×2 matrix and we have defined

$$D_R = \begin{pmatrix} d_R \\ s_R \end{pmatrix}, \qquad D_L = \begin{pmatrix} d_L \\ s_L \end{pmatrix}. \tag{1.62}$$

When going to the mass eigenstates basis $\{D'_L, D'_R\}$ through the introduction of two unitary matrices $\mathcal{U}$ and $\mathcal{V}$

$$D_L = \mathcal{U} D'_L \qquad D_R = \mathcal{V} D'_R, \tag{1.63}$$

the electromagnetic current does not change, whereas the charged and neutral currents do change as:

$$\begin{aligned} \bar{u}_L \gamma^\mu d_L &= \bar{u}_L \left(\cos\theta_c d'_L + \sin\theta_c s'_L\right), \\ \bar{d}_L \gamma^\mu d_L &= \left(\cos\theta_c \bar{d}'_L + \sin\theta_c \bar{s}'_L\right)\left(\cos\theta_c d'_L + \sin\theta_c s'_L\right), \end{aligned} \tag{1.64}$$

having defined

$$\mathcal{U} = \begin{pmatrix} \cos\theta_c & \sin\theta_c \\ -\sin\theta_c & \cos\theta_c \end{pmatrix}, \tag{1.65}$$

where $\theta_c \sim 13^\circ$ is the *Cabibbo angle*. The mixing between d and s, gives rise to flavor changing neutral currents like $\sim \cos\theta_c \sin\theta_c \, \bar{d}_L \gamma_\mu s_L$.

One of the consequences of the existence of these terms is that the rate of the decays $K_L^0 \to \mu^+\mu^-$ and $K^- \to \mu^- \bar{\nu}_\mu$ should be the same, since they are due respectively to the $\cos\theta_c \, \sin\theta_c \, \bar{d}_L \gamma^\mu s_L Z_\mu$ and $\sin\theta_c \, \bar{u}_L \gamma^\mu s_L \, W\dagger_\mu$ terms in Eq. (1.64). This is in contrast with experiments, where one observes

$$\begin{aligned} \mathcal{B}(K_L^0 \to \mu^+\mu^-) &= (63.54 \pm 0.14) \times 10^{-2}, \\ \mathcal{B}(K^- \to \mu^- \bar{\nu}_\mu) &= (6.84 \pm 0.11) \times 10^{-9}. \end{aligned} \tag{1.66}$$

This issue was solved in 1970, when Glashow, Iliopoulos and Maiani hypothesized the existence of a fourth quark, named *charm*, with the same quantum numbers of the u quark and which can thus form a weak isospin doublet together with s_L

$$\begin{aligned} &q_L^1 = \begin{pmatrix} u_L \\ d_L \end{pmatrix}_{Y=1/3}, \qquad q_L^2 = \begin{pmatrix} c_L \\ s_L \end{pmatrix}_{Y=1/3}, \\ &(u_R)_{Y=4/3}, \qquad (c_R)_{Y=4/3}, \qquad (d_R)_{Y=-2/3}, \qquad (s_R)_{Y=-2/3}. \end{aligned} \tag{1.67}$$

The interaction Lagrangian becomes now

$$\begin{aligned} \mathcal{L}_{int} = &- \frac{g}{\sqrt{2}} \left(\bar{U}_L \gamma^\mu D_L \, W_\mu^\dagger + \bar{D}_L \gamma^\mu U_L \, W_\mu\right) \\ &- e \, J_\mu^{\rm em} \, A^\mu - \frac{g}{2\cos\theta} \left[\bar{U}_L \gamma_\mu U_L - \bar{D}_L \gamma_\mu D_L - 2\sin^2\theta \, J_\mu^{\rm em}\right] Z^\mu, \end{aligned} \tag{1.68}$$

having defined also

$$U_{L(R)} = \begin{pmatrix} u_{L(R)} \\ c_{L(R)} \end{pmatrix}. \tag{1.69}$$

On the other hand the mass terms of Eq. (1.61) are rearranged into

$$\mathcal{L}_q^{\rm mass} = \bar{U}_R M^U U_L + \bar{D}_L M^D D_R + \text{h.c.}. \tag{1.70}$$

First we diagonalize M^U introducing $U_L = \mathcal{Z}U'_L$ and $U_R = \mathcal{W}U'_R$. Now D_L transforms accordingly to U_L, since they form a weak isospin doublet. Furthermore M^D is diagonalized by $\mathcal{U}$ and $\mathcal{V}$, so that we are left with

$$\mathcal{L}_q^{\text{mass}} = \bar{U}'_R \begin{pmatrix} m_u & 0 \\ 0 & m_c \end{pmatrix} U'_L + \bar{D}'_L \mathcal{Z}^\dagger \mathcal{U} \begin{pmatrix} m_d & 0 \\ 0 & m_s \end{pmatrix} D'_R + \text{h.c.}, \tag{1.71}$$

where $D'_R = \mathcal{V}D_R$.

The interaction Lagrangian in Eq. (1.68) is left unchanged if we switch to the fields U'_R, D'_R, U'_L, D'_L. However we need one more transformation on the D'_L fields to reach the mass eigenstates basis. Indeed, if we define

$$\mathcal{U}_{\text{GIM}} = \mathcal{U}^\dagger \mathcal{Z} \tag{1.72}$$

which is itself a unitary matrix [8], and we introduce

$$D''_L = \mathcal{U}_{\text{GIM}} D'_L, \tag{1.73}$$

then we diagonalize the down type mass terms and we induce a change *only* in the charged current terms

$$\frac{g}{\sqrt{2}} \left(\bar{U}'_L \gamma^\mu \mathcal{U}_{\text{GIM}} D''_L \, W^\dagger_\mu + \bar{D}''_L \gamma^\mu \mathcal{U}^\dagger_{\text{GIM}} U'_L \, W_\mu \right), \tag{1.74}$$

while the neutral currents are left diagonal in flavor space.

The process $K^0_L \to \mu^+\mu^-$ proceeds, thus, through the exchange of two charged vector bosons, as showed in Fig. 1.15. Taking the W propagator to be

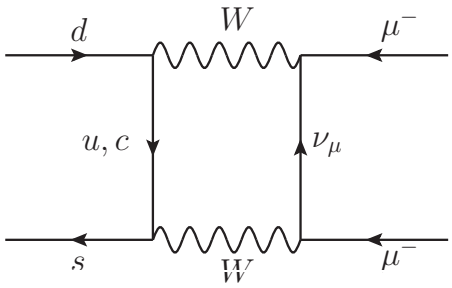

Figure 1.15. In a four quarks model with the addition of the charm quark the process $K^0_L \to \mu^+\mu^-$ proceeds through a loop diagram in which two charged vector bosons are exchanged.

$$\Delta_W(k) = \frac{-g_{\mu\nu} + \frac{k_\mu k_\nu}{M_W^2}}{k^2 - M_W^2}, \tag{1.75}$$

[8] We can thus redefine

$$\mathcal{U}_{\text{GIM}} = \begin{pmatrix} \cos\theta_c & \sin\theta_c \\ -\sin\theta_c & \cos\theta_c \end{pmatrix}.$$

the amplitude associated to the loop diagram in Fig. 1.15 is

$$\mathcal{A}_u \propto g^4 \cos\theta_c \sin\theta_c \left[\bar{\mu}_L \gamma^\mu \gamma^\alpha \gamma^\nu \mu_L\right] \left[\bar{s}_L \gamma^\rho \gamma^\beta \gamma^\sigma d_L\right] \int \frac{d^4k}{(2\pi)^4} \frac{k_\alpha}{k^2} \frac{k_\beta}{k^2 - m_u^2} \frac{-g_{\mu\sigma} + \frac{k_\mu k_\sigma}{M_W^2}}{k^2 - M_W^2} \frac{-g_{\nu\rho} + \frac{k_\nu k_\rho}{M_W^2}}{k^2 - M_W^2}. \tag{1.76}$$

By simple power counting one realizes that the divergence comes from the following term

$$\frac{1}{M_W^4} \int \frac{d^4k}{(2\pi)^4} \frac{k_\alpha}{k^2} \frac{k_\beta}{k^2 - m_u^2} \frac{k_\mu k_\sigma}{k^2 - M_W^2} \frac{k_\nu k_\rho}{k^2 - M_W^2} = \frac{T_{\alpha\beta\mu\sigma\nu\rho}}{M_W^4} \int \frac{d^4k}{(2\pi)^4} \frac{(k^2)^2}{(k^2 - m_u^2)(k^2 - M_W^2)^2} \tag{1.77}$$

Performing the integral with a cutoff on the Euclidean norm of k one obtains

$$\mathcal{A}_u \propto \left[\bar{\mu}_L \gamma^\mu \mu_L\right] \left[\bar{s}_L \gamma_\mu d_L\right] \; G_F^2 \cos\theta_c \sin\theta_c \int_0^1 dx \left[\frac{\Lambda^2}{2} + \frac{3}{2}\Delta \ln(\frac{\Delta}{\Lambda^2}) + \frac{5}{4}\Delta\right], \tag{1.78}$$

with $\Delta = M_W^2\, x + m_u^2(1-x)$. The same is valid for the c quark, substituting m_u with m_c and θ_c with $-\theta_c$. Each quark carries a term $\propto \Lambda^2$, but when we sum up $\mathcal{A}_u$ and $\mathcal{A}_c$ the quadratic divergent term cancels and we are left with

$$\mathcal{A}_u + \mathcal{A}_c \propto \left[\bar{\mu}_L \gamma^\mu \mu_L\right] \left[\bar{s}_L \gamma_\mu d_L\right] \; G_F^2 \cos\theta_c \sin\theta_c \left(m_c^2 - m_u^2\right) \left(1 + 3\ln(\frac{M_W^2}{\Lambda^2})\right) \tag{1.79}$$

The two diagrams cancel exactly in the limit of degenerate quark masses, $m_c = m_u$, whereas if $m_c \neq m_u$ then with a reasonably large cutoff ($\Lambda \sim \mathcal{O}(m_W)$) one succeeds in obtaining the experimental result choosing the mass of the *charm* quark to be

$$2 \text{ GeV} \leq m_c \leq 3 \text{ GeV}. \tag{1.80}$$

1.2.2 The discovery of charmonium and bottomonium

The 1976 Nobel Prize in physics was shared by a Massachusetts Institute of Technology researcher who used Brookhaven's Alternating Gradient Synchrotron (AGS) to discover a new particle and confirm the existence of a fourth quark flavor. Samuel Ting was credited for finding what he called the J particle [23], the same particle as the ψ found at nearly the same time at the Stanford Linear Accelerator Center by a group led by Burton Richter [24].

At the AGS a high intensity proton beam was fired on a Berillium target

$$p + Be \to e^+e^- + X, \tag{1.81}$$

at $\sqrt{s} \sim 7$ GeV. A narrow peak showed up in the e^+e^- invariant mass spectrum at 3.1 GeV. At almost the same time a resonance was observed in e^+e^- collisions at $\sqrt{s} = 3.105$ GeV in the following reactions

$$\begin{aligned} e^+e^- &\to e^+e^- \\ e^+e^- &\to \mu^+\mu^- \\ e^+e^- &\to \text{hadrons}. \end{aligned} \tag{1.82}$$

The width of this newly discovered particle, called J/ψ, was so small not to be readable directly off the resonance curve, $\Gamma_\psi \leq 3$ MeV. Nowadays we know that $\Gamma_\psi = 93.2 \pm 2.1$ KeV, of which the 87.7% is into hadrons, the 5.94% into e^+e^- and the 5.93% into $\mu^+\mu^-$.

The J^{PC} quantum numbers can be deduced studying the effect of the interference between the purely QED process $e^+e^- \to \gamma^\star \to \mu^+\mu^-$ and the production of $\mu^+\mu^-$ through J/ψ. A relevant aspect is the angular distribution of the particles in the final states. The QED one is well known and gives the typical $(1 + \cos^2\theta)$ behavior. If the J/ψ shared the same J^{PC} quantum numbers of the photon, then the angular distribution of the muon pair near the resonance should not be changed from the interference of the QED amplitude. In fact, experimentally, it was found to be $(1 + \cos^2\theta)$ near the resonance, clearly establishing the spin-parity of J/ψ to be 1^{--}.

To determine the isospin, one observes that the decay $J/\psi \to p\bar{p}$ occurs with a branching ratio of $\sim 0.2\%$, which cannot be explained by electromagnetic effects. Since $p\bar{p}$ can only have isospin $I = 0$ or $I = 1$, then also the J/ψ can be either $I = 0$ or $I = 1$. Now if it has $I = 1$, the decay $J/\psi \to \rho^0\pi^0$ should be strictly forbidden [9], while it is observed in the 0.6% of the times. If instead J/ψ has $I = 0$ then [10]

$$R = \frac{\Gamma(J/\psi \to \rho^0\pi^0)}{\Gamma(J/\psi \to \rho^+\pi^-) + \Gamma(J/\psi \to \rho^-\pi^+)} = \frac{1}{2}, \tag{1.83}$$

to be compared with the experimental measurement $R = 0.495575$. Thus one can conclude that J/ψ is an isoscalar state.

Although J/ψ itself does not carry any new quantum number, its unusually narrow width in spite of large available phase space, suggests that it is a bound state of $c\bar{c}$, where c is a quark with a flavor which is outside the three flavors u, d and s of $SU(3)$. The identification of this fourth quark with the *charm* came finally with the discovery of the D-mesons in 1976 [25, 26] and from the measurements of their weak decays. The quark c is assigned a new quantum number $C = 1$,whereas $C = 0$ for u, d and s quarks. The narrow width of the J/ψ compared to 100 MeV for ρ, can be qualitatively understood by the OZI rule, just as the suppression of $\phi \to 3\pi$ compared to $\phi \to KK$ is explained by this rule. While the decay into $D\bar{D}$ depicted in the left panel of Fig. 1.16, is OZI allowed, the one showed in the right panel is OZI suppressed. Nevertheless the decay $J/\psi \to D\bar{D}$ shown in Fig. 1 is forbidden by phase space, since $m_\psi < 2m_D$.

Beside being explained by the suppression due to the OZI rule, the narrowness of the J/ψ is a manifestation of asymptotic freedom.

The leptonic decay modes of the J/ψ can be explained as follows: the c and $\bar{c}$ come to a point and are converted into a virtual photon which in turn decays into a leptons pair: $c\bar{c} \to \gamma^\star \to l^+l^-$. The leptonic decay width thus reads

$$\Gamma(J/\psi \to l^+l^-) = 16\pi\alpha^2 \left(\frac{2}{3}\right)^2 \frac{|\Psi_S(0)|^2}{m_\psi^2}, \tag{1.84}$$

where $\Psi_S(0)$ is the non relativistic wave function of a $c\bar{c}$ pair in S-wave, and its square modulus represents the probability that the quark and the antiquark inside

[9] $|\rho^0\pi^0\rangle = |1,0\rangle|1,0\rangle = \sqrt{2/3}\,|2,0\rangle - \sqrt{1/3}\,|0,0\rangle$ in the $|I, I_z\rangle$ basis.

[10] $|\rho^+\pi^-\rangle = |1,1\rangle|1,-1\rangle = \sqrt{1/6}\,|2,0\rangle + \sqrt{1/2}\,|1,0\rangle + \sqrt{1/3}\,|0,0\rangle$ and $|\rho^-\pi^+\rangle = |1,-1\rangle|1,1\rangle = \sqrt{1/6}\,|2,0\rangle - \sqrt{1/2}\,|1,0\rangle + \sqrt{1/3}\,|0,0\rangle$ in the $|I, I_z\rangle$ basis.

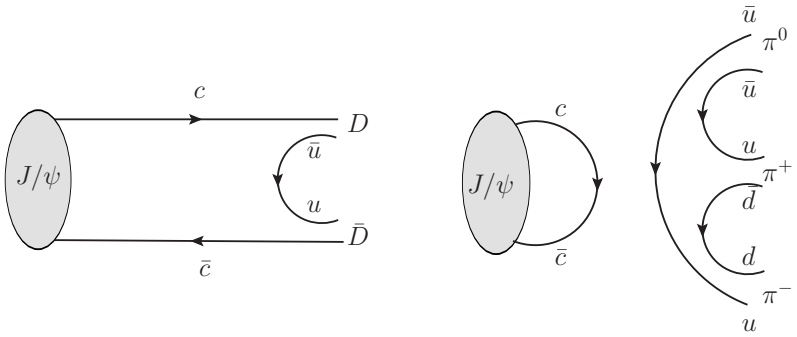

Figure 1.16. OZI allowed (left) and OZI forbidden (right) J/ψ decays.

the J/ψ meson come to a point. The leptonic width is thus proportional to the second power of the electromagnetic α: $\alpha^2(m_\psi) \sim 5.3 \times 10^{-5}$.

As for the hadronic final states, since J/ψ is a 1^{--} state, by C conservation it can decay in the lowest order into three gluons:

$$\Gamma(J/\psi \to \text{hadrons}) = \frac{160\pi(\pi^2 - 9)}{81\pi} \frac{\alpha_s^3(m_\psi)}{m_\psi^2} |\Psi_\psi(0)|^2. \tag{1.85}$$

On the other hand a 0^{-+} charmonium state, as the η_c, decays into hadrons through the emission of two gluons: Namely

$$\Gamma(\eta_c \to \text{hadrons}) = \frac{32\pi}{3} \frac{\alpha_s^2(m_{\eta_c})}{m_{\eta_c}^2} |\Psi_\psi(0)|^2 \tag{1.86}$$

With these observations we are able to: (i) compute the value of $\alpha_s(m_\psi) = 0.22$; (ii) explain why J/ψ is so narrow, and in particular narrower than η_c ($\Gamma_{\eta_c} \sim 20$ MeV); (iii) confirm the property of asymptotic freedom, since $\alpha_s(m_\phi) = 0.44$, $\alpha_s(m_\psi) = 0.22$ and $\alpha_s(m_\Upsilon) = 0.18$[11].

In 1977 it was indeed discovered the Υ meson [31], a $b\bar{b}$ bound state, with mass $m_\Upsilon = 9.5$ GeV and width $\Gamma_\Upsilon = 54$ KeV. It was observed by the E288 collaboration at Fermilab, in the $\mu^+\mu^-$ invariant mass spectrum produced in proton-nucleon collisions at $\sqrt{s} = 400$ GeV

$$p + (Cu, Pt) \to \mu^+\mu^- + \text{anything}. \tag{1.87}$$

A fifth flavor, the *bottom*, with mass $m_b \sim 4.7$ GeV was included in the picture and the sixth one, the *top*, was predicted in order to form the third weak doublet together with the b quark. The *top* was observed only 18 years after, in 1995, by the collaborations CDF and D$\emptyset$ at Fermilab [32, 33].

1.2.3 Spectrum

Motivation for a non relativistic approach. Heavy quarkonium states like $c\bar{c}$ and $b\bar{b}$ represent relative simple systems. Indeed to a good approximation the

[11] The expression of the leptonic and hadronic widths in Eq. (1.84) and Eq. (1.85) can be applied to the low lying $q\bar{q}$ mesons with $J^{PC} = 1^{--}$, such as ϕ and $\Upsilon(1S)$.

motion of the quarks inside the meson can be considered as non relativistic and thus described by the Schrödinger equation

$$\left[-\frac{\hbar^2}{2\mu}\boldsymbol{\nabla}^2 + V(\boldsymbol{r})\right]\Psi(\boldsymbol{r}) = E\Psi(\boldsymbol{r}), \tag{1.88}$$

where $\mu \sim m_{_Q}/2$ is the reduced mass of the system. Strong interactions at short distances generate a Coulomb like potential, and thus one can assume a central potential $V(\boldsymbol{r}) = V(r)$ and decompose the wave function in a radial and an orbital part

$$\Psi(\boldsymbol{r}) = Y_{l,m}(\theta,\phi)\, R(r). \tag{1.89}$$

The radial part $R(r)$ satisfies the equation

$$\frac{d^2R}{dr^2} + \frac{2}{r}\frac{dR}{dr} - \frac{L(L+1)}{r^2}R + \frac{2\mu}{\hbar^2}\left(E + \frac{\alpha_s}{r}\right)R = 0, \tag{1.90}$$

taking $V(r) \sim -\alpha_s/r$. Dimensional analysis states that

$$\left[\frac{2\mu\alpha_s}{\hbar^2 r}\right] = \left[\frac{1}{r^2}\right] \;\Rightarrow\; L \sim \frac{\hbar^2}{m_{_Q}\alpha_s}. \tag{1.91}$$

From the time-dependent Schrödinger equation we learn

$$i\hbar\frac{\partial\Psi}{\partial t} = H\Psi \;\Rightarrow\; \frac{\hbar}{T} \sim \frac{\alpha_s}{L} \;\Rightarrow\; T \sim \frac{\hbar^3}{m_{_Q}\alpha_s^2}. \tag{1.92}$$

Thus the average velocity of the heavy quark with respect to the antiquark is

$$v = \frac{L}{T} \sim \frac{\alpha_s}{\hbar} = \alpha_s \tag{1.93}$$

and in turn its kinetic energy is estimated by

$$E \sim m_{_Q}v^2 \sim \frac{m_{_Q}\alpha_s^2}{\hbar^2} = m_{_Q}\alpha_s^2. \tag{1.94}$$

In a hydrogen atom the energy levels are

$$E_n = -\frac{m_{_Q}\alpha_s^2}{n^2} \;\Rightarrow\; |E_{n+1} - E_n| \sim m_{_Q}\alpha_s^2 \tag{1.95}$$

thus

$$\frac{\Delta E}{m_{_Q}} \sim \alpha_s^2 \sim v^2 \tag{1.96}$$

From these relations one can obtain an estimate of v for charmonium and bottomonium. Using $m_c \sim 1.5$ GeV and $m_b \sim 4.7$ GeV we obtain

$$\begin{aligned}\frac{\Delta E_c}{m_c} &= \frac{m_{\psi'} - m_\psi}{m_c} \simeq 0.4 \sim v_c,\\ \frac{\Delta E_b}{m_b} &= \frac{m_{\Upsilon'} - m_\Upsilon}{m_b} \simeq 0.1 \sim v_b.\end{aligned} \tag{1.97}$$

Even if not truly justified the non relativistic approach appears to be more appropriate in the bottom sector than in the charm one.

Potential models. In the non relativistic limit heavy quarkonia resemble *positronium* states, e^+e^- bound states, or an atomic system. The interaction between quark ad antiquark is described by means of a non relativistic static potential which governs the Schödinger equation. The form of the potential can be inspired by the perturbative expansion of the interaction induced by one gluon exchange (OGE) between Q and $\bar{Q}$

$$V_{\rm OGE}(r) = -\frac{4}{3}\frac{\alpha_s}{r}. \tag{1.98}$$

However one can trust perturbation theory as long as the average distance between the quarks is much smaller than the typical distance at which QCD becomes strongly coupled, $\sim 1/\Lambda_{\rm QCD} \sim 1$ fm. From Eq. (1.91) we can estimate the typical size of a charmonium state as $r_{c\bar{c}} \sim 1/m_c \sim$ 0.1fm. It is thus necessary to resort to models for the interactions between quarks at medium and long distances. The idea of quark confinement has driven some of these models. The most successful choice is that of a linearly growing potential $V(r) = \sigma\, r$, where σ is the string tension of the chromo electric flux tube connecting the quark and the antiquark. One of the most developed models uses the *Cornell potential*, which is build up as a simple sum of the OGE potential and of a linearly confining term

$$V_{\rm Cornell}(r) = -\frac{\alpha}{r} + \sigma\, r, \tag{1.99}$$

where α and σ are phenomenological parameters to be fitted to data. Plugging this potential into the Schrödinger equation and including the relativistic corrections up to the v^2/c^2 order, which we will discuss hereafter, this model is able to reproduce the spectrum of the charmonium and bottomonium states which lie below the $D\bar{D}$ and $B\bar{B}$ thresholds respectively. The best fit values for α and σ in the c and b sector are [34]

$$\text{charm}: \qquad \alpha = 0.520, \qquad \sigma = 0.183 \text{ GeV}^2 \tag{1.100}$$

$$\text{bottom}: \qquad \alpha = 0.483, \qquad \sigma = 0.183 \text{ GeV}^2. \tag{1.101}$$

Relativistic corrections. One can further compute relativistic corrections to the interaction potential, through an expansion in powers of $1/c$ of the relativistic scattering amplitude. In the case of two electrons, where the interaction is mediated by the exchange of a photon (Fig. 1.17a), the scattering amplitude is a product of vector currents mediated by the photon propagator $D_{\mu\nu}(q)$

$$\mathcal{M} \sim e^2 \ \left[\bar{u}(p_1')\gamma^\mu u(p_1)\right] \ D_{\mu\nu}(q) \ \left[\bar{u}(p_2')\gamma^\nu u(p_2)\right]. \tag{1.102}$$

In the non relativistic limit the solution of the Dirac equation can be written as

$$\psi = \begin{pmatrix} \phi \\ \chi \end{pmatrix}, \tag{1.103}$$

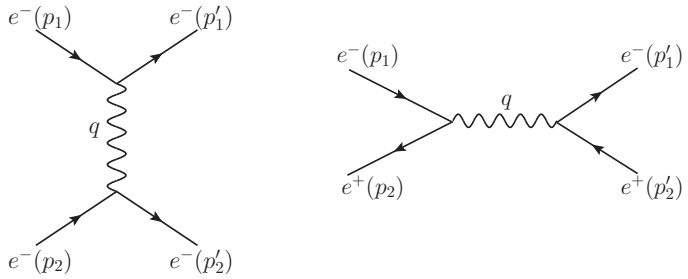

(a) t-channel **(b)** s-channel

Figure 1.17. e^-e^- and e^+e^- scattering diagrams.

with $\chi << \phi$. Since the relativistic energy includes also its rest energy mc^2 [12], this must be excluded in the non relativistic approximation and therefore we need to substitute $\psi \to \psi\, e^{-imc^2t/\hbar}$. Plugging ψ in the Dirac equation one finds that

$$\chi = \frac{\boldsymbol{\sigma}\cdot\boldsymbol{p}}{2mc}\phi \tag{1.104}$$

and in turn that in presence of an external electromagnetic field $A^\mu = (V_0, \boldsymbol{A})$ ϕ satisfies a Schrödinger equation with the following hamiltonian

$$i\hbar\frac{\partial\phi}{\partial t} = \hat{H}\phi = \left[\frac{1}{2m}\left(\boldsymbol{p} - \frac{e}{c}\boldsymbol{A}\right)^2 + eV_0 - \frac{e\hbar}{2mc}\boldsymbol{\sigma}\cdot\boldsymbol{H}\right]\phi, \tag{1.105}$$

at the firs order in $1/c$. It differs from the non relativistic version by the last term in the hamiltonian, which has the form of the potential energy of a magnetic dipole in the external field. If one wants to go beyond the first order in $1/c$, say up to $1/c^2$, one needs to replace ϕ by

$$\phi \to \left(1 - \frac{\boldsymbol{p}^2}{8m^2c^2}\right)\phi, \tag{1.106}$$

in order to find the wave equation corresponding to the Schrödinger equation. As a consequence

$$\chi \to \frac{\boldsymbol{\sigma}\cdot\boldsymbol{p}}{2mc}\left(1 - \frac{\boldsymbol{p}^2}{8m^2c^2}\right)\phi \xrightarrow{\mathcal{O}(1/c^2)} \frac{\boldsymbol{\sigma}\cdot\boldsymbol{p}}{2mc}\phi. \tag{1.107}$$

Now the general solution to the Dirac equation is $\psi \sim u(p)e^{-ipx}$ with

$$u(p) = \begin{pmatrix} \sqrt{\mathcal{E}+m}\; w \\ \sqrt{\mathcal{E}-m}\;\boldsymbol{\sigma}\cdot\hat{\boldsymbol{p}}\; w \end{pmatrix}. \tag{1.108}$$

If we want to find the non relativistic expansion up to $\mathcal{O}(1/c^2)$ of Eq. (1.102) we need to replace $u(p)$ with

$$u(p) \to \sqrt{2m}\begin{pmatrix} \left(1 - \frac{\boldsymbol{p}^2}{8m^2c^2}\right) w \\ \boldsymbol{\sigma}\cdot\hat{\boldsymbol{p}}\; w \end{pmatrix}. \tag{1.109}$$

[12] We indicate with m the electron mass.

At the lowest order, Eq. (1.102) reduces to

$$\mathcal{M}_{fi} = -4m^2\ w_1'^{\star} w_2'^{\star}\ U(\boldsymbol{q})\ w_1 w_2, \tag{1.110}$$

with $U(\boldsymbol{q})$ the Fourier transform of the Coulomb potential

$$U(\boldsymbol{q}) = \frac{4\pi e^2}{\boldsymbol{q}^2}. \tag{1.111}$$

Going to $\mathcal{O}(1/c^2)$ the transition amplitudes reads

$$\mathcal{M}_{fi} = -4m^2\ w_1'^{*} w_2'^{*}\ U(\boldsymbol{p}_1, \boldsymbol{p}_2, \boldsymbol{q})\ w_1 w_2, \tag{1.112}$$

with $U(\boldsymbol{p}_1, \boldsymbol{p}_2, \boldsymbol{q})$ the Fourier transform of

$$\begin{aligned}\hat{U}(\boldsymbol{p}_1, \boldsymbol{p}_2, \boldsymbol{r}) = &+ \frac{e^2}{r} - \pi\left(\frac{e\hbar}{mc}\right)^2 \delta(\boldsymbol{r}) - \frac{e^2}{2m^2c^2 r}\left(\boldsymbol{p}_1\cdot\boldsymbol{p}_2 + \frac{\boldsymbol{r}\cdot(\boldsymbol{r}\cdot\boldsymbol{p}_1)\boldsymbol{p}_2}{r^2}\right)\\ &+ \frac{e^2\hbar^2}{4m^2c^2r^3}\left[-(\boldsymbol{\sigma}_1\cdot 2\boldsymbol{\sigma}_2)\cdot\boldsymbol{r}\times\boldsymbol{p}_1 + -(\boldsymbol{\sigma}_2\cdot 2\boldsymbol{\sigma}_1)\cdot\boldsymbol{r}\times\boldsymbol{p}_2\right]\\ &+ \frac{1}{4}\left(\frac{e\hbar}{mc}\right)^2\left[-\frac{3(\boldsymbol{\sigma}_1\cdot\boldsymbol{r})(\boldsymbol{\sigma}_2\cdot\boldsymbol{r})}{r^5} - \frac{8\pi}{3}\boldsymbol{\sigma}_1\cdot\boldsymbol{\sigma}_2\delta(\boldsymbol{r})\right],\end{aligned} \tag{1.113}$$

where $\boldsymbol{r} = \boldsymbol{r}_1 - \boldsymbol{r}_2$. The first three terms are of purely orbital origin. The next terms, linear in the spin operators of the two electrons, are due to spin-orbit interaction. The last group of terms, quadratic in the spin operators, describes spin-spin interaction.

When considering, instead of two electrons, an electron and a positron, an additional term appears in the amplitude, associated to the annihilation diagram in Fig. 1.17b. The corresponding term in the potential is

$$\hat{U}_{\text{ann}}(\boldsymbol{r}) = \pi\frac{e^2\hbar^2}{2m^2c^2}(3 + \boldsymbol{\sigma}_1\cdot\boldsymbol{\sigma}_2)\delta(\boldsymbol{r}). \tag{1.114}$$

Taking into account that in a positronium state with spin $\boldsymbol{S}$, $\boldsymbol{p}_1 = -\boldsymbol{p}_2 = \boldsymbol{p}$ and that $(\boldsymbol{\sigma}_1 + \boldsymbol{\sigma}_2)/2 = \boldsymbol{S}$, one finally obtains the non relativistic interaction potential between electron and positron up to the second order in the $1/c$ expansion

$$\begin{aligned}\hat{U}(\boldsymbol{p}, \boldsymbol{r}) = \quad &-\frac{\boldsymbol{p}^4}{4m^3c^2} + 4\pi\mu_0^2\delta(\boldsymbol{r}) - \frac{e^2}{2m^2c^2 r}\left[\boldsymbol{p}^2 + \frac{\boldsymbol{r}\cdot(\boldsymbol{r}\cdot\boldsymbol{p})\boldsymbol{p}}{r^2}\right]\\ &+6\mu_0^2\frac{1}{r^3}\boldsymbol{l}\cdot\boldsymbol{S} - 2\mu_0^2\frac{1}{r^3}\left[\boldsymbol{S}^2 - \frac{3(\boldsymbol{S}\cdot\boldsymbol{r})(\boldsymbol{S}\cdot\boldsymbol{r})}{r^2}\right] + 4\pi\mu_0^2\left(\frac{7}{3}\boldsymbol{S}^2 - 2\right)\delta(\boldsymbol{r}),\end{aligned} \tag{1.115}$$

where $\mu_0 = e\hbar/2mc$ is the Bohr magneton and $\boldsymbol{L} = \hbar\boldsymbol{l} = \boldsymbol{r}\times\boldsymbol{p}$.

The same approach holds for a quarkonium state, $c\bar{c}$ or $b\bar{b}$, as long as one considers only short distance interactions, since one gluon exchange generates, apart from color factors, a Coulomb potential. As for the confining part of the potential in Eq. (1.99), it is necessary to make some hypotheses on the form of the relativistic interaction term which produces this linearly growing behavior: a scalar interaction has been discussed in [35, 36], while a vector one in [37, 38]. Finally the possibility that both a scalar and a vector interaction are at the origin of the confining term

has been considered in [39]. In this last case, the spin-orbit and spin-spin relativistic corrections can be generalized to the following form

$$\hat{V}(\boldsymbol{r}) = V_{LS}(r)(\boldsymbol{L}\cdot\boldsymbol{S}) + V_T(\boldsymbol{r})\left[\boldsymbol{S}^2 - \frac{3(\boldsymbol{S}\cdot\boldsymbol{r})(\boldsymbol{S}\cdot\boldsymbol{r})}{r^2}\right] + V_{SS}(r)\left[\boldsymbol{S}^2 - \frac{3}{2}\right], \quad (1.116)$$

with

$$V_{LS}(r) = \frac{1}{2m_c^2 r}\left(3\frac{dV_V}{dr} - \frac{dV_S}{dr}\right), \quad (1.117)$$

$$V_T(r) = \frac{1}{6m_c^2}\left(\frac{d^2V_V}{dr^2} - \frac{1}{r}\frac{dV_V}{dr}\right) \quad (1.118)$$

and

$$V_{SS}(r) = \frac{1}{3m_c^2}|\boldsymbol{\nabla}|^2 V_V. \quad (1.119)$$

One can verify that Eq. (1.116) reduces to Eq. (1.115) if V_S is set to zero.

In Chapter 3 we will consider a specific form of the vector potential and compute the relativistic corrections associated using some phenomenological parameters. The effect of the relativistic corrections has been tested experimentally. Let us consider the spin-orbit interaction. A quarkonium bound state is characterized by a definite value of the radial quantum number n_r, the total spin $S = 0, 1$, the orbital angular momentum $L = 0, 1, 2, \ldots$ and the total angular momentum $J = L \oplus S$. It is conventionally indicated by $n_r^{2S+1}L_J$, using capital letters $S, P, D, F, \ldots$ for $L = 0, 1, 2, 3, \ldots$. These quantum numbers also define the J^{PC} of the state, since

$$P = (-1)^{L+1}, \qquad C = (-1)^{L+S}. \quad (1.120)$$

The first orbital excitation of $c\bar{c}$ includes a spin 0 singlet h_c, and a spin 1 triplet $(\chi_{c0},\ \chi_{c1},\ \chi_{c2})$. The masses are determined by the expectation value of the hamiltonian on the definite quantum state: $m_{h_c} = \langle h_c|H|h_c\rangle$ and $m_{\chi_{cJ}} = \langle \chi_{cJ}|fH|\chi_{cJ}\rangle$. The hamiltonian H contains a non relativistic part $H^{\rm nr}$, which has the same expectation value on h_c and χ_{cJ} since it depends only on the radial part of the wave function, and a relativistic one $H^{\rm r}$, which contains the spin-orbit, spin-spin and tensor interactions. One can thus compute the expectation value of $H^{\rm r}$ on h_c and χ_{cJ} and determine their mass splitting in terms of V_{LS}, V_{SS} and V_T. While $\langle h_c|H^{\rm r}|h_c\rangle = 0$, one finds (see Appendix A)

$$\begin{aligned}
\langle \chi_{c0}|V_{LS}(r)\,\boldsymbol{L}\cdot\boldsymbol{S}|\chi_{c0}\rangle &= -2\times\langle V_{LS}\rangle \\
\langle \chi_{c1}|V_{LS}(r)\,\boldsymbol{L}\cdot\boldsymbol{S}|\chi_{c1}\rangle &= -1\times\langle V_{LS}\rangle \\
\langle \chi_{c2}|V_{LS}(r)\,\boldsymbol{L}\cdot\boldsymbol{S}|\chi_{c2}\rangle &= +1\times\langle V_{LS}\rangle
\end{aligned} \quad (1.121)$$

and

$$\begin{aligned}
\langle \chi_{c0}|V_T(r)\left(|\boldsymbol{S}|^2 - \frac{3(\boldsymbol{S}\cdot\boldsymbol{r})(\boldsymbol{S}\cdot\boldsymbol{r})}{r^2}\right)|\chi_{c0}\rangle &= +2\times\langle V_T\rangle \\
\langle \chi_{c1}|V_T(r)\left(|\boldsymbol{S}|^2 - \frac{3(\boldsymbol{S}\cdot\boldsymbol{r})(\boldsymbol{S}\cdot\boldsymbol{r})}{r^2}\right)|\chi_{c1}\rangle &= -1\times\langle V_T\rangle \\
\langle \chi_{c2}|V_T(r)\left(|\boldsymbol{S}|^2 - \frac{3(\boldsymbol{S}\cdot\boldsymbol{r})(\boldsymbol{S}\cdot\boldsymbol{r})}{r^2}\right)|\chi_{c2}\rangle &= +\frac{1}{5}\times\langle V_T\rangle
\end{aligned} \quad (1.122)$$

so that

$$\begin{cases} m_{\chi_{c0}} - m_{h_c} = -2\langle V_{LS}\rangle + 2\langle V_T\rangle \\ m_{\chi_{c1}} - m_{h_c} = -\langle V_{LS}\rangle - \langle V_T\rangle \\ m_{\chi_{c2}} - m_{h_c} = \langle V_{LS}\rangle + \frac{1}{5}\langle V_T\rangle \end{cases} \tag{1.123}$$

where by $\langle V_{LS}\rangle$ and $\langle V_T\rangle$ we mean the average on the $n_r = 0$ radial wave function. From Eq. (1.123) we can obtain a relation between the average mass of the χ_{cJ} triplet and the h_c mass

$$\frac{1}{9}\left(m_{\chi_{c0}} + 3\, m_{\chi_{c1}} + 5\, m_{\chi_{c2}}\right) = m_{h_c}, \tag{1.124}$$

which is confirmed by experiments, as we will detail in Section 3.3.1.

Also, an estimate of $\langle V_{LS}\rangle$ and $\langle V_T\rangle$ can be computed [40]

$$\begin{cases} \langle V_{LS}\rangle = \frac{1}{12}\left(5m_{\chi_{c2}} - 3m_{\chi_{c1}} - 2m_{\chi_{c0}}\right) \simeq 35 \text{ MeV} \\ \langle V_T\rangle = \frac{5}{36}\left(m_{\chi_{c2}} - 3m_{\chi_{c1}} + 2m_{\chi_{c0}}\right) \simeq -20 \text{ MeV} \end{cases} \tag{1.125}$$

States above thresholds. The non relativistic approach fails when going above the open-charm or open-bottom thresholds, since it does not envisage the possibility to create pair of light quarks from the vacuum. While nearly all of the $b\bar{b}$ mesons observed until now lie below the $B\bar{B}$ threshold, almost all the second radial excitations of charmonium appear above the $D\bar{D}$ threshold. To obtain reasonable predictions for their masses the coupling to pairs of open-charm or open-bottom mesons with the appropriate quantum numbers must be included. Many authors computed the effect of virtual or real D meson loops in shifting the masses of ordinary $c\bar{c}$ states, for a recent review see [41].

1.2.4 Decay rates

Heavy quarkonia decay mainly through: (*i*) annihilation processes, when the quark and the antiquark come to a point and are converted in photons or gluons leading to a final state containing leptons or light hadrons; (*ii*) radiative transitions, transitions between $Q\bar{Q}$ states with the emission of a photon; (*iii*) hadronic transitions, transitions between $Q\bar{Q}$ states with the emission of gluons materializing into light hadrons.

Annihilation processes. We distinguish between *electromagnetic* and *strong* annihilation.

Electromagnetic annihilation is due the conversion of a quarkonium state into one, two or three photon. For n^3S_1 vector states, the lowest order process is the annihilation into one virtual photon, which then can convert into a lepton pair or into hadrons. The total contribution of one photon annihilation amounts to $\mathcal{B}(J/\psi \to \gamma^\star \to X) \sim 25\%$ and $\mathcal{B}(\psi' \to \gamma^\star \to X) \sim 3.4\%$. Since, as showed by Eq. (1.84), the leptonic decay width is proportional to the wave function at the origin, the ratio $\mathcal{B}(J/\psi \to \gamma^\star \to X)/\mathcal{B}(\psi' \to \gamma^\star \to X)$ can be used as an estimate of the ratio $|\Psi_S(0)|^2/|\Psi_{2S}(0)|^2$. Besides the n^3S_1 vectors, also the n^3D_1 states have $J^{PC} = 1^{--}$ and thus could in principle annihilate into one photon. Nevertheless, in

the leading non relativistic approximation, the decay rate of a D-wave quarkonium vanishes, since its wave function at the origin vanishes: $\Psi_{nD}(0) = 0$. A non vanishing contribution appears when going at higher orders in the $1/c$ expansion. Two effects do contribute: the $n^3S_1 - n^3D_1$ mixing and a direct annihilation term proportional to the value at the origin of the second derivative of the wave function $\Psi''_{nD}(0)$. An example is the $\psi' - \psi(3770)$ system. These two states are considered as the result of the mixing between 2^3S_1 and 1^3D_1, the ψ' being mainly 2^3S_1 whereas the $\psi(3770)$ mainly 1^3D_1. From the leptonic width of $\psi(3770)$ is thus possible to obtain an estimate of the mixing angle $\theta \sim 0.2$ [42, 43].

States with even charge conjugation and $J \neq 1$ can annihilate into two photons. The S-wave decay rate is proportional to the wave function at the origin, whereas the P-wave one to the first derivative of the wave function computed at the origin

$$\begin{aligned}
\Gamma(^1S_0 \to 2\gamma) &= \frac{16 \times 3\,\pi\alpha^2}{m^2_{c\bar{c}}}(\frac{2}{3})^4|\Psi_S(0)|^2, \\
\Gamma(^3P_0 \to 2\gamma) &= \frac{2^6 \times 3^3\,\pi\alpha^2}{m^4_{c\bar{c}}}(\frac{2}{3})^4|\Psi'_P(0)|^2, \\
\Gamma(^3P_2 \to 2\gamma) &= \frac{2^8 \times 3^2\,\pi\alpha^2}{5m^4_{c\bar{c}}}(\frac{2}{3})^4|\Psi'_P(0)|^2.
\end{aligned} \tag{1.126}$$

It has to be noticed that since the P-wave decay into two photons is a relativistic effect of the second order in $1/c$, one expects that $\Gamma(\eta_c \to 2\gamma) > \Gamma(\chi_{cJ} \to 2\gamma)$, even if a precise knowledge of the wave functions at the origin is lacking. Experimentally one finds $\Gamma(\chi_{c0} \to 2\gamma) = (2.9 \pm 0.4)$ KeV, $\Gamma(\chi_{c2} \to 2\gamma) = (0.534 \pm 0.050)$ KeV and $\Gamma(\eta_c \to 2\gamma) = (6.3 \pm 0.2)$ KeV, which somewhat confirms the expected suppression.

An interesting annihilation process into two photons is the $1^1D_2 \to 2\gamma$ decay. The charmonium state 1^1D_2, a 2^{-+} resonance, has not yet been observed, even if the possibility that the exotic resonance $X(3872)$ could be a standard 1^1D_2 $c\bar{c}$ meson has been considered. We will discuss our personal result on this subject in Chapter 3. A measurement of the $1^1D_2 \to 2\gamma$ rate could indeed be of help in estimating the direct contribution to the D-wave annihilation, the value of $|\Psi''_{nD}(0)|^2$, since in this case no mixing with other states is involved

$$\Gamma(n^1D_2 \to 2\gamma) = \frac{2^8 \times 3\,\pi\alpha^2}{m^6_{c\bar{c}}}(\frac{2}{3})^4|\Psi''_{nD}(0)|^2. \tag{1.127}$$

Finally the three photon annihilation decay of the J/ψ has to be mentioned. This process happens at the third order in α and thus is highly suppressed, but its measurement does not appear unrealistic for the J/ψ. The interest in this quantity follows from the fact that the ratio $\Gamma(J/\psi \to 3\gamma)/\Gamma(J/\psi \to e^+e^-)$ is sensitive only to the QCD corrections.

Strong annihilation of quarkonium states can be described as a two stage process: first $Q\bar{Q}$ annihilate into gluons and then gluons evolve into hadrons. If one assumes a perfect gluon-hadron duality, that is if one assumes that the probability that gluons hadronize into hadrons is equal to unity, then the computation of strong annihilation rates consists in the computation of transition rates to on-shell gluons.

As we have already described in Section 1.2.2, n^3S_1 quarkonium states can annihilate into three gluons. This circumstance explains the extremely narrow width

of the J/ψ. The same holds for $\Upsilon(1S)$. Besides this process, vector resonances can decay into γgg. An estimate of the branching ratio of the mixed strong-electromagnetic annihilation $\mathcal{B}(J/\psi \to \gamma gg) \sim 6.7\%$ is in reasonable agreement with experimental data. Moreover a study of the spectrum of the direct photon [44] can give some insight on how the gluon-hadrons duality sets in.

C even states with $J \neq 1$ can annihilate into two gluons. The two gluons annihilation rate is simply related to the photon one as

$$\frac{\Gamma_{2g}}{\Gamma_{2\gamma}} = \frac{2\alpha_s^2}{9\alpha^2}(\frac{3}{2})^2. \tag{1.128}$$

Finally we consider the three-gluon annihilation of n^3P_1 and n^1P_1 states. For these levels the soft gluon radiation effect becomes relevant, as opposite to the other cases we have so far considered. Indeed when considering the three and two gluon annihilation of n^3S_1 and n^1S_0 states respectively, the emission of soft gluon can be neglected due to the the fact that we are approximating the heavy quarks as essentially static. When considering P-wave states we automatically include a relative motion of the quark and antiquark inside the meson. Already at the leading order two processes are possible ${}^3P_1 \to g_{\rm soft}[{}^3S_1]_8 \to g_{\rm soft} g^* \to g_{\rm soft} q\bar{q}$ and ${}^1P_1 \to g_{\rm soft}[{}^1S_0]_8 \to g_{\rm soft} gg$ [13]. These are $E1$ transitions, which conserve the spin of the heavy quark pair changing its orbital angular momentum. Thus both the hadronic widths of ${}^1P_1$ and ${}^3P_1$ states are proportional to α_s^3.

Radiative Transitions. The non relativistic approach to quarkonium allows to apply the standard multipole expansion in electrodynamics to compute the transitions between quarkonium levels with the emission of a photon. We distinguish $E1$ and $M1$ transitions associated to

$$H_{E1} = -e_Q e(\boldsymbol{r} \cdot \boldsymbol{E}), \qquad \text{and} \qquad H_{M1} = -\mu_Q(\boldsymbol{\Delta} \cdot \boldsymbol{B}). \tag{1.129}$$

respectively. $\boldsymbol{\Delta} = \boldsymbol{\sigma}_c - \boldsymbol{\sigma}_{\bar{c}}$ and $\boldsymbol{r}$ is the quark-antiquark relative position.

The $E1$ transitions are responsible for the decays $\psi' \to \gamma\chi_{cJ}$, $\chi_{cJ} \to \gamma J/\psi$ and $h_c \to \gamma\eta_c$. The associated decay rates are all proportional to the overlap integral between the S-wave and P-wave radial wave functions weighted by the r term coming from H_{E1},

$$I_{mP,\,nS} = \int r \times r^2\, dr\, \Psi_{nS}(r)\, \Psi_{mP}(r). \tag{1.130}$$

One obtains

$$\Gamma(2^3S_1 \to \gamma\, 1^3P_J) = (2J+1)\frac{4}{27}\left(\frac{2}{3}e\right)^2 \alpha\omega_\gamma^3 |I_{1P,\,2S}|^2 \tag{1.131}$$

$$\Gamma(1^3P_J \to \gamma\, 1^3S_1) = \Gamma(1^1P_1 \to \gamma\, 1^1S_0) = \frac{4}{9}\left(\frac{2}{3}e\right)^2 \alpha\omega_\gamma^3 |I_{1P,\,1S}|^2 \tag{1.132}$$

As for the M_1 transitions no coordinate dependence of the interaction hamiltonian is present in the static limit, *i.e.* in the zero recoil limit, and thus the overlap integral

[13] With the subscript 8 we indicate a $c\bar{c}$ state in color-octet configuration

can be computed using the orthonormality condition between the wave functions. The most interesting processes are $J/\psi \to \gamma\eta_c$ and $\psi' \to \gamma\eta_c$

$$\Gamma(n^3S_1 \to \gamma\, m^1S_0) = \frac{4}{3}\left(\frac{2}{3}e\right)^2 \alpha \frac{\omega_\gamma^3}{m_c^2}|I_{mn}|^2, \tag{1.133}$$

with

$$I_{mn} = \int r^2\, dr\, \Psi_{nS}(r)\, \Psi_{mS}(r). \tag{1.134}$$

Nevertheless the theoretical estimate of $\Gamma(J/\psi \to \gamma\eta_c) \sim 3.3$ KeV is far away from the experimental value ~ 1.2 KeV. A possible source of error may come from the value of the c quark mass or the c magnetic moment, but also eliminating these uncertainties using the $\eta_c \to \gamma\gamma$ amplitude, as suggested by Shifman [45], returns $\Gamma(J/\psi \to \gamma\eta_c) \sim 2.9$ KeV. This discrepancy could be resolved considering the possibility of a strong mixing in the 0^{-+} channel with light-quarks and gluon states [46].

Hadronic Transitions.

Hadronic transitions arise from the interactions of the quark-antiquark pair with the chromo-electric and chromo-magnetic fields of the gluons, in the same way as radiative transitions arise from the interaction with the electric and magnetic fields generated by photons.

Indeed the corresponding terms in the Hamiltonian are similar to those in Eq. (1.129) except for color matrices. In the multipole expansion in QCD [47] the leading order terms are the chromo-electric and chromo-magnetic dipole terms ($E1$ and $M1$) and the chromo-magnetic quadrupole term $M2$:

$$\begin{aligned} H_{E1} &= -\frac{1}{2}\xi^A\, \boldsymbol{r}\cdot\boldsymbol{E}^A(0), \qquad H_{M1} = -\frac{1}{2m_Q}\xi^A\left(\boldsymbol{\Delta}\cdot\boldsymbol{B}^A\right) \\ H_{M2} &= -\frac{1}{4m_Q}\xi^A S_j r_i\left(D^iB^j\right)^A, \end{aligned} \tag{1.135}$$

where $\xi^A = T^A_{\mathbf{3}_c} - T^A_{\bar{\mathbf{3}}_c}$, $\boldsymbol{S} = (\boldsymbol{\sigma}_c + \boldsymbol{\sigma}_{\bar{c}})/2$, $\boldsymbol{D}$ is the QCD covariant derivative and $\boldsymbol{E}$ and $\boldsymbol{B}$ are the chromo-electric and chromo-magnetic components of the gluon field strength tensor. Two observations are in order. First of all hadronic transition occur at least in the second order in the $E1$, $M1$ and $M2$ terms, since gluons are colored objects and one needs at least two gluons to obtain a color singlet. Secondly one can describe hadronic transitions as the interaction of a compact object with soft gluons, introducing a local colorless gluonic operator which produces light mesons in the final state. The transition amplitude thus factorizes into two parts: the heavy quarkonium part, determined by Eq. (1.135), times the production amplitude of light mesons due to the gluonic operator.

A colorless gluonic operator can produce one or two pseudoscalar mesons: $\pi^+\pi^-$, η or π^0. The relevant operators for these transitions are of the general form $G^A_{\mu\nu}\, G^A_{\lambda\sigma}$ or $G^A_{\mu\nu} D G^A_{\lambda\sigma}$, $G^A_{\mu\nu}$ being the gluon field strength tensor. The form of the matrix elements

$$\langle\pi^+\pi^-|G^A_\mu\nu\, G^A_{\lambda\sigma}|0\rangle, \quad \langle\pi^0|G^A_\mu\nu\, G^A_{\lambda\sigma}|0\rangle \ \text{ and } \ \langle\eta|G^A_\mu\nu\, G^A_{\lambda\sigma}|0\rangle \tag{1.136}$$

can be parametrized by only one unknown constant κ using the chiral algebra, the QCD anomaly in the trace of the energy-momentum tensor and the Adler zero condition [48, 49]. Since the transition to a single π^0 involves the isospin breaking, the associated matrix element must proportional to the $u-d$ mass difference [50].

Among the two pion transitions, one of the most studied is $\psi' \to J/\psi\ \pi^+\pi^-$. This decay process is due to two $E1$ terms and the relative amplitude can be written as

$$\mathcal{A}(\psi' \to J/\psi\ \pi^+\pi^-) = -\frac{1}{2}\alpha\langle\pi^+\pi^-|E_i^A E_j^A|0\rangle\alpha^{(ij)}, \tag{1.137}$$

where $\alpha^{(ij)}$ is the chromo-polarizability tensor of the quarkonium in analogy with the atomic properties in electric field. In the leading non relativistic approximation it can be reduced to a single scalar, which governs the over all rate of the decay. The shape of the $d\Gamma/dm_{\pi\pi}$ spectrum ($m_{\pi\pi}$ is the dipion invariant mass) is instead determined by the κ parameter. The values obtained from a fit to data are $\kappa \sim 0.2$ and $\alpha^{(12)} \sim 2$ Gev^{-3}. Considering the dipion as a whole, the partial wave with respect to J/ψ must be even to conserve parity, so that beyond the S-wave decay also a D-wave component will be present. The $S-D$ relative weight can be also expressed in terms of κ leading to a prediction well verified by experiments. Going beyond the leading order final state interactions between the two pions in the final state need to be considered. For a review on this subject see [51, 52].

Hadronic transitions with the emission of η or π^0 lead to the following decays: $\psi' \to J/\psi\,\eta$, $\psi' \to J/\psi\,\pi^0$, $\psi' \to h_c\,\pi^0$ and $h_c \to J/\psi\,\pi^0$.

The first one, $\psi' \to J/\psi\,\eta$, arise from gluonic operators containing one covariant derivative so that the associated amplitude comes out to be

$$\mathcal{A}(\psi' \to J/\psi\,\eta) = \frac{4\pi^2}{15}\sqrt{\frac{2}{3}}\frac{\alpha^{(12)}}{m_Q} f_\eta m_\eta^2 \epsilon_{klm} p^k \epsilon_1^l \epsilon_2^m, \tag{1.138}$$

where f_η is the η decay constant, $\boldsymbol{p}$ is the η momentum and $\boldsymbol{\epsilon}_{1,2}$ are the polarization vectors of ψ' and J/ψ respectively. In this way one obtains a prediction for the rate $\Gamma(\psi' \to J/\psi\,\eta)/\Gamma(\psi' \to J/\psi\,\pi^+\pi^-)$ in good agreement with the experimental measures $\sim 0.097 \pm 0.03$.

As for the second one $\psi' \to J/\psi\,\pi^0$, its decay width can be deduced from the one for $\psi' \to J/\psi\,\eta$ as

$$\frac{\Gamma(\psi' \to J/\psi\,\pi^0)}{\Gamma(\psi' \to J/\psi\,\eta)} = 3\left(\frac{m_d - m_u}{m_d + m_u}\right)^2 \frac{f_\pi^2}{f_\eta^2}\frac{m_\pi^4}{m_\eta^4}\frac{p_\pi^3}{p_\eta^3}. \tag{1.139}$$

The result turns out to be smaller than the observed one, indicating that likely the isospin violation induced by the light quark masses is not sufficient to describe data and that at least one of the two charmonia involved in the process contains a four quark component with isospin 1 [40].

Finally the transitions between n^3S_1 and 1^1P_1 states with the emission of a π^0 arise from the interference between $E1$ and $M1$ terms. The decay amplitude will be also proportional to the radial overlap integral between S and P states. The poor knowledge of this quantity could be the main source of error in the theoretical prediction of the branching ratios which turns out to be smaller than the measured values by one order of magnitude.

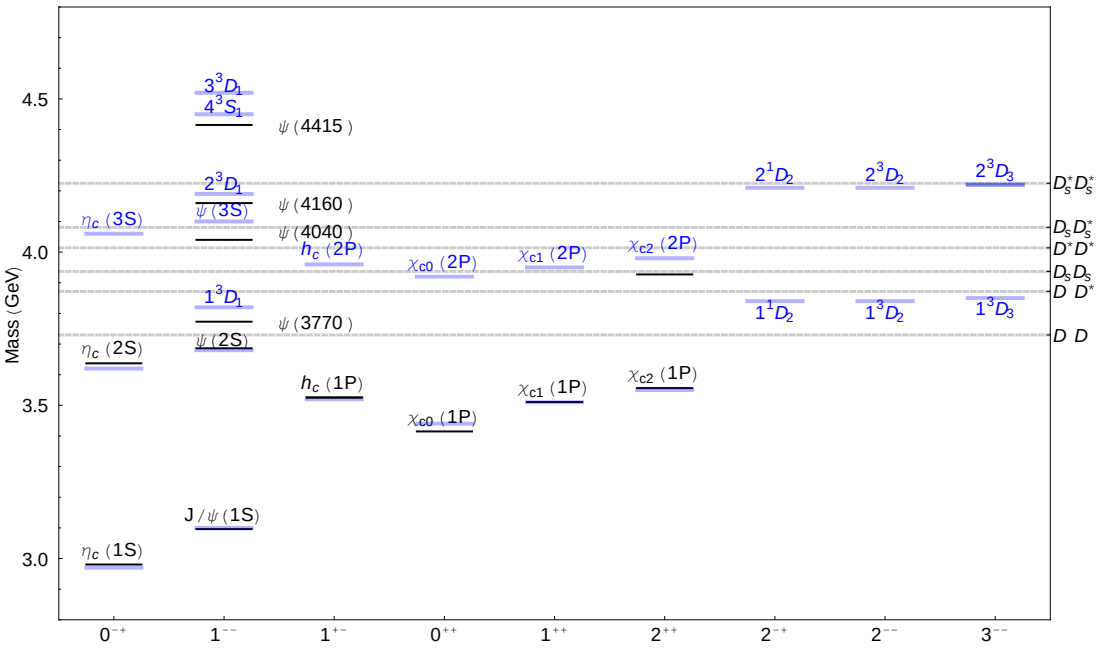

Figure 1.18. Blue lines represent the predictions from non relativistic potential models [55] for standard $c\bar{c}$ levels, compared to experimental values [53], black lines. Dashed lines show the onset of the $D_{(s)}^{(*)}\bar{D}_{(s)}^{(*)}$ open-charm thresholds.

1.2.5 Experimental data

Charmonium and bottomonium states have been widely studied in the last three decades, since the discovery of the J/ψ in 1974, both at e^+e^- and hadron colliders.

Three main e^+e^- colliders, PEP-II (Positron–Electron Project) at SLAC (Stanford Linear Accelerator, USA) KEK-B at KEK (Japan) and CESR (Cornell Electron Storage Ring) at LEPP (Laboratory of Elementary Particle–Physics,USA), have been running at a center of mass energy $\sqrt{s} \simeq m_{\Upsilon(4S)} \sim 10.5$ GeV. At the end of the 1990s, a new program began at CESR, known as CESR-c/CLEO-c. The physics focus shifted from the bottom quark to the lighter charm quark and the energy of CESR was lowered accordingly. Three general purpose detectors were installed at these facilities: the BaBar detector at PEP-II, the Belle detector at KEK-B and the CLEO detector at CESR (in three different configurations, CLEO-II/II.V/III).

The physics of quarkonium has also been under study at the TeVatron, a $\sqrt{s} \simeq$ 1.96 TeV $p\bar{p}$ hadron collider, through the CDF and D$\emptyset$ detectors.

Since 1974 it has been ascertained the existence of 13 charmonium states and 15 bottomonium states. Recently the h_c, the η_c', the χ_{c2}' have been added to the $c\bar{c}$ family, whereas the $b\bar{b}$ family has been enlarged by the observation of the η_b, the $1^3D_{0,1,2}$ triplet [53], the h_b and h_b' [54]. In Fig. 1.18 and Fig. 1.19 we show the comparison between theoretical predictions and experimental measurements for charmonium and bottomonium spectra respectively.

When searching for higher charmonium and bottomonium states a number of non conventional resonances have been uncovered, decaying into ordinary $c\bar{c}$ and $b\bar{b}$ mesons but not resembling any of the foreseen radial or orbital excitations. The

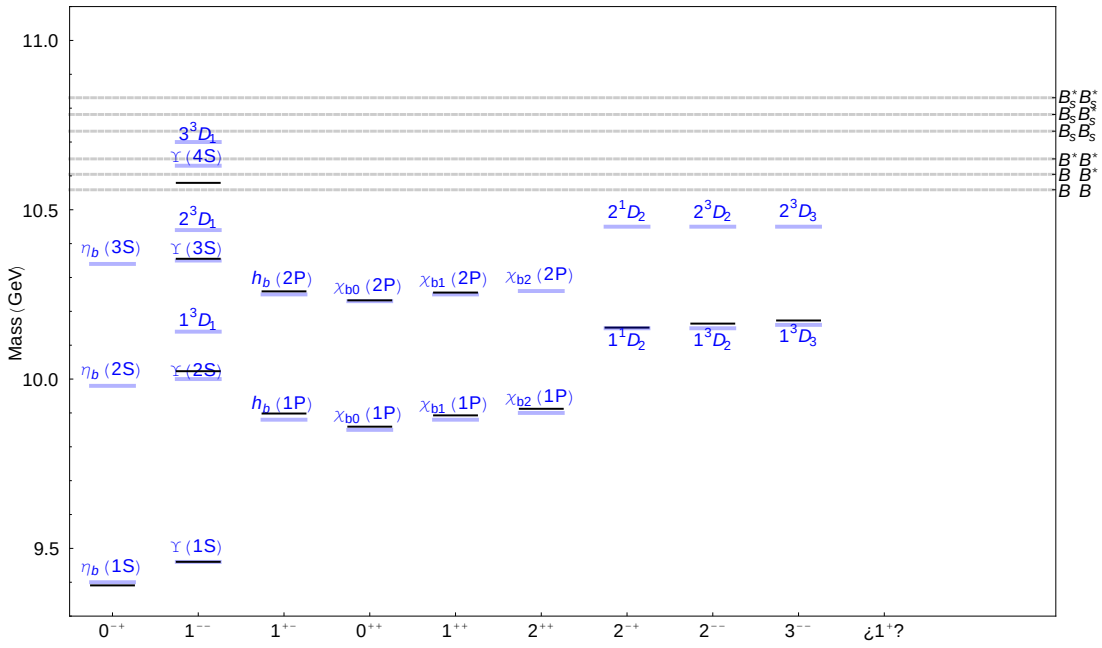

Figure 1.19. Blue lines represent the predictions from non relativistic potential models [55] for standard $b\bar{b}$ levels, compared to experimental values, black lines [53]. Dashed lines show the onset of the $B_{(s)}^{(*)}\bar{B}_{(s)}^{(*)}$ open-bottom thresholds.

possibility to make theoretical predictions for heavy quarkonia, both on the spectrum *and* the dynamics, allowed the identification of these new mesons as *exotic*, that is not predicted by the standard $Q\bar{Q}$ quark model.

Nevertheless, as we have said, the reliability of the non relativistic predictions for heavy quarkonium decreases when crossing the $D\bar{D}$ and $B\bar{B}$ thresholds. Thus one needs to rely on more than one property for each new state to conclude that they are actually non conventional: its mass, its prominent decay modes, its production rate.

In the next chapter we will list the established exotic mesons in the charm and bottom sector. Then we will present some of the theoretical interpretations that have been proposed during the years.

Chapter 2

Exotic mesons

As anticipated in the previous chapter, during the search for orbital and radial excitations of charmonium and bottomonium states, non conventional mesons decaying into the lowest $c\bar{c}$ and $b\bar{b}$ levels have been found. In Section 2.1 a summary of the most recent experimental data is presented. These non conventional states elude an explanation in terms of quark antiquark bound states, and they are thus referred to as *exotic* and usually called XYZ resonances. It is worth to observe that the identification of exotic mesons is much easier in the heavy sector than in the light one. In the mass region where heavy quarkonia are expected, one can rely on the non relativistic approach, which has proved to be an acceptable effective theory for QCD in that energy range.

For these exotic states many theoretical interpretations have been proposed. For some of them a standard explanation is still foreseen, since a refinement of the predictions for masses and decay rates of heavy quarkonia above the open-charm and open-bottom thresholds is always possible.

Many of these newly discovered mesons have been indicated as candidates to be *multiquark states*, made up of two quarks and two antiquarks $\sim Q\bar{Q}q\bar{q}$[1]. Two different forms of multiquark states can be considered: tetraquark states, if the color is saturated over all the four constituents, or meson-antimeson molecules, if the color is saturated separately on the two quark-antiquark pairs.

The existence of *hybrid mesons*, gluon-quark-antiquark bound states, has also been investigated. Finally a peculiar form of multiquark state has been recently proposed: *hadroquarkonium*, a standard heavy quarkonium embedded inside light hadronic matter.

For each of these possibilities, after a brief theoretical explanation, we will list the candidates among the XYZ mesons. In this chapter we will pass in review the molecular (Section 2.2), hybrid (Section 2.3) and hadroquarkonium (Section 2.4) hypotheses. The next chapter will be instead entirely dedicated to tetraquarks.

2.1 Experimental data

In this section we summarize the experimental data available on the XYZ mesons. Data have been collected at e^+e^- colliders operating mainly at the $\Upsilon(4S)$ center

[1] $q = u, d, s$ and $Q = c, b$.

of mass energy, as described in Section 1.2.5, and at the $p\bar{p}$ collider at Fermilab, the Tevatron, with the CDF and D$\emptyset$ detectors. Data from the LHC (pp collider), especially from the LHCb experiment, are forthcoming. Some preliminary results are already available, but we will not include them in our review.

***X*(3872).** $X(3872)$ was first discovered by the Belle collaboration in 2003 produced in $B \to KX(3872)$ and decaying into $J/\psi\,\pi^+\pi^-$ [56, 57]. After few time it was also observed in $p\bar{p}$ collisions in the same final state, by the CDF [58, 59, 60, 61] and D$\emptyset$ [62] collaborations. In particular in [59] the dipion mass spectrum has been measured and the fraction of $X(3872)$ originated from b-hadrons has been estimated to be $16.1 \pm 4.9(\text{stat}) \pm 0.7(\text{syst})\%$, establishing that a consistent amount of the $X(3872)$ observed was due to prompt production. Also BaBar confirmed the resonance [63, 64, 65, 66].

During the years other decay modes have been ascertained: $X(3872) \to J/\psi\,\omega$ by Belle [67] and BaBar [68]; $X(3872) \to J/\psi\,\gamma$ by Belle [67, 69] and BaBar [70, 71]; $X(3872) \to \psi'\gamma$ by Belle [69] and BaBar [71]; $X(3872) \to D^0\bar{D}^{0*}$ by Belle [72, 73] and BaBar [74]. Branching ratios for each decay mode have been measured by the various experiments. In [75] these different values have been combined giving the results reported in Table 2.1.

Table 2.1. Measured $X(3872)$ product branching fractions (PBF), separated by production and decay mechanism. When more than a publication is present the combination is performed assuming gaussian uncorrelated errors. The last two columns report the results in terms of absolute X branching fraction (B_{fit}) and of the branching fraction normalized to $J/\psi\,\pi^+\pi^-$ (R_{fit}). Ranges and limits are provided at 68% and 90% C.L. respectively.

B decay mode	X decay mode	PBF($\times 10^5$)	B_{fit}	R_{fit}
$XK^\pm$	$X \to J/\psi\,\pi^+\pi^-$	0.82±0.09 [66, 57]	$[0.035, 0.075]$	N/A
XK^0	$X \to J/\psi\,\pi^+\pi^-$	0.53±0.13 [66, 57]	N/A	N/A
$XK^\pm$	$X \to D^0\bar{D}^{0*}$	13±3 [74, 72]	$[0.54, 0.8]$	$[7.2, 16.2]$
XK^0	$X \to D^0\bar{D}^{0*}$	19±6 [74, 72]	N/A	N/A
XK	$X \to J/\psi\,\gamma$	0.22±0.05 [71, 67]	$[0.0075, 0.0195]$	$[0.19, 0.33]$
XK	$X \to \psi'\gamma$	1.0 ± 0.3 [71]	$[0.03, 0.09]$	$[0.75, 1.55]$
XK	$X \to J/\psi\,\pi^+\pi^-\pi^0$	– [67]	$[0.015, 0.075]$	$[0.42, 1.38]$
XK^*	$X \to J/\psi\,\pi^+\pi^-$	< 0.34 [57]	N/A	N/A

A noticeable feature of this particle is represented by the vicinity of its mass to the $D^0\bar{D}^{0*}$ threshold. The most precise mass determination in the $J/\psi\,\pi^+\pi^-$ channel is [61] [2]

$$M_{X(3872)} = (3871.61 \pm 0.16 \pm 0.19)\ \text{MeV}, \tag{2.1}$$

while in $D^0\bar{D}^{0*}$ slightly higher values are measured [73, 74] which average to

$$M_{X(3872)} = (3874.0 \pm 1.2)\ \text{MeV}. \tag{2.2}$$

Furthermore the $X(3872)$ is an extremely narrow resonance. The different measurements of its width are reported in Table 10 of [53]. The average in the

[2] Everywhere in the text the first error is statistical and the second one systematic.

$J/\psi\,\pi^+\pi^-$ final state is

$$\Gamma_{X(3872)} = (1.3 \pm 0.6)\ \text{MeV}, \tag{2.3}$$

whereas in the $D^0\bar{D}^{0*}$ one

$$\Gamma_{X(3872)} = (3.5^{+1.6}_{-1.0})\ \text{MeV}. \tag{2.4}$$

The fact that $X(3872)$ decays with nearly the same strength into $J/\psi\,\pi^+\pi^-$, where the two pions come from a ρ, and into $J/\psi\,\pi^+\pi^-\pi^0$, where the three pions come from an ω [67],

$$\frac{\mathcal{B}(X \to \pi^+\pi^-\pi^0 J/\psi)}{\mathcal{B}(X \to \pi^+\pi^- J/\psi)} = 1.0 \pm 0.4 \pm 0.3, \tag{2.5}$$

indicates a high level isospin violation which seems to forbid a standard $c\bar{c}$ interpretation.

As for the J^{PC} quantum numbers, the earliest angular analysis on the $J/\psi\,\pi^+\pi^-$ mode by Belle [76] favored the 1^{++} assignment. An angular analysis by CDF on the same final state indicated that 1^{++} and 2^{-+} were equally probable [60]. Finally came the BaBar analysis on the $J/\psi\,\pi^+\pi^-\pi^0$ events, which stated that the 2^{-+} option is the most likely [68].

***X*(3940)**, ***Y*(3940)**, ***Y*(3915)**, ***X*(3915)** and ***Z*(3930)**. In the 3940 MeV mass region five resonant structures have been revealed by the BaBar and Belle collaborations.

The first of them, found by Belle, is the $X(3940)$ (statistical significance of 5 σ), produced in $e^+e^- \to J/\psi\,X(3940)$ and decaying into $D\bar{D}^*$ [77]. Its production mode suggests that it is a scalar resonance and thus its J^{PC} quantum numbers are likely to be $0^{\pm+}$. However its decay mode forbids the 0^{-+} assignment and thus one can conclude that if it is a scalar state it needs to have positive parity. A resonance in the $J/\psi\,\omega$ invariant mass spectrum was searched at the same mass without finding any evidence of a signal ($B(X(3940) \to J/\psi\ \omega) < 26\%$ at 90% C.L.). In [78] the mass and width of the resonance have been measured

$$\begin{aligned} M_{X(3940)} &= (3942^{+7}_{-6} \pm 6)\ \text{MeV} \\ \Gamma_{X(3940)} &= (37^{+26}_{-15} \pm 8)\ \text{MeV}. \end{aligned} \tag{2.6}$$

Un upper limit for the branching ratio into $D\bar{D}^*$ is known

$$B(X(3940) \to D\bar{D}^*) < 41\%\ \text{at}\ 90\%\,\text{C.L.}. \tag{2.7}$$

An additional resonance named $Y(3940)$ has been found always by Belle (statistical significance of 8.1σ) at almost the same mass being produced in $B \to KY(3940)$ and decaying into $J/\psi\,\omega$ [79]. Its mass and width are

$$\begin{aligned} M_{Y(3940)} &= (3943 \pm 11 \pm 13)\ \text{MeV} \\ \Gamma_{Y(3940)} &= (87 \pm 22 \pm 26)\ \text{MeV}, \end{aligned}$$

whereas its branching ratio into $J/\psi\,\omega$ is

$$\mathcal{B}(B \to KY(3940) \times \mathcal{B}(Y(3940) \to J/\psi\,\omega) = (7.1 \pm 1.3 \pm 3.1) \times 10^{-5}. \tag{2.8}$$

There isn't any indication on the J^P quantum numbers of $Y(3940)$, but its charge conjugation must be $C = +1$.

The BaBar collaboration [80] confirmed the existence of a resonance (statistical significance of 5.2σ) in the $J/\psi\,\omega$ invariant mass spectrum, but measuring a lower mass and width with respect to $Y(3940)$

$$M_{Y(3915)} = (3914.6^{+3.8}_{-3.4} \pm 2.0)\ \text{MeV} \tag{2.9}$$
$$\Gamma_{Y(3915)} = (34^{+12}_{-8} \pm 5)\ \text{MeV}. \tag{2.10}$$

The product of branching fractions is

$$\mathcal{B}(B^+ \to K^+Y(3915) \times \mathcal{B}(Y(3915) \to J/\psi\,\omega) = (4.9^{+1.0}_{-0.9} \pm 0.5) \times 10^{-5}$$
$$\mathcal{B}(B^0 \to K^0Y(3915) \times \mathcal{B}(Y(3915) \to J/\psi\,\omega) = (1.3^{+1.3}_{-1.1} \pm 0.2) \times 10^{-5}.$$

Subsequently a peak (statistical significance of 7.7σ) at nearly the same mass and width has been revealed by the Belle collaboration produced in $\gamma\gamma$ collisions and decaying into $J/\psi\,\omega$ [81]

$$M_{X(3915)} = (3915 \pm 3 \pm 2)\ \text{MeV}$$
$$\Gamma_{X(3915)} = (17 \pm 10 \pm 3)\ \text{MeV}.$$

The possible J^{PC} quantum numbers are $J^{PC} = 0^{\pm+}, 1^{\pm+}, 2^{\pm+}$.

Finally the Belle collaboration also found a resonance named $Z(3930)$ [82] (statistical significance of 5.3σ) produced in $\gamma\gamma$ collisions and decaying in $D\bar{D}$. BaBar confirmed the state [83]. Its mass and width have been estimated to be

$$M_{Z(3930)} = (3926.7 \pm 2.7 \pm 1.1)\ \text{MeV}$$
$$\Gamma_{Z(3930)} = (21.3 \pm 6.8 \pm 3.6)\ \text{MeV},$$

and an angular analysis has established its quantum numbers: $J^{PC} = 2^{++}$. Finally the branching ratio into $D\bar{D}$ has been measured

$$\Gamma_{\gamma\gamma} \times \mathcal{B}(Z(3930) \to D\bar{D}) = (0.24 \pm 0.05 \pm 0.04)\ \text{KeV}. \tag{2.11}$$

The $Z(3930)$ is a strong candidate to be a standard $\chi_{c2}(2P)$ state, as discussed in [53].

As for the other four states, three of them are likely to be one single state: $Y(3940)$, $Y(3915)$ and $X(3915)$. If this were the case it would be the second resonance to be observed in two production modes, B-decays and $\gamma\gamma$ collisions.

***G*(3900)**. During a study of exclusive production of the $D\bar{D}$ system through initial-state radiation, the BaBar collaboration [84] revealed a broad enhancement at 3900 MeV, besides confirming the 1^{--} radial excitations of charmonium: $\psi(3770)$,

$\psi(4040)$, $\psi(4160)$ and $\psi(4415)$. A Gaussian fit to the $D\bar{D}$ invariant mass spectrum returned

$$\begin{aligned} M_{G(3900)} &= (3.909 \pm 0.021)\ \text{MeV} \\ \Gamma_{G(3900)} &= (50 \pm 7)\ \text{MeV}. \end{aligned}$$

Later, also the Belle collaboration confirmed the resonance [85].

***Y*(4008)**. A measurement of the $e^+e^- \to J/\psi\,\pi^+\pi^-$ cross section via initial state radiation at Belle [86] has shown that a structure is present at ~ 4.05 GeV (statistical significance of 7.4σ), beside confirming the $Y(4260)$, see hereafter. A fit to the $J/\psi\,\pi^+\pi^-$ invariant mass spectrum gives

$$\begin{aligned} M_{Y(4008)} &= (4008 \pm 40^{+114}_{-28})\ \text{MeV} \\ \Gamma_{Y(4008)} &= (226 \pm 44 \pm 87)\ \text{MeV}. \end{aligned}$$

The production mode constraints the J^{PC} quantum numbers to be 1^{--}. An analogous study by BaBar [87] does not confirm the existence of this broad peak.

***Y*(4140)**, ***Y*(4274)** and ***X*(4350)**. The CDF collaboration [88] reported the observation of a resonant state with even charge conjugation, named $Y(4140)$, in the $J/\psi\,\phi$ invariant mass spectrum of the $B \to KJ/\psi\,\phi$ decay. The measured mass and decay width are [89]

$$\begin{aligned} M_{Y(4140)} &= (4143.0^{+2.9}_{-3.0} \pm 0.6)\ \text{MeV} \\ \Gamma_{Y(4140)} &= (15.3^{+10.4}_{-6.1} \pm 2.5)\ \text{MeV}, \end{aligned}$$

whereas the product of branching ratios is [90]

$$\mathcal{B}(B^+ \to Y(4140)K^+) \times \mathcal{B}(Y(4140) \to J/\psi\,\phi) = (9.0 \pm 3.4 \pm 2.9) \times 10^{-6}. \quad (2.12)$$

The statistical significance of the signal is greater than 5σ.

In [89] CDF has also found evidence at 3.1σ level for a second structure with mass and width of

$$\begin{aligned} M_{Y(4274)} &= (4274.4^{+8.4}_{-6.7})\ \text{MeV} \\ \Gamma_{Y(4274)} &= (32.3^{+21.9}_{-15.3})\ \text{MeV}. \end{aligned}$$

The Belle collaboration searched for the $Y(4140)$ in the same process [91] without finding any evidence of a signal, but putting an upper limit on the $J/\psi\,\phi$ branching ratio

$$\mathcal{B}(B^+ \to Y(4140)K^+) \times \mathcal{B}(Y(4140) \to J/\psi\,\phi) < 6 \times 10^{-6}, \quad (2.13)$$

which is not in contradiction with CDF measurement, considering its large uncertainty. The theoretical interpretations of $Y(4140)$ as a $D_s^{*+}\bar{D}_s^{*-}$ molecule predicted a sizable value for the product of the two-photon width times the branching ratio into $J/\psi\,\phi$. A search for this state in $\gamma\gamma$ collisions by Belle found no evidence of it [92], and set un upper limit of

$$\Gamma_{\gamma\gamma}(Y(4140))\mathcal{B}(Y(4140) \to J/\psi\,\phi) < 39\ \text{eV}. \quad (2.14)$$

Nevertheless a 3.2σ evidence was found at

$$\begin{aligned} M_{X(4350)} = &\quad (4350.6^{+4.6}_{-5.2} \pm 0.7)\ \text{MeV} \\ \Gamma_{Y(4350)} = &\quad (13^{+18}_{-9} \pm 4)\ \text{MeV}, \end{aligned}$$

adding a further $C = +1$ meson to the list.

***X*(4160)**. During a study of $X(3940)$ [78], the Belle collaboration observed another charmonium-like state decaying into $D^*\bar{D}^*$ and produced in association with a J/ψ in e^+e^- collisions. The mass and width parameters of this resonance, denoted as $X(4160)$, are

$$\begin{aligned} M_{X(4160)} = &\quad (4156^{+25}_{-20} \pm 15)\ \text{MeV} \\ \Gamma_{X(4160)} = &\quad (139^{+111}_{-61} \pm 21)\ \text{MeV}, \end{aligned}$$

whereas the statistical significance of the signal is 5.5σ. Only the charge conjugation is known for this state: $C = +1$.

***Y*(4260)**, ***Y*(4350)** and ***Y*(4660)**. Studying the initial-state radiation events $e^+e^- \to \gamma_{\text{ISR}} J/\psi\,\pi^+\pi^-$, the BaBar collaboration observed a resonant structure (statistical significance between 5σ and 7σ) near 4260 MeV [93]. The mass and width of this state, named $Y(4260)$, are [87]

$$\begin{aligned} M_{Y(4260)} = &\quad (4252 \pm 6^{+2}_{-3})\ \text{MeV} \\ \Gamma_{Y(4260)} = &\quad (105 \pm 18^{+4}_{-6})\ \text{MeV} \end{aligned}$$

and the product of branching ratios is

$$\Gamma_{ee}(Y(4260))\mathcal{B}(Y(4260) \to J/\psi\,\pi^+\pi^-) = (7.5 \pm 0.9 \pm 0.8)\ \text{eV}. \tag{2.15}$$

The Belle collaboration [94, 86] subsequently confirmed the state in the same production and decay mode (statistical significance of 11σ). CLEO also observed $Y(4260)$ in direct production in e^+e^- collisions at $\sqrt{s} = 3970 \div 4260$ MeV [95, 96] and via initial state radiation in e^+e^- collisions at $\sqrt{s} = m_{\Upsilon(4S)} \div m_{\Upsilon(4S)}$ [97]. In particular in [95] $Y(4260)$ has been found also in the $J/\psi\,\pi^0\pi^0$ (statistical significance of 5.1σ) and $J/\psi\,K^+K^-$ (statistical significance of 3.7σ) final states, beside $J/\psi\,\pi^+\pi^-$ (statistical significance of 11σ).

Belle [98, 85] and BaBar [99, 100] searched for a $Y(4260)$ signal in the $D^{(*)}\bar{D}^{(*)}$ invariant mass spectrum without finding evidence of a signal. In [100] the following limits on the associated branching ratios have been set:

$$\begin{aligned} \frac{\mathcal{B}(Y(4260)\to D^*\bar{D})}{\mathcal{B}(J/\psi\,\pi^+\pi^-)} &< 34 \\ \frac{\mathcal{B}(Y(4260)\to D^*\bar{D}^*)}{\mathcal{B}(J/\psi\,\pi^+\pi^-)} &< 40. \end{aligned} \tag{2.16}$$

A study in the $D_s^{(*)}\bar{D}_s^{(*)}$ channel has been performed by BaBar [101] and Belle [102]

with the following upper limits on the branching ratios

$$\begin{aligned} \frac{\mathcal{B}(Y(4260)\to D_s\bar{D}_s)}{\mathcal{B}(J/\psi\,\pi^+\pi^-)} &< 0.7 \\ \frac{\mathcal{B}(Y(4260)\to D_s^*\bar{D}_s)}{\mathcal{B}(J/\psi\,\pi^+\pi^-)} &< 44 \\ \frac{\mathcal{B}(Y(4260)\to D_s^*\bar{D}_s^*)}{\mathcal{B}(J/\psi\,\pi^+\pi^-)} &< 30. \end{aligned} \tag{2.17}$$

Studying the decay $B^{+,0} \to K^{+,0}Y(4260)$, BaBar set an upper limit on the product of branching ratios

$$\mathcal{B}(B \to KY(4260))\mathcal{B}(Y(4260) \to J/\psi\,\pi^+\pi^-) < 2.9 \times 10^{-5}. \tag{2.18}$$

An investigation of the $e^+e^- \to \psi'\pi^+\pi^-$ process using initial state radiation revealed the existence of a new 1^{--} resonance, denoted as $Y(4350)$ [103, 104], with statistical significance of more than 8σ. This state has mass and width equal to

$$\begin{aligned} M_{Y(4350)} &= (4361 \pm 9 \pm 9)\ \text{MeV} \\ \Gamma_{Y(4350)} &= (74 \pm 15 \pm 10)\ \text{MeV}. \end{aligned}$$

In [104] the Belle collaboration observed an additional state (statistical significance of 5.8σ), the $Y(4660)$, not present in the BaBar analysis [103]. The measured peak position and width are

$$\begin{aligned} M_{Y(4660)} &= (4664 \pm 11 \pm 5)\ \text{MeV} \\ \Gamma_{Y(4660)} &= (48 \pm 15 \pm 3)\ \text{MeV}. \end{aligned}$$

The production mode of these three resonances constraints the J^{PC} quantum numbers to be 1^{--}.

$Y(4630)$. In [105] Belle performed a study of the exclusive $e^+e^- \to \Lambda_c^+\Lambda_c^-$ cross section as a function of center-of-mass energy near the $\Lambda_c^+\Lambda_c^-$ threshold finding a resonance (statistical significance of 8.2σ), the $Y(4630)$, with the following mass and width

$$\begin{aligned} M_{Y(4630)} &= (4634^{+8}_{-7}\ {}^{+5}_{-8})\ \text{MeV} \\ \Gamma_{Y(4630)} &= (92^{+40}_{-24}\ {}^{+10}_{-21})\ \text{MeV}. \end{aligned}$$

The branching ratio into $\Lambda_c^+\Lambda_c^-$ is measured to be

$$\mathcal{B}(Y(4630) \to \Lambda_c^+\Lambda_c^-) = (0.68^{+0.16}_{-0.15}\ {}^{+0.07}_{-0.11} \pm 0.28(\text{sys.})) \times 10^{-6}. \tag{2.19}$$

The production mode constraints the J^{PC} quantum numbers to be 1^{--}.

$Z_1^+(4050)$, $Z_2^+(4250)$ and $Z^+(4430)$. The existence of charged states containing $c\bar{c}$ would represent an unquestionable signal of the existence of multiquark mesons. Three charged states were discovered by the Belle collaboration in B-decays, but never confirmed by BaBar.

The first one to be revealed was the $Z^+(4430)$ [106], as a peak in the $\psi'\pi^+$ invariant mass spectrum in the $B \to K\psi'\pi^+$ process. The mass and width of the charged resonance resulted [107]

$$\begin{aligned} M_{Z^+(4430)} &= (4433^{+15}_{-12}\ {}^{+19}_{-13})\ \text{MeV} \\ \Gamma_{Z^+(4430)} &= (107^{+86}_{-43}\ {}^{+74}_{-56})\ \text{MeV}, \end{aligned}$$

with a product of branching ratios

$$\mathcal{B}(B^0 \to K^- Z^+(4430)) \times \mathcal{B}(Z^+(4430) \to \psi'\pi^+) = (3.2^{+1.8}_{-0.9}\ {}^{+5.3}_{-1.6}) \times 10^{-5}. \quad (2.20)$$

and a statistical significance of 5.4σ. Unfortunately BaBar did not confirm the charged state [108] (with a statistical significance between 1.9σ and 3.1σ), setting an upper limit on the product of branching ratios which is contrast with the Belle measurement

$$\mathcal{B}(B^0 \to K^- Z^+(4430)) \times \mathcal{B}(Z^+(4430) \to \psi'\pi^+) < 3.1 \times 10^{-5} \qquad \text{at } 95\%\text{C.L.} \quad (2.21)$$

Two additional charged states were uncovered in $\bar{B}^0 \to K^-\chi_{c1}\pi^+$ decays by the Belle collaboration [109]. The mass and width parameters are

$$\begin{aligned} M_{Z_1^+} &= (4051 \pm 14^{+20}_{-41})\ \text{MeV} \\ \Gamma_{Z_1^+} &= (82^{+21}_{-17}\ {}^{+47}_{-22})\ \text{MeV}, \end{aligned}$$

$$\begin{aligned} M_{Z_2^+} &= (4248^{+44}_{-29}\ {}^{+180}_{-35})\ \text{MeV} \\ \Gamma_{Z_2^+} &= (177^{+54}_{-39}\ {}^{+316}_{-61})\ \text{MeV}. \end{aligned}$$

The significance of each of the $\pi^+\chi_{c1}$ structures exceeds 5σ.

Y_b(10890). Belle studied the $\Upsilon(1S)\pi^+\pi^-$, $\Upsilon(1S)K^+K^-$, $\Upsilon(2S)\pi^+\pi^-$ and $\Upsilon(3S)\pi^+\pi^-$ production in e^+e^- collisions near the $\Upsilon(5S)$ peak: $\sqrt{s} \sim 10.87$ GeV [110]. Attributing the signals to the $\Upsilon(5S)$ resonance, the values of the partial widths $\Gamma(\Upsilon(5S) \to \Upsilon(1S)\pi^+\pi^-)$ and $\Gamma(\Upsilon(5S) \to \Upsilon(2S)\pi^+\pi^-)$ exceed by more than two orders of magnitude the previously measured partial widths for dipion transitions between lower Υ states.

In a subsequent analysis [111] the observed enhancement was explained fitting the data with an additional resonance, beside the $\Upsilon(5S)$ one. A fit using a Briet-Wigner resonance shape yields a peak mass of

$$\begin{aligned} M_{Y_b} &= (10888.4^{+2.7}_{-2.6} \pm 1.2)\ \text{MeV} \\ \Gamma_{Y_b} &= (30.7^{+8.3}_{-7.0} \pm 3.1)\ \text{MeV}. \end{aligned}$$

The production mode constraints the J^{PC} quantum numbers to be 1^{--}.

Z_b^+(10610) and Z_b^+(10650). The discovery of two charged states in the bottom sector was led by the search for the $^1P_0$ bottomonium state, the h_b. The analogous

state in the charm sector, the h_c, was found by CLEO [112] in e^+e^- collisions at $\sqrt{s} \sim 4.260$ GeV, near the $Y(4260)$ peak. The $Y_b(10890)$ appears similar in many respects to the $Y(4260)$ and this suggested to look for the h_b in e^+e^- collisions near the $Y_b(10890)$ peak. This study not only revealed the $h_b(1P)$ and $h_b(2P)$ [54], but uncovered also the existence of two intermediate charged states decaying into $\Upsilon(1S, 2S, 3S)\pi^\pm$ and $h_b(1P, 2P)\pi^\pm$ [113]. The measured masses and widths of the two structures averaged over the five final states are

$$\begin{aligned} M_{Z_b^+(10610)} &= (10608.4 \pm 2.0)\ \text{MeV} \\ \Gamma_{Z_b^+(10610)} &= (15.6 \pm 2.5)\ \text{MeV}, \end{aligned}$$

$$\begin{aligned} M_{Z_b^+(10650)} &= (10653.2 \pm 1.5)\ \text{MeV} \\ \Gamma_{Z_b^+(10650)} &= (14.4 \pm 3.2)\ \text{MeV}. \end{aligned}$$

Analysis favors quantum numbers of $I^G(J^P) = 1^+(1^+)$ for both states.

All the experimental information contained in this Section is summarized in Table 2.2 and 2.3.

Table 2.2. Summary table of the experimental information available for the XYZ states (Section 2.1).

State	J^{PC}	Mass (MeV)	Width (MeV)	Production/Decay	Experiments (Stat. Significance)
$X(3872)$	$1^{++}/2^{-+}$	$3871.61 \pm 0.16 \pm 0.19$	1.3 ± 0.6	$B \to K\,X \to K(J/\psi\,\pi^+\pi^-)$ $p\bar{p} \to X + \text{All},\ X \to J/\psi\,\pi^+\pi^-$	Belle [56, 57], BaBar [63, 64, 65, 66] CDF [58, 59, 60, 61], DØ [62]
		3874.0 ± 1.2	$3.5^{+1.6}_{-1.0}$	$B \to KX \to K(D^0\bar{D}^{0*})$	Belle [72, 73], BaBar [74]
				$B \to KX \to K(J/\psi\,\pi^+\pi^-\pi^0)$	Belle [67], BaBar [68]
				$B \to KX \to K(J/\psi\,\gamma)$	Belle [67, 69], BaBar [70, 71]
				$B \to KX \to K(\psi'\,\gamma)$	Belle [69], BaBar [71]
$X(3940)$	$?^{?+}$	$(3942^{+7}_{-6} \pm 6)$	$(37^{+26}_{-15} \pm 8)$	$e^+e^- \to J/\psi\,X \to J/\psi(D\bar{D}^*)$	Belle [77, 78] (5σ)
$Y(3940)$	$?^{?+}$	$3943 \pm 11 \pm 13$	$87 \pm 22 \pm 26$	$B \to K\,Y \to K(J/\psi\omega)$	Belle [79] (8.1σ)
$Y(3915)$	$?^{?+}$	$3914.6^{+3.8}_{-3.4} \pm 2.0$	$34^{+12}_{-8} \pm 5$	$B \to K\,Y \to K(J/\psi\omega)$	BaBar [80] (5.2σ)
$X(3915)$	$?^{?+}$	$3915 \pm 3 \pm 2$	$17 \pm 10 \pm 3$	$\gamma\gamma \to X \to (J/\psi\omega)$	Belle [81] (7.7σ)
$Z(3930)$	2^{++}	$3926.7 \pm 2.7 \pm 1.1$	$21.3 \pm 6.8 \pm 3.6$	$\gamma\gamma \to Z \to D\bar{D}$	Belle [82] (5.3σ), BaBar [83] (5.8σ)
$G(3900)$	1^{--}	3.909 ± 0.021	50 ± 7	$e^+e^- \to \gamma G \to \gamma(D\bar{D})$	BaBar [84], Belle [85]
$Y(4008)$	1^{--}	$4008 \pm 40^{+114}_{-28}$	$226 \pm 44 \pm 87$	$e^+e^- \to \gamma Y \to \gamma(J/\psi\,\pi^+\pi^-)$	Belle [86] (7.4σ)
$Y(4140)$	$?^{?+}$	$4143.0^{+2.9}_{-3.0} \pm 0.6$	$15.3^{+10.4}_{-6.1} \pm 2.5$	$B \to KY \to K(J/\psi\,\phi)$	CDF [88] ($> 5\sigma$)
$Y(4274)$	$?^{?+}$	$4274.4^{+8.4}_{-6.7}$	$32.3^{+21.9}_{-15.3}$	$B \to KY \to K(J/\psi\,\phi)$	CDF [89] (3.1σ)
$X(4350)$	$?^{?+}$	$4350.6^{+4.6}_{-5.2} \pm 0.7$	$13^{+18}_{-9} \pm 4$	$\gamma\gamma \to X \to J/\psi\,\phi$	Belle [92] (3.2σ)
$X(4160)$	$?^{?+}$	$4156^{+25}_{-20} \pm 15$	$139^{+111}_{-61} \pm 21$	$e^+e^- \to J/\psi X \to J/\psi(D^*\bar{D}^*)$	Belle [78] (5.5σ)

Table 2.3. Summary table of the experimental information available for the XYZ states (Section 2.1).

State	J^{PC}	Mass (MeV)	Width (MeV)	Production/Decay	Experiments (Stat. Significance)
$Y(4260)$	1^{--}	$4252 \pm 6^{+2}_{-3}$	$105 \pm 18^{+4}_{-6}$	$e^+e^- \to \gamma Y \to \gamma(J/\psi\,\pi^+\pi^-)$	BaBar [93](5σ-7σ), Belle [94, 86](11σ) CLEO [97](5.4σ)
				$e^+e^- \to Y \to J/\psi\,\pi^+\pi^-$	CLEO [95, 96] (11σ)
				$e^+e^- \to Y \to J/\psi\,\pi^0\pi^0$	CLEO [95] (5.1σ)
				$e^+e^- \to Y \to J/\psi\,K^+K^-$	CLEO [95] (3.7σ)
$Y(4350)$	1^{--}	$4361 \pm 9 \pm 9$	$74 \pm 15 \pm 10$	$e^+e^- \to \gamma Y \to \gamma(\psi'\pi^+\pi^-)$	BaBar [103, 104] (8σ)
$Y(4660)$	1^{--}	$4664 \pm 11 \pm 5$	$48 \pm 15 \pm 3$	$e^+e^- \to \gamma Y \to \gamma(\psi'\pi^+\pi^-)$	Belle [104] (5.8σ)
$Y(4630)$	1^{--}	$4634^{+8\ +5}_{-7\ -8}$	$92^{+40\ +10}_{-24\ -21}$	$e^+e^- \to Y \to \Lambda_c^+\Lambda_c^-$	Belle [105] (8.2σ)
$Z^+(4430)$		$4433^{+15\ +19}_{-12\ -13}$	$107^{+86\ +74}_{-43\ -56}$	$B \to KZ^+ \to K(\psi'\pi^+)$	Belle [106] (5.4σ) not confirmed by BaBar [108] (1.9σ - 3.1σ)
$Z_1^+(4050)$		$4051 \pm 14^{+20}_{-41}$	$82^{+21\ +47}_{-17\ -22}$	$\bar{B}^0 \to K^-Z_1^+ \to K^-(\chi_{c1}\pi^+)$	Belle [109] ($> 5\sigma$)
$Z_2^+(4250)$		$4248^{+44\ +180}_{-29\ -35}$	$177^{+54\ +316}_{-39\ -61}$	$\bar{B}^0 \to K^-Z_2^+ \to K^-(\chi_{c1}\pi^+)$	Belle [109] ($> 5\sigma$)
$Y_b(10890)$	1^{--}	$10888.4^{+2.7}_{-2.6} \pm 1.2$	$30.7^{+8.3}_{-7.0} \pm 3.1$	$e^+e^- \to Y_b \to \Upsilon(1S,2S)\pi^+\pi^-$	Belle [111]
$Z_b^+(10610)$	1^+	10608.4 ± 2.0	15.6 ± 2.5	$e^+e^- \to \pi^\mp Z_b^\pm \to \pi^\mp(\Upsilon(1S,2S,3S)\pi^\pm)$ $e^+e^- \to \pi^\mp Z_b^\pm \to \pi^\mp(h_b(1P,2P)\pi^\pm)$	Belle [113]($> 10\sigma$)
$Z_b^+(10650)$	1^+	10653.2 ± 1.5	14.4 ± 3.2	$e^+e^- \to \pi^\mp Z_b^\pm \to \pi^\mp(\Upsilon(1S,2S,3S)\pi^\pm)$ $e^+e^- \to \pi^\mp Z_b^\pm \to \pi^\mp(h_b(1P,2P)\pi^\pm)$	Belle [113]($> 10\sigma$)

In Fig. 2.1 and Fig. 2.2 we show a summary of the experimental information available on the charmonium-like states, classifying them according to the production and decays modes respectively. Fig. 2.3 contains instead the bottomonium-like states.

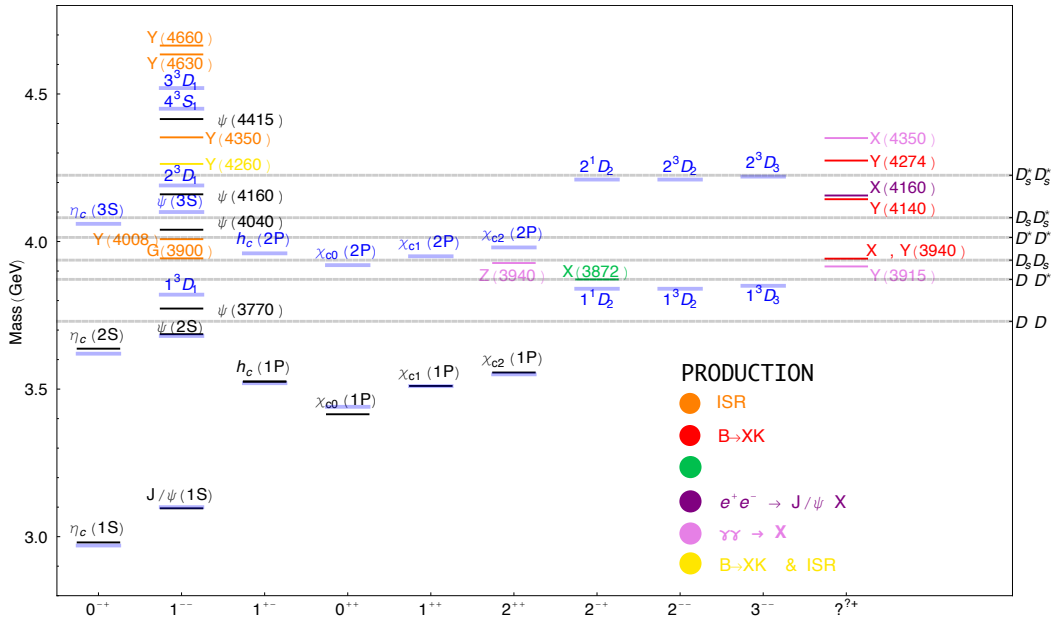

Figure 2.1. Spectrum of the XYZ mesons in the charm sector superimposed to the standard charmonia (blue lines show predictions, black lines experiments). The exotic states are classified according to their production mechanism. The dashed lines indicate the onset of the open-charm thresholds.

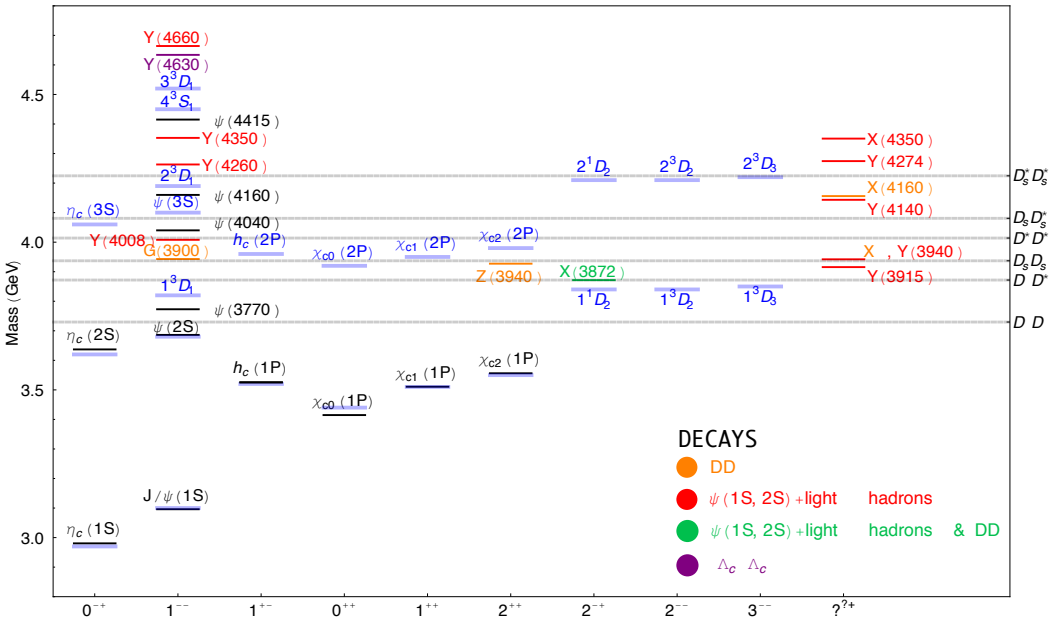

Figure 2.2. As in Fig. 2.1 but with the XYZ states classified according to their decay mechanism.

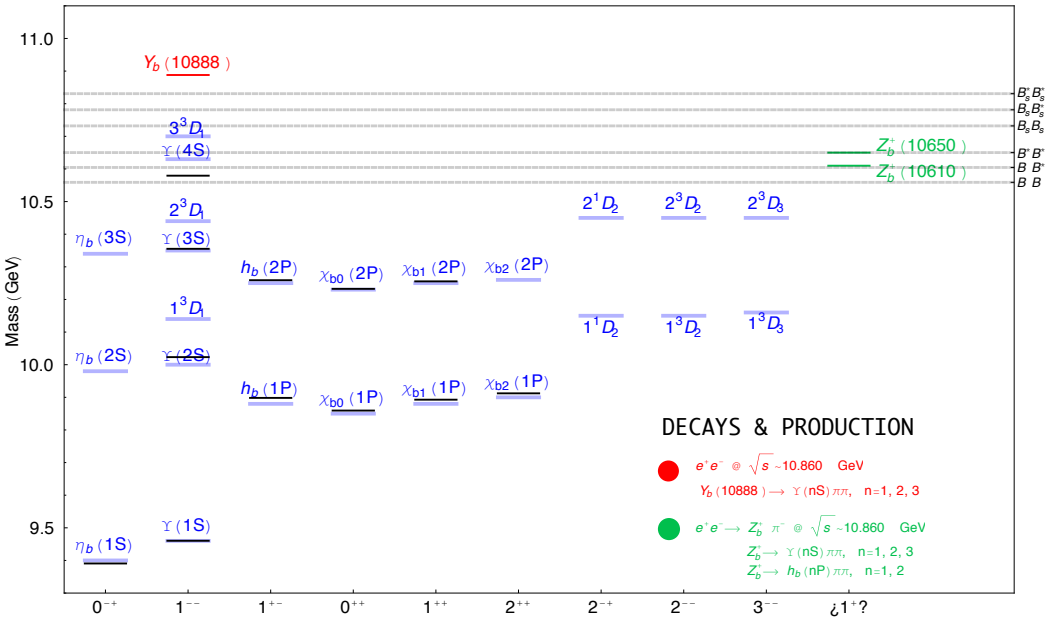

Figure 2.3. Spectrum of the XYZ mesons in the bottom sector superimposed to the standard bottomonia (blue lines show predictions, black lines experiments). The legend explains the production and decay modes. The dashed lines indicate the onset of the open-bottom thresholds.

2.2 Molecules

Meson molecules are bound states of two (or more) mesons. Hadronic molecules were proposed a long time ago to describe the deuteron as a bound state of nucleons. Later molecular candidates have been identified among the 0^+ light mesons. The first molecular interpretation in the charm meson sector was proposed for the $\psi(4040)$, observed in e^+e^- annihilations [114, 115].

Before analyzing the details of the dynamics we give some distinctive phenomenological signatures of meson molecules [116]:

1. In the light sector J^{PC} and flavor quantum numbers should be compatible with those of an $L = 0$ meson pair (nuclear forces which bind the two mesons together are short ranged so that a P-wave bound state seems unlikely). In the heavy mesons sector there is the possibility of P-wave bound states but this would imply the existence of more deeply bound S-wave molecules [117].

2. Binding energies should be of the order of 50 MeV for the light mesons and of the order of 10 MeV for the heavy ones. This is because the minimum distance required for the hadrons to maintain separate identities is $R \sim 1$ fm and the binding energy is $E_B \sim 1/(2\mu R^2)$ (where μ is the reduced mass). As an example $K\bar{K}$ molecules have $\mu \sim 500$ MeV and thus $E_B < 50$ MeV, whereas $D\bar{D}$ molecules have $\mu \sim 1$ GeV and thus $E_B < 10$ MeV, and finally for $B\bar{B}$ molecules $\mu \sim 5$ GeV leading to $E_B < 4$ MeV.

3. Large branching ratios into final states containing the constituent mesons despite the reduced phase space available.

4. Anomalous electromagnetic coupling with respect to ordinary charmonium states.

Binding mechanism. The spectrum of hadron bound states can be predicted once a model for the interaction between the hadrons has been proposed. The interaction between two hadrons varies with the distance:

Gluon Exchange. At short distance quarks inside the hadron interact with each other through the exchange of gluons. At first order in the strong coupling constant the non relativistic potential associated with one gluon exchange is Coulomb like. To this the typical linear term in the distance, which mimics confinement, is added:

$$V_{ij}^c = \left(-\frac{\alpha_s}{r_{ij}} + \frac{3}{4} b r_{ij}\right) \frac{\lambda_i^a}{2} \left(-\frac{\lambda_j^{a*}}{2}\right), \tag{2.22}$$

where r_{ij} is the distance between the i-th and j-th quarks or antiquarks which constitute the hadrons and b is a string tension parameter.

Relativistic corrections to the potential can be included, *i.e.* the spin-orbit and contact spin-spin interaction respectively

$$V_{ij}^r = -\frac{8\pi}{3} \frac{\alpha_s}{m_i m_j} \left(\frac{\sigma^3}{\pi^{3/2}} e^{-\sigma^2 r_{ij}^2}\right) (\vec{s}_i \cdot \vec{s}_j) \frac{\lambda_i^a}{2} \left(-\frac{\lambda_j^{a*}}{2}\right) + V^{SO}. \tag{2.23}$$

Table 2.4. Spin-isospin factor in the one-pion-exchange potential. $(\boldsymbol{\tau}_1 \cdot \boldsymbol{\tau}_2)(\boldsymbol{\sigma}_1 \cdot \boldsymbol{\sigma}_2) = \frac{1}{4}\left[I(I+1) - \frac{3}{2}\right]\left[S(S+1) - \frac{3}{2}\right]$.

S \ I	0	1
0	9/16	−3/16
1	−3/16	+1/16

The hyperfine term can be understood as a dipole-dipole interaction: to each quark is associated a chromo-magnetic dipole moment which is proportional, just as in the electron case, to the strong coupling e_s and to the inverse of its mass. This spin-spin term is weighted by a smeared delta function, usually a gaussian, which accounts for the short distance nature of the interaction. Using this potential to reproduce the conventional meson and baryon spectra one can obtain the value of the phenomenological parameters. There is generally a quite broad agreement in the literature [118, 119, 120].

Meson exchange. At long distance the exchange of mesons (π, ω, ρ, ...) between the hadrons themselves is dominant. The existence of bound states of two mesons due to one-pion-exchange was proposed for the first time by Tornqvist in [121]. The inspiration came from the deuteron, a bound state of two nucleons which interact through the long range potential:

$$V_\pi(\boldsymbol{r}) = \frac{g_{\pi N}^2}{3}(\boldsymbol{\tau}_1 \cdot \boldsymbol{\tau}_2)\left[(3(\boldsymbol{\sigma}_1 \cdot \hat{\boldsymbol{r}})(\boldsymbol{\sigma}_2 \cdot \hat{\boldsymbol{r}}) - \boldsymbol{\sigma}_1 \cdot \boldsymbol{\sigma}_2) W(r) + (\boldsymbol{\sigma}_1 \cdot \boldsymbol{\sigma}_2)\right] \frac{e^{-m_\pi r}}{r}, \tag{2.24}$$

where

$$W(r) = 1 + \frac{3}{(m_\pi r)^2} + \frac{3}{m_\pi r} \tag{2.25}$$

$\boldsymbol{\sigma}_{1,2}$ are the spins of the nucleons, and $\boldsymbol{\tau}_{1,2}$ their isospins. The potential contains a scalar term proportional to the spin-isospin factor with a pure Yukawa interaction, and a tensor term, which is a higher order correction. In the deuteron case the spin-isospin factor gives an indication of the binding channels (see Table 2.4):

$$(\boldsymbol{\tau}_1 \cdot \boldsymbol{\tau}_2)(\boldsymbol{\sigma}_1 \cdot \boldsymbol{\sigma}_2) = \frac{1}{4}\left[I(I+1) - \frac{3}{2}\right]\left[S(S+1) - \frac{3}{2}\right]. \tag{2.26}$$

The binding is expected in the $(S = 0, I = 1)$ channel and in the $(S = 1, I = 0)$ channel, the deuteron one. The first possibility is ruled out when including also the tensor term, which instead strengthens the attraction in the second configuration adding a D-wave component.

Tornqvist speculated on the possibility that such a potential could bind pairs of mesons, calling *deusons* these deuteron-like bound states. Since the pion is very light, deusons can be very large, much larger than ordinary $q\bar{q}$ mesons. For ground state mesons there are two possibilities: pseudoscalar-vector mesons

and vector-vector mesons, since bound states of pseudoscalar-pseudoscalar mesons are forbidden by parity. In these cases π mesons are exchanged in P-wave. If one allows higher values of the relative orbital angular momentum between the mesons, the spectroscopy becomes more complicated and more detailed calculation are needed. Moreover in [117, 122] the possibility for the exchange of pions in S-wave has been considered.

Manohar and Wise studied in [123] the interaction between two heavy-light mesons $Q\bar{q}$ and considered the possibility that a BB bound state could exist. Their derivation of the potential proceeds from the Heavy Quark Effective Theory formalism combined with the chiral Lagrangian approach to describe the light pseudoscalar mesons. Their potential agrees with Eq. (2.24) . The same calculation scheme is applied by Tornqvist in [124] to meson-antimeson bound states. The only parameter of the model, besides the mesons masses, is the pion-meson-meson coupling g. Its value can be deduced from the πN coupling exploiting the relation

$$\frac{g_{\pi N}^2}{4\pi} = \frac{25}{9}\frac{g^2}{f^2}m_\pi^2 \tag{2.27}$$

where f is the decay constant of the pion. The measured value $g_{\pi N}^2 \sim 1$ leads to $g^2 \sim 0.6$. A striking confirmation of this estimate is the prediction of the D^* width of $\sim$70 KeV. The potential is computed for each of these states paying attention to the fact that there will be some coupled channels (states with same J and S but different L will mix with each other).

Nevertheless, because of the singular nature of the tensor part of the potential, *i.e.* the first term in (2.24), a regularization procedure is needed. The most natural method is to introduce a form factor at the πN vertex, which gives to the pion source a spherical extension with radius $R \sim 1/\Lambda$, Λ being an ultraviolet cutoff. Even if the phenomenological knowledge of the cutoff Λ is rather poor, it may be fixed by comparison with nuclear physics. From NN interactions Λ must be in the range 0.8-1.5 GeV, while to reproduce the deuteron binding energy one needs Λ $\sim$0.8 GeV. The value employed in [124] and in the literature in general is Λ $\sim$1.2 GeV, which seems appropriate for D mesons. It is crucial here to emphasize that the existence or otherwise of meson-antimeson bound states depends strongly on the value chosen for Λ [121, 119].

Spectra. We briefly review the results for the spectra of possible molecular states as obtained in the two approaches.

Gluon exchange. This interaction scheme has been used mainly to study the light sector. Either a Schrödinger equation has been solved using the OGE potential of Eq. (2.22,2.23), or an effective potential between the two mesons has been derived by the Born order scattering amplitude.

The scalars $f_0(975)$, $a_0(980)$ have been indicated as candidates to be $K\bar{K}$ states [125, 126, 118], while the $f_1(1420)$ as a $K^*\bar{K}$ bound state [127, 128].

Meson exchange. Bound states of mesons due to one-pion-exchange have been studied in [123, 124] and many others. In [124] the Schroedinger equation with the one-pion-exchange potential of Eq. (2.24) has been solved with numerical methods. The results in the hidden-charm and hidden-bottom sector are summarized in Table 2.5. The general pattern is that for pseudoscalar-vector mesons the binding is more likely in $J^{PC} = 0^{-+}, 1^{++}$, while for vector-vector ones in $J^{PC} = 0^{-+}, 0^{++}, 1^{+-}, 2^{++}$. In both cases the favored isospin configuration is $I = 0$. In [129] Swanson obtained the same results for the vector-vector heavy-heavy mesons bound states, except for the fact that he found only one $D^*\bar{D}^*$ bound state with $J^{PC} = 0^{++}$.

Table 2.5. Hidden charm and hidden bottom meson-antimeson bound states found in [124]. The $D^{(*)}\bar{D}^{(*)}$ are predicted to be almost at threshold, compatible with zero binding energy, while for the $B^{(*)}\bar{B}^{(*)}$ molecule the typical binding energy is of the order of 50 MeV.

Constituents	M (MeV)	J^{PC}	Λ(GeV)
$D\bar{D}^*$	~ 3870	0^{-+}	> 1.5
	~ 3870	1^{++}	1.2
$D^*\bar{D}^*$	~ 4015	0^{-+}	1.5
	~ 4015	0^{++}	1.2
	~ 4015	1^{+-}	1.3
	~ 4015	2^{++}	1.2
$B\bar{B}^*$	~ 10545	0^{-+}	1.2
	~ 10562	1^{++}	1.2
$B^*\bar{B}^*$	~ 10590	0^{-+}	1.2
	~ 10582	0^{++}	1.2
	~ 10608	1^{+-}	1.2
	~ 10602	2^{++}	1.2

Decays. The decay modes of a meson-meson bound state can be divided into two classes: *long-distance* decay modes and *short-distance* decay modes.

The former class consists of the decay modes of the constituent mesons. The partial decay widths of the molecular state in these modes are related to those of its constituent mesons. If the binding energy is very small, nearly zero, the partial decay widths of the molecule in these channels will be almost equal to the ones of its constituents, whereas for deeply bound states one expects large deviation from the free meson widths. In particular a large binding energy tends to stabilize the meson when it is bound.

The latter class of decay modes, the short-distance one, is a manifestation of the existence of some inelastic channels in the meson-meson scattering mechanism. The associated partial decay widths are proportional to the probability that the two mesons come together at a point, which is given by the square modulus of the bound state wave function at the origin $|\Psi(0)|^2$.

2.2.1 Candidates

$X(3872)$. The vicinity of the $X(3872)$ mass to the $D^0\bar{D}^{0*}$ threshold led many authors to interpret this resonance as a $D^0\bar{D}^{0*}$ S-wave molecule

$$\frac{|D\bar{D}^*\rangle \pm |\bar{D}D^*\rangle}{\sqrt{2}}, \tag{2.28}$$

in the hypothesis of $J^{PC} = 1^{++}$. Potential models [124, 130, 120] predict that $I = 0$ states are favored with respect to $I = 1$ ones. This would imply an equal contribution of the charged and neutral meson components:

$$|D\bar{D}^*\rangle = \frac{|D^0\bar{D}^{0*}\rangle + |D^+D^{-*}\rangle}{\sqrt{2}}. \tag{2.29}$$

Nevertheless since the $D^{+*}D^-$ threshold (∼3879 MeV) lies ∼8 MeV above the $D^{0*}\bar{D}^0$ threshold (∼3871 MeV) $D^*\bar{D}$ should have a smaller weight than $D^{0*}\bar{D}^0$ in the wave function, which means that there will be a strong $I = 1$ component in the state [131, 132, 133].

It is worth to notice that using one-pion-exchange Suzuki in [134] concluded that the X cannot be regarded as an analog of the deuteron. The author considers more likely that the binding proceeds through the coupling to charmonium states, due to u, d quark exchange.

For what concerns the width of the state the main arguments follow from the *low-energy universality* [135] of such a loosely bound molecule: its properties depend only on the scattering length a and are insensitive to the details of the interactions between D^0 and $\bar{D}^{0*}$. Indeed an S-wave $D^0\bar{D}^{0*}$ molecule with an extremely small binding energy $E_B \sim 0.25$ MeV, much smaller than the typical energy scale m_π^2/μ ∼20 MeV, exhibits an unnaturally large scattering length $a = \sqrt{2\mu E_B} \sim 8$ fm. Low energy universalities implies that short-distance decay modes, like J/ψ + light hadrons, are suppressed by a factor $\sim 1/a$. They have been studied in detail in [136]. On the other hand the long-distance decays, the constituents ones, contribute at most with ∼ 100 KeV. Their effects on the line shapes of the resonance have been considered in [137, 138]. The line shapes have been also studied in [139, 140, 141, 142]. Other decay modes have been considered in the hypothesis of X being a loosely bound $D^0\bar{D}^{0*}$ molecule: $X \to \chi_{cJ}\pi^0$ [143, 144] and $X \to D\bar{D}\gamma$ [145].

The production of a $D^0\bar{D}^{0*}$ molecule necessarily proceeds through the production of a D meson pair. This production mechanism has been extensively studied in B decays [146, 147]. The prompt production in $p\bar{p}$ collisions will be extensively discussed in the next chapter, where we will present our original results.

$Y(3940)$ and **$Y(4140)$**. The molecular nature of the $Y(3940)$ has been considered as a possibility by a number of authors [148, 149, 150, 151]. According to this picture, the hadronic wave function would be

$$\frac{|D^{*+}D^{*-}\rangle + |D^{*0}\bar{D}^{*0}\rangle}{\sqrt{2}}, \tag{2.30}$$

with $J^{PC} = 0^{++}$ or 2^{++}. In this scenario the $Y(3940)$ would have a molecular partner, the $Y(4140)$, with composition $D_s^*\bar{D}_s^*$, quantum numbers $J^{PC} = 0^{++}$ or

2^{++} and a similar binding energy of about 80 MeV [152, 153, 154]. This idea is supported by the fact that the mass difference between these two mesons is approximately the same as the mass difference between the ϕ and ω mesons: $m_{Y(4140)} - m_{Y(3940)} \sim m_\phi - m_\omega \sim 210$ MeV. However, with a meson exchange mechanism to bind the two charmed mesons, it seems natural to expect a more deeply bound system in the case that pions can be exchanged between the two charmed mesons, as in D^*D^*, than when only η and ϕ mesons can be exchanged, as $D_s^*D_s^*$ [155]. The molecule picture predicts that the decays proceed via rescattering to hidden and open charm states at the same rate, so that decays to $D\bar{D}$ and $D\bar{D}^*$ are foreseen. Another prediction of the molecular hypothesis is that the constituent mesons can decay independently, leading to $D_s^{*+}D_s^-\gamma$ and $D_s^{*-}D_s^+\gamma$ [148, 156, 157]. Predictions for the radiative decays $Y(3940)/Y(4140) \to \gamma\gamma$ in [151, 158] yield similar results for the J^{PC} 0^{++} and 2^{++} assignments. In addition, a $D^{*+}D_s^{*-}$ molecule is predicted with a mass of about 4040 MeV, decaying to $J/\psi\,\rho$ [159].

***X*(4350)**. Due to its production mechanism and its decay mode, the possibility that $X(4350)$ could be interpreted as a molecular $D_s^{*+}D_{s0}^{*-}$ state has been considered in [154, 160]. In [161] a QCD sum rules study has been performed to test whether the $X(4350)$ can be an exotic $J^{PC} = 1^{-+}$ $D_s^*D_{s0}^*$ (or $D^*D_0^*$) molecular state. The mass value obtained is inconsistent with the experimental measurement.

***Y*(4260)** and ***Y*(4350)**. In [117] a possible interpretation of the $Y(4260)$ and $Y(4350)$ as D_1D^* molecular states has been proposed: pion exchange between D_1 and D^* here happens in S-wave, whereas in the $D^0\bar{D}^{0*}$ interpretation of $X(3872)$ it occurs in P-wave. A distinctive decay channel would be $D\bar{D}3\pi$. Other molecular assignments have been proposed: $\rho^0\chi_{c1}$ [162] or $\omega\chi_{c1}$ [163] or $D_1\bar{D}/D_0\bar{D}^*$ [164].

***Y*(4660)**. Due to the proximity of its mass to the $\psi' f_0(980)$ threshold, the $Y(4660)$ state, was considered as a $\psi' f_0(980)$ bound state in [165]. If this interpretation of the $Y(4660)$ were correct, heavy quark spin symmetry would imply the existence of a $\eta_c' f_0(980)$ bound state [166]. This state would decay mainly into $\eta_c'\pi\pi$, and the authors of [166] predicted the mass of such a state to be $\simeq 4616$ MeV. The enhancement at ~ 4630 MeV in the $\Lambda_c^+\Lambda_c^-$ distribution has been suggested to be a final state interaction effect of the $Y(4660) \to \Lambda_c^+\Lambda_c^-$ [167].

***Z*$^+$(4430)**. An interpretation as a $\bar{D}_1D^*$ molecular state has been discussed in [168, 169, 170, 171, 172]. Considering the $Z^+(4430)$ as a loosely bound S-wave D^*D_1 molecular state, the allowed angular momentum and parity are $J^P = 0^-,\ 1^-,\ 2^-$, although the 2^- assignment is probably suppressed in the $B^+ \to Z^+K$ decay by the small phase space. Among the remaining possible 0^- and 1^- states, the former will be more stable as the latter can also decay to DD_1 in S-wave. Moreover, one expects a bigger mass for the $J^P = 1^-$ state as compared to a $J^P = 0^-$ state. The molecule explanation predicts that the $Z^+(4430)$ decays into $D^*\bar{D}^*\pi$ [168] through the decay of its constituents and into $\psi(2S)\pi$ via rescattering [173].

There is also a quenched lattice QCD calculation that finds attractive interaction for the D^*D_1 system in the $J^P = 0^-$ channel [174]. The authors of [174] also find positive scattering length. Based on these findings, they conclude that although

the interaction between the two charmed mesons is attractive in this channel, it is unlikely that they can form a genuine bound state right below the threshold.

$Z_1^+(4050)$, $Z_2^+(4250)$. Due to the closeness of the $Z_1^+(4050)$ and $Z_2^+(4250)$ masses to the $D^*\bar{D}^*$ and $D_1\bar{D}$ thresholds, these states could be interpreted as molecular states or threshold effects. However, since the mass of $Z_1^+(4050)$ is above the $D^*\bar{D}^*$ threshold, the molecular interpretation is disfavored, even if studies present in the literature give contradictory results: strong attraction for the $D^*\bar{D}^*$ system with $J^P = 0^+$ is found in [175] using a meson exchange model, whereas the author of [176] concluded that that the interpretation of $Z_1^+(4050)$ as a $D^*\bar{D}^*$ molecule is not favored using a boson exchange model. In the case of $Z_2^+(4250)$ again a meson exchange model indicates that its interpretation as a $D_1\bar{D}$ or $D_0\bar{D}^*$ molecule is disfavored [164].

$Z_b^+(10610)$ and $Z_b^+(10650)$. The proximity of the masses of $Z_b^+(10610)$ and $Z_b^+(10650)$ to the $B\bar{B}^*$ and $B^*\bar{B}^*$ thresholds favored the molecular interpretation of these states. This interpretation would indeed explain the similar decay rates into Υ and h_b, bottomonia with $S = 1$ and $S = 0$ respectively [177]. As detailed in Appendix C, B and B^* are associated to the bilinears $\bar{b}\gamma^5 q$ and $\bar{b}\gamma^i q$ respectively, see Table C.1. In the non relativistic limit they reduce to $\bar{b}q$ and $\bar{b}\sigma^i q$, in the Weyl basis. Thus the $B\bar{B}^*$ and $B^*\bar{B}^*$ bound states with $J^P = 1^+$ are

$$\begin{aligned} |B\bar{B}^*\rangle + |B^*\bar{B}\rangle \quad &\sim (\bar{b}q)(\bar{q}'\sigma^i b) + (\bar{b}\sigma^i q)(\bar{q}' b) \\ &\sim (\bar{b}\sigma^i b)(\bar{q}' q) + (\bar{b}b)(\bar{q}'\sigma^i q) \sim (\bar{b}b)_{1^-}\ (\bar{q}'q)_{0^-} + (\bar{b}b)_{0^-}\ (\bar{q}'q)_{1^-} \end{aligned} \tag{2.31}$$

$$\begin{aligned} |B\bar{B}^*\rangle \quad &\sim \epsilon_{ijk}(\bar{b}\sigma^j q)(\bar{q}'\sigma^k b) \\ &\sim (\bar{b}\sigma^k b)(\bar{q}' q) - (\bar{b}b)(\bar{q}'\sigma^k q) \sim (\bar{b}b)_{1^-}\ (\bar{q}'q)_{0^-} - (\bar{b}b)_{0^-}\ (\bar{q}'q)_{1^-}, \end{aligned} \tag{2.32}$$

where we have used the Fierz identity for Pauli matrices in Eq. (D.11) of Appendix D[3]. The two bound states contain 0^- and 1^- $b\bar{b}$ states with the same weight, so that no spin flip is thus required for such states to decay into Υ and h_b. It was also argued [178] that including $Z_b^+(10610)$ and $Z_b^+(10650)$ one can explain the anomalous $\Upsilon(2S)\pi^+\pi^-$ production observed in the $\Upsilon(5S)$ decay, without invoking the existence of a $[bq][\bar{b}\bar{q}]$ tetraquark state.

Sum rules have been used to determine the mass of a $B\bar{B}^*$ S-wave molecule finding good agreement with the experimental value [179]. Assuming the molecular nature of these resonances, the existence of an isospin multiplet of similar states is predicted in [180]. A dynamical study was carried out in [181], whereas the similarity of $Z_b(10610)$ to $X(3872)$ was studied in [182, 183, 184]. In [185] the one-boson-exchange model was applied to test the likelihood of the binding.

2.3 Hybrids

Beside envisaging the possibility of four quark mesons, the QCD Lagrangian contains also the gluons, which can act as dynamical degrees of freedom besides being the

[3] $(\bar{b}q)(\bar{q}'\sigma^i b) = (\bar{b}\sigma^i b)(\bar{q}' q) + (\bar{b}b)(\bar{q}'\sigma^i q) + i\epsilon_{jik}(\bar{b}\sigma^k b)(\bar{q}'\sigma^j q)$
$(\bar{b}\sigma^i q)(\bar{q}' b) = (\bar{b}\sigma^i b)(\bar{q}' q) + (\bar{b}b)(\bar{q}'\sigma^i q) + i\epsilon_{ijk}(\bar{b}\sigma^k b)(\bar{q}'\sigma^j q)$.

particles which mediate strong interactions. One can indeed suppose the existence of *gluonic hadrons*, bound states of gluons and quarks. There are two kinds of gluonic hadrons: the *glueballs*, which are bound states of only gluons, and the *hybrids* which are $q\bar{q}g$ bound states, *i.e.* $q\bar{q}$ states with a gluonic excitation. This is not surprising from the point of view of color, since $q\bar{q} \in \mathbf{8}_c \oplus \mathbf{1}_c$ and $g \in \mathbf{8}_c$ and one can pick a singlet component from the $\mathbf{8}_c \otimes \mathbf{8}_c$ configuration. In this section we will focus on hybrid mesons.

The existence of hybrid mesons was suggested in 1976 by Jaffe and Johnson [186] and Vainsthein and Okun [187]. Hybrids have been studied using different approaches [188]: (*i*) the MIT bag model; (*ii*) an adiabatic heavy-quark bag model; (*iii*) constituent gluon models; (*iv*) heavy quark lattice gauge theory; (*v*) the flux-tube model. The average mass obtained for the lightest hybrid with light quarks is about 1.5-2 GeV. Hybrids can exhibit exotic J^{PC} quantum numbers, and thus can be easily identified experimentally.

The MIT [189, 190] bag model predicts the existence of a lightest hybrid mesons mulitplet at $\sim$1.5 GeV and the presence of an exotic 1^{-+} state in this multiplet. The exotic J^{PC} quantum numbers are due to the boundary conditions in the bag.

For the heavy quarks a spherical bag would be quite unrealistic, and thus an adiabatic bag model was introduced by Hasenfratz, Horgan, Kuti and Richard in [191]. In this model the bag was allowed to deform in the presence of a fixed $Q\bar{Q}$ source. The resulting potential was used in a Schrödinger equation to compute the mass of the hybrids. The lightest hybrid for $c\bar{c}$ was found at $\simeq$3.9 GeV, whereas it lies at $\simeq$10.5 GeV for $b\bar{b}$. For a recent result on adiabatic potentials in QCD string models see [192].

Constituent gluon models treat the gluon as the constituent quark model treat the quarks. These models have been introduce by Horn and Mandula in [193] and later developed by Tanimoto, Iddir et al. [194, 195, 196] and Ishida et al. [197, 198]. The gluon has a fixed orbital angular momentum l_g relatively to the $q\bar{q}$ pair which is in a defined orbital and spin configuration $(l_{q\bar{q}}, s_{q\bar{q}})$. The quantum numbers of such a bound state are somewhat different from the ones predicted in other models: $P = (-1)^{l_g + l_{q\bar{q}}}$ and $C = (-1)^{l_{q\bar{q}} + s_{q\bar{q}} + 1}$. The lightest hybrid states in this model have $l_g = 0$ and thus non exotic quantum numbers, such as 1^{--}, are obtained using P-wave $q\bar{q}$ states with $s_{q\bar{q}} = 1$, while exotic quantum numbers, like 1^{-+}, require $s_{q\bar{q}} = 0$.

Lattice QCD is supposed to give the most reliable predictions for absolute hybrid masses. In heavy quark lattice QCD in which the $Q\bar{Q}$ pair is kept fixed while the gluonic degrees of freedom are allowed to be excited, the lightest charmonium hybrid was predicted in [199] to have a mass of $\simeq$ 4.2 GeV for $c\bar{c}$ and $\simeq$ 10.81 GeV for $b\bar{b}$.

Finally the flux-tube model, which is the most widely used model for hybrids. In lattice QCD two separated color sources are confined by approximately cylindrical regions of color fields if they are sufficiently far apart. The flux-tube model describes this confinement in a simple dynamical way, approximating the confining region between quarks with a string of massive points. This approach is motivated by the strong coupling expansion of lattice QCD. Since in a lattice gauge theory the flux lines can be expanded only in transverse directions, in the flux-tube models one allows only for transverse spatial fluctuations of the massive point positions. In the first studies with this model an adiabatic separation of the quark and gluon degrees

of freedom was carried out, exploiting the fast dynamical response of the flux-tube degrees of freedom with respect to the heavy quarks time scales. This separation allows to fix the $Q\bar{Q}$ separation at some value R and compute the eigen energy of the system in some fixed configuration of the flux-tube: $E_\Lambda(R)$. The ground state $\Lambda = 0$ gives the ordinary mesons spectrum. Hybrids are obtained for $\Lambda > 0$ and can be studied using the excited potential $E_\Lambda(R)$. The lightest hybrid state is the one in which the string has a single orbital excitation about the $Q\bar{Q}$ axis. In initial models the adiabatic potentials were determined in the approximation of small fluctuations relatively to the $Q\bar{Q}$ axis. This approximation was removed by Barnes, Close and Swanson in [188]. In the charmonium family, hybrids are predicted in the mass region of 4.3 GeV, with an estimated uncertainty of $100 \div 200$ MeV. As for the bottom sector, hybrids are predicted in the region $10.7 \div 11.0$ GeV.

While the masses of hybrid mesons are computable in all the models listed above, and in particular in lattice QCD, the decay dynamics is more difficult to study. The only model which offers a description of the decay dynamics is the flux-tube model. Indeed in this context the decay occurs when the flux-tube breaks at any point along its length, producing in the process a $q\bar{q}$ pair in a relative $J^{PC} = 0^{++}$ state. A similar model has been applied to the ordinary $Q\bar{Q}$ mesons, since, as we stated before, the flux-tube model in its ground state describes ordinary mesons. The distance from the $Q\bar{Q}$ axis at which the light pair is created is controlled by the transverse distribution of the flux-tube. This distribution varies when going from the non-excited flux-tube to the first excited flux-tube configuration. Exploiting the empirical success of this model in describing the ordinary mesons decay dynamics, Close and Page derived the decay pattern for hybrids in [200]. They found that in a two meson decays the unit of orbital angular momentum of the incoming hybrid around the $Q\bar{Q}$ axis is exactly absorbed by the component of the angular momentum of one of the two outgoing mesons along this axis. In [200] they treated explicitly the light flavor case, but a generalization to hybrid charmonia is straightforward. The final state should be in this case $D^{(*,**)}\bar{D}^{*,**}$, where D^{**} indicates a D-meson which is formed from P-wave $c\bar{q}$ ($q = u, d$) pairs. However, since the masses predicted in the flux-tube model are $\simeq$4.3 GeV, *i.e.* below the DD^{**} threshold, it is possible that this final state is kinematically forbidden giving a rather narrow resonance decaying into charmonium plus light hadrons. These modes offer a clear experimental signature and furthermore should have large branching fractions if the total width is sufficiently small.

2.3.1 Candidates

$\boldsymbol{X(3940)}$, $\boldsymbol{Y(4140)}$, $\boldsymbol{Y(4260)}$, $\boldsymbol{Y(4350)}$ and $\boldsymbol{Y(4660)}$. The hybrid interpretation for the $Y(4260)$ has been proposed in [201, 202, 203]. Its mass lies infact in the ball park predicted by lattice QCD [204] and flux tube models. Actually, recent lattice simulations [205] and QCD string models calculations [206], predict that the lightest charmonium hybrid has a mass of about 4400 MeV, which is closer to the mass of the $Y(4350)$, thus not excluding the interpretation of the latter as an hybrid.

A prediction of the hybrid hypothesis is that the dominant open charm decay mode, would be a meson pair with one S-wave D meson (D, D^*, D_s, D_s^*) and one P-wave D meson (D_1, D_{s1}) [207, 201, 200]. In the case of the $Y(4260)$ this

suggests dominance of the decay mode $D\bar{D}_1$. Therefore, a large $D\bar{D}_1$ signal could be understood as a strong evidence in favor of the hybrid interpretation for the $Y(4260)$. Up to now the Belle experiment did not find evidence for such a signal [208, 209].

In the case of the $Y(4350)$ and $Y(4660)$, since their masses are well above the $D\bar{D}_1$ threshold, their decay rates into $D\bar{D}_1$ should be very large if they were charmonium hybrids.

Another prediction of the hybrid scenario is the existence of partner states: the flux tube model predicts a multiplet of states nearby in mass with conventional quantum numbers (0^{-+}, 1^{+-}, 2^{-+}, 1^{++}, 1^{--}) and states with exotic quantum numbers (0^{+-}, 1^{-+}, 2^{+-}) [173]. Among them a possible candidate for the 1^{-+} resonance has been identified in the $Y(4140)$ [159, 210], whereas the non exotic 0^{-+} could be the $X(3940)$, explaining thus why it does not decay into $D\bar{D}$ [211]. Indeed spin dependent splittings place two states, 0^{-+} and 1^{-+}, below the vector 1^{--} with equal mass gaps of the order of 100 MeV [189, 190, 212, 213].

2.4 Hadroquarkonium

Recently [214] a new interpretation has been proposed for the states with $J^{PC} = 1^{--}$ in the region $4.2 - 4.6$ GeV, namely $Y(4260)$-$Y(4350)$-$Y(4660)$, and for the only charged state observed at 4.43 GeV, namely the $Z^+(4430)$.

These states show a common feature, they decay prominently either into J/ψ or into $\psi(2S)$. None of them is observed in both final states. Furthermore the decay into open-charm mesons is highly suppressed. These evidences have been explained hypothesizing that a standard charmonium state can get stuck inside a light hadron, drawing inspiration from the much discussed case of charmonium states bound inside a nucleus. This exotic structure has been called *hadrocharmonium*. The light hadronic matter acts as a spatial extended environment in which the more compact J/ψ or $\psi(2S)$ moves. This picture is at least able to explain why the decay into J/ψ or $\psi(2S)$ is favored or suppressed, depending on which charmonium state is bound inside the hadron.

The $c\bar{c}$ chromo-electric dipole moment interacts with the chromo-electric field generated by the light hadronic matter as in hadronic transitions, Section 1.2.4. This interaction can be treated with the multipole expansion in QCD. The chromo-electric dipole moment is proportional to the chromo-electric field $\mathbf{E}^a$ through the chromo-polarizability α, so that the effective interaction hamiltonian takes the form:

$$H_{eff} = -\frac{1}{2}\alpha_{ij}^{(12)} E_i^a E_j^a, \tag{2.33}$$

where

$$\alpha_{ij}^{(12)} = \frac{1}{16}\langle 1S|\xi^a r_i \mathcal{G} r_j \xi^a|2S\rangle, \tag{2.34}$$

$\mathcal{G}$ being the two point Green function of the heavy quark pair in a color octet configuration. In the leading non relativistic order for transitions in S-wave, $\alpha_{ij}^{(12)}$ actually reduces to a scalar $\alpha^{(12)}$, which can be deduced from the decay $\psi' \to J/\psi\,\pi^+\pi^-$, discussed in Section 1.2.4. On the other hand the average value of the product of chromo-electric fields over the light hadron X can be estimated using the

conformal anomaly relation in QCD:

$$\langle X|\frac{1}{2}\mathbf{E}^a \cdot \mathbf{E}^a|X\rangle \geq \frac{8\pi^2}{9}M_X. \tag{2.35}$$

In this way one is able to estimate the strength of the interaction between the light hadronic matter and the quarkonium system bound inside it. The possibility that such a bound state exists depends on the relation between the mass M_X and the spatial extension of the light hadron. In particular in [215] it has been shown that a quarkonium state does form a bound state inside a sufficient highly excited light hadron. Furthermore the authors in [215] found that for this kind of bound state the decay into open heavy flavor mesons is suppressed exponentially as $\exp\left(-\sqrt{\Lambda_{QCD}}/M_Q\right)$, which would explain the non observation of the decay of the Y resonances into pairs of charmed mesons.

Chapter 3

Tetraquarks

Tetraquarks can be described as *diquark-antidiquark* bound states. In Section 3.1 we will clarify why diquarks are likely to be stable bound states of two quarks, behaving as point like objects. Then, in Section 3.2 and 3.3, we will build tetraquarks from diquarks and discuss theoretical predictions. In particular we will construct a string model for $L = 1$ tetraquarks, P-wave diquark-antidiquark bound states: first, to test the model, we will show how well it describes the standard charmonium and bottomonium spectra (Section 3.3.1), then we will exploit it to interpret two of the XYZ mesons as two subsequent radial excitations of a $L = 1$ tetraquark (Section 3.3.2).

3.1 Diquarks

A tetraquark state is built out of two quarks and two antiquarks. Indeed a color neutral state can be obtained out of two quarks and two antiquarks since

$$\mathbf{3}_c \otimes \mathbf{3}_c \otimes \bar{\mathbf{3}}_c \otimes \bar{\mathbf{3}}_c = \mathbf{1}_c \oplus \mathbf{8}_c^a \oplus \mathbf{8}_c^s \oplus \mathbf{10}_c. \tag{3.1}$$

There are indications, both experimental and theoretical, that is very likely that two quarks in antisymmetric color configuration $\bar{\mathbf{3}}_c$ bind into a point like object called *diquark*: $\mathfrak{q} = [q_1 q_2]_{\bar{\mathbf{3}}_c}$. An antidiquark is instead a bound state of two antiquarks in color $\mathbf{3}_c$ configuration: $\bar{\mathfrak{q}} = [\bar{q}_1 \bar{q}_2]_{\mathbf{3}_c}$.

We will first give some hints on the phenomenological indications in favor of diquarks and we will classify them in terms of flavor and spin-parity quantum numbers. Then assuming the diquarks as colored point like objects, we will build tetraquarks as diquark-antidiquark bound states focusing on the hidden-charm and hidden-bottom sector which is relevant in the study of the XYZ mesons.

One Gluon Exchange. At the lowest order in perturbation theory the interaction between two quarks or between quark and antiquark is mediated by the exchange of a single gluon , as depicted in Fig. 3.1. The associated color factor is

$$Q(R_1 \otimes R_2) = \sum_{A,B} T^A_{ji} T^B_{lk} \delta_{AB} \equiv \sum_A T^A_{R_1} T^A_{R_2}, \tag{3.2}$$

where T^A_R is the $SU(3)_c$ generator in the representation R, and δ_{AB} comes from the gluon propagator. With R_1 and R_2 we indicate the $SU(3)_c$ representation to which

the two two fermionic lines belong to. If we are dealing with a quark and an antiquark then $R_1 = \mathbf{3}_c$ and $R_2 = \bar{\mathbf{3}}_c$, if we are dealing with two quarks then $R_1 = R_2 = \mathbf{3}_c$. Eq. (3.2) represents the product of color charges of the quark-antiquark or quark-

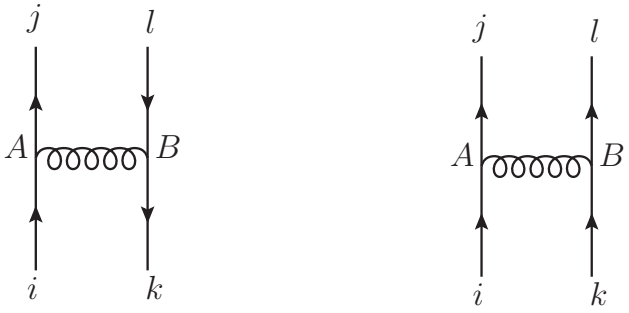

Figure 3.1. Feynman diagrams for the one gluon exchange between quark and antiquark (left) and between two quarks (right).

quark aggregate. To expect the binding, in this simple perturbative approach, one requires this product to be negative. Evidently it will depend on which is the tensor representation $R = R_1 \otimes R_2$ we are considering, since as detailed in Appendix B, we can rewrite Eq. (3.2) in the form

$$Q(R) = \frac{1}{2}\left(C(R) - C(R_1) - C(R_2)\right), \qquad \text{with } R = R_1 \otimes R_2. \tag{3.3}$$

$C(R)$ is defined as

$$\sum_A \left(T_R^A\right)^2 = C(R)\mathbf{1} \tag{3.4}$$

and is related to the constant $k(R)$, which fixes the generator normalization[1], by

$$C(R) = k(R)\frac{\dim(G)}{\dim(R)}. \tag{3.5}$$

with $\dim(G)$ the group dimension and $\dim(R)$ the representation dimension.

We are interested in

$$qq \in \mathbf{3}_c \otimes \mathbf{3}_c = \bar{\mathbf{3}}_c \oplus \mathbf{6}_c, \tag{3.6}$$

$$q\bar{q} \in \mathbf{3}_c \otimes \bar{\mathbf{3}}_c = \mathbf{1}_c \oplus \mathbf{8}_c. \tag{3.7}$$

To understand the decompositions of Eq. (3.6)-(3.7) we remind that each quark belongs to the fundamental representation of the $SU(3)$ color group and can be indicated with a vector with upper index

$$v^i \in \mathbf{3}_\mathrm{c}. \tag{3.8}$$

On the other hand an antiquark is represented as a vector with lower index

$$v_i \in \bar{\mathbf{3}}_\mathrm{c}. \tag{3.9}$$

[1] $\mathrm{tr}(T_R^A T_R^B) = k(R)\delta^{AB}$

A qq state will thus transform as $v^i w^j$

$$v^i w^j = \frac{v^i w^j + v^j w^i}{2} + \frac{1}{2}\epsilon^{ijk}\epsilon_{klm} v^l w^m, \tag{3.10}$$

which can be easily proved using the relation

$$\epsilon^{ijk}\epsilon_{klm} = \delta^i_l \delta^j_m - \delta^j_l \delta^i_m. \tag{3.11}$$

From Eq. (3.10) one obtains the decomposition of Eq. (3.6), where the symmetric part belongs to $\mathbf{6}_\mathrm{c}$ (a symmetric 3×3 tensor has 6 independent components)

$$\frac{v^i w^j + v^j w^i}{2} \in \mathbf{6}_\mathrm{c}, \tag{3.12}$$

whereas the antisymmetric one belongs to $\bar{\mathbf{3}}_\mathrm{c}$ (an antisymmetric 3×3 tensor has 3 independent components)

$$\epsilon_{klm} v^l w^m \in \bar{\mathbf{3}}_\mathrm{c}. \tag{3.13}$$

On the other hand a $q\bar{q}$ state transforms as $v^i w_j$

$$v^i w_j = \left(v^i w_j - \frac{1}{3}\delta^i_j v^k w_k\right) + \frac{1}{3}\delta^i_j v^k w_k. \tag{3.14}$$

The first term in brackets is a 3×3 traceless tensor and thus contains eight independent elements

$$\left(v^i w_j - \frac{1}{3}\delta^i_j v^k w_k\right) \in \mathbf{8}_\mathrm{c}, \tag{3.15}$$

whereas the second one belongs to the singlet representation

$$\frac{1}{3}\delta^i_j v^k w_k \in \mathbf{1}_\mathrm{c}. \tag{3.16}$$

Having obtained the tensor decompositions of a standard $q\bar{q}$ meson and of a diquark, we now compute the $C(R)$ factors. We choose the normalization of the fundamental representation of $SU(3)$ to be

$$k(\mathbf{3}) = k(\bar{\mathbf{3}}) = 1/2 \tag{3.17}$$

and we assume $k(\mathbf{1}) = 0$. Exploiting Eq.(B.31) in Appendix B, one obtains

$$\begin{aligned} k(\mathbf{1}) + k(\mathbf{8}) &= 2 \times \dim(\mathbf{3}) k(\mathbf{3}), \\ k(\mathbf{3}) + k(\mathbf{6}) &= 2 \times \dim(\mathbf{3}) k(\mathbf{3}). \end{aligned} \tag{3.18}$$

As highlighted in Table 3.1, the product of color charges is negative only in two configurations: $qq \in \bar{\mathbf{3}}_c$ (diquark in antisymmetric color state) and $q\bar{q} \in \mathbf{1}_c$ (standard meson). The strength of the interaction between two quarks in $\bar{\mathbf{3}}_c$ is only one half of the one which is responsible for the binding of standard mesons.

Diquarks inside baryons. The diquark-quark description of baryons, stems from a very simple interpretation of the ratio of Deep Inelastic Scattering (DIS) neutron and proton structure functions in the $x \to 1$ limit. Indeed it is known that experimentally the ratio $F_1^{(n)}(x)/F_1^{(p)}(x) \to 1/4$ as the fraction x of the momentum carried

Table 3.1. Color charges computed in the One Gluon Exchange model for all the possible $q\bar{q}$ and qq color configurations.

$R_1 \otimes R_2 \in R$	$\mathbf{3} \otimes \bar{\mathbf{3}} \in \mathbf{1}$	$\mathbf{3} \otimes \bar{\mathbf{3}} \in \mathbf{8}$	$\mathbf{3} \otimes \mathbf{3} \in \bar{\mathbf{3}}$	$\mathbf{3} \otimes \mathbf{3} \in \mathbf{6}$
$k(R)$	0	3	1/2	5/2
$C(R)$	0	3	4/3	10/3
$Q(R)$	-4/3	1/6	$-2/3$	1/3

by the parton involved in DIS tends to 1. It results that $F_1^{(\text{nucleon})}(x) = \frac{1}{2}\sum_i f_i(x)\, Q_i^2$, where f_i is the parton distribution function for the i quark species. As the quark participating to DIS gets closer to carry the entire nucleon momentum, the remaining quarks are frozen in their lowest energy state. If diquark bound states exist, these will further lower the energy. But, as shown by lattice simulations, diquarks of the form $[uu]$ or $[dd]$ cannot be formed. Thus the lowest energy configurations for the spectator quarks in DIS are reached when we have a $[ud]$ diquark in the neutron with a d quark involved in DIS and again a $[ud]$ diquark in the proton with a u quark in DIS. Since $Q_d = -1/3$ and $Q_u = 2/3$, the experimental fact $F_1^{(n)}(x)/F_1^{(p)}(x) \to 1/4$ $(x \to 1/4)$ is understood as due to the ratio of charges $Q_d^2/Q_u^2 = 1/4$.

Also, a recent study by 't Hooft [216] showed that using a classical string picture to describe baryons, the stable configuration has a single open string with two quarks at the end points and one quark moving around on the string. Because of the attraction between two quarks into a $\bar{\mathbf{3}}_c$ bound state (as opposed to the $\mathbf{6}_c$), one expects quantum effects eventually to favor the configuration of one quark at one end and a diquark at the other end of a single open string.

Recent evidences. The existence of diquarks received a renewed interest when in January of 2003 evidence was reported of a very narrow baryon with strangeness one and charge one, of mass ~ 1540 MeV, the Θ^+, with minimum quark content $uudd\bar{s}$ [217]. In [218] Jaffe and Wilczek proposed to interpret this resonance as a diquark-diquark-antiquark bound state. Nevertheless as time passed several experiments reported negative results on the existence of the Θ^+. At any rate the Θ^+ led many authors to reconsider the possibility of the occurrence of exotic mesons, especially when the unexpected XYZ resonances started to appear in the charmonium and bottomonium spectra.

A further phenomenological indication in favor of the existence of diquarks, is due to 't Hooft *et al.* [219]. Using a diquark-antidiquark picture for the light 0^+ mesons, they obtain the best fit of their decay rates.

Classification of diquarks. Diquarks can be classified according to their J^{PC} quantum numbers and to their flavor content.

The J^{PC} quantum numbers of a diquark can be understood by simple considerations: (i) the spin of a diquark can be $S = 0$, with antisymmetric wave function, or $S = 1$, with symmetric wave function; (ii) the lightest diquarks are expected to have vanishing orbital angular momentum $L = 0$ [220]. The parity of the low-lying

diquarks is thus always positive $P = (-1)^L = +1$ and the possible J^P quantum numbers are 0^+ and 1^+. The spin-parity configurations 0^- and 1^- are associated with orbital excitations and they are expected to be heavier. In Table 3.2 the spin-parity quantum numbers are listed together with the fermi bilinears $\bar{q}_C \Gamma q$ associated to them. All the details about how to compute the $J^{P(C)}$ quantum numbers of quark-antiquark and diquark Fermi bilinears are reported in Appendix C.

Table 3.2. J^P classification of qq states.

J^P	Bilinear
0^-	$\bar{q}_C q$, $\bar{q}_C \gamma^0 q$
0^+	$\bar{q}_C \gamma^5 q$, $\bar{q}_C \gamma^0 \gamma^5 q$
1^-	$\bar{q}_C \gamma^i \gamma^5 q$, $\bar{q}_C \sigma^{ij} q$
1^+	$\bar{q}_C \gamma^i q$, $\bar{q}_C \sigma^{0i} q$

The wave function of diquarks accounts for color, flavor, spin and orbital angular momentum. Assuming $L = 0$ diquarks the spatial part is symmetric and thus we need to take into account only color, flavor and spin.

Light-Light Diquarks: if one deals with light-light diquarks Fermi statistics requires an antisymmetric wave function under the exchange of quarks labels. Since the color part of the wave function is antisymmetric, the product of the flavor and spin components must be symmetric. Thus the scalar diquark must be antisymmetric in flavor, whereas the vector one must be symmetric in flavor;

$$\begin{aligned} |0^+\rangle_{\mathtt{q}} &= |\bar{\mathbf{3}}_c, \bar{\mathbf{3}}_f\rangle \qquad \text{good diquark} \\ |1^+\rangle_{\mathtt{q}} &= |\bar{\mathbf{3}}_c, \bar{\mathbf{6}}_f\rangle \qquad \text{bad diquark} \end{aligned}$$

Evidence in favor of an attractive diquark (antidiquark) channel in the scalar configuration, the so-called *good diquarks* in the characterization of Jaffe [221] has also emerged from more than one Lattice QCD study [222, 223, 224, 225, 226, 227] for the light quark systems. On the other hand, no evidence is found on the lattice for an attractive diquark channel for the so-called *bad diquarks* [228].

Heavy-Light Diquarks: the situation is different for heavy-light diquarks. First of all Fermi statistics is not relevant since the particles in the diquarks are not identical. Second the effective QCD Lagrangian is spin-independent in the heavy quark limit and thus also the bad diquarks, $[cq]_{1^+}$ and $[bq]_{1^+}$, are likely to be in an attractive channel. This implies that the spectrum of hidden-charm and hidden-bottom tetraquarks is richer than the one we expect in the light sector. The interest in the spectrum of these states came when some resonances among the XYZ were identified as possible candidates to be tetraquarks [229, 230, 231, 232, 233]. We will describe the theoretical predictions and the experimental evidences about $[Qq][\bar{Q}\bar{q}']$ states in the next section. Lattice studies of the hidden-charm and hidden-bottom tetraquark

spectra have been carried out by the TWQCD collaboration [234, 235, 236] and by the CLQCD collaboration [174].

3.2 $L = 0$ tetraquarks

We consider here the spectra of $L = 0$ tetraquark states (S-wave diquark-antidiquark bound states) containing $c\bar{c}$ and $b\bar{b}$. The orbital angular momentum between diquark and antidiquark vanishes for these states. We will discuss the spectra in the framework of a non relativistic hamiltonian including chromo-magnetic spin-spin interactions between the quarks within a diquark and between quark and antiquark belonging to different diquarks. For a $[Qq_1][\bar{Q}\bar{q}_2]$ state, where $Q = c, b$, $q_1 = u, d, s$ and $q_2 = u, d, s$, we have

$$H = m_{[Qq_1]} + m_{[Qq_2]} + H_{SS}^{(qq)} + H_{SS}^{(q\bar{q})}, \tag{3.19}$$

with

$$H_{SS}^{(qq)} = 2\kappa_{(Qq_1)_{\bar{\mathbf{3}}}}\, \boldsymbol{S}_Q \cdot \boldsymbol{S}_{q_1} + 2\kappa_{(Qq_2)_{\bar{\mathbf{3}}}}\, \boldsymbol{S}_{\bar{Q}} \cdot \boldsymbol{S}_{\bar{q}_2}, \tag{3.20}$$

$$H_{SS}^{(q\bar{q})} = 2\kappa_{Q\bar{q}_2}\, \boldsymbol{S}_Q \cdot \boldsymbol{S}_{\bar{q}_2} + 2\kappa_{\bar{Q}q_1}\, \boldsymbol{S}_{\bar{Q}} \cdot \boldsymbol{S}_{q_1} + 2\kappa_{q_1\bar{q}_2}\, \boldsymbol{S}_{q_1} \cdot \boldsymbol{S}_{\bar{q}_2} + 2\kappa_{Q\bar{Q}}\, \boldsymbol{S}_Q \cdot \boldsymbol{S}_{\bar{Q}}. \tag{3.21}$$

The κ's are spin-spin couplings, whereas $m_{[Qq]}$ are the constituent diquark masses.

The spin-spin couplings can be obtained from the spectra of the $L = 0$ mesons and baryons assuming also for them a non relativistic hamiltonian

$$H_{\text{standard}} = \sum_i m_i + \sum_{i,j} 2\kappa_{ij}(\boldsymbol{S}_i \cdot \boldsymbol{S}_j), \tag{3.22}$$

where the sum runs over the hadron constituents.

The quark-antiquark spin couplings within a tetraquark $\kappa_{(q\bar{q}')}$ are related to the ones within a standard meson $\kappa_{(q\bar{q}')_{\mathbf{1}_c}}$ by [229]

$$\kappa_{(q\bar{q}')} = \frac{1}{4}\kappa_{(q\bar{q}')_{\mathbf{1}_c}}. \tag{3.23}$$

This is because of the color structure. The tetraquark color wave function is

$$\begin{aligned}[Qq_1][\bar{Q}\bar{q}_2] &= \epsilon_{ijk}Q^j(q_1)^k\, \epsilon^{ilm}\bar{Q}_l(\bar{q}_2)_m \\ &= \left(\delta^l_j\delta^m_k - \delta^m_j\delta^l_k\right)\, Q^j(q_1)^k\, \bar{Q}_l(\bar{q}_2)_m,\end{aligned} \tag{3.24}$$

where we have used Eq. (3.11) at the first step. We now use the Fierz identity derived in Appendix D

$$\delta^m_j\delta^l_k = \frac{1}{3}\delta^l_j\delta^m_k + \frac{1}{2}\boldsymbol{\lambda}^l_j \cdot \boldsymbol{\lambda}^m_k \tag{3.25}$$

to obtain

$$\begin{aligned}[Qq_1][\bar{Q}\bar{q}_2] &= \left(\frac{2}{3}\delta^l_j\delta^m_k - \frac{1}{2}\boldsymbol{\lambda}^l_j \cdot \boldsymbol{\lambda}^m_k\right)\, Q^j(q_1)^k\, \bar{Q}_l(\bar{q}_2)_m \\ &= \frac{2}{3}Q^l\bar{Q}_l\, (q_1)^m(\bar{q}_2)_m - \frac{1}{2}Q^j\boldsymbol{\lambda}^l_j\bar{Q}_l\, \cdot\, (q_1)^k\boldsymbol{\lambda}^m_k(\bar{q}_2)_k \\ &= \frac{2}{3}(Q\bar{Q})_{\mathbf{1}_c}\, (q_1\bar{q}_2)_{\mathbf{1}_c} - \frac{1}{2}(Q\bar{Q})_{\mathbf{8}_c}\, (q_1\bar{q}_2)_{\mathbf{8}_c}.\end{aligned} \tag{3.26}$$

From the expression above one understands that the probability to find inside a tetraquark a particular $q\bar{q}'$ pair in color octet is half the probability to find it in color singlet, so that

$$\kappa_{q\bar{q}'} = \frac{1}{3}\kappa_{(q\bar{q}')_{\mathbf{1}_c}} + \frac{2}{3}\kappa_{(q\bar{q}')_{\mathbf{8}_c}}. \tag{3.27}$$

From standard mesons we have no insight into the quantity $\kappa_{(q\bar{q}')_{\mathbf{8}_c}}$, thus we resort again to the one gluon exchange model. Since the chromo-magnetic interactions are originated by the exchange of gluons at the lowest order in perturbation theory, we can write

$$\kappa_{(q\bar{q}')_R} \propto C(R) - C(\bar{\mathbf{3}}) - C(\bar{\mathbf{3}}), \tag{3.28}$$

which in turn implies

$$\kappa_{(q\bar{q}')_{\mathbf{8}_c}} = -\frac{1}{8}\kappa_{(q\bar{q}')_{\mathbf{1}_c}}. \tag{3.29}$$

Plugging this relation in Eq. (3.27) we finally get to Eq. (3.23).

The quark-quark couplings $\kappa_{(qq')}$ are instead determined from the masses of the baryons with $J = 1/2$ and $J = 3/2$.

The values of the constituent quark masses and of the chromo-magnetic couplings from baryons and mesons have been computed in a number of papers ([229] for hidden-charm and [237] for hidden-bottom) and are summarized in Table 3.3 and 3.4 taken from [75].

Table 3.3. Constituent quark masses determined from mesons [75]. $(q = u, d)$.

	q	s	c	b
m_i (MeV)	305	490	1534	4720

Table 3.4. Quark-antiquark spin couplings within a meson $\kappa_{(q\bar{q}')_{\mathbf{1}_c}}$ and quark-quark spin couplings $\kappa_{qq'}$ [75]. $(q = u, d)$.

	$q\bar{q}$	$s\bar{q}$	$s\bar{s}$	$c\bar{q}$	$c\bar{s}$	$c\bar{c}$	$b\bar{q}$	$b\bar{s}$	$b\bar{c}$	$b\bar{b}$
$\kappa_{(q\bar{q}')_{\mathbf{1}_c}}$ (MeV)	315	195	121	70	72	59	23	23	20	36
$\kappa_{qq'}$ (MeV)	103	64	22	25	72	6	8			

The diquark masses can be determined once at least one tetraquark state has been identified in the data. In what follows we assume that $X(3872)$ has $J^{PC} = 1^{++}$ and interpret it as a tetraquark with wave function

$$\frac{[cq]_{1^+}[\bar{c}\bar{q}]_{0^+} + [cq]_{0^+}[\bar{c}\bar{q}]_{1^+}}{\sqrt{2}}.$$

In Section 3.3.2 we will briefly discuss the spectrum of $L = 0$ tetraquark states in the hypothesis of $J^{PC} = 2^{-+}$ quantum numbers.

To obtain the other diquarks masses we use

$$\begin{aligned} m_{[cs]} &= m_{[cq]} - m_q + m_s, \\ m_{[bq]} &= m_{[cq]} - m_c + m_b, \\ m_{[bs]} &= m_{[bq]} - m_c + m_s. \end{aligned} \tag{3.30}$$

In Table 3.5 we report the results on the diquark mass values obtained in [75].

Table 3.5. Diquark masses obtained in [75].

	$[cq]$	$[cs]$	$[bq]$	$[bs]$
$m_{q_1q_2}$ (MeV)	1933	2118	5119	5304

Combining scalar and vector diquarks one can form J^P eigenstates. In the $|S, S_z\rangle$ basis we have:

two $J^P = 0^+$ tetraquarks

$$|0,0\rangle_1 = |0;0\rangle_{Qq_1}|0;0\rangle_{\bar{Q}\bar{q}_2}$$
$$|0,0\rangle_2 = \frac{|1;1\rangle_{Qq_1}|1;-1\rangle_{\bar{Q}\bar{q}_2} - |1;0\rangle_{Qq_1}|1;0\rangle_{\bar{Q}\bar{q}_2} + |1;-1\rangle_{Qq_1}|1;1\rangle_{\bar{Q}\bar{q}_2}}{\sqrt{3}}$$

three $J^P = 1^+$ tetraquarks

$$|1,S_z\rangle_1 = |1;S_z\rangle_{Qq_1}|0;0\rangle_{\bar{Q}\bar{q}_2}$$
$$|1,S_z\rangle_2 = |0;0\rangle_{Qq_1}|1;S_z\rangle_{\bar{Q}\bar{q}_2}$$
$$|1,S_z\rangle_3 = \begin{cases} |1,1\rangle = \frac{|1;1\rangle_{Qq_1}|1;0\rangle_{\bar{Q}\bar{q}_2} - |1;0\rangle_{Qq_1}|1;1\rangle_{\bar{Q}\bar{q}_2}}{\sqrt{2}} \\ |1,0\rangle = \frac{|1;1\rangle_{Qq_1}|1;-1\rangle_{\bar{Q}\bar{q}_2} - |1;-1\rangle_{Qq_1}|1;1\rangle_{\bar{Q}\bar{q}_2}}{\sqrt{2}} \\ |1,-1\rangle = \frac{|1;-1\rangle_{Qq_1}|1;0\rangle_{\bar{Q}\bar{q}_2} - |1;0\rangle_{Qq_1}|1;-1\rangle_{\bar{Q}\bar{q}_2}}{\sqrt{2}} \end{cases}$$

one $J^P = 2^+$ tetraquark

$$|2,S_z\rangle = \begin{cases} |2,2\rangle = |1;1\rangle_{Qq_1}|1;1\rangle_{\bar{Q}\bar{q}_2} \\ |2,1\rangle = \frac{|1;1\rangle_{Qq_1}|1;0\rangle_{\bar{Q}\bar{q}_2} + |1;0\rangle_{Qq_1}|1;1\rangle_{\bar{Q}\bar{q}_2}}{\sqrt{2}} \\ |2,0\rangle = \frac{|1;1\rangle_{Qq_1}|1;-1\rangle_{\bar{Q}\bar{q}_2} + 2|1;0\rangle_{Qq_1}|1;0\rangle_{\bar{Q}\bar{q}_2} + |1;-1\rangle_{Qq_1}|1;1\rangle_{\bar{Q}\bar{q}_2}}{\sqrt{6}} \\ |2,-1\rangle = \frac{|1;-1\rangle_{Qq_1}|1;0\rangle_{\bar{Q}\bar{q}_2} + |1;0\rangle_{Qq_1}|1;-1\rangle_{\bar{Q}\bar{q}_2}}{\sqrt{2}} \\ |2,-2\rangle = |1;-1\rangle_{Qq_1}|1;-1\rangle_{\bar{Q}\bar{q}_2} \end{cases} \quad (3.31)$$

If $q_1 = q_2$ one can build J^{PC} eigenstates:

two $J^{PC} = 0^{++}$ tetraquarks

$$|0,0\rangle_1 \quad \text{and} \quad |0,0\rangle_2$$

one $J^{PC} = 1^{++}$ tetraquark

$$\frac{|1,S_z\rangle_1 + |1,S_z\rangle_2}{\sqrt{2}}$$

two $J^{PC} = 1^{+-}$ tetraquarks

$$|1,S_z\rangle_3 \quad \text{and} \quad \frac{|1,S_z\rangle_1 - |1,S_z\rangle_2}{\sqrt{2}}$$

one $J^{PC} = 2^{++}$ **tetraquark**

$$|2, S_z\rangle$$

To obtain the masses of these states, the hamiltonian of Eq. (3.19) needs to be diagonalized. To do that one has to compute the expectation values of scalar product of spin operators between $|S, S_z\rangle$ states.

As an example let us consider ${}_1\langle 0,0|\boldsymbol{S}_Q \cdot \boldsymbol{S}_{q_1}|0,0\rangle_1$. In [233] a non relativistic notation has been introduced for diquarks, which has proved to be very useful in this computation. This notation follows from the non relativistic limit of the diquarks bilinears listed in Appendix C. As reported in Table C.2, a scalar $[qq']_{0^+}$ diquark is created by the $\bar{q}_C\gamma^5 q'$ operator, whereas the vector $[qq']_{1^+}$ by $\bar{q}_C\gamma^i q'$. In the non relativistic limit the two operators become $q^T\sigma^2 q'$ and $q^T\sigma^2\sigma^i q'$ respectively, so that

$$|0,0\rangle_1 = [Q^T\sigma^2 q_1]\,[\bar{Q}\sigma^2\bar{q}_2^T]. \tag{3.32}$$

The action of $\boldsymbol{S}_Q \cdot \boldsymbol{S}_{q_1}$ on this state is

$$\begin{aligned}\boldsymbol{S}_Q \cdot \boldsymbol{S}_{q_1}|0,0\rangle_1 &= \frac{1}{4}\left[Q^T(\boldsymbol{\sigma})^T\sigma^2 \cdot \boldsymbol{\sigma} q_1\right]\ \left[\bar{Q}\sigma^2\bar{q}_2^T\right] \\ &= -\frac{1}{4}\left[Q^T\sigma^2\,\boldsymbol{\sigma}\cdot\boldsymbol{\sigma}\,q_1\right]\ \left[\bar{Q}\sigma^2\bar{q}_2^T\right] \\ &= -\frac{1}{4}\times 3\ \left[Q^T\sigma^2 q_1\right]\ \left[\bar{Q}\sigma^2\bar{q}_2^T\right],\end{aligned} \tag{3.33}$$

where we have used $\boldsymbol{\sigma}^T\sigma^2 = -\sigma^2\boldsymbol{\sigma}$ at the first step and Eq. (D.4) of Appendix D to compute $\boldsymbol{\sigma}\cdot\boldsymbol{\sigma}$ at the second step. Thus ${}_1\langle 0,0|\boldsymbol{S}_Q \cdot \boldsymbol{S}_{q_1}|0,0\rangle_1 = -3/4$, as expected.

The mass spectra of hidden-charm and hidden-bottom states have been computed in [75] including all flavors for the light degrees of freedom. In Fig. 3.2 and 3.3 we plot the mass values as a function of the third isospin component I_3. Flavor multiplicities for each level are explained in [75] in detail.

3.2.1 Candidates

***X*(3872)**. In the 1^{++} assignment $X(3872)$ would be a $X_q = [cq]_{0^+}[\bar{c}\bar{q}]_{1^+} + \text{c.c.}$ tetraquark. It is expected to be narrow like all diquark-antidiquark systems below the baryon-antibaryon threshold. Furthermore unnatural spin parity forbids the decay to $D^0\bar{D}^0$, while the decay to J/ψ plus vector meson is allowed with conservation of the spin of the heavy quark pair. This can be checked using the Fierz identity for Pauli matrices in Eq. (D.11) of Appendix D. It results that $[cq]_{0^+}[\bar{c}\bar{q}]_{1^+} + [cq]_{1^+}[\bar{c}\bar{q}]_{0^+} \sim \epsilon_{ijk}[\bar{q}\sigma^k q]\,[\bar{c}\sigma^j c]$, indicating that the decay $J/\psi\,\rho$ or $J/\psi\,\omega$ conserves the spin of the heavy quark pair.

The isospin quantum number is related to the light quark content of the tetraquark. The two flavor eigenstates X_u and X_d mix through self energy diagrams giving two mass eigenstates

$$X_{low} = \cos\theta X_u + \sin\theta X_d, \tag{3.34}$$

$$X_{high} = -\sin\theta X_u + \cos\theta X_d. \tag{3.35}$$

In the small mixing limit $\cos\theta \sim 1$ and $\sin\theta \sim \theta$, one obtains an almost maximal isospin breaking. The mass difference between the two states is $M(X_{high}) -$

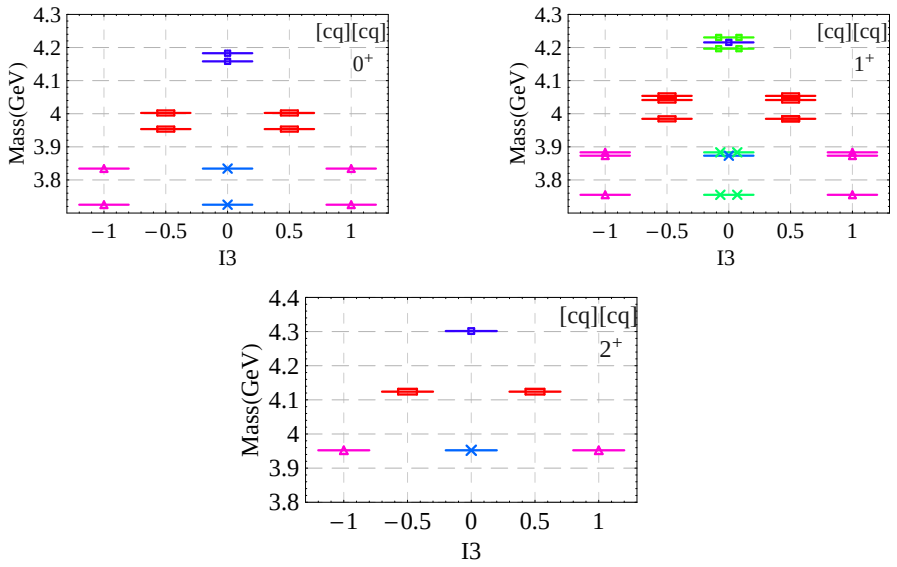

Figure 3.2. *Hidden-charm multiplets with $L = 0$ taken from [75].*

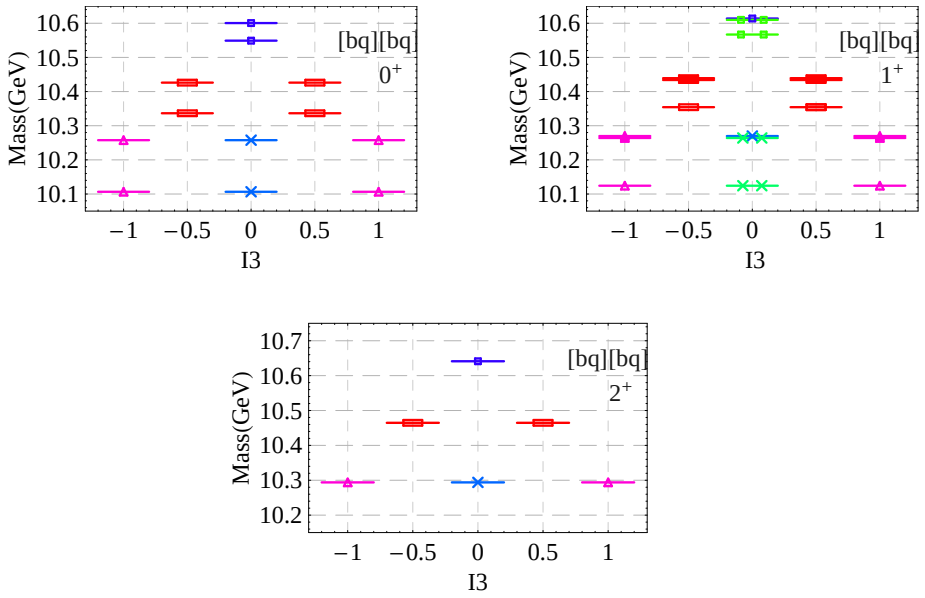

Figure 3.3. *Hidden-bottom multiplets with $L = 0$ taken from [75].*

$M(X_{low}) = (m_d - m_u)/\cos 2\theta$. The existence of multiple structures nearby in mass, indicated by the earliest data, has been widely tested in [74, 57, 73, 66, 61], resulting in an upper limit on the mass difference between the two resonances of 3.2 MeV at 90% C.L.. An alternative mechanism to explain the isospin violation in the tetraquark picture is the possibility of a $\omega - \rho^0$ mixing, as proposed in [238].

The mass of the $X(3872)$ is used to fit the mass of the $[cq]$ diquark[2] [229, 231]: $m_{[cq]}$ =1933 MeV.

Besides these two neutral states, two charged states arise as a natural prediction of the tetraquark picture $X^+ = [cu][\bar{c}\bar{d}]$ and $X^- = [cd][\bar{c}\bar{u}]$. The lack of any observation of these two states constitutes the main drawback to the tetraquark assignment.

***Y*(4140)**. The interpretation of $Y(4140)$ in terms of a $[cs][\bar{c}\bar{s}]$ tetraquark state has been considered in [239, 240]. Using a constituent quark model with chromo-magnetic interactions the spectrum of $[cs][\bar{c}\bar{s}]$ tetraquarks has been computed, favoring $J^{PC} = 1^{++}$, even if $J^{PC} = 0^{++}$ cannot entirely be excluded. However tetraquarks will fall apart into a pair of charmed mesons very easily. As a tetraquark, the width of $Y(4140)$ would be around several hundred MeV instead of 12 MeV as observed by CDF.

***X*(4350)**. The possibility for the $X(4350)$ to be a 1^{++} $[cs][\bar{c}\bar{s}]$ tetraquark has been considered in [241].

***Z*$^+$(4430)**. In [242] $Z^+(4430)$ has been identified as a $J^P = 1^+$ radial excitation of a $[cq][\bar{c}\bar{q}]$, a charged partner of $X(3872)$. A similar conclusion was drawn in [243] based on a QCD string model, whereas QCD sum rules indicated [244] that $J^P = 0^-$ are the favored quantum numbers. The tetraquark model also predicts a second nearby state with mass ~ 4340 MeV, decaying into $\psi'\pi^+$ [242].

3.3 $L = 1$ tetraquarks: a string model

We consider now diquark-antidiquark bound states with non vanishing orbital angular momentum L

$$\Big([Qq_1][\bar{Q}\bar{q}_2]\Big)_{L-\text{wave}}. \tag{3.36}$$

The parity of such states is $P = (-1)^L$, since the lightest diquarks come only in the positive parity configurations 0^+ and 1^+.

To compute the spectrum of these states we need to include in the non-relativistic hamiltonian of Eq. (3.19) the energy due to the orbital motion. In [245] a term proportional to $L(L+1)$ was introduced to study 1^{--} $qs\bar{q}\bar{s}$ tetraquarks. The same model was used to study orbitally excited states with hidden-charm and strangeness in [233].

In [3] we first proposed a different approach, later developed in [2]. We considered a generalization of the Chew-Frautschi formula, a relativistic model of spinning string first discussed in [246, 247] by Selem and Wilczek.

Let us consider a relativistic string with tension T spinning around a given axis. Attached at the two ends of the string there are two masses m_1 and m_2. The rest energy in the laboratory frame is

$$\mathcal{E}_0 = m_1\gamma_1 + m_2\gamma_2, \tag{3.37}$$

[2] One assumes that the scalar and axial diquark have the same mass.

where

$$\gamma_i = \frac{1}{\sqrt{1-(\omega r_i)^2}} \tag{3.38}$$

with r_i the distance of the particle with mass m_i from the rotation axis and ω the angular velocity. To obtain the total energy of the system one has to consider the rotational energy. The rest frame energy of an infinitesimal string segment of length dr is

$$d\mathcal{E}_r^* = T dr^*. \tag{3.39}$$

In the laboratory frame one gains the Lorentz factor and obtains ($\omega dr = dv$)

$$d\mathcal{E}_r = T\frac{dr}{\sqrt{1-v^2}} = \frac{T}{\omega}\frac{dv}{\sqrt{1-v^2}}. \tag{3.40}$$

The total energy of the system is thus:

$$\mathcal{E} = m_1\gamma_1 + m_2\gamma_2 + \frac{T}{\omega}\int_0^{\omega r_1}\frac{dv}{\sqrt{1-v^2}} + \frac{T}{\omega}\int_0^{\omega r_2}\frac{dv}{\sqrt{1-v^2}}. \tag{3.41}$$

We want also to determine the orbital angular momentum of the system. The two masses attached at the ends contribute with

$$L_0 = m_1\omega r_1^2\gamma_1 + m_2\omega r_2^2\gamma_2 \tag{3.42}$$

Furthermore the orbital angular momentum can be written in terms of the moment of inertia I of the system

$$dL = \omega dI. \tag{3.43}$$

Remind that

$$I = \int r^2\frac{d\mathcal{E}}{dr}\,dr \Rightarrow dI = r^2\,d\mathcal{E} = \frac{v^2}{\omega^2}d\mathcal{E}, \tag{3.44}$$

so that

$$dL = \frac{v^2}{\omega}d\mathcal{E} = \frac{T}{\omega^2}\frac{v^2\,dv}{\sqrt{1-v^2}}. \tag{3.45}$$

Finally we obtain

$$L = m_1\omega r_1^2\gamma_1 + m_2\omega r_2^2\gamma_2 + \frac{T}{\omega^2}\int_0^{\omega r_1}\frac{v^2\,dv}{\sqrt{1-v^2}} + \frac{T}{\omega^2}\int_0^{\omega r_2}\frac{v^2\,dv}{\sqrt{1-v^2}} \tag{3.46}$$

Carrying out the integrals gives

$$\begin{cases} \mathcal{E} = & m_1\gamma_1 + m_2\gamma_2 + \frac{T}{\omega}\left(\arcsin(\omega\, r_1) + \arcsin(\omega\, r_2)\right) \\ L = & m_1\gamma_1 + m_2\gamma_2 \\ & +\frac{1}{2}\frac{T}{\omega^2}\left(-\omega\, r_1\sqrt{1-(\omega r_1)^2} + \arcsin(\omega\, r_1) - \omega\, r_2\sqrt{1-(\omega r_2)^2} + \arcsin(\omega\, r_2)\right) \end{cases} \tag{3.47}$$

Using Eq.(3.38) and the fact that the same centrifugal force, given by the tension T of the string, acts on each mass

$$T = m_1\gamma_1^2\omega^2 r_1 = m_2\gamma_2^2\omega^2 r_2, \tag{3.48}$$

one can write γ_i and r_i as a function of T, m_i and ω:

$$\gamma_i = \left(\frac{1}{2} + \frac{1}{2} \sqrt{1 + 4 \left(\frac{T}{m_i \omega} \right)^2} \right)^{1/2}, \tag{3.49}$$

$$r_i = \frac{1}{\omega} \sqrt{1 - \frac{1}{\gamma_i^2}}. \tag{3.50}$$

Plugging Eq. (3.49) and (3.50) inside Eq. (3.47) one obtains an expression of the energy and the orbital angular momentum in terms of the masses m_1 and m_2, the string tension T and the angular velocity ω:

$$\begin{cases} \mathcal{E} &= \mathcal{E}(m_1, m_2, T, \omega) \\ L &= L(m_1, m_2, T, \omega) \end{cases} \tag{3.51}$$

We compute the expressions above in two limits[3]:

$m_1 = m_2 = m$ and $\epsilon = T/m\omega >> 1$

$$\begin{cases} \mathcal{E} &= \frac{\pi T}{\omega} + \frac{2M}{\sqrt{\epsilon}} + 2\sqrt{\epsilon} \left(\frac{m}{4} - \frac{T}{\omega} \right) + \mathcal{O}(\epsilon^{3/2}) \simeq \sqrt{\frac{m^3 \omega}{4T}} + \frac{\pi T}{\omega} \\ L &= \frac{\pi T}{2\omega^2} + \mathcal{O}(\epsilon^{3/2}) \simeq \frac{\pi T}{2\omega^2} \end{cases} \tag{3.52}$$

One can derive an analytic expression of the energy as a function of the orbital angular momentum:

$$\mathcal{E} = (\sigma L)^{1/2} + \frac{\sqrt{\pi} m^{3/2}}{2} (\sigma L)^{-1/4}, \tag{3.53}$$

where the string tension T is related to that of Regge phenomenology σ by $T = \sigma/2\pi$. This model reproduces the linear behavior of the Regge Trajectories for light mesons $\mathcal{E}^2 \simeq \sigma L$ with $\sigma = 1.1$ GeV^2 or $T = 0.175$ GeV^2 [247].

$m_1 = m_2 = M$ and $\epsilon = T/M\omega << 1$

$$\begin{cases} \mathcal{E} &= 2M + \epsilon \frac{2T}{\omega} + \epsilon^2 M + \mathcal{O}(\epsilon^3) \simeq 2M + \frac{3T^2}{M\omega^2} \\ L &= \epsilon \frac{2T}{\omega^2} + \mathcal{O}(\epsilon^3) \simeq \frac{2T^2}{M\omega^3} \end{cases} \tag{3.54}$$

The energy as a function of the orbital angular momentum reads

$$\mathcal{E} = 2M + \frac{3}{(16\pi^2 M)^{1/3}} (\sigma L)^{2/3}. \tag{3.55}$$

This model can describe either standard $L \neq 0$ $q\bar{q}$ mesons, either $L \neq 0$ $\mathfrak{q}\bar{\mathfrak{q}}$ tetraquarks.

In the next section we will test this model on the spectrum of $L = 1$ and $L = 2$ charmonium and bottomonium states. To do so we will include also the relativistic correction terms: spin-orbit interactions and spin-spin interactions.

In Section 3.3.2 we will consider the case of three 1^{--} XYZ resonances, $Y(4350)$ and $Y(4630)/Y(4660)$, and explain why an interpretation in terms of P-wave diquark-antidiquark bound states seems to be supported by experimental data.

[3] $[T/m\omega] = [m\omega/T] = M^0$ since $[T] = [dE/dr] = M/L = M^2$ and $[\omega] = 1/T = M$.

3.3.1 Test on standard charmonium and bottomonium [2]

Eq. (3.55) represents in our picture the energy of a heavy quark-antiquark pair with $L \neq 0$ orbital angular momentum. This is a characteristically different Regge trajectory from that of light quarks $\mathcal{E} \simeq \sqrt{\sigma L}$. It has recently been demonstrated that the spectra of bottomonia does not fit with the standard Regge trajectory [248], and indeed we shall argue that the trajectory of Eq. (3.55) is the correct one to fit the data.

It is worth to notice that the expression in Eq. (3.55) had been previously mentioned in the literature [249], but not confronted directly with the meson spectrum. Furthermore we note with interest that the same result, Eq. (3.55), arises in the Bohr-Sommerfeld quantization of the standard Cornell potential used in quark model calculations [250]. It shall come as no surprise, then, that the results presented here do not differ drastically from those of other models.

Our interest in developing a model for charmonia and bottomonia orbital excitations stems from the recent claim of the BaBar collaboration [68] about the J^{PC} quantum numbers of $X(3872)$, which indicates the 2^{-+} assignment more likely than the 1^{++} one. In this scenario the charmonium interpretation of $X(3872)$ as a 1^1D_2 state needs to be reconsidered. We will obtain a prediction of the mass of the 1^1D_2 state in the framework of our spinning string model and compare it to data.

We use Eq. (3.55) to predict the masses of the orbitally excited mesons with zero quark spin, yielding for the P- and D-wave spin singlets [4],

$$M(^1P_1) = 2M + \Delta, \tag{3.56}$$

$$M(^1D_2) = 2M + 2^{2/3}\Delta, \tag{3.57}$$

where $\Delta = 3\left(T^2/4M\right)^{1/3}$. For the states with nonzero spin, we improve Eq. (3.55) including relativistic corrections: spin-spin, spin-orbit, and tensor interactions. We thus write the mass formula for states with given total spin S, orbital angular momentum L, and total angular momentum J:

$$M(^{2S+1}L_J) = 2M + \Delta\, L^{2/3} + M_{SS}\langle 2\boldsymbol{S}_q \cdot \boldsymbol{S}_{\bar{q}}\rangle + M_{LS}\langle \boldsymbol{L}\cdot\boldsymbol{S}\rangle + M_{\mu\mu}\langle \boldsymbol{S}^2 - 3\,(\boldsymbol{S}\cdot\boldsymbol{n})^2\rangle, \tag{3.58}$$

where here $\boldsymbol{S}_q$ and $\boldsymbol{S}_{\bar{q}}$ are the quark and antiquark spins coupled to $\boldsymbol{S}$, and the unit vector $\boldsymbol{n} = \boldsymbol{R}/|\boldsymbol{R}|$, with $\boldsymbol{R}$ the vector connecting the quark and the antiquark. The mass shifts M_{SS}, M_{LS} and $M_{\mu\mu}$ for spin-spin, spin-orbit and tensor interactions are the analogues of the interaction potentials used in quark potential model calculations. The difference is that in this semiclassical approach, instead of taking matrix elements of these R-dependent functions between meson wave functions we can evaluate the expectation values directly using the fixed value of the meson radius. We will derive explicit expressions for these mass shifts but first we investigate some general predictions of the model arising from Eq. (3.58).

We assume that the spin-spin interaction splits only states with zero orbital angular momentum, for which the $Q\bar{Q}$ pair tends to be at much lower average distance. Assuming that M_{SS} is common to both $^1S_0$ and $^3S_1$, the masses of these

[4] In what follows we always refer to radial ground states so that $n_r = 0$ is understood in the atomic notation.

states are

$$M(^1S_0) = 2M - \frac{3}{2}M_{SS} \tag{3.59}$$

$$M(^3S_1) = 2M + \frac{1}{2}M_{SS} \tag{3.60}$$

Equations (3.56)-(3.57) and (3.59)-(3.60) yield a single linear relation among the masses

$$M(^1D_2) = 2^{2/3}M(^1P_1) + \frac{1-2^{2/3}}{4}\left(M(^1S_0) + 3M(^3S_1)\right) \tag{3.61}$$

and a parameter-independent prediction of the mass of the $^1D_2$ state in terms of the masses of the h_c, J/ψ and η_c,

$$M(^1D_2) \simeq 3795 \text{ MeV}. \tag{3.62}$$

The predicted mass is in reasonable agreement with other models, as we discuss later, but is considerably lower than the mass of the $X(3872)$. In what follows we refine the model, adjusting the parameters to fit also the χ_c states, but ultimately our predicted $M(^1D_2)$ changes very little. Thus, our conclusion is that the $X(3872)$, whose mass exceeds our prediction by some 80 MeV, is difficult to reconcile with a $^1D_2$ interpretation.

In what follows we verify that the application of the same mass formula in the bottomonia sector is in remarkable agreement with data, supporting the validity of our prediction.

The spin-orbit and tensor terms split the states with $S = 1$ and nonzero L, although we will assume, as is usual, that for these states spin-spin contact interactions are negligible. Applying Eq. (3.58) to the P-wave family yields the following expressions (see Appendix A):

$$M(^3P_0) = M(^1P_1) - 2M_{LS}^{(\mathrm{P})} + 2M_{\mu\mu}^{(\mathrm{P})} \tag{3.63}$$

$$M(^3P_1) = M(^1P_1) - M_{LS}^{(\mathrm{P})} - M_{\mu\mu}^{(\mathrm{P})} \tag{3.64}$$

$$M(^3P_2) = M(^1P_1) + M_{LS}^{(\mathrm{P})} + \frac{1}{5}M_{\mu\mu}^{(\mathrm{P})}, \tag{3.65}$$

where we have labeled the mass shifts M_{LS} and $M_{\mu\mu}$ with a superscript to denote that they are dependent on the meson radius R, and hence the partial wave. Eliminating these terms yields a linear relation among the masses of the four members of the P-wave family

$$M(^1P_1) = \frac{1}{9}\left(M(^3P_0) + 3M(^3P_1) + 5M(^3P_2)\right). \tag{3.66}$$

The accuracy of this relation can be tested both in the charmonia and bottomonia sector, where the h_b, the $^1P_1$ state, has been recently observed [54]. Using the χ_{cJ} and χ_{bJ} mass values as input, one predicts $M(h_c) = (3525.30 \pm 0.1)$ MeV and $M(h_b) = (9892.46 \pm 0.42)$ MeV, in remarkable agreement with the experimental data $M(h_c) = (3525.67 \pm 0.32)$ MeV [251] and $M(h_b) = (9898.3 \pm 1.1^{+1.0}_{-1.1})$ MeV [54]. We note in passing that the good agreement also justifies the neglect of spin-spin interactions for nonzero L which, if present, would modify Eq. (3.66).

Recent data [252] on the masses of the $^3D_{1,2,3}$ states of the bottom sector allow us to apply the analogous approach, arriving at a new prediction for the mass of the as-yet unidentified $^1D_2$ state. In Appendix A we derive the mass formulas

$$M(^3D_1) = M(^1D_2) - 3M_{LS}^{(\mathrm{D})} + M_{\mu\mu}^{(\mathrm{D})}, \tag{3.67}$$

$$M(^3D_2) = M(^1D_2) - M_{LS}^{(\mathrm{D})} - M_{\mu\mu}^{(\mathrm{D})}, \tag{3.68}$$

$$M(^3D_3) = M(^1D_2) + 2M_{LS}^{(\mathrm{D})} + \frac{2}{7}M_{\mu\mu}^{(\mathrm{D})}, \tag{3.69}$$

which lead to the linear relation

$$M(^1D_2) = \frac{1}{15}\left(3M(^3D_1) + 5M(^3D_2) + 7M(^3D_3)\right). \tag{3.70}$$

We thus predict the mass of the unobserved $^1D_2$ state

$$M(\eta_{b2}) = (10165.84 \pm 1.8)\ \mathrm{MeV}. \tag{3.71}$$

We are now in a position to test the validity of our mass formula (3.61) in the bottomonia sector. We use as input the experimental values for the η_b, Υ and h_b masses. The mass relation (3.61) yields a predicted $^1D_2$ mass of $M(\eta_{b2}) = 10168.72^{+1.4}_{-1.8}$ MeV, in striking agreement with the above value extracted from the experimental data, and therefore we can be confident in the reliability of the corresponding prediction for the $^1D_2$ charmonium state.

The remarkable accuracy of the model can be seen by plotting the Regge trajectory of equation (3.55). For the center of gravity of the $1S$ states we use

$$\mathcal{E}(L=0) = \frac{1}{4}\left(3M(\Upsilon) + M(\eta_b)\right) = 9442.45^{+1.20}_{-1.07}\ \mathrm{MeV}, \tag{3.72}$$

for $\mathcal{E}(L=1)$ we use the experimental value of $M(h_b)$ and for $\mathcal{E}(L=2)$ the value of $M(\eta_{b2})$ in Eq. (3.71).

In the upper part of Fig. 3.4 we plot these three data points in the $\mathcal{E}$-$L^{2/3}$ plane, and one sees immediately the accuracy with which the model fits the data. On the same plot (indicated by stars) we show our prediction for the masses of the higher L spin-singlet states, $M(^1F_3) = 10391$ MeV and $M(^1G_4) = 10591$ MeV, the identification of which would be a good test of our model. Both of these states should be narrow since they lie below the threshold for $B^*\bar{B}$, the lightest open flavor pair to which they can decay.

In the lower part of the same figure we plot the corresponding Regge trajectory for the $c\bar{c}$ system. Here we have only two data points: $\mathcal{E}(L=0)$, which we determine from the masses of the J/ψ and η_c as above, and $\mathcal{E}(L=1) = M(h_c)$. We indicate by stars our predictions for $M(^1D_2) = 3795$ MeV, $M(^1F_3) = 4020$ MeV and $M(^1G_4) = 4221$ MeV, although the masses of the latter pair may not be as reliable as in the bottomonia case because of the coupling to the open $D^*\bar{D}$ threshold.

A striking feature of Fig. 3.4 is that the slopes of the trajectories for $b\bar{b}$ and $c\bar{c}$ are almost identical. Since the slope is given by $3(T^2/4M)^{1/3}$, this implies that the effective string tension scales with the square root of the quark mass, in contrast to many potential models in which a common string tension is used for different quark

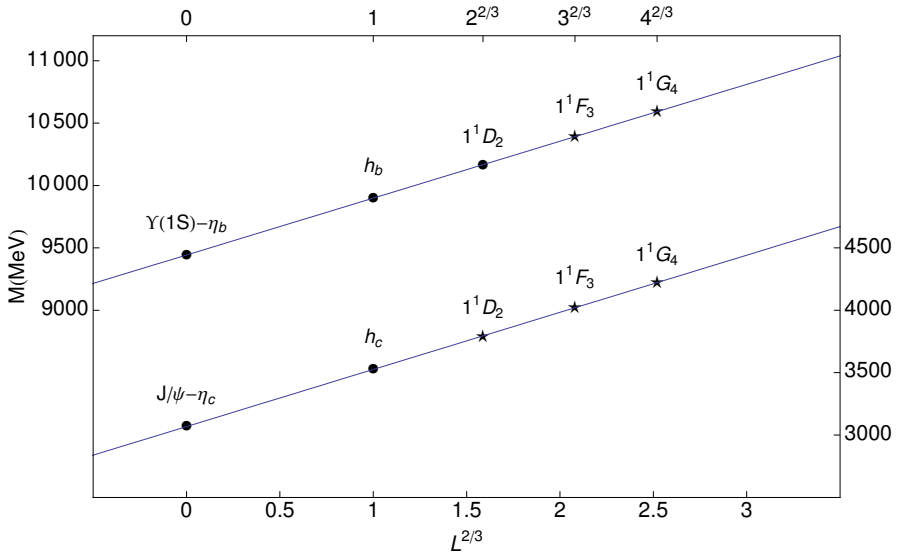

Figure 3.4. Regge trajectories for bottomonia (upper left) and charmonia (lower right) states. The closed circles indicate experimental masses (or those of the center of gravity where appropriate) for a given L; stars indicate predictions for unobserved states.

masses; we determine the best fit values $T_b = 0.257$ GeV^2 and $T_c = 0.148$ GeV^2. From the intercept of the trajectories we determine the quark masses $m_b = 4721$ MeV and $m_c = 1533$ MeV.

We return now to the derivation of the mass shifts M_{SS}, M_{LS}, and $M_{\mu\mu}$ in terms of the parameters of the string model.

Spin-spin interactions are contact interactions and thus the associated term in the potential is

$$V_{SS}(\boldsymbol{R}) = \kappa_{c\bar{c}}\delta^3(\boldsymbol{R}). \tag{3.73}$$

The corresponding mass shift is thus proportional to the square of the wave function at the origin, assuming that the magnetic coupling and the wave function at the origin do not depend on the total spin of the pair

$$M_{SS} = \langle V_{SS}(\boldsymbol{R})\rangle = \kappa_{c\bar{c}}\ |\psi_{1S}(0)|^2\,. \tag{3.74}$$

In our model we treat $\kappa' = \kappa|\psi(0)|^2$ as a free parameter.

The mass shift M_{LS} is due to the coupling of the magnetic moment of one quark to the magnetic field created by the moving charge of the other quark; this is the essence of the spin-orbit coupling,

$$M_{LS} = A\frac{1}{R}\frac{\partial\mathcal{E}(R)}{\partial R}, \tag{3.75}$$

where A is a constant to be determined and $\mathcal{E}$ is the energy of the string. As explained in Section 1.2.3, the form of the spin-orbit potential depends on the type of interaction between the constituents of the meson. We assume that only a vector interaction of the kind $\bar{Q}\gamma^\mu Q$ exists between the heavy quarks and this is responsible for the string energy. To obtain the form of $\mathcal{E}$ we exploit the expansion of the

energy in Eq. (3.54). In the heavy quark limit, we can compute the dependence of $\mathcal{E}$ on the distance between the masses, using Eq. (3.48) to eliminate ω in favor of $R = 2r = r_1/2 = r_2/2$:

$$\omega^2 = (1 - (\omega r)^2)\frac{T}{Mr} \Rightarrow \omega = \sqrt{\frac{T}{Mr + r^2 T}}. \tag{3.76}$$

One finds

$$\begin{cases} \mathcal{E} &= 2M + \frac{3RT}{2} + \frac{3R^2T^2}{4M} \\ L &= \frac{T^2}{4M}\left(\frac{2MR+R^2T}{T}\right)^{3/2} \end{cases} \tag{3.77}$$

From the first of these two relations it is evident that this relativistic string model well describes the confinement, the energy being a growing function of the distance between the quark and the antiquark inside the meson. The second of the relations in (3.77) allows to write the distance R between the quarks in terms of the orbital angular momentum, the mass, and the tension:

$$R = -\frac{M}{T} + \frac{\sqrt{M^2T^{2/3} + (4LMT^2)^{2/3}}}{T^{4/3}} \approx \left(\frac{2L^2}{MT}\right)^{1/3}, \tag{3.78}$$

which means as expected that R grows when the orbital angular momentum grows.

The tensor mass shift $M_{\mu\mu}$ arises from the interaction between the magnetic moment of one of the two quarks with the static magnetic field generated by the other one,

$$M_{\mu\mu} = B\frac{1}{R^3} \tag{3.79}$$

where the constant B is again to be determined.

Following standard electromagnetism, one can parametrize A and B in terms of the gyromagnetic factor and of the charge of the heavy quarks bound to form the meson. The interaction between the magnetic dipole and the magnetic field generated from a moving charge carries a factor $ge/2m^2$, whereas the Thomas precession gives $-e/2m^2$ so that

$$A = \frac{(g_Q - 1)e_Q}{2m_Q^2}, \tag{3.80}$$

where e_Q is the electric charge of the heavy quark. As for the tensor coupling B, we expect it to be related to the product of the Bohr magnetons of the quark and the antiquark. The magnetic field generated from a magnetic moment $\boldsymbol{\mu_1}$ is

$$\boldsymbol{H}_1 = \frac{3\,\boldsymbol{n}\,(\boldsymbol{\mu}_1 \cdot \boldsymbol{n}) - \boldsymbol{\mu}_1}{R^3}. \tag{3.81}$$

The interaction energy is

$$V_{\mu\mu} = -\boldsymbol{\mu}_2 \cdot \boldsymbol{H}_1 - \boldsymbol{\mu}_1 \cdot \boldsymbol{H}_2 = -\frac{3\,(\boldsymbol{\mu}_2 \cdot \boldsymbol{n})\,(\boldsymbol{\mu}_1 \cdot \boldsymbol{n}) - \boldsymbol{\mu}_2 \cdot \boldsymbol{\mu}_1}{R^3} + (1 \leftrightarrow 2), \tag{3.82}$$

where $\boldsymbol{n}$ is the unit vector in the direction between the two heavy quarks. Now $\boldsymbol{\mu}_i$ is the Bohr magneton

$$\boldsymbol{\mu}_i = \frac{ge_i}{2m_i}\boldsymbol{S}_i \tag{3.83}$$

and the following relation holds

$$2\left[\boldsymbol{S}_1 \cdot \boldsymbol{S}_2 - 3\left(\boldsymbol{S}_1 \cdot \boldsymbol{n}\right)\left(\boldsymbol{S}_2 \cdot \boldsymbol{n}\right)\right] = \boldsymbol{S}^2 - 3\left(\boldsymbol{S} \cdot \boldsymbol{n}\right)^2 . \tag{3.84}$$

One finds

$$V_{\mu\mu} = -\left(\frac{g_Q e_Q}{2m_Q}\right)^2 \frac{1}{R^3}\left[\boldsymbol{S}^2 - 3\left(\boldsymbol{S} \cdot \boldsymbol{n}\right)^2\right], \tag{3.85}$$

which allows to identify

$$B = -\left(\frac{g_Q e_Q}{2m_Q}\right)^2 . \tag{3.86}$$

As we are dealing with a constituent quark model we do not expect the g_Q values to be comparable to those of a point like structureless particle. Thus, we leave g_Q as a free parameter and, as expected, we find best fit values larger than 2. We use $e_c = 2e/3$ and $e_b = e/3$.

We test the validity of our model on the charmonia and bottomonia spectra with $L = 1, 2$. In the heavy quark limit we expect the model to work better at fitting the bottomonia states, and we fit the η_b, Υ, $\chi_{b0}, \chi_{b1}, \chi_{b2}$ [251], and $\Upsilon(1D_1), \Upsilon(1D_2), \Upsilon(1D_3)$ [252]. The splitting between η_b and Υ is not a feature of the string model *per se*, since it is controlled by the parameter κ_b' which is not correlated with any other masses. The masses of the remaining states are controlled by two parameters (T_b and g_b), and we find the best fit values

$$\begin{cases} T_b = 0.258 \text{ GeV}^2, \\ g_b = 11.5. \end{cases} \tag{3.87}$$

The string tension is close to the value used to fit Regge trajectories of light mesons ($T \approx 0.175$ GeV^2) and differs only very slightly from the value obtained earlier by fitting the spin-averaged masses. The resulting spectrum is summarized in Table 3.6, where we also compare our results with the predictions obtained in the potential models in [34] and [55]. The agreement is remarkable. The splitting between the center of gravities of the S-, P-, and D-wave sectors has already been confronted with data; the new feature is that with the same parameters we are also able to describe the splitting among the ${}^3P_{0,1,2}$ and ${}^3D_{1,2,3}$ states. A comparison of the theoretical and experimental spectra is presented in Figs. 3.5 and 3.6.

The same work can be done for charmonia. In this case a priori we do not expect such a remarkable agreement with data. Still, as we will see, the agreement with the $L = 1$ states is rather good. We include in our fit the following charmonia [251]: η_c, J/ψ, h_c, $\chi_{c0}, \chi_{c1}, \chi_{c2}$, and $\psi(3770)$, which we identify with the 1^3D_1 state. The best fit is obtained with the following values for the parameters:

$$\begin{cases} T_c = 0.147 \text{ GeV}^2, \\ g_c = 5.7. \end{cases} \tag{3.88}$$

Here the agreement of the value obtained for the string tension with the one used for light mesons is better than in the $b\bar{b}$ case, and again it differs very little from the value obtained in the spin-averaged case. It is worth saying that performing the

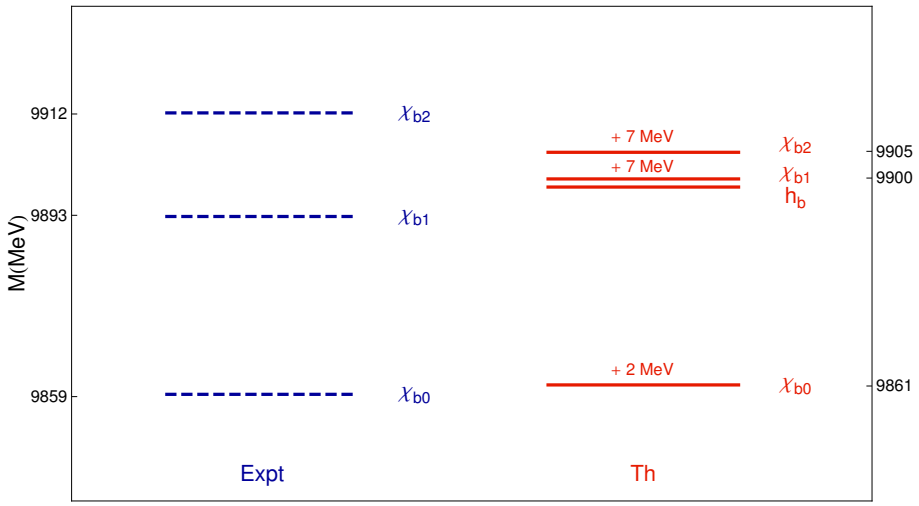

Figure 3.5. Results of the fit to the $L = 1$ bottomonia with the parameters in Eq. (3.87).

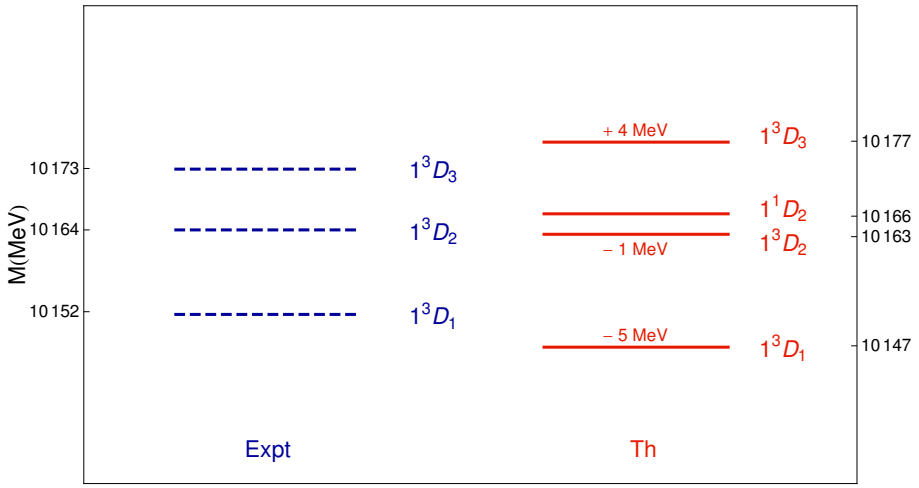

Figure 3.6. Results of the fit to the $L = 2$ bottomonium states with the parameters in Eq. (3.87).

Table 3.6. Theoretical values of the masses obtained by the fit with the parameters in Eq. (3.87) compared to the experimental values and to other theoretical determinations [34, 55]. All mass values are in MeV.

	M_{exp}	$\sigma(M_{exp})$	M_{th}	M_{th} [34]	M_{th} [55]
η_b	9391	3.2	**9388**	9366	9400
$\Upsilon(1S)$	9460	0.26	**9460**	9460	9460
h_b			**9898**	9924	9880
χ_{b0}	9859	0.5	**9861**	9888	9850
χ_{b1}	9893	0.4	**9900**	9913	9880
χ_{b2}	9912	0.4	**9905**	9939	9900
$\Upsilon(1^1D_2)$			**10166**	10166	10150
$\Upsilon(1^3D_1)$	10152	1	**10147**	10153	10140
$\Upsilon(1^3D_2)$	10164	0.9	**10163**	10163	10150
$\Upsilon(1^3D_3)$	10173	1	**10177**	10174	10160

same fit procedure numerically with the full expression for the energy, *i.e.*, without any expansion, and orbital momentum (see Eq. (3.47)), the best fit parameters are essentially the same as the ones quoted above, both for the charmonium and the bottomonium sectors.

The experimental masses [251] are compared to the results of the fit in Table 3.7, where we again compare with the predictions of [34, 55], and in Figs. 3.7 and 3.8. The agreement is very good, although unlike [34, 55] our model fails to reproduce the mass of the $\psi(3770)$, which is around 45 MeV above our predicted value. The effect of the mixing with the nearby $\psi'(3686)$ could be advocated as a possible resolution of this mismatch. However, since the mixing angle between the two states is only $\phi = (12 \pm 2)^\circ$ [42, 43], it could account for an upward shift of at most ~ 5 MeV with respect to the fitted value, giving the $\psi(3770)$ at 3735 MeV.

Table 3.7. Theoretical values of the masses obtained by the fit with the parameters in Eq. (3.88) compared to the experimental values and to other theoretical determinations [34, 55]. All mass values are in MeV.

	M_{exp}	$\sigma(M_{exp})$	M_{th}	M_{th} [34]	M_{th} [55]
η_c	2980	1	**2981**	2965	2970
J/ψ	3096	0.1	**3097**	3095	3100
h_c	3526	0.32	**3525**	3525	3520
χ_{c0}	3415	0.31	**3427**	3415	3440
χ_{c1}	3510	0.07	**3518**	3508	3510
χ_{c2}	3556	0.09	**3548**	3555	3550
$X(3872)[1^1D_2]$	3872	0.24	**3793**	3810	3840
$\psi(3770)$ $[1^3D_1]$	3772	0.35	**3727**	3762	3820
1^3D_2			**3779**	3797	3840
1^3D_3			**3831**	3840	3850

Our predicted value of 3793 MeV for the mass of the 1^1D_2 state is only slightly different from that which we obtained using the formula (3.62), and our conclusion

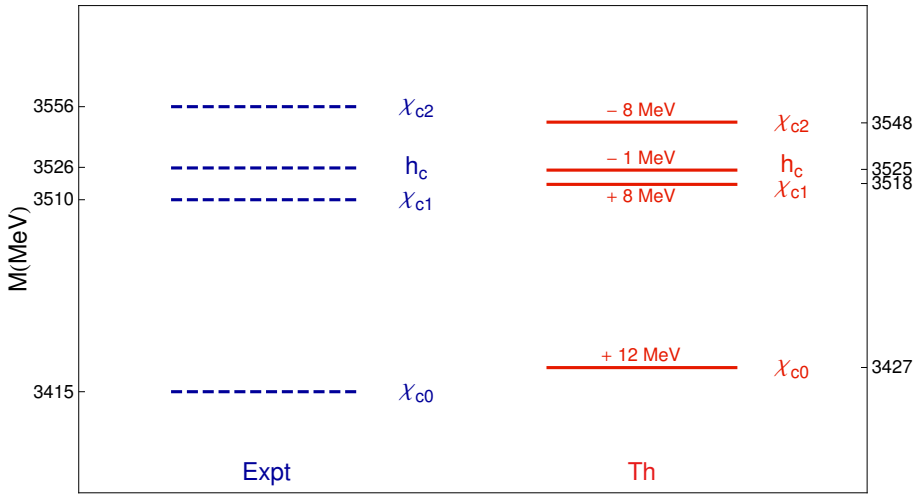

Figure 3.7. Results of the fit to the $L = 1$ charmonium states with the parameters in Eq. (3.88). The agreement between data and the results of our string model are remarkable in the $L = 1$ sector.

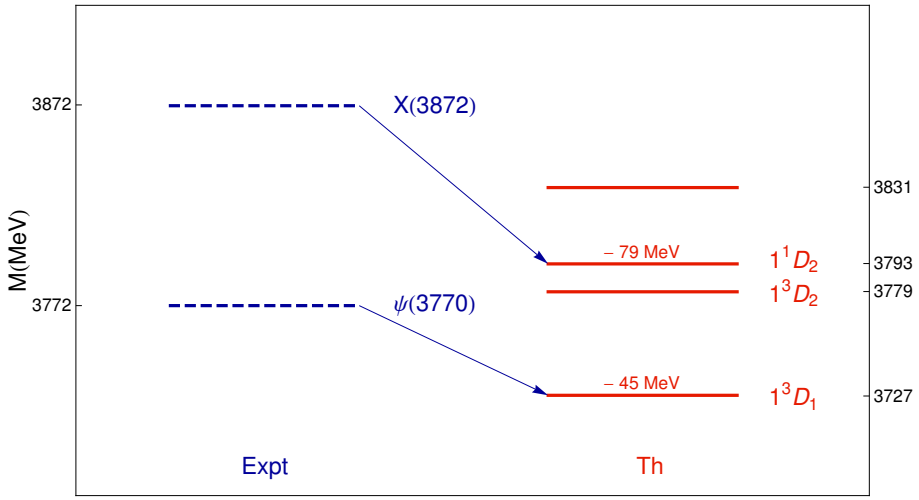

Figure 3.8. The same as in Fig. 3.7 but for the $L = 2$ states. We tentatively identify the $X(3872)$ with the 1^1D_2 charmonium state and the $\psi(3770)$ with the 1^3D_1.

remains the same: the mass of the $X(3872)$ is difficult to reconcile with the charmonium interpretation. Indeed it is evident in Figs. 3.7 and 3.8 the most difficult identification to make is that of the $X(3872)$ as a 1^1D_2 state. As can be seen in Table 3.7, the same is also true for the potential models [34] and [55]. Reference [253] compiles the mass predictions for a variety of different potential models, and five out of the six cases (including the two which we have quoted in the tables) predict the mass of the 1^1D_2 is some 50-100 MeV lighter than that of the $X(3872)$. The exception is that of Fulcher [254] who predicted a 1^1D_2 with a mass of none other

than 3872 MeV; notwithstanding the remarkable agreement of that model with the $X(3872)$ mass, we find rather more compelling the broad agreement of our model with the predictions of the majority of other approaches. We note in passing, however, that lattice QCD predicts a somewhat higher 2^{-+} mass of 3907 ± 32 MeV [255], consistent with the $X(3872)$.

At any rate the charmonium option cannot be dismissed only on the base of the mass spectrum. One has to consider also the decay pattern. First of all the charmonium interpretation fails to describe the isospin violation seen by experiments: the $J/\psi\,\rho$ and $J/\psi\,\omega$ modes are observed with the same strength $\mathcal{B}(X \to J/\psi\,\omega)/\mathcal{B}(X \to J/\psi\,\pi^+\pi^-) = 1.0 \pm 0.4$ (stat.) ± 0.3 (syst.) [256], in obvious contradiction to the expectations for a standard $c\bar{c}$ state which is a pure isoscalar. However the isospin violation is not so severe if one considers the different phase space volumes available to $J/\psi\,\pi^+\pi^-$ and $J/\psi\,\pi^+\pi^-\pi^0$ final states. Because of the different decay widths of ρ and ω one finds the ratio between the $I = 1$ and $I = 0$ amplitudes $\mathcal{A}_{I=1}/\mathcal{A}_{I=0} \approx 0.5$, consistent with the experimental value. A further possibility is that the $J/\psi\,\pi^+\pi^-$ and $J/\psi\,\pi^+\pi^-\pi^0$ modes are fed by rescattering from intermediate $D^*\bar{D}$ states, and isospin is broken by the mass difference between the neutral and charged states [257].

Historically, the literature on the 1^1D_2 state has assumed that it lies below the $D^*\bar{D}$ threshold in which case it would decay dominantly by radiative transitions, hadronic transitions with pion emission, and annihilation into gluons. Among the radiative transitions, the dominant mode is expected to be [258]

$$X(3872) \to h_c\gamma \to J/\psi\,\pi^0\gamma, \tag{3.89}$$

with a branching ratio of 0.004. Using the $X(3872)$ mass, Ref. [253] predicts a $h_c\gamma$ width of 0.460 MeV, somewhat larger than an earlier prediction of 0.278 MeV which assumed a lower mass [259]. Reference [253] also predicts a considerable $\psi(3770)\gamma$ mode with a partial width of 0.045 MeV. By contrast, the observed $J/\psi\,\gamma$ and $\psi'\gamma$ are rather at odds with expectations. Because of the orthogonality of the spin and spatial wave functions of the heavy quark pair, these transitions are expected to be small, although the $\psi'\gamma$ would be enhanced due to its $1D$ component, as it is presumably the orthogonal partner of the dominantly $1D$ $\psi(3770)$. In a recent paper [260] the 2^{-+} hypothesis has been tested on the radiative decays of $X(3872)$. Using potential non-relativistic QCD (coupled to electromagnetism to describe single photon transitions), they found upper bounds on $\mathcal{B}(1^1D_2 \to J/\psi(\psi')\gamma)$ which are 1 order of magnitude smaller than the experimental lower bounds obtained from BaBar measurements. The estimate for the $1^1D_2 \to \psi'\gamma$ takes into account the $S - D$ wave mixing in the ψ' wave function, which turns out to be not sufficient to accommodate theoretical predictions with experimental data. The approach used in [260], first derived in [261], relies on the use of charmonium potential models in order to compute overlap integrals of radial wave functions. The stability of the results is checked using different potentials. Furthermore in recent news Belle does not confirm the $X(3872) \to \psi'\gamma$ decay [262], in contrast to the BaBar result with an estimated branching ratio $\mathcal{B}(X \to \psi'\gamma) \simeq 6\%$ [263].

As for the hadronic transitions, Refs. [259, 253] indicate that the dominant hadronic decay mode with two pions in the final state is $1^1D_2 \to \eta_c\pi\pi$, and the latter

authors predict a partial width of 0.21 ± 0.11 MeV. As described in [47], this result is obtained using a multipole expansion of the color gauge field. In atomic physics the analogous process is the emission of atomic electrons or e^+e^- pairs by nuclei. This expansion leads to some selection rules which at leading order imply that quark spin is conserved. Thus the operator responsible for the transition connects quarkonium states with the same spin S, namely 1^1D_2 and 1^1S_0, the η_c. The observation or the absence of this decay would be crucial and thus we encourage the experimental search in this direction.

Reference [264] considered the $D^{0*}\bar{D}^0$ decays of a heavier 1^1D_2 and predicted a partial width of 0.03 MeV for a state with mass 3872 MeV, increasing to 1.7 MeV if it were somewhat higher at 3880 MeV; experimentally, the $X(3872)$ is known to lie much closer to 3872 MeV and these partial widths are consistent with the experimental width.

In conclusion if the $X(3872)$ were a 1^1D_2 charmonium, the $h_c\gamma$ and $\eta_c\pi\pi$ decay modes ought to be prominent. Furthermore the verification or otherwise of $\psi'\gamma$ may help clarify the situation.

3.3.2 The case of Y(4630) and Y(4660) [3, 2]

As reported in Section 2.1, $Y(4660)$ and $Y(4630)$ are two 1^{--} states produced in initial state radiation events and decaying into $\psi'\,\pi^+\pi^-$ and $\Lambda_c^+\Lambda_c^-$ respectively.

Experimental data. In [3] we performed a re-analysis of data from the Belle experiment on the decay of the $Y(4660)$ resonance in $\psi'\pi^+\pi^-$ [104] and of the $Y(4630)$ in $\Lambda_c^+\Lambda_c^-$ [105]. We fit the invariant mass spectra in Fig. 3.9 with a binned likelihood, adopting a consistent signal model: a relativistic Breit-Wigner with comoving width, as detailed in [245]. Background is parameterized with a second order polynomial multiplied by the phase space. The individual fits to the charmonium and baryonic modes return:

$$Y(4660) \to \psi'\pi^+\pi^- : \begin{cases} M_{Y_B} = (4661 \pm 9)\ \text{MeV} \\ \Gamma_{Y_B} = (61 \pm 23)\ \text{MeV} \end{cases} \quad \text{with } \chi^2/\text{d.o.f.} = 7/20 \tag{3.90}$$

and

$$Y(4630) \to \Lambda_c^+\Lambda_c^- : \begin{cases} M_{Y_B} = (4661 \pm 14)\ \text{MeV} \\ \Gamma_{Y_B} = (63 \pm 23)\ \text{MeV} \end{cases} \quad \text{with } \chi^2/\text{d.o.f.} = 51/35 \tag{3.91}$$

respectively. The two results are consistent, strongly supporting the hypothesis that the two structures are evidences of the *same resonance*, which we named Y_B[5]. From the same fits we also extract

$$\frac{\mathcal{B}(Y_B \to \Lambda_c^+\Lambda_c^-)}{\mathcal{B}(Y_B \to \psi'\pi^+\pi^-)} = 25 \pm 7, \tag{3.92}$$

a result which highlights a strong affinity of the Y_B to the baryon-antibaryon decay mode[6].

[5] We use the results of the first, and more accurate, fit as reference

[6] It is to be noted that omitting interference, the ratio of the peak cross sections is about 11.

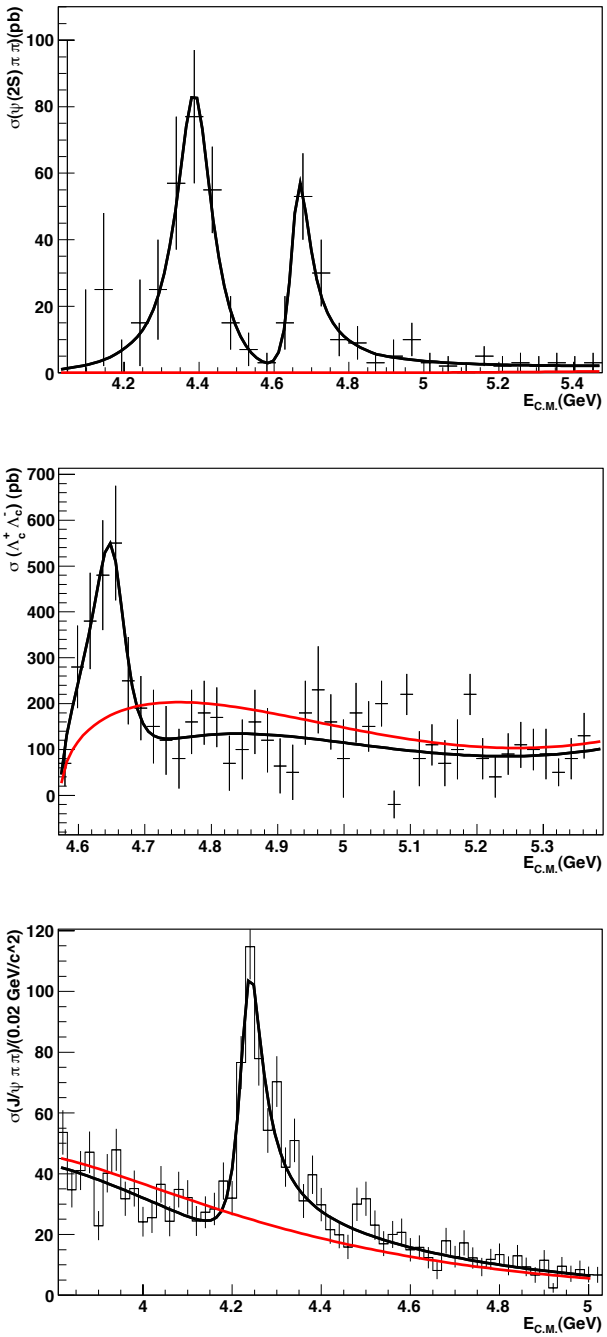

Figure 3.9. Fit of the cross section from the data of Belle Collaboration [104, 105] for the process $e^+e^- \to \psi'\pi^+\pi^-$ (top) and $e^+e^- \to \Lambda_c^+\Lambda_c^-$ (center) and from the BaBar Collaboration [87] for the process $e^+e^- \to J/\psi\,\pi^+\pi^-$ (bottom) . The black line represents the fit results, the red one shows the polynomial background.

There are three other interesting experimental facts which we observed in [3] for the first time. First the absence of the decay of $Y_B \to J/\psi\,\pi^+\pi^-$ on which we put an upper limit

$$\frac{\mathcal{B}(Y_B \to J/\psi\,\pi^+\pi^-)}{\mathcal{B}(Y_B \to \psi'\,\pi^+\pi^-)} < 0.46 \qquad \text{at } 90\% \text{ C.L.}. \tag{3.93}$$

Second the contribution of σ and f_0 in the two pion invariant mass spectrum measured by Belle in the mass region of the Y_B [104] (see Fig. 3.10). In absence of background (see Fig. 3.9), we fit for the sum of two relativistic Breit-Wigner functions describing the σ and $f_0(980)$. The resulting fitted masses and widths are $m_\sigma = (714 \pm 77)$ MeV, $\Gamma_\sigma = (499 \pm 176)$ MeV and $m_{f_0} = (955.3 \pm 4.5)$ MeV, $\Gamma_{f_0} = (14 \pm 15)$ MeV, in agreement with the standard knowledge about the light scalar mesons. Since these mesons are the best currently known candidates for tetraquarks [265, 219] in the light sector, the four-quark nature of the Y_B is naturally suggested. Furthermore we extracted the ratio

$$\mathcal{B}(Y_B \to \psi(2S)\sigma(600))/\mathcal{B}(Y_B \to \psi(2S)f_0(980)) = 2.0 \pm 0.3. \tag{3.94}$$

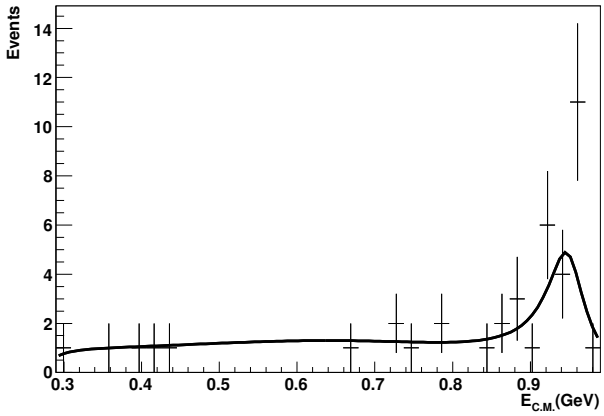

Figure 3.10. Fit of the dipionic mass distribution in the mass region for $\psi(2S)\pi^+\pi^-$: 4.0 GeV $< m_{\pi^+\pi^-\psi(2S)} <$ 4.5 GeV [105] including the contributions of σ and $f_0(980)$. Removing the σ, the lower part of the spectrum gives a sensibly worse fit.

Finally by fitting consistently the $\psi'\pi^+\pi^-$ spectrum in Fig. 3.9 we extract the parameters of the $Y(4350)$ resonance $M = (4353 \pm 13)$ MeV and $\Gamma = (118 \pm 25)$ MeV and we also find that

$$\mathcal{B}(Y(4350) \to J/\psi\,\pi\pi)/\mathcal{B}(Y(4350) \to \psi(2S)\pi\pi) < 3.4 \times 10^{-3} \qquad \text{at } 90\% \text{ C.L.}. \tag{3.95}$$

Tetraquark interpretation. The prominence of the baryon-antibaryon decay mode over the charmonium one can be interpreted as the evidence of a $[cq][\bar{c}\bar{q}]$ diquark-antidiquark structure of the Y_B meson. The diagram **A** in Fig. 3.11 is a representation of a $[cq][\bar{c}\bar{q}]$ tetraquark where the two diquarks are connected by a string neutralizing their color. To obtain 1^{--} quantum numbers one needs at least

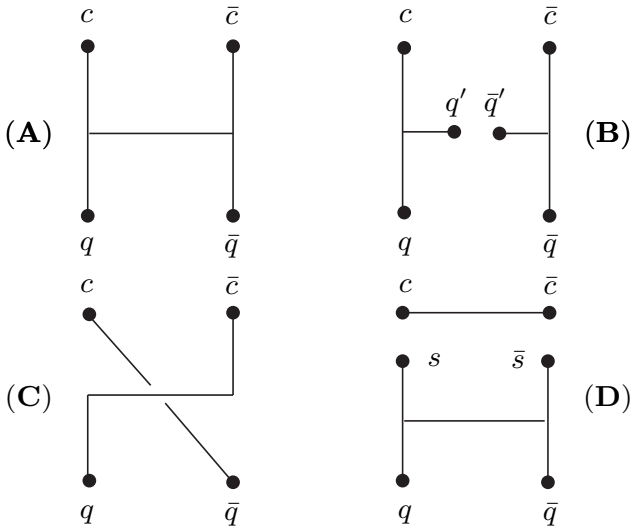

Figure 3.11. Phase space allows **A** → **B** ($Y_B \to \Lambda_c \bar{\Lambda}_c$), **A** → **C** ($Y_B \to D\bar{D}^*$), **A** → **D** ($Y \to \psi' f_0(980)$).

a unit of orbital angular momentum between the diquark and the antidiquark. The Y_B tetraquark wave function is either $([cq]_{0^+}[\bar{c}\bar{q}]_{0^+}))_{L=1}$ or $([cq]_{0^+}[\bar{c}\bar{q}]_{1^+}))_{L=1}$ − c.c..

The $L = 1$ centrifugal potential favors configurations with the diquarks at an higher average relative distance with respect to the $L = 0$ case, stretching the color string which eventually breaks as in diagram **B** of Fig. 3.11 (baryon-antibaryon decay). Breaking the color string in two points rather than in one, as shown in **C** or in **D** in Fig. 3.11, allows either the $D\bar{D}^*$ or the ψf_0 decay. To estimate the spectrum of orbital excitations we resort to the expression of Eq. (3.54), where $M = m_{[cq]}$ is the mass of the diquark and T should be the string tension of the diquark antidiquark system.

Our predictions depend on the value we use for the diquark mass. We thus distinguish two circumstances.

X(3872) with $J^P = 1^+$. In this case $X(3872)$ is a $L = 0$ diquark-antidiquark bound state and the expression of its mass in terms of $m_{[cq]}$ and the chromo-magnetic couplings is

$$M_{X(3872)} = 2m_{[cq]} - \kappa_{(cq)_{\bar{\mathbf{3}}}} + \frac{1}{2}\kappa_{q\bar{q}} - \kappa_{c\bar{q}} + \frac{1}{2}\kappa_{c\bar{c}} \tag{3.96}$$

which gives $m_{[cq]} = 1933$ MeV. With this value of the diquark mass and using the tension T_c derived from the $c\bar{c}$ spectrum, Eq. (3.88), we obtain from Eq. (3.55)

$$\begin{aligned} M(L = 1, n_r = 0) &= 4289 \text{ MeV} \\ M(L = 3, n_r = 0) &= 4745 \text{ MeV}, \end{aligned} \tag{3.97}$$

where n_r is the radial quantum number. We cannot exclude a priori that Y_B could be a $L = 3$ state, so we quote the relative prediction for its mass. If we

want to estimate the mass of the radial excitations of a $\mathfrak{q}\bar{\mathfrak{q}}$ $L = 1$ state, we can borrow the mass gap between the ground state and the first radial excitation of the P-wave charmonia. Using the results in [266] gives $\Delta M_{\rm rad} \simeq 0.440$ GeV so that

$$M(L = 1, n_r = 1) = 4729 \text{ MeV}, \tag{3.98}$$

which is the closer value to the Y_B mass, 70 MeV away from the experimental measure. Thus the most likely assignment is that Y_B is the first radial excitation of a $L = 1$ tetraquark state. Moreover one is tempted to identify $Y(4350)$, with the radial ground state, its mass being only 60 MeV away from the predicted value Eq. (3.97).

To refine the model we investigate whether the decay patterns of the $Y(4350)$ and Y_B are consistent with the assigned quantum numbers: from data we see that both $Y(4350)$ and Y_B prefer to decay into $\psi'\pi^+\pi^-$ rather than into $J/\psi\,\pi^+\pi^-$, even if the latter mode is phase space enhanced. The measured spectra show that the $\pi\pi$ pair comes from phase space (or, equivalently a σ) apart from the case of the Y_B where there seems to be a 30 % component due to $f_0(980)$, see Eq. (3.94). We therefore attempt an explanation of the observed Y's decay pattern describing the S-wave transition $\langle\psi(1S, 2S)\mathfrak{a}|Y\rangle$ as

$$\langle\psi(\eta, q)\mathfrak{a}(k)|Y(\epsilon, p)\rangle = g\ \epsilon\cdot\eta, \tag{3.99}$$

where $\mathfrak{a} = \sigma, f_0$. We find the eigenfunctions Ψ of the linear part of the Cornell potential $V(r) = -k/r + r/a^2$ ($k = 0.52$, $a = 2.3$ GeV^{-1}) for the $\psi(1S, 2S)$ and the charmonium-like Y, namely $\Psi = Y_{L,m}R_{n_r,L}$. Interpreting the Y's as charmonium-like bound states made up by a diquark and an antidiquark we can write

$$g \propto \int d^3r\ R^\dagger_{(\psi)}(r)R_{(Y)}(r). \tag{3.100}$$

We are interested in estimating the following ratio of decay widths

$$\Gamma_{\mathfrak{a}}(Y) \equiv \Gamma(Y \to \psi(1S)(\pi\pi)_{\mathfrak{a}})/\Gamma(Y \to \psi(2S)(\pi\pi)_{\mathfrak{a}}). \tag{3.101}$$

We find the values reported in the Table 3.8. We report separately the σ and f_0 contributions. The results show that the radial excitation would explain the preference of Y_B tetraquark to decay into $\psi'\sigma$ whereas with this simple model we cannot explain why the $Y(4350)$ seems to prefer the ψ' channel. This aspect remains puzzling.

X(3872) with $J^P = 2^-$. In this case, which we have considered in [2], $X(3872)$ is a $L = 1$ diquark-antidiquark bound state. Neglecting the chromo-magnetic interactions the diquark mass can be extracted directly from Eq. (3.55) giving $m_{[cq]} = 1716$ MeV.

The entire spectrum of $L = 0$ states, discussed in Section 3.2, is shifted downwards in mass once the new input value is the 2^{-+} $X(3872)$: the average mass will be around $2m_{[cq]} \simeq 3430$ MeV. Thus a striking prediction of the tetraquark model is that there is a set of positive parity states in the same mass region as the $\chi_{c0,1,2}$ and h_c. The full spectrum of tetraquark states is

Table 3.8. $\Gamma_{\mathfrak{a}}(Y)$ as in Eq. (3.101), $\mathfrak{a} = \sigma, f_0$. The square of the matrix element in Eq. (3.100) weights the three-body phase space where the two pions are the decay products of an intermediate scalar resonance. The Breit-Wigner ansatz we use is a rough approximation for the description of a very broad σ meson whereas is rather suitable for the $f_0(980)$.

n_r	L	$\Gamma_\sigma(Y_B(4660))$	$\Gamma_{f_0}(Y_B(4660))$
1	1	0.1	0.5
n_r	L	$\Gamma_\sigma(Y(4350))$	$\Gamma_{f_0}(Y(4350))$
0	1	15.8	–

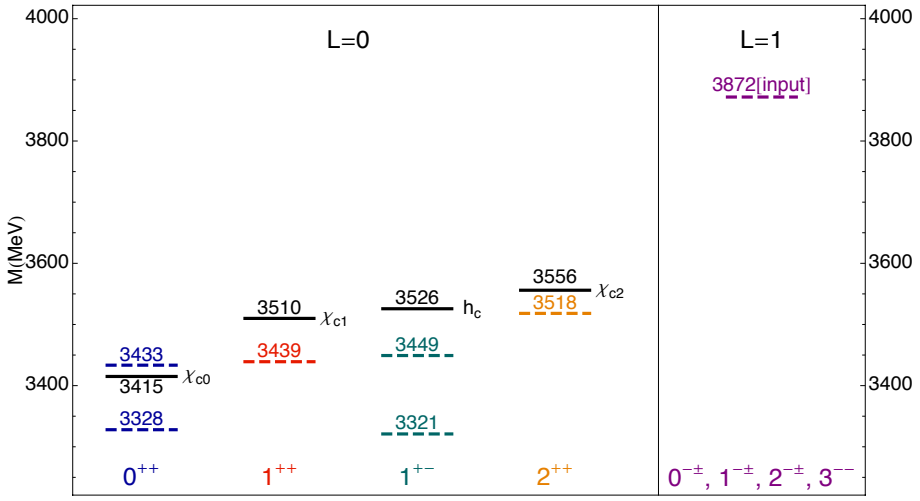

Figure 3.12. Dashed lines represents the full spectrum of the tetraquark $[cq][\bar{c}\bar{q}]$ states with $L = 0$ and $L = 1$, whereas the solid lines are the standard charmonium levels with $L = 1$.

reported in Fig. 3.12. Among the $L = 0$ states the 0^{++} tetraquark is very close in mass to the standard charmonium state χ_{c0}, while the others are some 40 MeV lighter than the charmonia with the same J^{PC}.

As for the $L = 1$ part of the spectrum, a closer look is required for the 1^{--} states. The new value of the diquark mass pushes the masses of the $L = 1$ states down to the $3800 - 3900$ MeV region. In this scheme the $Y(4350)$ and the Y_B could thus be the two successive radial excitations of the 1^{--} state at about 3870 MeV [7]. For a rough estimate of the mass splitting between the first and second radial excitations, we borrow again the results obtained in [266]

[7] Observe that using the tension obtained from the fit to the charmonium states, the mass of $L = 1$ and $L = 3$ tetraquarks would be 3872 MeV and 4353 MeV respectively. We choose not to consider the $L = 3$ assignment.

Table 3.9. $\Gamma_{\mathfrak{a}}(Y)$ as in Eq. (3.101), $\mathfrak{a} = \sigma, f_0$.

n_r	L	$\Gamma_\sigma(Y_B(4660))$	$\Gamma_{f_0}(Y_B(4660))$
2	1	0.6	1.9
n_r	L	$\Gamma_\sigma(Y(4350))$	$\Gamma_{f_0}(Y(4350))$
1	1	0.3	–

$\Delta M'_{\rm rad} = 370$ MeV, which gives

$$\begin{aligned} M(n_r = 1, L = 1) &= 4320 \text{ MeV} \\ M(n_r = 2, L = 1) &= 4690 \text{ MeV} \end{aligned} \tag{3.102}$$

The advantage of this assignment is that it explains the suppression of the $Y(4350) \to J/\psi\,\pi^+\pi^-$ and $Y_B \to J/\psi\,\pi^+\pi^-$ decays with respect to the corresponding $\psi^{'}$ decay modes. Within this new picture we repeat the estimate of the ratio in Eq. (3.99) and (3.100) and we find the results reported in Table 3.9.

In this case, although it cannot reproduce entirely the experimental suppression of the $J/\psi\,\pi^+\pi^-$ mode, the ansatz contained in Eq. (3.100) is able to account for some enhancement of $\psi'\pi^+\pi^-$ despite the phase space suppression.

As we already said, the prediction of such a large number of unobserved states is the main drawback of the tetraquark model. In what follows we investigate the decay dynamics of the $L = 0$ and $L = 1$ tetraquarks that emerges in the case of the $J^P = 2^-$ assignment for $X(3872)$, considering also that the low-lying states overlap with the standard $c\bar{c}$ ones. Our intention is to indicate a selection rule which prevents some of the predicted states to be observable, because of a too large decay width.

Each tetraquark wave function contains an admixture of color singlet meson pairs, and one therefore expects that hadronic decays will be dominated by a "fall-apart" mechanism in which the tetraquark dissociates into meson pairs, either charmed mesons or a charmonium plus light meson(s), and also radiative decays in which a light quark pair annihilates into a photon. The $X(3872)$ decays in all three ways.

We show in Table 3.10 the J^{PC} allowed hadronic and radiative decays of $L = 0$ and $L = 1$ tetraquarks and the corresponding partial waves. We also identify selection rules which arise due to the spin part of the decay amplitude, the details of which are derived in Section D.1.1 of Appendix D. Entries without parentheses indicate that the fall-apart decay can proceed by a spin-conserving process, which is to say that the diquark-antidiquark spin wave function recouples directly into the spin wave functions of the final state mesons. Those with parentheses require a spin flip, either of the light or heavy-light quark pair (round brackets), or the heavy quark pair (square brackets); we expect the latter to be a stronger selection rule. Such arguments have been used before in the context of the $X(3872)$ as a 1^{++} tetraquark [229] or molecule [143], where

Table 3.10. Hadronic and radiative decays of tetraquark states in given partial waves S, P, D, F. Partial waves in parentheses indicate that the decay can take place only by spin-flip, either of the light or heavy-light quark pair (round brackets) or the heavy quark pair (square brackets). In applying the rule to decays involving the σ, we assume that they proceed through an intermediate $q\bar{q}$ with $^3\mathrm{P}_0$ quantum numbers which then feeds the physical σ.

	0^{++}	1^{++}	2^{++}	0^{-+}	1^{-+}	2^{-+}
$\eta_c\pi^0$	S		[D]		(P)	
$\eta_c\eta$					(P)	
$J/\psi\,\rho$				(P)	(P,F)	(P,F)
$J/\psi\,\omega$				(P)	(P,F)	(P,F)
$\eta_c'\pi^0$					(P)	
$D\bar{D}$					(P)	
$D^*\bar{D}$				P	P	P
$\eta_c\sigma$		[P]	[P]	S		D
$\chi_0\pi$				S		D
$\chi_1\pi$					S,D	D
$\chi_2\pi$				D	D	S,D
$J/\psi\,\gamma$	S,D	S,D	S,D	(P)	(P,F)	(P,F)
$\psi'\,\gamma$				(P)	(P,F)	(P,F)
$h_c\gamma$				S,D	S,D	S,D

	1^{+-}	0^{--}	1^{--}	2^{--}	3^{--}	
$J/\psi\,\pi^0$	S,D	(P)	(P)	(P,F)	(F)	
$J/\psi\,\eta$		(P)	(P)	(P,F)	(F)	
$\eta_c\rho$		[P]	(P)	[P,F]	[F]	
$\eta_c\omega$		[P]	(P)	[P,F]	[P,F]	
$\psi'\pi^0$		(P)	(P)	(P,F)	(F)	
$D\bar{D}$			P		(F)	
$D^*\bar{D}$		P	P	P	(F)	
$J/\psi\,\sigma$	(P)		S,D	D	D	
$h_c\pi$			S,D	[D]	[D]	
$\chi_0\gamma$	(P)		S,D	D	D	
$\chi_1\gamma$		S,D	S,D	S,D	D	
$\chi_2\gamma$			S,D	S,D	S,D	
$\eta_c\gamma$	S,D	[P]	(P)	[P,F]	[F]	
$\eta_c'\gamma$		[P]	(P)	[P,F]	[F]	

the wave function in either case necessarily has the $c\bar{c}$ in spin-one, consistent with the dominance of the $J/\psi\,\pi^+\pi^-$ and $J/\psi\,\pi^+\pi^-\pi^0$ modes.

The J^+ states present something of a problem from a phenomenological point of view, insofar as they are as light or even lighter than the corresponding h_c and χ_c states, sharing the same quantum numbers and hence decay modes, and yet there is apparently no experimental evidence for their existence. Recall that among the neutral states we would expect four additional 0^{++} and 1^{+-}, and two additional 1^{++} and 2^{++} states. Referring to Table 3.10, we note that

the two most numerous of the expected additional states, 0^{++} and 1^{+-}, can decay in S-wave to $\eta_c\pi$ and $J/\psi\,\pi$ respectively, and one could argue that they simply "fall-apart" broadly in such a way as to be effectively unobservable. The remaining states $L = 0$ cannot be dismissed in this way. The 1^{++} states, because of their unnatural parity, cannot decay into $\eta_c\pi$ and we thus expect them to be comparatively narrow. The corresponding χ_{c1} state has a width of less than 1 MeV; the tetraquark analogue may be broader on account of fall-apart decay into $\eta_c\pi\pi$ via the low mass tail of the broad σ, however this is forbidden in the limit of heavy quark spin conservation, since the 1^{++} tetraquark necessarily has the $c\bar{c}$ in spin 1, as discussed above. The 2^{++} states could decay to $\eta_c\pi$ in D-wave, but this is also forbidden by heavy quark spin conservation. In the tetraquark picture we thus expect light, narrow 1^{++} and 2^{++} states in the χ_c mass region decaying into $\eta_c\pi$ and $J/\psi\,\gamma$.

Because of their higher mass the J^- states have many more available decay modes and considerably more phase space, and it is plausible that most of them decay broadly so as to be effectively unobservable.

The $X(3872)$ with 2^{-+} quantum numbers may be a unique exception. Because of its unnatural spin-parity it cannot decay to $\eta_c\pi$, $\eta_c\eta$, or $D\bar{D}$; its observed decays into $J/\psi\,\rho$, $J/\psi\,\omega$ and $D^0\bar{D}^{0*}$ are all P-wave with very little phase space, naturally implying a small width in accordance with the experimental data, $\Gamma_X = 3.0^{+2.1}_{-1.7}$ MeV. Moreover, we note that the J/ψ modes are suppressed by the conservation of quark spin, even if only the light quark spin needs to flip and thus this selection rule may be badly violated. Indeed the very observation of these modes confirms that the rule is broken, but without further model-dependent assumptions it is difficult to ascertain to what extent the narrowness of the $X(3872)$ is due to the limited phase space and to what extent it is due to this weak selection rule. We note also that the observed $J/\psi\,\gamma$ and $\psi'\,\gamma$ decays also imply the non conservation of light quark spin: the $q\bar{q}$ pair can only annihilate into a photon if it has spin one, and the wave function of the $X(3872)$ does not contain such a component (see Appendix D). In a diquark-antidiquark model the P-wave tetraquark wave function contains a $c\bar{c}$ pair at large distance due to the P-wave, and thus it may be anticipated that $\chi_c\pi$ modes, particularly $\chi_{c2}\pi$, and $h_c\gamma$, should be large. We thus urge a search for these challenging modes which, if observed to be prominent, would support the tetraquark hypothesis, although as noted earlier $h_c\gamma$ should also be large in the 1^1D_2 case.

The pattern of allowed decays for the 0^{-+} states is very similar to those of the 2^{-+} states, largely because of their shared unnatural spin-parity. The $\eta_c\sigma$ decay goes in S- rather than D-wave, and in a model approach [229] one expects tetraquark states to couple strongly to final states which themselves have four-quark content, as the σ is generally accepted to have. This coupling may be so strong as to make the width of the 0^{-+} much larger than that of the 2^{-+}, which may therefore make it more difficult to identify. If such a mechanism is not in place then the 0^{-+} states should exist and will be as narrow as the $X(3872)$. Indeed, they may be even narrower: due to spin-orbit splittings one expects the 0^{-+} to be lighter than the 2^{-+} [233], which would

close the $D^{0*}\bar{D}^0$ mode and reduce the effective phase space for $J/\psi\rho$ and $J/\psi\,\omega$. Such a state should, like the $X(3872)$, decay radiatively into $J/\psi\,\gamma$, and there is apparently no signal in the data [71].

Among the remaining states we expect the unnatural spin-parities 0^{--} and 2^{--} to be the most narrow, although they will presumably be broader than the corresponding 0^{-+} and 2^{-+} states due to the much greater phase space available to $J/\psi\,\pi$ and $J/\psi\,\eta$ compared to $J/\psi\,\rho$ and $J/\psi\,\omega$. If their mass is sufficient the $D^*\bar{D}$ mode could be prominent, while $\eta_c\rho$ and $\eta_c\omega$ are forbidden by the conservation of heavy quark spin. We expect dominant radiative decays to $\chi_{c1}\gamma$ and, for the 2^{--}, $\chi_{c2}\gamma$.

The remaining 1^{--}, 3^{--}, and the J^{PC} exotic 1^{-+} states have many decay modes available and with ample phase space, so we expect that they should be the least stable of all the possible $L = 1$ tetraquark configurations. This may be helpful from a phenomenological point of view. The spectra of 1^{--} states in the $3800 \div 3900$ MeV mass region has been very well studied and there is apparently no evidence of an overpopulation of states, whereas in the tetraquark picture one expects a further eight neutral states alone. The phenomenology is thus only consistent with the assumption that the 1^{--} states, due to the large number of decay modes available and ample phase space, do not exist as stable resonances. It may be, however, that their radial excitations are more stable on account of the spatial separation of the $c\bar{c}$ pair, as discussed earlier in the context of the $Y(4350)$ and Y_B. If it is indeed the case that the radial ground states of the $L = 1$ tetraquark states with 1^{--} quantum numbers do not exist as stable resonances, then one can infer, judging by the overall similarity of their decay patterns to those of the 1^{--} states, that the 3^{--} and 1^{-+} states are likewise unstable and probably do not exist.

3.3.3 Other candidates

$Y(4260)$. $Y(4260)$ was considered as a $[cs]_{0^+}[\bar{c}\bar{s}]_{0^+}$ in a P-wave state in [267, 230] . Studying the uncertainty in the determination of the orbital term, a mass of $M = (4330 \pm 70)$ MeV was estimated, in nice agreement with the mass of $Y(4260)$ but also consistent with the mass of $Y(4350)$. However, from the $\pi\pi$ mass distribution, none of these two states, $Y(4260)$ and $Y(4350)$ has a decay with an intermediate state consistent with $f_0(980)$ and, therefore, it is not clear whether they should have an $s\bar{s}$ pair in their structure. Furthermore, in [267] the authors estimate that the mass of a $[cs]_{0^+}[\bar{c}\bar{s}]_{0^+}$ tetraquark in a P-wave state would be 200 MeV higher than the $Y(4260)$ mass, concluding that it is more natural to interpret the $Y(4260)$ as a $[cq]_{0^+}[\bar{c}\bar{q}]_{0^+}$ tetraquark in a P-wave state.

$Y_b(10890)$. In [237, 268, 269] Ali and collaborators proposed to explain the anomalous production of $\Upsilon(1S, 2S)\pi^+\pi^-$ in e^+e^- collisions at $\sqrt{s} \sim 10.890$ GeV introducing a new resonance, $Y_b(10890)$, with a $([bq][\bar{b}\bar{q}])_{L=1}$ tetraquark structure. This state contributes to the production of $\Upsilon(1S, 2S)\pi^+\pi^-$ through resonant channels, $Y_b \to \Upsilon(1S)(\sigma, f_0(980), f_2(1270))$ and $Y_b \to \Upsilon(2S)\sigma$, and non resonant channels. The resonant channels with σ and $f_0(980)$ are expected to be large, since Y_b as a

tetraquark should have a high affinity to these light mesons, which are the strongest tetraquark candidates in the light sector.

Chapter 4

X(3872): decays and production

In this chapter we focus our attention on the $X(3872)$ resonance, the first among the XYZ mesons to be observed in 2003. It is by far the particle for which the most experimental information is available, nevertheless it is still not possible to establish weather its J^P quantum numbers are 1^+ or 2^-. We will consider each hypothesis from the point of view of the decay and production processes.

In Section 4.1 we compute the strong coupling constants for the three prominent decay modes: $J/\psi\,\rho$, $J/\psi\,\omega$ and $D^0\bar{D}^{0*}$. We do not make any hypothesis on the nature of the resonance and thus our conclusions are model independent and could serve as a benchmark for other estimates of the same couplings. We will use these values in the next chapter to quantify the role of $X(3872)$ in the renowned phenomenon of J/ψ suppression in heavy ions collisions.

In Section 4.2 we study the prompt production, *i.e.* not from B-decays, cross section in $p\bar{p}$ collisions. We consider two possible interpretations of $X(3872)$: a loosely bound $D^0\bar{D}^{0*}$ molecule in the $J^{PC} = 1^{++}$ case and a 1^1D_2 charmonium in the $J^{PC} = 2^{-+}$ one. We compute predictions for the prompt production cross section at the Tevatron, $p\bar{p}$ collider at $\sqrt{s} \sim 1.96$ TeV, and compare the results with the experimental measurements. We conclude that both interpretations fail to reproduce the experimental data from CDF.

4.1 Decays [4]

There are still two open possibilities for the J^{PC} quantum numbers of this resonance. Indeed, as explained in Section 2.1, the BaBar collaboration recently took issue with the statement that the $X(3872)$ is a 1^{++} resonance, as was widely accepted, raising the hypothesis of 2^{-+} quantum numbers [68], yet to be confirmed by Belle or LHC experiments.

In [4] we considered the decays of $X(3872)$ under the hypothesis that it is a 1^{++} state, let us call it X_1, or a 2^{-+} state, call it X_2, but making no assumptions on its structure (charmonium, molecule, tetraquark).

We will define a general parameterization of the transition matrix elements, describing the known decays in terms of a set of strong coupling constants. Using the experimental information available and summarized in Table 4.1, we will determine the strong couplings in the 1^{++} and 2^{-+} cases by the explicit computation of decay

widths. In our fits we also use the data on $X \to J/\psi\,\omega$ decay reported in [68].

Table 4.1. Branching ratios $\mathcal{B}$ and one sigma errors $\sigma(\mathcal{B})$ for the observed decays of $X(3872)$ [75].

Decay Mode	$\mathcal{B}$	$\sigma(\mathcal{B})$
$X \to J/\psi\,\pi^+\pi^-$	0.055	0.020
$X \to J/\psi\,\pi^+\pi^-\pi^0$	0.045	0.030
$X \to J/\psi\,\gamma$	0.0135	0.0060
$X \to D^0\bar{D}^{0*}$	0.67	0.13

We will not attempt any theoretical determination of the strong coupling constants we are going to define. This would require to formulate some hypotheses on the structure of the X and the use of approaches such as quark models or QCD sum rules. This work could be done elsewhere and confronted with the coupling strengths found here.

We also confirm that using data in [68], the negative parity assignment for the X is indeed favored: as opposite to an earlier analysis by CDF [60] on the $J/\psi\,\pi^+\pi^-$ angular distribution, indicating that both the 1^{++} and 2^{-+} assignments are equally possible, we will show that the 2^{-+} assignment would be the preferred one.

4.1.1 Transition matrix elements

We start with the parameterization of the transition matrix elements for the decay processes in Table 4.1 in terms of coupling strengths whose numerical values are then extracted by comparison with experimental data. The transition matrix elements are related to the M_{fi} matrix elements by

$$T_{fi} = (2\pi)^4\delta^4(p_i - \sum_f p_f)\; M_{fi}. \tag{4.1}$$

As for the normalization of states in M_{fi} the standard $1/\sqrt{2EV}$ is used.

We require that strong transition matrix elements are parity even Lorentz scalars obtained by combining the momenta and polarizations of the initial and final particles. The conservation of angular momentum fixes the decay wave of $A \to BC$: $J_A = (J_B \oplus J_C) \oplus L_{BC}$, L_{BC} being the relative orbital angular momentum in the final state. For each unit of orbital angular momentum in the final state there must be factor of a spatial component of the momentum in the transition matrix element (ψ and J/ψ are used interchangeably hereafter).

The $J^{PC} = 1^{++}$ case. The decay $X_1 \to \psi V$, with $V = \rho, \omega$ is an $L = 0$ decay, since from the point of view of the J^P quantum numbers it corresponds to $1^+ \to 1^-1^-$. There is only one combination of momenta and polarizations which has all the properties we enumerated above

$$\langle\psi(\epsilon,p)V(\eta,q)|X_1(\lambda,P)\rangle = g_{_{1\psi V}}\;\epsilon^{\mu\nu\rho\sigma}\;\lambda_\mu(P)\;\epsilon^*_\nu(p)\;\eta^*_\rho(q)\;P_\sigma. \tag{4.2}$$

Indeed, in the rest frame of the decaying particle $P_\sigma = (m_{_X}, \mathbf{0})$ and one can write

$$\begin{aligned}\langle\psi(\epsilon,p)V(\eta,q)|X_1(\lambda,P)\rangle =& g_{_{1\psi V}}\;m_{_X}\;\epsilon^{ijk0}\;\lambda_i(P)\;\epsilon^*_j(p)\;\eta^*_k(q)\\ =& g_{_{1\psi V}}\;m_{_X}\;\left(\boldsymbol{\lambda}(P)\times\boldsymbol{\epsilon}^*(p)\right)\cdot\boldsymbol{\eta}^*(q)\end{aligned} \tag{4.3}$$

which is the scalar product of two polar vectors, the first coming from the vector product between an axial vector $\boldsymbol{\lambda}$ and a polar vector $\boldsymbol{\epsilon}$. Moreover Eq. (4.3) does not contain any spatial component of the momenta and thus accounts for an S-wave process.

The decay $X_1 \to D^0 \bar{D}^{0*}$ is also an $L = 0$ decay, since it corresponds to $1^+ \to 0^- 1^-$. The matrix element can be written in terms of a second coupling strength, $g_{_{1DD^*}}$, as follows

$$\langle D^0(p)\bar{D}^{0*}(\epsilon, q)|X_1(\lambda, P)\rangle = g_{_{1DD^*}}\ \lambda^\mu(P)\ \epsilon^*_\mu(q). \tag{4.4}$$

In order to conserve charge conjugation one should consider the final state $D^0\bar{D}^{0*} + \bar{D}^0 D^{0*}$. As explained in Section E.4.1 of Appendix E, we can consider only the $D^0\bar{D}^{0*}$ component in what follows, provided that we replace $g_{_{1DD^*}}$ with $\sqrt{2}\, g_{_{1DD^*}}$ in Eq. (4.4).

The $J^{PC} = 2^{-+}$ case. In this case, both the decays $X_2 \to \psi V$ and $X_2 \to D^0\bar{D}^{0*}$ are $L = 1$ processes, since they correspond to $2^- \to 1^-1^-$ and $2^- \to 0^-1^-$ transitions respectively.

The spin of the X_2 is described by a symmetric traceless polarization tensor $\pi^{\mu\nu}$ satisfying $P_\mu \pi^{\mu\nu} = 0$. In the rest frame the five independent components can be set in a 3×3 traceless tensor π^{ij}. For the sum over polarizations we have [270]

$$\begin{aligned}\sum_{\text{pol}} \pi_{\mu\nu}(P)\pi^*_{\alpha\beta}(P) &= \frac{1}{2}\left(g_{\mu\alpha}g_{\nu\beta} + g_{\mu\beta}g_{\nu\alpha} - g_{\mu\nu}g_{\alpha\beta}\right) \\ &- \frac{1}{2m^2}\left(g_{\mu\alpha}P_\nu P_\beta + g_{\nu\beta}P_\mu P_\alpha + g_{\mu\beta}P_\nu P_\alpha + g_{\nu\alpha}P_\mu P_\beta\right) \\ &+ \frac{1}{6}\left(g_{\mu\nu} + \frac{2}{m^2}P_\mu P_\nu\right)\left(g_{\alpha\beta} + \frac{2}{m^2}P_\alpha P_\beta\right)\end{aligned} \tag{4.5}$$

with $P^2 = m_X^2$.

For the decay $X_2 \to \psi V$, we have to determine the transition matrix element $\langle\psi(\epsilon, p)V(\eta, q)|X_2(\pi, P)\rangle$. There are two ways of combining momenta and polarizations which give a parity even Lorentz scalar[1]:

(*i*) a polarization vector contracts with the left index of the π tensor. If that of the ψ we have

$$\epsilon^{*\alpha}(p)\ \pi_{\alpha\mu}(P)\ \epsilon^{\mu\nu\rho\sigma}\ p_\nu\ q_\rho\ \eta^*_\sigma(q) \tag{4.6}$$

or if the V one does

$$\eta^{*\alpha}(p)\ \pi_{\alpha\mu}(P)\ \epsilon^{\mu\nu\rho\sigma}\ q_\nu\ p_\rho\ \epsilon^*_\sigma(q); \tag{4.7}$$

(*ii*) a momentum contracts with the left index of the π tensor. One can have

$$p^\alpha\ \pi_{\alpha\mu}(P)\ \epsilon^{\mu\nu\rho\sigma}\ q_\nu\ \epsilon^*_\rho(p)\ \eta^*_\sigma(q) \tag{4.8}$$

and the remaining combinations of momenta obtained by replacing pq by pp, qq, qp.

[1] An $\epsilon^{\mu\nu\rho\sigma}$ tensor is needed to obtain even parity. Moreover one cannot contract the two indices of the symmetric π tensor with two of the indices of the completely antisymmetric ϵ tensor.

Since we have a P-wave decay, we should not have non-zero terms proportional to $p_i q_j$, where i and j are spatial indices. In the X rest frame such terms are absent in Eq. (4.6) and (4.7) since they would be proportional to $\boldsymbol{p} \times \boldsymbol{q}$ - which vanishes only in the rest frame of the decaying particle. The only non zero combination of the type of Eq. (4.8), not containing the $p_i q_j$ terms is

$$Q^\alpha \, \pi_{\alpha\mu}(P) \, \epsilon^{\mu\nu\rho\sigma} \, P_\nu \, \epsilon^*_\rho(p) \, \eta^*_\sigma(q), \tag{4.9}$$

where $Q = p - q$ and $P = p + q$.

In conclusion we find that there are only three invariant amplitudes one can form by combining these tensors

$$T_1 = \epsilon^{*\alpha}(p) \, \pi_{\alpha\mu}(P) \, \epsilon^{\mu\nu\rho\sigma} \, p_\nu \, q_\rho \, \eta^*_\sigma(q) + \eta^{*\alpha}(q) \, \pi_{\alpha\mu}(P) \, \epsilon^{\mu\nu\rho\sigma} \, p_\nu \, q_\rho \, \epsilon^*_\sigma(p), \tag{4.10}$$

$$T_2 = \epsilon^{*\alpha}(p) \, \pi_{\alpha\mu}(P) \, \epsilon^{\mu\nu\rho\sigma} \, p_\nu \, q_\rho \, \eta^*_\sigma(q) - \eta^{*\alpha}(q) \, \pi_\alpha \mu(P) \, \epsilon^{\mu\nu\rho\sigma} \, q_\nu \, p_\rho \, \epsilon^*_\sigma(p), \tag{4.11}$$

$$T_3 = Q^\alpha \, \pi_{\alpha\mu}(P) \, \epsilon^{\mu\nu\rho\sigma} \, P_\nu \, \epsilon^*_\rho(p) \, \eta^*_\sigma(q) \tag{4.12}$$

which carry three implicit polarization indices. The first two correspond to the sum and the difference of Eq. (4.6) and (4.7), which it turns out to be useful to further reduce the number of independent tensors. Indeed one can show that T_1 and T_3 are one and the same tensor. To do this we prove that the following relation among sums over polarizations holds

$$\Big(\sum_{\text{pol}} T_1 T_3^*\Big)^2 = \Big(\sum_{\text{pol}} |T_1|^2\Big)\Big(\sum_{\text{pol}} |T_3|^2\Big). \tag{4.13}$$

The above condition implies that the two tensors are equal up to a constant if the sum over polarizations has the properties of an inner product. The Schwarz inequality states indeed that for all vectors $\boldsymbol{v}$, $\boldsymbol{w}$

$$|\langle \boldsymbol{v}, \boldsymbol{w} \rangle|^2 \leq \langle \boldsymbol{v}, \boldsymbol{v} \rangle \langle \boldsymbol{w}, \boldsymbol{w} \rangle, \tag{4.14}$$

where $\langle \cdot, \cdot \rangle$ is an inner product: the equality holds only if the two vectors are linearly dependent, *i.e.*, if they are parallel. Given two vectors $\boldsymbol{v}$, $\boldsymbol{w} \in \mathbb{C}^n$, the inner product is defined as $\langle \boldsymbol{v}, \boldsymbol{w} \rangle = \sum_{n=1}^N v_n w_n^* = \sum_{n=1}^N v_n^* w_n$. Here we are evaluating sums over polarizations, labeled by n, which means

$$\sum_{\text{pol}} T_i T_j^* = \sum_{n=1}^{5\times3\times3} T_i^{(n)} (T_j^{(n)})^*, \tag{4.15}$$

where we are summing over the 5 polarizations of the X_2 and the 3 of the vectors. Therefore Eq. (4.13) implies that for each polarization configuration, T_1 and T_3 are equal up to a constant, and we can choose one out of the two for our basis of linearly independent tensors. We choose to keep T_3 and eliminate T_1. The final choice for the parameterization is

$$\langle \psi(\epsilon, p) V(\eta, q) | X_2(\pi, P) \rangle = g_{2_\psi V} T_2 + g'_{2_\psi V} T_3, \tag{4.16}$$

where $V = \rho, \omega$.

Finally we consider $X_2 \to D^0\bar{D}^{0*}$. One can easily build a parity even Lorentz scalar by contracting the π tensor with the D^{0*} polarization vector and the D^0 momentum

$$\langle D^0(p)\bar{D}^{0*}(\epsilon,q)|X(\pi,P)\rangle = g_{_{2DD^*}}\pi^{\mu\nu}\epsilon^*_\mu(q)p_\nu. \tag{4.17}$$

The even parity can be easily understood. In the rest frame of the X one has

$$\langle D^0(p)\bar{D}^{0*}(\epsilon,q)|X(\pi,P)\rangle = g_{_{2DD^*}}\pi^{ij}\epsilon^*_i(q)\,p_j = g_{_{2DD^*}}\,(\boldsymbol{a}\cdot\boldsymbol{\epsilon}^*(q))\otimes(\boldsymbol{v}\cdot\boldsymbol{p})$$

where $\boldsymbol{a}$ and $\boldsymbol{v}$ are an axial and a polar vector respectively defined by $\pi^{ij} = a^i\otimes v^j + v^i\otimes a^j$. The same considerations on how to take into account the $D^0\bar{D}^{0*}+\bar{D}^0D^{0*}$ final state made in the case of $J^{PC}=1^{++}$ apply here ($g_{_{2DD^*}}\to\sqrt{2}\,g_{_{2DD^*}}$ in Eq. (4.17)).

4.1.2 Decay widths and determination of the strong couplings

The $\boldsymbol{J^{PC}=1^{++}}$ case. Since ω and ρ have different isospin quantum numbers in principle one needs to use different couplings to describe these decays: $g_{_{1\psi\omega}}$ and $g_{_{1\psi\rho}}$. To determine these two values we write the partial decay widths for $X\to J/\psi\ \rho$ and $X\to J/\psi\ \omega$ as in Eq. (E.12) and (E.34) in Appendix E. For $X\to J/\psi\ \rho\to J/\psi\ \pi^+\pi^-$ we have

$$\begin{aligned}\Gamma(X\to J/\psi\ \pi^+\pi^-) =& \frac{1}{3}\frac{1}{8\pi m_X^2}\int ds\ \sum_{\rm pol}|\langle\psi\rho(s)|X\rangle|^2 \\ &\times p^*(m_X^2,m_\psi^2,s)\frac{1}{\pi}\frac{m_\rho\Gamma_\rho\,\mathcal{B}(\rho\to\pi\pi)}{(s-m_\rho^2)^2+(m_\rho\Gamma_\rho)^2}\frac{m_\rho}{\sqrt{s}}\frac{p^*(s,m_{\pi^+}^2,m_{\pi^-}^2)}{p^*(m_\rho^2,m_{\pi^+}^2,m_{\pi^-}^2)}.\end{aligned} \tag{4.18}$$

Here $\mathcal{B}$ denotes a branching fraction, Γ_ρ is the width of the ρ resonance, $\langle\psi\rho(s)|X\rangle$ is the M_{fi} matrix element we have derived in the previous section [2], and p^* is the decay momentum in the rest frame of the decaying particle, see Appendix E.

In the calculations we will substitute $m_\rho\Gamma_\rho\to\sqrt{s}\ \Gamma_\rho(s)\to(s/m_\rho)\Gamma_\rho$, the comoving width (see Eq. (E.20)). Similarly for $X\to J/\psi\,\omega\to J/\psi\ \pi^+\pi^-\pi^0$ we get

$$\begin{aligned}\Gamma(X\to J/\psi\ \pi^+\pi^-\pi^0) =& \frac{1}{3}\frac{1}{8\pi m_X^2}\int ds\ \sum_{\rm pol}|\langle\psi\,\omega(s)|X\rangle|^2 p^*(m_X^2,m_\psi^2,s) \\ &\times\frac{1}{\pi}\frac{m_\omega\Gamma_\omega\,\mathcal{B}(\omega\to3\pi)}{(s-m_\omega^2)^2+(m_\omega\Gamma_\omega)^2}\frac{\Phi^{(3)}(\sqrt{s},m_{\pi^+},m_{\pi^-},m_{\pi^0})}{\Phi^{(3)}(m_\omega,m_{\pi^+},m_{\pi^-},m_{\pi^0})},\end{aligned} \tag{4.19}$$

where $m_\omega\Gamma_\omega\to(s/m_\omega)\Gamma_\omega$. The meaning of $\Phi^{(3)}$ is explained in Eq. (E.28).

The width of $X\to D^0\bar{D}^{0*}\to D^0\bar{D}^0\pi^0$ can be written as the one for $X\to J/\psi\ \rho\to J/\psi\ \pi^+\pi^-$. Using the expressions for the invariant amplitudes in terms of the couplings constants in the preceding section, we obtain $g_{_{1\psi\rho}}=0.14\pm0.03$, $g_{_{1\psi\omega}}=0.36\pm0.01$ and $g_{_{1DD^*}}=(3.5\pm0.7)$ GeV.

The $\boldsymbol{J^{PC}=2^{-+}}$ case. We will use four different couplings to describe the

[2] By $\langle\psi\rho(s)|X\rangle$ we mean $\langle\psi(\epsilon,p)\rho(\eta,q)|X(\lambda,P)\rangle$ with $q^2=s$. s is thus the invariant mass of the $\pi^+\pi^-$ pair coming from the ρ. In what follows we will use the same notation for the transition matrix element to a final state containing an unstable particle.

decays $X_2 \to J/\psi\ \rho$ and $X_2 \to J/\psi\ \omega$: $g_{2\psi\rho}$, $g'_{2\psi\rho}$ and $g_{2\psi\omega}$, $g'_{2\psi\omega}$. As for the $J/\psi\ \gamma$ channel, one can assume that the decay proceeds through a hadronic channel: X_2 first decays to $J/\psi\ \rho$ or $J/\psi\ \omega$ and later ρ or ω convert into a photon. Using vector meson dominance one can write

$$\begin{aligned}\langle J/\psi\ \gamma|X_2\rangle &= \langle\gamma|\omega\rangle\frac{1}{m_\omega^2}\langle J/\psi\ \omega(q^2=0)|X_2\rangle + \langle\gamma|\rho(q^2=0)\rangle\frac{1}{m_\rho^2}\langle J/\psi\ \rho|X_2\rangle \\ &= \frac{f_\omega}{m_\omega^2}\langle J/\psi\ \omega(q^2=0)|X_2\rangle + \frac{f_\rho}{m_\rho^2}\langle J/\psi\ \rho(q^2=0)|X_2\rangle.\end{aligned} \tag{4.20}$$

We use the decay constants for ρ and ω derived from the e^+e^- partial decay width of the two mesons: $f_\rho = 0.121$ GeV^2 and $f_\omega = 0.036$ GeV^2 [271]. The matrix element for the decay of $X_2 \to J/\psi\ \gamma$ is thus also written in terms of $g_{2\psi\omega}$, $g'_{2\psi\omega}$ and $g_{2\psi\rho}$, $g'_{2\psi\rho}$. We are left with four couplings to be determined and only three input values for the branching ratios: $\mathcal{B}(X \to \psi\omega)$, $\mathcal{B}(X \to \psi\rho)$ and $\mathcal{B}(X \to \psi\gamma)$. To perform the fit of the coupling we therefore use the data on the 3π invariant mass spectrum taken from [68].

In [68] 3π events are selected from a sample of $J/\psi\ \omega$ events with an invariant mass in the interval 3.8625 GeV $< m_{J/\psi\ \omega} <$ 3.8825 GeV. To perform the fit we simulate the decay of a 2^{-+} particle extracting its squared mass $x_i = m_i^2$ randomly with a Breit-Wigner distribution centered at $m_X = 3.8723$ GeV and with a width $\Gamma_X = 0.003$ GeV [75]. For each value x_i we require that $x_i > 0$ and that 3.8625 GeV $< \sqrt{x_i} <$ 3.8825 GeV. Having assigned m_i^2, the expected number of 3π events with a definite invariant mass $m_{3\pi}^2 = s$, is proportional to the distribution with respect to s of the decay width $\Gamma(X_2 \to J/\psi\ \pi^+\pi^-\pi^0)$

$$N_i(m_{3\pi}^2 = s) \propto \frac{d\Gamma(X_2 \to J/\psi\ \pi^+\pi^-\pi^0)}{ds}, \tag{4.21}$$

which can be computed using Eq. (4.19). Neglecting the overall numerical normalization we obtain

$$\begin{aligned}N_i(m_{3\pi}^2 = s) \propto &\frac{1}{m_i^2}\sum_{\text{pol}}|\langle J/\psi\ \omega|X_2(m_i^2)\rangle|^2\frac{1}{(s-m_\omega^2)^2 + (\frac{s}{m_\omega}\Gamma_\omega)^2} \\ &\times p^*(m_i^2, m_\psi^2, s)\Phi^{(3)}(\sqrt{s}, m_\pi^+, m_\pi^-, m_\pi^0)\end{aligned} \tag{4.22}$$

if $m_i > m_\psi + \sqrt{s}$. Thus the total number of events at fixed s is

$$N(m_{3\pi}^2 = s) = \sum_i N_i(m_{3\pi}^2 = s)\ \theta(m_i - m_\psi - \sqrt{s}). \tag{4.23}$$

In Fig. 4.1 we show the agreement obtained with data ($\chi^2/\text{DOF} = 4.03/4$) and we compare it with the experimental fit obtained using a Blatt-Weisskopf factor to account for the $L = 1$ decay, as was done in [68].

To compute the normalization factor we exploit the partial decay width of $\Gamma(X \to \psi\omega) = \mathcal{B}(X \to \psi\omega)\Gamma_X$ as written in Eq. (4.19). We obtain $g_{2\psi\omega} = (1.58 \pm 0.16)$ GeV^{-1} and $g'_{2\psi\omega} = (-0.74 \pm 0.34)$ GeV^{-1}. Using the known experimental data on $\mathcal{B}(X \to \psi\rho)$ and $\mathcal{B}(X \to \psi\gamma)$ we obtain two possible solutions for $g_{2\psi\rho}$ and $g'_{2\psi\rho}$. Since the $J/\psi\rho \to X_2 \to D^0\bar{D}^{0*}$ cross section turns out to be roughly the same using the two

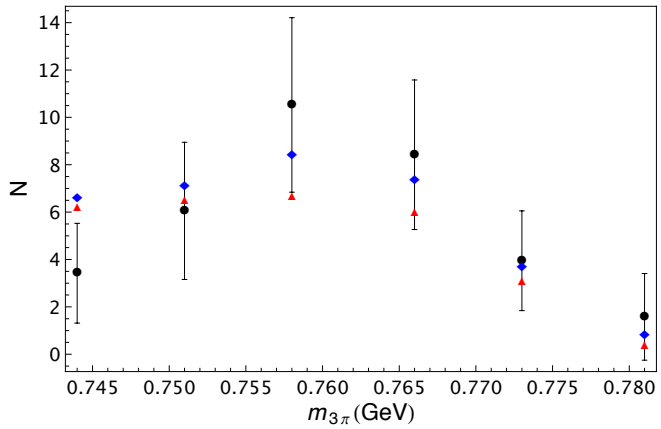

Figure 4.1. Our fit from Eq. (4.23) (Red Triangles) compared with experimental data (Black Disks) and the fit in [68] (Blue Diamonds). $\chi^2/\text{DOF} = 4.03/4$

sets of couplings, we choose to use one of them, namely $g_{2\psi\rho} = (-0.29 \pm 0.08)\ \text{GeV}^{-1}$, $g'_{2\psi\rho} = (0.28 \pm 0.09)\ \text{GeV}^{-1}$.

If one fits the same data set assuming $J^{PC} = 1^{++}$ a $\chi^2/\text{DOF} \sim 9/4$ is obtained, which means that the probability of the 1^{++} hypothesis is smaller by a factor of 6 than the 2^{-+} one. For the decay $X_2 \to D^0\bar{D}^{0*}$ we use the same method to extract the coupling and we obtain $g_{2DD^*} = 189 \pm 36$.

The results are summarized in Table 4.2. As a consequence of the fact that $\mathcal{B}(X \to D^0\bar{D}^{0*}) > \mathcal{B}(X \to \psi\omega)$ and $\mathcal{B}(X \to D^0\bar{D}^{0*}) > \mathcal{B}(X \to \psi\rho)$ we find that the adimensional coupling g_{2DD^*} is much larger than $g_{1\psi\omega}$ and $g_{1\psi\rho}$. On the other hand all the dimensional couplings turn out to be of the same order of magnitude of the mass scales involved.

Table 4.2. Fitted values for the effective couplings of $X(3872)$ to $D\bar{D}^{0*}$, $J/\psi\ \omega$ and $J/\psi\ \rho$ for the two J^{PC} assignments.

	$J^{PC} = 1^{++}$	$J^{PC} = 2^{-+}$	
$g_{(J)DD*}$	(3.5 ± 0.7) GeV	189 ± 36	
$g_{(J)\omega\psi}$	0.36 ± 0.01	$1.58 \pm 0.16\ \text{GeV}^{-1}$	$-0.74 \pm 0.34\ \text{GeV}^{-1}$
$g_{(J)\rho\psi}$	0.14 ± 0.03	$(-0.29 \pm 0.08)\ \text{GeV}^{-1}$	$(0.28 \pm 0.09)\ \text{GeV}^{-1}$

4.2 Prompt production in $p\bar{p}$ collisions

4.2.1 Loosely bound molecule [5, 6]

In the hypothesis of $J^{PC} = 1^{++}$ quantum numbers one of the most popular interpretation of $X(3872)$ is that of a $D^0\bar{D}^{0*}$ S-wave molecule, as we have extensively discussed in Section 2.2.1. Its binding energy would be extremely small, namely

compatible with zero

$$E_B = \left| M_{X(3872)} - M_{D^0} - M_{D^{0*}} \right| \simeq (-0.25 \pm 0.40) \text{ MeV}. \tag{4.24}$$

This striking property implies an extremely large spatial extension of this state, as compared to standard hadrons. If one assumes that the mechanism which binds the

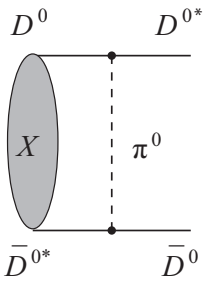

Figure 4.2. One pion exchange between D^0 and D^{0*} bound inside $X(3872)$.

two D mesons is pion exchange, as depicted in Fig. 4.2, one obtains an estimate of the size of this bound state using E_B

$$\frac{\hbar^2}{2\mu r_0^2} - \frac{g^2}{4\pi} \frac{\exp^{-m_\pi r_0}}{r_0} \equiv E_B, \tag{4.25}$$

where μ is the reduced mass of the $D^0 \bar{D}^{0*}$ system, g is the Yukawa strong coupling which we estimate taking into account that $g^2/4\pi \sim 10$. From Eq. (4.25) we obtain

$$r_0 = (8.6 \pm 1.1) \text{ fm}. \tag{4.26}$$

Having in mind a naive gaussian ansatz for the bound state wave function, we can use the minimal uncertainty principle to obtain the gaussian momentum spread

$$\Delta k \sim 1/2r_0 \sim 12 \text{ MeV}, \tag{4.27}$$

where k represents the modulus of the spatial part of the relative momentum between the two D-mesons. On the other hand a good estimate of the central value of the relative momentum is the center of mass momentum

$$k_0 = \sqrt{\lambda(m_X^2, m_D^2, m_D^{*2})}/2m_X \simeq 27 \text{ MeV}. \tag{4.28}$$

We are thus supposing that the $X(3872)$ wave function in momentum space has a Gaussian form, with mean value $k_0 \sim 27$ MeV and spread $\Delta k \sim 12$ MeV. This means that the probability that $k_0 - \Delta k < k < k_0 + \Delta k$ is equal to 68%. As one would have expected naively the constituent of a bound state with a nearly vanishing binding energy cannot have a large relative momentum, *i.e.* they are almost collinear.

With this picture in mind we consider the problem of the prompt production of $X(3872)$ in $p\bar{p}$ collisions observed at the Tevatron, taking into account an analysis by the CDF collaboration on the fraction of $X(3872)$ produced promptly, *i.e.* not originated from B-decays.

In the molecular hypothesis the production of $X(3872)$ must proceeds through the production of $D^0\bar{D}^{0*}$ pairs with suitable relative momentum k. We employ standard Monte Carlo tools as Herwig [272] and Pythia [273] to compute the production of D^0 and $\bar{D}^{0*}$ hadrons in proton-antiproton collisions at Tevatron energies. Open charm meson pairs produced are ordered as a function of their relative three-momentum and of their center of mass momentum. We select those which pass the kinematical cuts used in the analysis made by the CDF collaboration.

As we will explain below, we can estimate an *upper bound* for the theoretical cross section and a *lower bound* for the experimental one. The comparison of the two should give a qualitative answer whether the production of $X(3872)$ is exclusively due to the formation of a molecular bound state. In the following considerations we will not make use of any particular model. The only model dependency in our calculations is that hardwired in the hadronization schemes of Herwig and Pythia. Indeed, to add weight to our conclusions, a comparison between the results obtained with both MC's will be carried out.

4.2.1.1 Prompt production cross section of $X(3872)$ at CDF

In [274] the CDF collaboration performed an analysis on the lifetime distributions of the $\psi(2S)$ and $X(3872)$ mesons in the $J/\psi\,\pi^+\pi^-$ final state, observed in $p\bar{p}$ collisions. This analysis is based on a an integrated luminosity of about 220 pb^{-1} of $p\bar{p}$ collisions at $\sqrt{s} = 1.96$ TeV, taken between February 2002 and August 2003.

Considering nearly identical kinematic cuts on transverse momentum and pseudorapidity for the event selection, they estimate the fraction of $\psi(2S)$ and $X(3872)$ originated from the decay of B-mesons. They found

$$f_{\text{long lived}}(\psi(2S)) = (28.3 \pm 1.0 \pm 0.7)\% \tag{4.29}$$

$$f_{\text{long lived}}(X(3872)) = (16.1 \pm 4.9 \pm 2.0)\%, \tag{4.30}$$

where the long-lived fraction have a mean lifetime of (468±19) μm and (439±107) μm for $\psi(2S)$ and $X(3872)$ respectively. Both these values are comparable with the B^0 and B^+ lifetimes.

In [274] one can find also the yields of $\psi(2S)$ and $X(3872)$, which amount to

$$N(\psi(2S)) = 4940 \pm 110, \tag{4.31}$$

$$N(X(3872)) = 605 \pm 91. \tag{4.32}$$

Assuming the same detection efficiency for $\psi(2S)$ and $X(3872)$, one can thus obtain an estimate of the following quantity ($f_{\text{prompt}} = 1 - f_{\text{long lived}}$):

$$\begin{aligned} &\frac{N(X(3872))f_{\text{prompt}}(X(3872))}{N(\psi(2S))f_{\text{prompt}}(\psi(2S))} \\ &\simeq \frac{\sigma(p\bar{p} \to X(3872) + \text{All})_{\text{prompt}} \times \mathcal{B}(X(3872) \to J/\psi\,\pi^+\pi^-)}{\sigma(p\bar{p} \to \psi(2S) + \text{All})_{\text{prompt}} \times \mathcal{B}(\psi(2S) \to J/\psi\,\pi^+\pi^-)} \end{aligned} \tag{4.33}$$

Using the value reported in [251] for $\mathcal{B}(\psi(2S) \to J/\psi\,\pi^+\pi^-)$ one obtains

$$\frac{\sigma(p\bar{p} \to X(3872) + \text{All})_{\text{prompt}} \times \mathcal{B}(X(3872) \to J/\psi\,\pi^+\pi^-)}{f_{\text{prompt}}(\psi(2S))\sigma(p\bar{p} \to \psi(2S) + \text{All})} = (4.7 \pm 0.8)\% \tag{4.34}$$

The acceptance of the $\psi(2S)$ and $X(3872)$ candidates is not specified in [274], but from the CDF II detector geometry and the indicated candidates selection we can conservatively assume that the above ratio applies for $p_\perp > 5$ GeV and $|y| < 1$.

Furthermore in [275] a measurement of the $\psi(2S)$ inclusive cross section gives

$$\sigma(p\bar{p} \to \psi(2S) + \text{All}) \times \mathcal{B}(\psi(2S) \to \mu^+\mu^-) = (0.69 \pm 0.01 \pm 0.06)\ \text{nb}, \quad \text{for}\, p_T > 5\ \text{GeV and}\, |y| < 0.6 \tag{4.35}$$

so that

$$\sigma(p\bar{p} \to X(3872) + \text{All})_{\text{prompt}} \times \mathcal{B}(X(3872) \to J/\psi\,\pi^+\pi^-) = (3.1 \pm 0.7)\ \text{nb}. \tag{4.36}$$

A measure of $\mathcal{B}(X(3872) \to J/\psi\,\pi^+\pi^-)$ can be found in [65] resulting in

$$0.042 \leq \mathcal{B}(X(3872) \to J/\psi\,\pi^+\pi^-) \leq 0.093, \tag{4.37}$$

which can be finally translated in a range for the $X(3872)$ prompt production cross section from $p\bar{p}$ collisions

$$33\ \text{nb} < \sigma(p\bar{p} \to X(3872) + \text{All})_{\text{prompt}} < 72\ \text{nb}, \quad \text{for}\, p_T > 5\ \text{GeV and}\, |y| < 0.6. \tag{4.38}$$

This is the experimental range with which we will compare our theoretical prediction.

4.2.1.2 Monte Carlo simulation

Assuming a molecular structure for the $X(3872)$ we can write its prompt production cross section at the Tevatron as:

$$\sigma(p\bar{p} \to X(3872) + \text{All}) \quad \sim \left| \int d^3\boldsymbol{k} \langle X | D\bar{D}^*(\boldsymbol{k})\rangle \langle D\bar{D}^*(\boldsymbol{k}) + \text{All}\,|p\bar{p}\rangle \right|^2, \tag{4.39}$$

where $\boldsymbol{k}$ is the relative three-momentum between the $D(\mathbf{p_1}), D^*(\mathbf{p_2})$ mesons and $\psi(\boldsymbol{k}) = \langle X|D\bar{D}^*(\boldsymbol{k})\rangle$ is some normalized bound state wave function characterizing the $X(3872)$ in momentum space. For the considerations we made in the beginning, in the hypothesis of a Gaussian form for the wave function there is a limited integration region $\mathcal{R} \sim \{\boldsymbol{k}\,|\,0 < |\boldsymbol{k}| < k_0 + \Delta k\}$ where $\psi(\boldsymbol{k})$ is significantly different from zero, so that a good approximation for Eq. (4.39) is given by

$$\sigma(p\bar{p} \to X(3872) + \text{All}) \quad \sim \left| \int d^3\boldsymbol{k} \langle X | D\bar{D}^*(\boldsymbol{k})\rangle \langle D\bar{D}^*(\boldsymbol{k}) + \text{All}\,|p\bar{p}\rangle \right|^2 \tag{4.40}$$

$$\simeq \left| \int_{\mathcal{R}} d^3\boldsymbol{k} \langle X | D\bar{D}^*(\boldsymbol{k})\rangle \langle D\bar{D}^*(\boldsymbol{k}) + \text{All}\,|p\bar{p}\rangle \right|^2. \tag{4.41}$$

The Cauchy-Schwartz inequality [3] allows to write

$$\left|\int_{\mathcal{R}} d^3\boldsymbol{k}\langle X|D\bar{D}^*(\boldsymbol{k})\rangle\langle D\bar{D}^*(\boldsymbol{k})+\mathrm{All}\,|p\bar{p}\rangle\right|^2 \leq \int_{\mathcal{R}} d^3\boldsymbol{k}|\psi(\boldsymbol{k})|^2\int_{\mathcal{R}} d^3\boldsymbol{k}|\langle D\bar{D}^*(\boldsymbol{k})+\mathrm{All}\,|p\bar{p}\rangle|^2$$
$$\leq \int_{\mathcal{R}} d^3\boldsymbol{k}|\langle D\bar{D}^*(\boldsymbol{k})+\mathrm{All}\,|p\bar{p}\rangle|^2 \sim \sigma^{\mathrm{th.}}_{\mathrm{max}}, \tag{4.42}$$

where at the second step we have used the fact that $\psi(\boldsymbol{k})$ is a normalized wave function.

The squared matrix element $|\langle D\bar{D}^*(\boldsymbol{k})+\mathrm{All}\,|p\bar{p}\rangle|^2$ can be computed using standard matrix-element/hadronization Monte Carlo programs like Herwig and Pythia. To do so, we require our MC tools to generate $2\to 2$ QCD events with some loose partonic cuts. Configurations with one gluon recoiling from a $c\bar{c}$ pair, are those configurations expected to produce two collinear charm quarks and in turn collinear open charm mesons. The parton shower algorithms in Herwig and Pythia treat properly these configurations at low $p_\perp$ whereas they are expected to be less important at higher $p_\perp$. We will discuss also these processes at the parton level.

We tune our MC tools on CDF data on D^0D^{*-} pair production cross section distributions in the $\Delta\phi$ variable, ϕ being the azimuthal angle in the transverse plane to the beam axis z; see Figs. 4.3 and 4.4. We notice that we can reproduce rather well the cross section distributions in azimuth intervals $\Delta\phi$ for open charm production at CDF (see for example [277] and the relative CDF internal notes), provided that we adopt some rescaling factors as to get the right normalizations.

In the hadron samples produced by the shower/hadronization algorithm we list the events containing $D^0\bar{D}^{*0}$ as a function of their center of mass relative momentum. At this level, the only cuts are those on partons: $p_\perp^{\mathrm{part}} > 2$ GeV and $|y^{\mathrm{part}}| < 6$. If more than one $D^0\bar{D}^{*0}$ pair is found in the event, we select the pair having the smaller relative three-momentum k. Following Eq. (4.42) we restrict the integration region over $|\boldsymbol{k}|$ to a ball $\mathcal{R}$ of radius $\simeq [0, 35]$ MeV.

We have used Herwig and Pythia to compute hadron final states from $2\to 2$ QCD parton processes, reaching a Monte Carlo luminosity $\mathcal{L}\sim 100$ nb^{-1}. In Fig. 4.5 we show the integrated cross section as a function of the center of mass relative momentum in the $D^0\bar{D}^{*0}$ molecule obtained using Herwig. To get the minimal experimental value of $\sigma\sim(3.1\pm 0.7)$ nb we need to include $D^0\bar{D}^{*0}$ configurations having up to $k=(205\pm 20)$ MeV. Molecule candidates in the ball of relative momenta $\mathcal{R}$ can account only for 0.071 nb. Repeating the same calculation with Pythia, see Fig. 4.6, we get $k=(130\pm 15)$ MeV whereas in $\mathcal{R}$ we integrate 0.11 nb.

Simulating the real experimental situation of prompt production of $X(3872)$ at CDF would require a further increase of just a factor of 10^4 in the Monte Carlo

[3] The Cauchy-Schwartz inequality states that [276]

$$|\phi(g,f)|^2 \leq \phi(g,g)\phi(f,f),$$

where $\phi(g,f)$ is the inner product between the $\mathbb{C}$-functions g and f

$$\phi(g,f)=\int_a^b g^\star(x)f(x)dx.$$

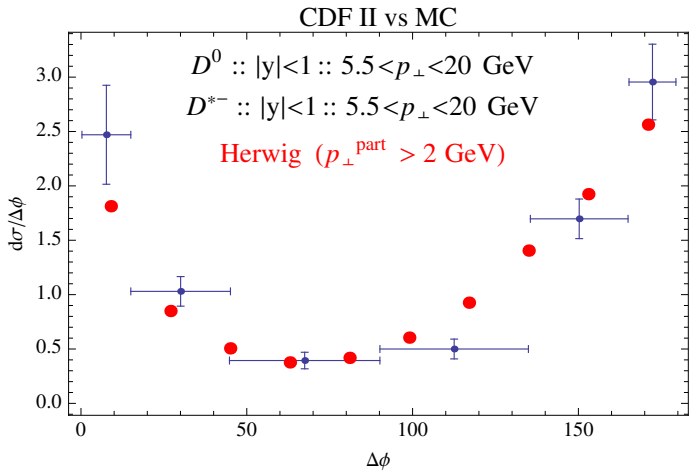

Figure 4.3. The $D^0 D^{*-}$ pair cross section as function of $\Delta\phi$ at CDF Run II. The transverse momentum, $p_\perp$, and rapidity, y, ranges are indicated. Data points with error bars, are compared to the leading order event generator Herwig. The cuts on parton generation are $p_\perp^{\rm part} > 2$ GeV and $|y^{\rm part}| < 6$. We have checked that the dependency on these cuts is not significative. We find that we have to rescale the Herwig cross section values by a factor $K_{\rm Herwig} \simeq 1.8$ to best fit the data on open charm production.

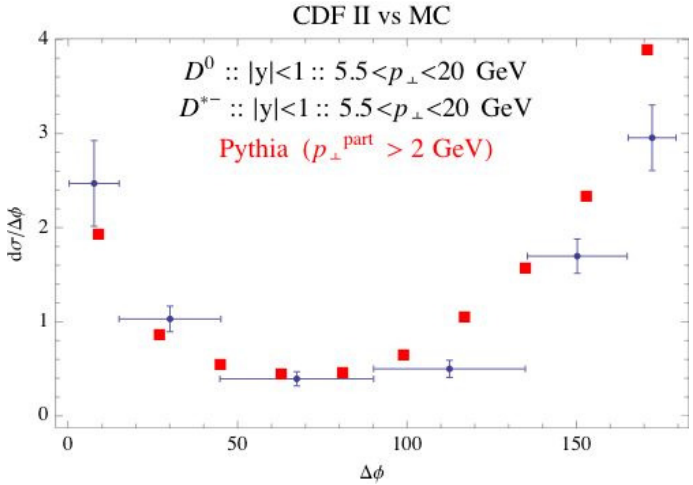

Figure 4.4. The same as in Fig. 4.3 but using Pythia. We find that we have to rescale the Pythia cross sections by a factor $K_{\rm Pythia} \simeq 0.74$ to best fit the data on open charm production. In both cases the agreement of the Monte Carlo distribution with data is remarkable.

luminosity which is extremely CPU demanding. Yet, in consideration of the stability of our results, we do not expect significant variations from what here observed.

In conclusion we study $gc\bar{c}$ events with one gluon at $p_\perp > 5$ GeV recoiling from the $c\bar{c}$ pair which in turn can hadronize into open charm mesons very close in phase space. We perform this computation at the parton level using ALPGEN [278] and assuming that the fragmentation functions into open charm mesons to be set to one. This corresponds to an upper bound estimation. The results obtained point at a definitely negligible contribution from these configurations, being in the range of

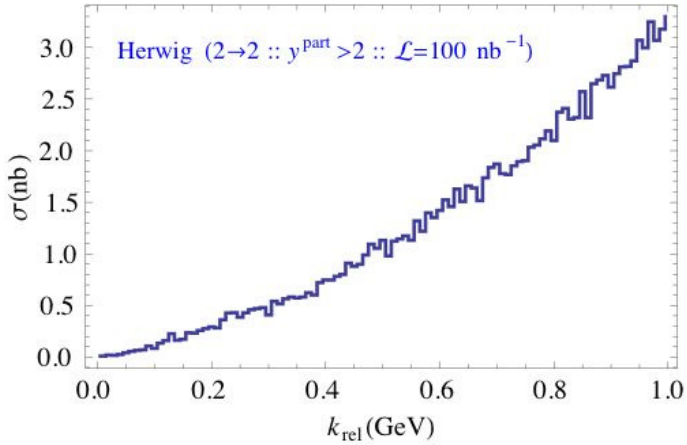

Figure 4.5. The integrated cross section obtained with Herwig as a function of the center of mass relative momentum of the mesons in the $D^0\bar{D}^{*0}$ molecule. This plot is obtained after the generation of 55×10^9 events with parton cuts $p_\perp^{\text{part}} > 2$ GeV and $|y^{\text{part}}| < 6$. The cuts on the final D mesons are such that the molecule produced has a $p_\perp > 5$ GeV and $|y| < 0.6$.

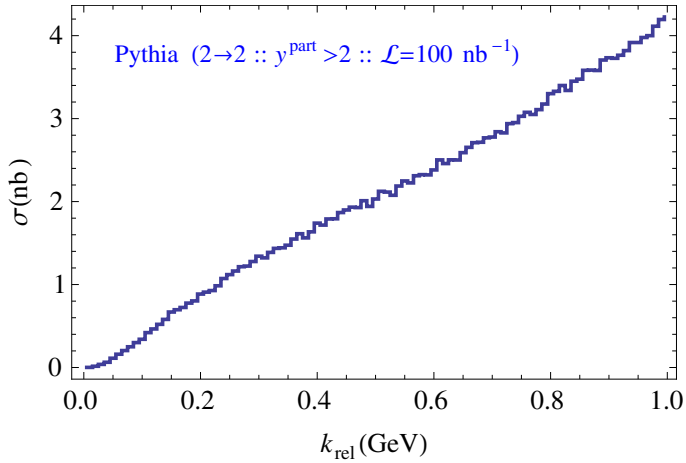

Figure 4.6. Same plot as in Fig. 4.5 but using Pythia. We show these curves in a wide range of k_{rel} to give an idea of the remarkable Monte Carlo stability against fluctuations achieved on account of the very high statistics used.

few picobarns. The results are shown in Fig. 4.7.

We can thus estimate the upper bound for the theoretical prompt production cross section of $X(3872)$ at CDF, averaging the results obtained with Herwig and Pythia. We find this to be approximately

$$\sigma(p\bar{p} \to X(3872) + \text{All})^{\text{th. max}}_{\text{prompt}} \sim 0.085 \text{ nb} \tag{4.43}$$

in the most reasonable region of center of mass relative momenta $|\boldsymbol{k}| \in [0, 35]$ MeV of the open charm meson pair constituting the molecule. This value has to be compared with the lower bound on the experimental cross section in Eq. (4.38), namely 33 nb,

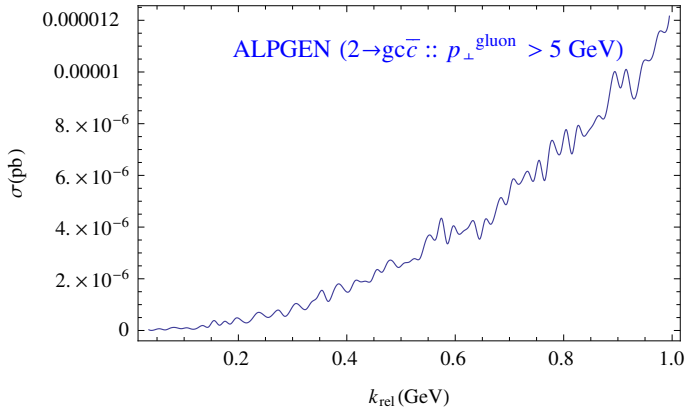

Figure 4.7. The integrated cross section in picobarn obtained with the parton level generator ALPGEN. $2 \to gc\bar{c}$ processes with a gluon recoiling from the $c\bar{c}$ pair can produce D mesons at very small relative momentum. At lower $p_\perp^{\text{gluon}}$, Herwig and Pythia are efficient at generating this configurations from showering.

extracted from CDF data. One obtains

$$\frac{\sigma_{\text{min}}^{\text{exp.}}}{\sigma_{\text{max}}^{\text{th.}}} \sim 300. \tag{4.44}$$

The intuitive expectation that S-wave resonant scattering is unlikely to allow the formation of a loosely bound $D^0\bar{D}^{*0}$ molecule in high energy hadron collisions is confirmed by this analysis.

4.2.1.3 Final State Interactions

In [279] Braaten and Artoisenet reconsidered the theoretical estimate of the $X(3872)$ prompt production cross section using MC event generators.

The authors of [279] starts from Eq. (4.42), the prompt production cross section for the system $D^0\bar{D}^{0*}$ with relative momentum $\boldsymbol{k}$

$$d\sigma[D^{*0}\bar{D}^0(\boldsymbol{k})] = \frac{1}{\text{flux}} \sum_{\text{All}} \int d\phi_{D^*\bar{D}+\text{All}} |\langle D^0\bar{D}^{*0}(\boldsymbol{k}) + \text{All}\,|p\bar{p}\rangle|^2 \frac{d^3\boldsymbol{k}}{(2\pi)^3 2\mu}. \tag{4.45}$$

They include Final State Interactions (FSI) using the results of the Migdal-Watson theorem [280]

$$d\sigma[D^{*0}\bar{D}^0(\boldsymbol{k})] = \frac{1}{\text{flux}} \sum_{\text{All}} \int d\phi_{D^*\bar{D}+\text{All}} \left| \frac{\langle D^0\bar{D}^{*0}(\boldsymbol{k}) + \text{All}\,|p\bar{p}\rangle}{f(\boldsymbol{k})} \right|^2 \times \frac{1}{k^2 + 2\mu E_B} \frac{d^3\boldsymbol{k}}{(2\pi)^3 2\mu}. \tag{4.46}$$

A factor $1/(k^2 + 2\mu E_B)$ is added and the transition matrix element is divided by the S-wave scattering amplitude $f(k)$. Since the dependence of the transition matrix element on the relative momentum k is all contained in $f(k)$, one can make the following approximation

$$\left| \frac{\langle D^0\bar{D}^{*0}(\boldsymbol{k}) + \text{All}\,|p\bar{p}\rangle}{f(\boldsymbol{k})} \right|^2 \sim \left| \frac{\langle D^0\bar{D}^{*0}(k_{max}) + \text{All}\,|p\bar{p}\rangle}{f(k_{max})} \right|^2. \tag{4.47}$$

In which conditions Eq. (4.46) does apply? As one can read from [280], FSI are those interactions among the particles produced in a reaction process which sensibly affect the property of the reaction cross section. The importance in analyzing and recognizing the role played by these interactions lies partly in the observation that they may greatly modify the angular distribution and energy spectra of the produced particles and yet play no important role in the primary mechanism by which the reaction takes place. The possibility to separate the effect of these two mechanism, that is the *primary mechanism* of the reaction and the FSI, allows to simplify the analysis of this phenomenon.

The modifications induced by FSI are expected to be sizable and quantifiable with the Migdal-Watson theorem *only if* four conditions are met.

- The primary interaction should be a short-range interaction, *i.e.* confined in a certain volume $V \simeq a^3_{\text{primary}}$.
- The effect of FSI is relevant only for pairs of particles with *sufficiently small* relative momentum: $ka_{\text{FSI}} << 1$, where a_{FSI} is the range of the potential which causes FSI. Since we are dealing with strong interactions, both for the primary and FSI stages of the reaction, $a_{\text{primary}} = a_{\text{FSI}} = a = 1$ fm, so that only particles with relative momentum $k << 200$ MeV undergo FSI.
- FSI must be strong and attractive.
- *Only two particles*, among all the particles produced in the reaction, must meet the conditions for FSI to be relevant.

Thus as far as the Migdal-Watson theorem is concerned, Eq. (4.46) applies only for $k << 200$ MeV, whereas the authors of [279] choose $k_{max} \sim \mathcal{O}(m_\pi)$. The fact that k_{max} should be well below 200 MeV, as we estimated $k < 35$ MeV, can be also understood considering that the maximum value of the orbital angular momentum is given by $L_{max} = ka$. Since we are dealing with S-wave scattering we need $L_{max} << 1$ which implies again $k << 1/a$.

The authors of [279] integrate Eq. (4.46) over $d^3\boldsymbol{k}$ with $k_{max} \sim \mathcal{O}(1/a)$. Taylor expanding the result of the integration ($\sqrt{2\mu E_B} << 1/a$) one obtains

$$\int \frac{1}{k^2 + 2\mu E_B} \frac{d^3\boldsymbol{k}}{(2\pi)^3\mu} \propto \int_0^{k_{max}} \frac{1}{k^2 + 2\mu E_B} \frac{4\pi\, k^2\, dk}{8\pi^3\mu} \sim \frac{\sqrt{2\mu E_B}}{2\pi\mu} \tag{4.48}$$

Moreover the S-wave scattering amplitude $f(k)$ is

$$f(k) = \frac{1}{k\cot\delta_0 - ik} \xrightarrow{k\sim 0} \frac{1}{-\sqrt{2\mu E_b} - ik}, \tag{4.49}$$

so that for $k = k_{max}$ we can neglect $\sqrt{2\mu E_B}$ in the denominator

$$|f(k_{max})|^2 \sim 1/k^2_{max}. \tag{4.50}$$

Eq. (4.46) becomes

$$\sigma^{\text{FSI}}(p\bar{p} \to X(3872) + \text{All}) \sim \frac{1}{\text{flux}} \sum_{\text{All}} \int d\phi_{D^0\bar{D}^{*0}+\text{All}} |\langle D^0\bar{D}^{*0}(k_{max}) + \text{All}\,|p\bar{p}\rangle|^2 \times k^2_{max} \frac{\sqrt{2\mu E_X}}{2\pi\mu} \tag{4.51}$$

On the other hand the integration of Eq. (4.45) gives the prompt production cross section of $X(3872)$ not including the effect of FSI

$$\sigma^{\text{NO FSI}}(p\bar{p} \to X(3872) + \text{All}) \sim \frac{1}{\text{flux}} \int d\phi_{D^0\bar{D}^{*0}+all} |\langle D^0\bar{D}^{*0}(k_{max}) + \text{All}\,|p\bar{p}\rangle|^2 \times \frac{k_{max}^3}{12\pi^2\mu}, \tag{4.52}$$

which is the cross section we have discussed in Section 4.2.1.2. Comparing Eq. (4.52) and Eq. (4.51) one obtains

$$\sigma^{\text{FSI}}(p\bar{p} \to X(3872) + \text{All}) \sim \sigma^{\text{NO FSI}}(p\bar{p} \to X(3872) + \text{All}) \times \frac{6\pi\sqrt{2\mu E_X}}{k_{max}}. \tag{4.53}$$

In conclusion two corrections should be made to our previous calculation according to:

(*i*) the ball $\mathcal{R}$ should be enlarged to include momenta up to $k_{max} \sim \mathcal{O}(m_\pi)$ (in [279] three values are considered $k_{max} = m_\pi, 2m_\pi, 3m_\pi$);

(*ii*) a correction factor $6\pi\sqrt{2\mu E_X}/k_{max}$ should be added so that the actual cross section includes the full effect of final state interactions.

In this way Braaten and Artoisenet are able to reconcile the results of MC simulations with the experimental data from CDF.

Nevertheless in [6] we casted some doubts on the possibility that final state interactions can indeed play such a pivotal role as described in [279].

First of all, as we have said before, we remind that Watson formulae [280] used in [279] are valid for S-wave scattering, whereas a relative three-momentum $k \sim 300$ MeV indicates that higher partial waves should be taken into account.

Most importantly, we have verified in our MC simulations that as the relative momentum k in the center of mass of the molecule is taken to be up to 300 MeV, then other hadrons (on overage more than two) have a relative momentum $k < 100$ MeV with the D or the D^* constituting the molecule (see Fig. 4.8). On the other hand the Migdal-Watson theorem for final state interactions requires that *only two* particles in the final state participate to the strong interactions causing them to rescatter. In other words the extra hadrons involved in the process do necessarily interfere in an unknown way with the mesons assumed to rescatter into an $X(3872)$. This is particularly true as one further enlarges the dimensions of the momentum ball $\mathcal{R}$ as required in [279].

4.2.2 D-wave charmonium [2]

In the 2^{-+} hypothesis the molecular interpretation of $X(3872)$ is completely ruled out. A 2^{-+} state formed out of $D^{0*}\bar{D}^0$ would require a relative P-wave, and it is unlikely that π exchange could bind such a state, given that even in S-wave it is not clear whether the attraction is sufficiently strong [134]. Even if such a state exists, there remains the further problem that unless spin-dependent forces prevent the binding, one should expect partner states with 0^{-+} and the J^{PC}-exotic 1^{-+} state, for which there is no experimental evidence. A P-wave 2^{-+} molecule would

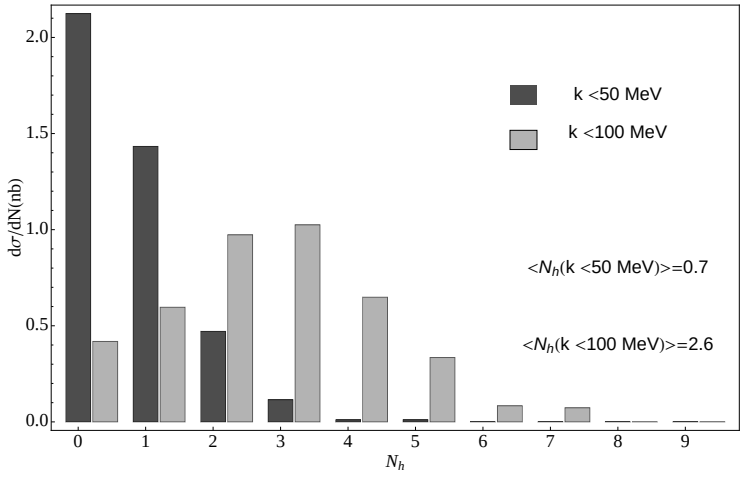

Figure 4.8. The cross section integrated in bins containing $N_h = 0, 1, 2, ...$ extra hadrons having a relative momentum $k < 50$ or 100 MeV with respect the D or the D^* composing the $X(3872)$ molecule. Following [279] we assume that the molecule is formed in S-wave with a relative k in the center of mass of D and D^* as large as 300 MeV.

also imply the existence of a more deeply bound S-wave 1^{++} molecule, which would be extremely narrow. Alternatively, to form a 2^{-+} bound state in S-wave would require $D_2 D$ or $D_1 D^*$, which not only implies an immense binding energy of some 500 MeV, but one loses the appealing connection between the mass of the $X(3872)$ and the $D^{0*}\bar{D}^0$ threshold.

The charmonium option 1^1D_2 should thus be reconsidered. In Section 3.3.1 we have tested this assignment from the point of view of the spectrum and of the dominant decay modes. Here we wish to complete this test analyzing the prompt production rate of a 1^1D_2 standard charmonium in $p\bar{p}$ collisions at the Tevatron [2].

On general grounds one expects it to be small. The production cross section is proportional to a fragmentation function, which describes the probability that quarks and gluons hadronize into bound states. This function can be expressed as a perturbative expansion in the quark velocity v. For the production of a 1^1D_2 state the function begins at order $O(v^7)$, and so one expects a smaller cross section than for $1P$ states, whose functions are $O(v^5)$, which are themselves suppressed with respect to $1S$ states, $O(v^3)$.

For the fragmentation functions we draw upon the result of Cho and Wise [281], who calculated the production cross section of a 1^1D_2 state at the Tevatron. They observed that despite the aforementioned kinematic suppression, large numerical prefactors in the amplitudes implied that such states could be produced in large enough measure to be observed in prompt production. These authors argue that color octet contributions are subleading with respect to color singlet in the heavy quark velocity expansion and thus are neglected. We use their result for the gluon fragmentation function $D_{g\to 1^1D_2^{(h)}}(z;\mu)$ which describes the production of a 1^1D_2 quarkonia with helicity h, quark longitudinal momentum fraction z, and

renormalisation scale μ. We compute the production cross section,

$$\frac{d\sigma}{dp_\perp}(p\bar{p} \to 1^1\mathrm{D}_2 + \mathrm{All}) = \sum_{h=0}^{2} \int_0^1 dz \frac{d\sigma}{dp_\perp}(p\bar{p} \to g(p_\perp/z) + \mathrm{All}; \mu) \times D_{g \to 1^1 D_2^{(h)}}(z;\mu) \tag{4.54}$$

using recent gluon distribution functions. We find that the ratio between the MRSD0 gluon distribution functions used in [281] and the most recent MSTW20008NNLO set amounts to about a factor of 0.7 in the most relevant Bjorken x region, $x \simeq \sqrt{\hat{s}/s}$, which at Tevatron energies is $x \simeq \sqrt{M_\perp^2/1960^2} \simeq 0.02$, where $M_\perp = \sqrt{M^2 + p_\perp^2}$. Indeed we have $M = 3872$ MeV, $p_\perp \gtrsim 5$ GeV, and $|y| \leq 0.6$ to fulfil the kinematical cuts used in the CDF analysis. Here the factorization scale μ is set $\mu = M_\perp$.

The integrated prompt production cross section we find over the interval $p_\perp \geq 5$ GeV is

$$\sigma(p\bar{p} \to 1^1D_2 + all) = 0.6 \text{ nb}, \tag{4.55}$$

some 50 and 120 times smaller than the estimated experimental cross section in Eq. (4.38). It is difficult, therefore, to reconcile the observed prompt production cross section of the $X(3872)$ with the expectations for a 1^1D_2 state.

4.3 Summary about $X(3872)$

Hereafter we summarize the pros and cons of the various interpretations proposed for the $X(3872)$, depending on its J^{PC} quantum numbers.

$J^{PC} = 1^{++}$:

Standard Charmonium : $X(3872) \sim 2^3P_1 = \chi'_{c1}$.

- ✗ Isospin breaking,
- ✗ Too small radiative decay modes
- ✓ $M(2^1P_1) \sim m_{X(3872)}$

S-wave tetraquark : $X(3872) \sim [cq]_{0^+}[\bar{c}\bar{q}]_{1^+} + [cq]_{1^+}[\bar{c}\bar{q}]_{0^+}$.

- ✗ Charged partners not observed.
- ✓ Isospin breaking
- ✓ Narrow because $X(3872)$ lies below the $\Lambda_c^+\Lambda_c^-$ threshold
- ✗ $X(3872) \to J/\psi\,\rho(\omega)$ and $X(3872) \to D^0\bar{D}^{0*}$ conserve the $c\bar{c}$ spin

S-wave $D^0\bar{D}^{0*}$ molecule : $X(3872) \sim D^0\bar{D}^{0*} + \bar{D}^0D^{0*}$

- ✗ Too small prompt production cross section
- ✓ Isospin breaking, large decay into $D^0\bar{D}^{0*}$
- ✓ $m_{X(3872)} \simeq m_{D^0} + m_{D^{0*}}$

$J^{PC} = 2^{-+}$:

Standard Charmonium : $X(3872) \sim 1^1D_2$

- ✗ Isospin breaking

- ✗ $M(1^1D_2) << m_{X(3872)}$
- ✗ Too small prompt production cross section.
- **?** Search for distinctive decay mode: $X(3872) \to h_c\gamma$, $X(3872) \to \eta_c\pi\pi$

P-wave tetraquark : $X(3872) \sim ([cq]_{0^+}[\bar{c}\bar{q}]_{1^+} + [cq]_{1^+}[\bar{c}\bar{q}]_{0^+})_{P-\text{wave}}$

- ✗ Charged partners not observed
- **?** S-wave tetraquarks in the ~ 3400 MeV mass region.
- ✓ Isospin breaking
- ✓ Narrow because $X(3872)$ lies below the $\Lambda_c^+\Lambda_c^-$ threshold
- ✓ $X(3872) \to J/\psi\,\rho(\omega)$ and $X(3872) \to D^0\bar{D}^{0*}$ with conservation of the $c\bar{c}$ spin

P-wave $D^0\bar{D}^{0*}$ molecule : $X(3872) \sim \left(D^0\bar{D}^{0*} + \bar{D}^0D^{0*}\right)_{P-\text{wave}}$

- ✗ A P-wave bound state with nearly zero binding energy is unlikely
- ✗ S-wave molecule not observed

$X(3872)$ represents a paradigmatic example for the XYZ mesons.

First of all we showed that the incompleteness of the experimental picture forbids the definitive exclusion or confirmation of a particular model. For example the 1^1D_2 charmonium assignation could be further tested if the two decay modes $h_c\gamma$ and $\eta_c\pi\pi$ would be searched. These are indeed expected to be the prominent decay channels for a 1^1D_2 charmonium state below the $D\bar{D}^*$ threshold. This is also the case of the hybrid interpretation of the $Y(4260)$, which could be excluded or confirmed looking for the $D\bar{D}_1$ final state. For a more comprehensive experimental picture we should wait for the upcoming results from the LHC and the SuperB factories. Nevertheless we could gain some insight on where we stand now, studying processes in which the XYZ mesons behave as indirect states. This will be the subject of the next chapter.

Secondly in this chapter we proved how the prompt production mechanism could serve as a crucial table test for various interpretations. We succeeded in giving a theoretical framework which allows to obtain a prediction of the prompt production cross-section of a loosely bound molecule. Also we exploit a previous calculation to give an estimate of the same quantity in the D-wave charmonium option. It would be very interesting to consider the prompt production mechanism in the case of tetraquarks. The Monte Carlo event generators, which proved to be efficient in the case of the molecule, could be modified including among their final states $[Qq][\bar{Q}\bar{q}]$ mesons. This project could be the subject of a PhD thesis on its own.

Chapter 5

Indirect Searches

In this chapter we present two processes which allow an indirect search for the XYZ exotic mesons, *i.e.* processes in which XYZ play their role as intermediate states. We intend to underscore that the XYZ particles being discovered in the last few years might have impact on a wide class of elementary processes. Furthermore this kind of searches could be of help in clarifying if there are more exotic resonances to be discovered, beyond the ones we established to exist until now. A direct observation is obviously needed, but this implies a huge amount of data analysis, which we hope will be undertaken in the next few years both on the *old* data from B-factories and Tevatron, and on the new data from the LHC and from the forthcoming SuperB factories.

In Section 5.1 we reconsider the phenomenon of J/ψ suppression observed in heavy ion collisions. It has always been indicated as one of the most compelling signal of Quark Gluon Plasma formation in the first stages after ultra relativistic collisions between heavy ions. Nevertheless in many recent works the J/ψ interaction with the hadron gas which is supposed to appear after or in place of the QGP, has been identified to be an important background to the J/ψ suppression induced by QGP. We have updated the previous analyses on two different aspects. First we take into account the effect of the hot hadron medium on the masses and widths of the open charm mesons, in which the J/ψ can be dissociated. Secondly we add the contribution of the resonant scattering process $J/\psi\,\rho(\omega) \to X(3872) \to D^0\bar{D}^{0*}$ finding that this is non negligible if $X(3872)$ has $J^{PC} = 2^{-+}$. We finally perform a comparison with the most recent data from RHIC.

In Section 5.2 we will instead discuss the possibility that XYZ mesons can help in solving the discrepancy between theory and data on the decay momentum distribution of the J/ψ's coming from B-decays. Beside including the contribution of exotic mesons, we will also update the previous theoretical predictions on the standard channels.

5.1 J/ψ suppression in heavy ion collisions

5.1.1 Heavy ion collisions and Quark Gluon Plasma

The fundamental theory of strong interactions QCD is an asymptotically free theory, as we have reviewed in the first chapter. This implies that interactions between quarks

and gluons become weaker as the mutual distance decreases or as the exchanged momentum increases. As a consequence at very high temperatures and large densities strong forces, which are responsible for the confinement of quarks and gluons inside hadrons, are sufficiently weak to make hadrons disappear: quarks and gluons become the effective degrees of freedom. This *deconfined* phase is known as Quark Gluon Plasma.

The Standard Cosmology Model states that space, time, and all the matter and radiation in the Universe were formed during the big-bang some 15 billion years ago. The Universe as we know it nowadays is an evolution of a cosmic fireball created at that moment. It is widely accepted that almost equal amounts of matter and antimatter were formed and that they subsequently annihilated as soon as the Universe started to expand and thus to cool down. At the time of this annihilation process, some 20 μs after the big-bang, protons and neutrons already existed. Before the hadronization took place, the space was filled with the primordial state of hadronic matter, the QGP.

The purpose of heavy ion collision experiments is exactly to reproduce this deconfined phase of matter, which seems to be an inescapable consequence of our knowledge about strong interactions. In high energy collisions between heavy ionized nuclei a huge quantity of energy is released and one can hope to reach a sufficiently high temperature for QGP to be formed.

heavy ion collision experiments started in the seventies, and met the interest both of particle and nuclear physicists. The initial experimental program was launched at the Lawrence Berkeley Laboratory, LBL, at Berkeley, USA, and at the Joint Institute for Nuclear Research, JINR, in Dubna, USSR. At LBL nuclear projectiles were accelerated at $1A$ GeV [1]. Nevertheless the temperatures reached in the collisions were too low to allow quarks and gluons to be released and move freely in the reaction volume.

The hope to reach the experimental conditions to produce in laboratories the QGP, gave birth to the research programs at the BNL (Brookhaven National Laboratory) and at CERN (Centre Europeen pour la Recherche Nucleaire). Two generations of experiments have been carried on: in the 90s the AGS (Alternating Gradient Synchrotron) and SPS (Super Proton Synchrotron) facilities, since the year 2000 the RHIC (Relativistic heavy ion Collider) and LHC (Large Hadron Collider) facilities In Table 5.1 we report the relevant parameters for each experiment.

The energy density of ordinary nuclear matter is

$$\epsilon_{\text{nucl}} = 0.17 \text{ GeV fm}^{-3}, \tag{5.1}$$

whereas experimental results have shown that ultra relativistic heavy ion collisions lead to the formation of a dense hadronic fireball, with an energy density of the order of

$$\epsilon_{\text{heavy ions}} \sim 1 \text{ GeV fm}^{-3}. \tag{5.2}$$

One can associate a temperature to the hadron fireball once a statistical description of it is introduced. The typical temperatures involved are of the order of 10^2 MeV which means

$$T_{\text{heavy ions}} \sim 100 \text{ MeV} = 116 \times 10^{10} \text{ K}, \tag{5.3}$$

[1] By $1A$ GeV we intend 1 GeV per nucleon, A being the mass number of the colliding nuclei.

Table 5.1. Relevant parameters for the heavy ion collisions experiments.

Facility	Beam	C.O.M Energy (GeV/A)	Date
AGS	^{28}Si	5.4	1986
	^{197}Au	4.8	1994
SPS	^{16}O	19	1986
	^{32}S	19	1987
	^{208}Pb	17	1994
RHIC	^{197}Au	200	2000
LHC	^{208}Pb	2760	2008

an extremely high temperature if one recalls that the center of the sun is expected to be at $T_{\text{sun}} = 11 \times 10^6$ K.

The dependence of the energy density on the temperature is expected to have an abrupt change when the critical temperature for the transition to QGP is crossed. One can indeed estimate this dependence considering that

$T < T_c$: a hot pion gas is expected to be produced in the collisions, since the colliding nuclei are made by u and d quarks. The energy density of a hot massless pion gas can be computed using the Bose-Einstein distribution as

$$\epsilon_{\pi\text{ gas}} = \int \frac{d\boldsymbol{p}}{(2\pi)^3} \sum_i \frac{E_i}{e^{E_i/T} - 1} \simeq N_\pi \times \int_0^\infty \frac{p^3\, dp}{2\pi^2} \frac{1}{e^{p/T} - 1} = N_\pi \times \frac{\pi^2}{30} T^4, \tag{5.4}$$

with $N_\pi = 3$.

$T > T_c$: a gas of free quarks and gluons is expected to be produced above the critical temperature

$$\epsilon_{\text{quark gas}} = \int \frac{d\boldsymbol{p}}{(2\pi)^3} \sum_i \frac{E_i}{e^{E_i/T} + 1} \simeq N_q \times \int_0^\infty \frac{p^3\, dp}{2\pi^2} \frac{1}{e^{p/T} + 1} = N_q \times \frac{7\pi^2}{240} T^4,$$

$$\epsilon_{\text{gluon gas}} = \int \frac{d\boldsymbol{p}}{(2\pi)^3} \sum_i \frac{E_i}{e^{E_i/T} - 1} \simeq N_g \times \int_0^\infty \frac{p^3\, dp}{2\pi^2} \frac{1}{e^{p/T} - 1} = N_g \times \frac{\pi^2}{30} T^4,$$

so that

$$\epsilon_{QGP} = \epsilon_{\text{quark gas}} + \epsilon_{\text{gluon gas}} = \left(N_q \times \frac{7\pi^2}{240} + N_g \times \frac{\pi^2}{30} \right) T^4, \tag{5.5}$$

where $N_q = 2 \times 2 \times 3 \times n_f$ and $N_g = 2 \times 8$.

Below the critical temperature $\epsilon/T^4 \sim 1$, whereas above the critical temperature $\epsilon/T^4 \sim 12$, for two quark flavors. Lattice QCD studies at finite temperature have been performed [282] and they have found this behavior, as shown in Fig. 5.1. The critical temperature results to be $T_c = (175 \pm 15)$ MeV. As we will explain later in this section, one can also estimate the critical temperature for the transition to a deconfined phase using the Hagedorn model to describe a gas of hadrons and obtain similar results.

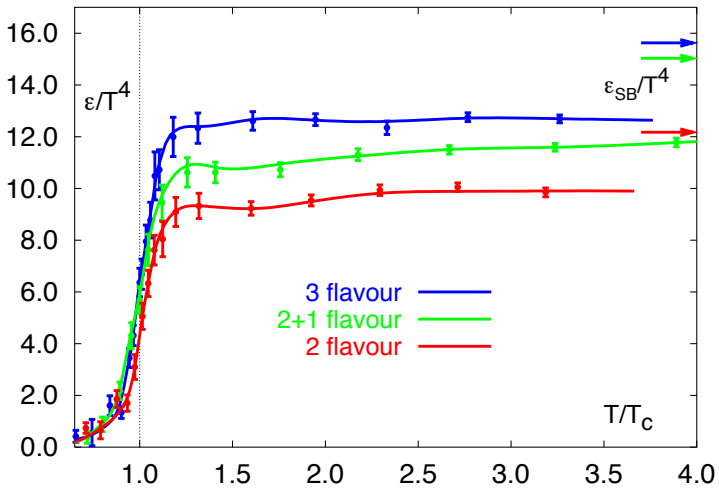

Figure 5.1. Energy density as a function of the temperature from lattice QCD studies [282].

High Energy Density Released. To understand the capability of the various experiments to explore the QGP phase one can exploit the Bjorken relation [283] to estimate the energy density released in a ultra relativistic heavy ion collision by measuring the transverse energy per unit rapidity

$$\epsilon_{Bj} = \frac{dE_T}{dy}\frac{1}{\tau_0 \pi r^2}, \tag{5.6}$$

where τ_0, the formation time, is usually taken as 1 fm, and πr^2 is the effective area of the collision.

One should also consider that the energy density released depends on the centrality of the collision, since the higher the centrality the higher is the number of nucleons participating to the reaction. The centrality of a collision can be measured by the impact parameter b, the distance between the centers of the two colliding ions. Small values of b correspond to high centralities, *i.e.* for $b = 0$ the two nuclei overlaps completely.

At very high energies the two ions approaching one another can be considered as two discs, Lorentz contracted in the direction of the motion. The nucleons will be then distributed on a surface rather than in a volume. The number of nucleons involved in the reaction is $2 \times \rho_{\rm nucl} V(b)$, with $\rho_{\rm nucl}$ the standard nuclear matter density and $V(b)$ the overlapping portions of the spheres representing the two nuclei. The nucleons are distributed on a surface $S(b)$, which is the overlapping area between the two discs representing the approaching Lorentz contracted ions.

Thus the energy density in a ultra relativistic heavy ion collision with impact parameter b is then

$$\epsilon(b) \propto 2 \times \frac{\rho_{\rm nucl} V(b)}{S(b)} = \frac{A}{S} g(b/R), \tag{5.7}$$

where

$$g(b/R) = \frac{\pi}{2} \frac{(1 - b/2R)^2 (b/4R + 1)}{\arccos(b/2R) - (b/2R)\sqrt{1 - b^2/4R^2}} \tag{5.8}$$

and $S = \pi R^2$, R being the nucleus radius.

To obtain the geometrical factor $g(b/R)$ one needs to compute $S(b)$ and $V(b)$. As can be understood looking at Fig. 5.2 $S(b)$ reads

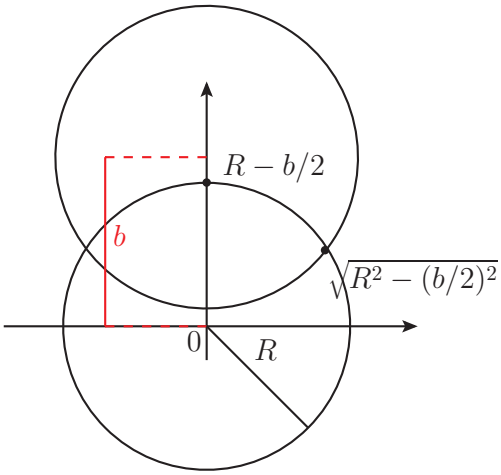

Figure 5.2. In ultra relativistic collisions the two approaching ions are Lorentz contracted in the direction of the motion and thus can be approximated by to discs. b is the impact parameter of the collisions, R is the nucleus radius.

$$\begin{aligned} S(b) &= 4 \times \left[\int_0^{\sqrt{R^2 - b^2/4}} \sqrt{R^2 - x^2} dx - \frac{b}{2} \sqrt{R^2 - b^2/4} \right] \\ &= 2R^2 \arccos\left(\frac{b}{2R}\right) - \frac{b}{2}\sqrt{4R^2 - b^2}. \end{aligned} \tag{5.9}$$

As a byproduct of this calculation we obtain also an estimate of the number of participants to the collisions as a function of the impact parameter b

$$N_{\text{part}} \sim S(b) \times \frac{2A}{\pi R^2}. \tag{5.10}$$

The dependence of the number of participants in a collisions, and thus of the energy density, on the impact parameter can be deduced from more refined nuclear model, like the Glauber model, yielding however similar results to the ones obtained here, see for example [284].

On the other hand the overlapping volume $V(b)$ of two spheres with impact parameter b is

$$\begin{aligned} V(b) &= 2 \times \left[\int_0^{\sqrt{R^2 - b^2/4}} \sqrt{R^2 - r^2}\, r dr - \frac{b}{2} \pi (R^2 - b^2/4) \right] \\ &= \frac{\pi}{12} (b - 2R)^2 (b + 4R), \end{aligned} \tag{5.11}$$

which leads to the ratio

$$\frac{V(b)}{S(b)} = \frac{\pi}{12} \frac{(b/2R-1)^2(b+4R)}{\arccos(b/2R) - (b/2R)\sqrt{1-(b/2R)^2}}. \tag{5.12}$$

To get to Eq. (5.7) one needs only to observe that

$$\rho_{\rm nucl} = \frac{2A}{\frac{4}{3}\pi R^3} = \frac{1}{2}\frac{A}{S}\frac{3}{R}. \tag{5.13}$$

Therefore a simple estimate of the ratio of the energy density for two different values of b is given by

$$\frac{\epsilon(b)}{\epsilon(b_0)} = \frac{g(b/R)}{g(b_0/R)} \Rightarrow \epsilon(b) = \frac{\epsilon(b_0)}{g(b_0/R)} g(b/R). \tag{5.14}$$

Using the Bjorken relation, the various experiment have measured the energy density released at some fixed value of the impact parameter b_0:

SPS: in [285] the NA50 collaboration finds that in Pb-Pb collisions the energy density at a given centrality b_0 is

$$\epsilon^{\rm NA50}(b_0 = 9.2 \text{ fm}) = 1.9 \text{ GeV/fm}^3. \tag{5.15}$$

RHIC: in [286] the PHENIX collaboration finds that in Au-Au collisions with 90 participants, which corresponds to $b_0 \simeq 9$ fm (see Eq. (5.10)), the energy density amounts to

$$\epsilon^{\rm PHENIX}(b_0 = 9 \text{ fm}) = 2.4 \text{ GeV/fm}^3. \tag{5.16}$$

LHC: in [287, 288, 289] one finds some indications on the energy density released in Pb-Pb collisions at the LHC

$$\epsilon^{\rm ATLAS}(b_0) \sim 3 \times \epsilon^{\rm PHENIX}(b_0). \tag{5.17}$$

Form Eq. (5.14) one obtains the dependence of the energy density on the centrality of the collisions. The results for the three experiments are shown in Fig. 5.3. Looking at Fig. 5.1 one can estimate which is the temperature region probed by the various experiments: $T \lesssim 1.2\,T_c$ at SPS, $T \lesssim 1.3\,T_c$ at RHIC and $T \lesssim 1.6\,T_c$ at LHC.

The exploration of the phase transition to QGP is in the reach of all these experiments. Indeed both SPS and RHIC observed some indications of QGP phase transition, as we will discuss hereafter.

Vanishing baryon chemical potential. As indicated in Fig. 5.3 the energy density released in the collisions grows with the beam energy. This is not the only consequence of the growth of the beam energy. The ultra relativistic domain can indeed be separated into two regimes: the *stopping region*, where baryons contained inside the colliding ions are fully or partly stopped by each other, forming a fairly baryon rich matter in the middle of the reaction zone, and the *transparent region* at higher energies, where the initial baryon charge will not be slowed down completely, so that the middle of the reaction zone will be essentially baryon free. In this second

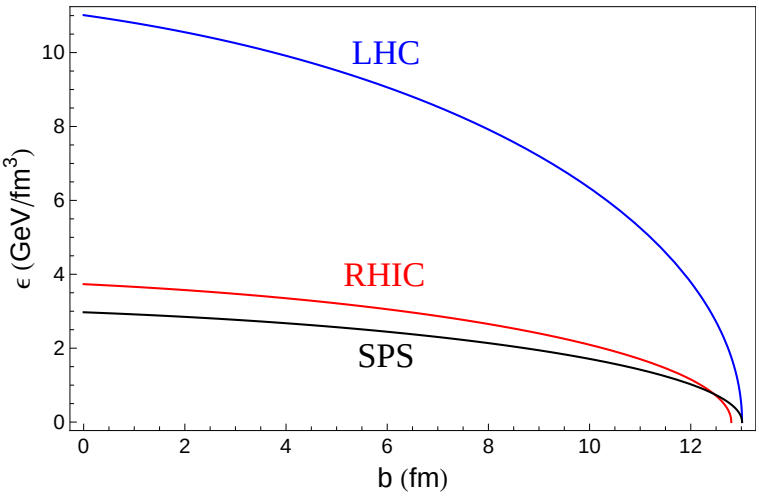

Figure 5.3. Energy density released in Pb-Pb collisions (SPS and LHC) and Au-Au collisions (RHIC) as a function of the impact parameter.

region a baryon free QGP is likely to be formed. This is the regime where the theoretical model calculations are more straightforward and furthermore this form of high energy density and low baryon density matter is the one which was present in the early Universe before hadrons were formed. SPS, RHIC and above all LHC are in the region of very low, nearly zero, baryon chemical potential, as shown in Fig. 5.4.

High gluonic density. High energy of the incoming beams means also *high gluonic density*. This can be understood looking at the form of the Parton Density Functions of hadrons. At very high energy hadrons have contributions to their wave functions from gluons and quarks of all species. The momentum fraction carried by each constituent is

$$x = \frac{E_{\text{const}}}{E_{\text{hardron}}}. \tag{5.18}$$

The gluon and quark distributions are shown in Fig. 5.5. For $x \leq 10^{-1}$ gluons dominate the wave function. The gluon component grows without bound as $x \to 0$. The small x limit is also the high energy limit since for a minimal gluon energy of order Λ_{QCD}, $x \sim \Lambda_{\text{QCD}}/E_{\text{hadron}}$. The size of a hadron does not grow rapidly as energy approaches infinity. The growth of the cross size is limited by he Froissart bound. Since the number of gluons is growing rapidly but the size of a hadron is not, the high energy limit of QCD is also the high gluon density limit. The first stage of the heavy ion collision can be thus represented by two *Color Glassed Condensates* (CGC), highly coherent and high energy density ensembles of gluon states, approaching one another. The collisions of these CGC's produces the *Glasma*, which has properties much different from those of the CGC and is produced in a very short time after the collision. The Glasma represents the transition from CGC's to QGP. Finally as the QGP expands it evolves in a hot hadron gas. The time evolution of a heavy ion collision is depicted in Fig. 5.6.

Strangeness Production. Strangeness was one of the first proposed signatures

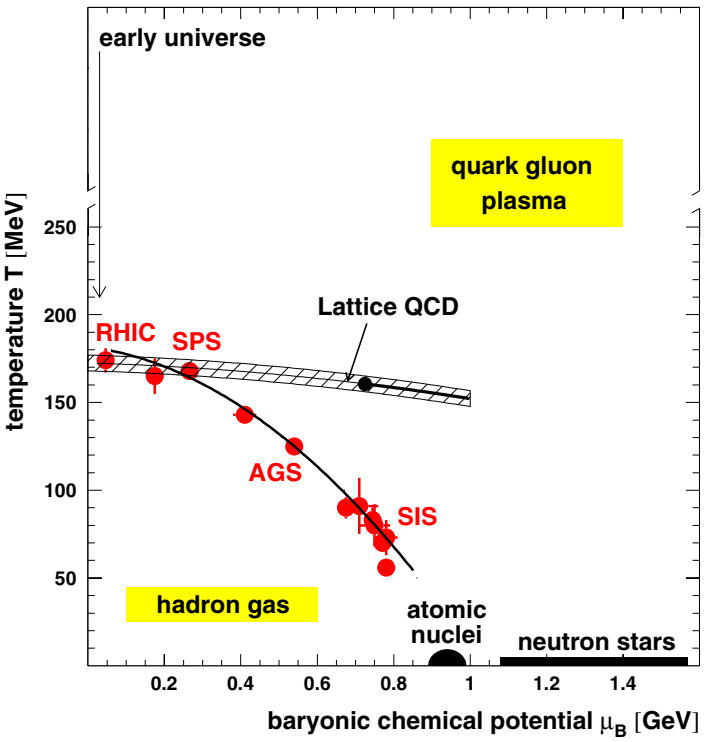

Figure 5.4. The phase diagram of strongly interacting matter from [290].

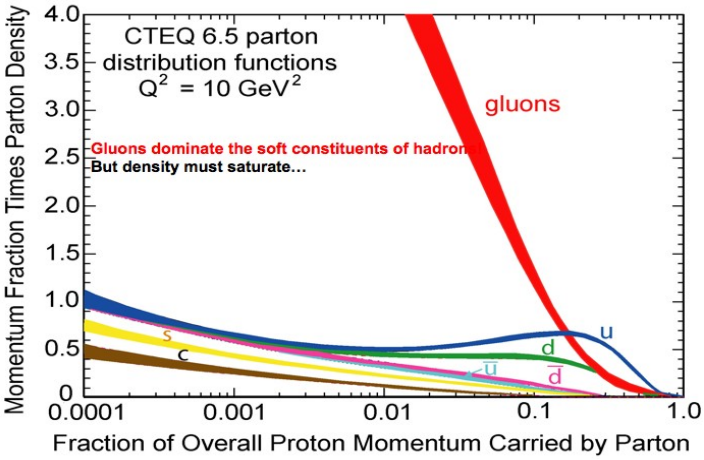

Figure 5.5. Parton content of a proton probed at $Q^2 = 10$ GeV^2.

of the deconfined phase [292]. The quarks u and d from which the stable matter around us is made are easily produced as quark-antiquark pairs because they have small masses. The mass of strange quarks and antiquarks is of the same magnitude as the temperature T at which protons, neutrons, and other hadrons are expected to dissolve into quarks, the QGP critical temperature. This means that the abundance of strange quarks is sensitive to the conditions, structure, and dynamics of the deconfined-matter phase. The dominant mechanism to produce strangeness from

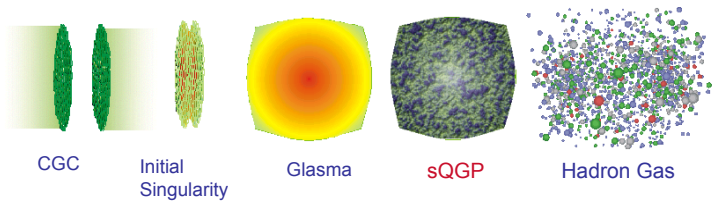

Figure 5.6. Time evolution of a ultra relativistic heavy ion collision [291].

QGP was demonstrated to be gluon-gluon fusion $gg \to s\bar{s}$ [293]. The quarks and antiquarks produced in the QGP evolve into a multitude of final state particles with different quark content, as depicted in Fig. (5.7) The detection of strange particles

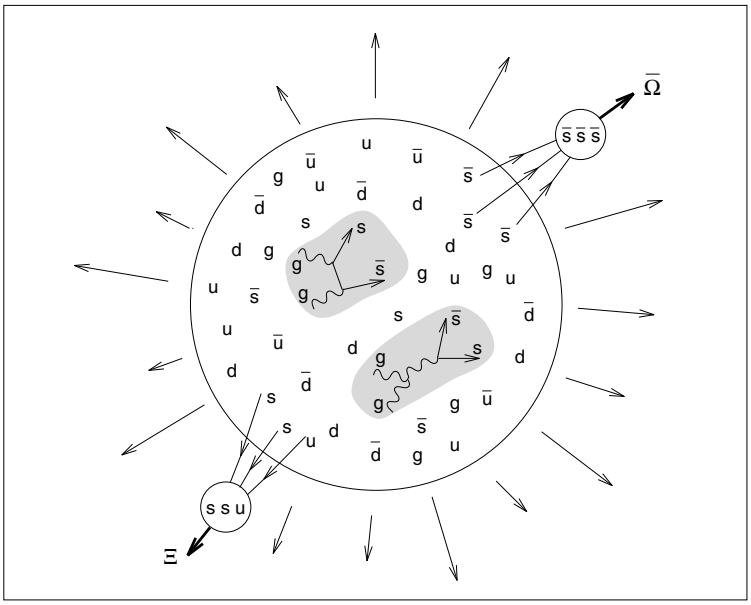

Figure 5.7. Qualitative picture describing the production of hadrons containing strange quarks [294].

is relatively easy to perform in this kind of experimental scenario. Strange quarks decay into the lighter ones through weak interactions, thus on a time scale much longer compared to the typical nuclear collision times. It is important to observe that since strange quarks are not brought into the reaction by the colliding nuclei, the production of strange particles is originated by the kinetic energy of the colliding ions. The most interesting qualitative signature of strangeness in QGP is the yield of multi-strange antibaryons. Given the ready supply of strange quarks and antiquarks, otherwise rarely produced strange particles will be emerging from a deconfined phase. In Fig. 5.8 we show the production of (multi)-strange baryons and antibaryons as measured by the NA57 experiment at CERN.

J/ψ suppression due to color screening. The production of $c\bar{c}$ pairs must occur at the very first instants after the collision, since it involves energies much higher than those needed to produce light quarks. Thus charmonium production

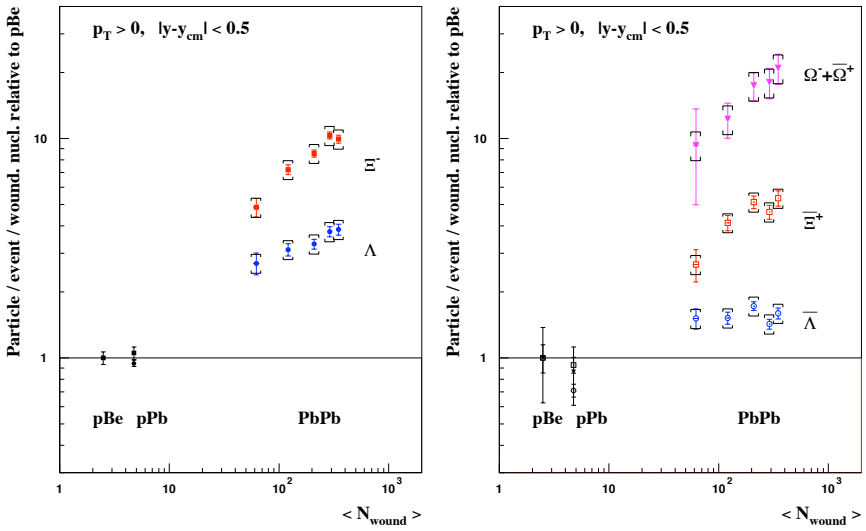

Figure 5.8. Strangeness enhancement measured by the NA57 experiment. The enhancements are defined as the particle yields normalized by the number of participating nucleons in the collisions, and divided by the observed yield in p-Be collisions.

should be tightly related to the formation of QGP, if this phase really exists. If the QGP phase is formed, these charmed quarks have less chance of forming a charmonium state, because the gluons present within the plasma hinder their binding or break the bound states.

Debye screening is responsible for this phenomenon. An electric charge in high density atomic matter at temperature T is partially screened by the other surrounding charges, so that the associated Coulomb potential reduces its range becoming

$$\frac{e}{r} \to \frac{e \exp^{-r/r_D(T)}}{r}, \tag{5.19}$$

where r is the distance from the charge e and r_D is the Debye screening radius, inversely proportional to the charge density.

To derive Eq. (5.19) let us consider high density ionic matter. We start from the Poisson equation for the electrostatic potential $\Phi(r)$:

$$|\boldsymbol{\nabla}|^2 \Phi(\boldsymbol{r}) = -\rho(\boldsymbol{r}), \tag{5.20}$$

ρ being the charge density distribution. This can be expressed in terms of the charges and the spatially varying number densities of the individual ions as

$$\rho(\boldsymbol{r}) = \sum_i q_i c_i(\boldsymbol{r}) \tag{5.21}$$

One assumes that $c_i(r)$ is given by a Boltzmann distribution in the electrostatic interaction energy between the ions and the point charge:

$$c_i(\boldsymbol{r}) = \frac{1}{Z_i} \exp^{-(q_i \Phi(\boldsymbol{r})/k_B T)}, \tag{5.22}$$

with Z_i the partition functions defined through the density of each ion species

$$n_i = \frac{1}{V}\int d\boldsymbol{r} c_i(\boldsymbol{r}) = \frac{1}{VZ_i}\int d\boldsymbol{r}\exp^{-(q\Phi(\boldsymbol{r})/k_BT)}. \tag{5.23}$$

For weak electrostatic potentials we can make the following approximation

$$\rho(\boldsymbol{r}) \simeq \sum_i q_i \frac{1}{Z_i}\left(1 - \frac{q_i\Phi(\boldsymbol{r})}{k_BT}\right). \tag{5.24}$$

At lowest order we can also deduce from Eq. (5.23) $Z_i \sim 1/n_i$. Now, recalling that in the spherically symmetric $\Phi(\boldsymbol{r}) = \Phi(r)$ case the differential operator can be written as

$$|\boldsymbol{\nabla}|^2\Phi(r) = \frac{1}{r^2}\frac{d}{dr}\left[r^2\frac{d}{dr}\Phi(r)\right], \tag{5.25}$$

the Poisson equation reads

$$\frac{1}{r^2}\frac{d}{dr}\left[r^2\frac{d}{dr}\Phi(r)\right] = -\sum_i\left(n_iq_i - \frac{n_iq_i^2\Phi(\boldsymbol{r})}{k_BT}\right). \tag{5.26}$$

The first term on the right hand side vanishes since the whole system is electrically neutral $\sum_i n_iq_i = 0$, so we are left with a linear differential equation in $\Phi(r)$, which can easily be solved

$$\frac{1}{r^2}\frac{d}{dr}\left[r^2\frac{d}{dr}\Phi(r)\right] = \sum_i \frac{n_iq_i^2\Phi(\boldsymbol{r})}{k_BT} \Rightarrow \Phi(r) = \frac{e\,\exp^{-r/r_D(T)}}{r}, \tag{5.27}$$

with

$$r_D^2(T) = \frac{k_BT}{\sum_i n_iq_i^2}. \tag{5.28}$$

The higher the atomic matter density the shorter the screening length r_D is, so that the electrons are no more bound to their own nucleus.

A similar mechanism should be at work in high density strong interacting matter, like the QGP [295]. In particular one can focus on how the QGP modifies the potential which is responsible for the binding of $c\bar{c}$. As we have said in the beginning $c\bar{c}$ bound states should be formed at the very initial stages of the collision, as an example the formation time of a J/ψ is $\sim 0.9\text{fm}/c$. Matsui and Satz suggested for the first time in [296] that the J/ψ production could be used as a probe of the existence of QGP. As we have explained in Section 1.2.3, the effective potential between $c\bar{c}$ at zero temperature is well approximate by the Cornell potential

$$V(r) = -\frac{\alpha}{r} + \sigma\, r. \tag{5.29}$$

At finite temperature $V(r)$ should be modified due to the Debye screening of the color charge: above the critical temperature the term responsible for confinement must disappear and the Coulomb-like term is attenuated as

$$V(r,T) \xrightarrow{T>>T_c} -\frac{\alpha\exp^{-r/r_D(T)}}{r} \tag{5.30}$$

Now, when the screening radius r_D becomes less than the binding radius r_H of the quark system, *i.e.* less than the hadron radius, the confining force can no longer hold the quarks together and hence deconflnement sets in. The general form of the interacting potential at finite temperature $V(r,T)$ must give $V(r)$ as $T \to 0$. Introducing the *Debye screening mass* $\mu_D(T) = 1/r_D(T)$, $V(r,T)$ reads

$$V(r,T) = \frac{\sigma}{\mu_D(T)}\left(1 - \exp^{-\mu_D(T)r}\right) - \frac{\alpha}{r}\exp^{-\mu_D(T)r} \tag{5.31}$$

The screening mass $\mu_D(T)$ is an increasing function of temperature. When $\mu_D(T = 0) \to 0$, Eq. (5.29) is recovered. At finite temperature, as $r \to 0$ the $1/r$ behavior is dominant, while as $r \to \infty$ the range of the potential decreases with $\mu_D(T)$, making the binding less effective.

This deconfining medium has an effect on the binding of c and $\bar{c}$ quarks into J/ψ mesons. The energy of the bound states may be estimated semi-classically by

$$E(r,T) = 2m_c + \frac{1}{2m_c r^2} + V(r,T) \tag{5.32}$$

including the c and $\bar{c}$ rest masses and their kinetic energies. In Fig. 5.9 we plot the energy $E(r,T)$ at $T = 0$ and $T = 178$ MeV taking $\mu_D(178\text{ MeV}) = 357$ MeV. If the QGP is created just after the collision the probability to produce excited charmonium states, like $\psi(2S)$, χ_{cJ} and $\psi(3770)$, diminishes consistently, since the onset of the continuum part of the spectrum starts just above the J/ψ mass. Thus the J/ψ produced from radiative and hadronic decays, $\psi(2S) \to J/\psi\,\pi\pi$ or $\chi_{cJ} \to J/\psi\,\gamma$, will be produced less copiously with respect to what happens, for example, in proton proton collisions.

The observation of a suppression of the J/ψ yield with respect to what observed in Drell-Yan production lead the NA50 collaboration to claim the evidence for the existence of QGP [297]. A suppression in the J/ψ production with respect to the one expected from nuclear absorption was observed for high values of the transverse energy E_T. As detailed in [284] the higher E_T the higher is the centrality of the collision. The E_T value at which the dip in the production occurs indicates the centrality needed to reach sufficiently high temperatures for the QGP to be formed.

Is this a solid signal of the existence of QGP? In a series of recent works a competitive mechanism to the Debye screening due to QGP has been considered. This mechanism is the J/ψ dissociation due to the interaction with the hadron gas at the last stage of the time evolution of the collisions, see Fig. 5.6.

In [4] we updated these considerations comparing theoretical predictions with the last data from RHIC and we discussed the possible contribution from resonant scattering through $X(3872)$.

5.1.2 Scattering in hot hadronic matter: the role of $X(3872)$ [4]

Processes like

$$J/\psi\ (\pi, \eta, \rho, \omega, \phi, K^{(*)}, ...) \to D^{(*)}\bar{D}^{(*)}, \tag{5.33}$$

which are at work in a hypothetical hadron gas formed in place or after the deconfined phase of quarks and gluons, may also provide a source of attenuation of J/ψ. These

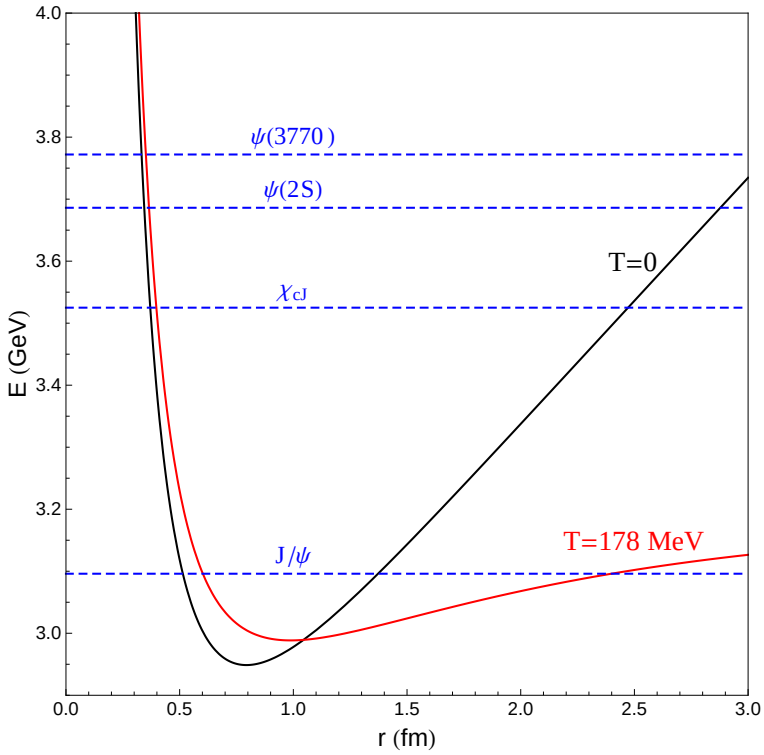

Figure 5.9. Energy as in Eq. (5.32) for $T = 0$ (black line) and $T = 178$ MeV (red line) with a Debye screening mass $\mu_D(178\text{ MeV}) = 357$ MeV. Dashed blue lines represents the lowest charmonium levels.

contributions might also take place at a different stage of the hadronization process – once the plasma has converted into hadrons under the hypothesis that the hadron gas is itself in thermal equilibrium. Such situations have been extensively studied in the past. Here we take into account also the in-medium effects on the open charm mesons discussed in [298, 299, 300, 301, 302, 303, 304, 305, 306] and update analyses such as those in [307, 308, 309, 310, 311, 312, 313] and lattice studies like [314]. Similar studies can be found in [315] or in [316, 317], where a critical temperature (Mott transition) is introduced to reproduce the dip observed in J/ψ suppression in correspondence of a particular centrality; see also [318, 319, 320].

Recently the PHENIX collaboration published new data on the J/ψ suppression in heavy ion collisions observed at RHIC [321], which have been discussed for example in [322]. These data, together with the upcoming ones from the LHC - ALICE collaboration, have encouraged us to consider the study of the contribution of the $X(3872)$ to the J/ψ suppression by a hot hadron gas and to revise some previous results on this topic.

In addition to previous works, we consider here a resonant channel mediated by $X_{1,2}$ [2] which turns out to be relevant if in-medium effects on open charm mesons are considered. Due to the narrowness of the $X(3872)$, one would expect the contribution

[2] We remind that X_1 indicates $X(3872)$ in the $J^{PC} = 1^{++}$ assignment, whereas X_2 indicates $X(3872)$ in the 2^{-+} one.

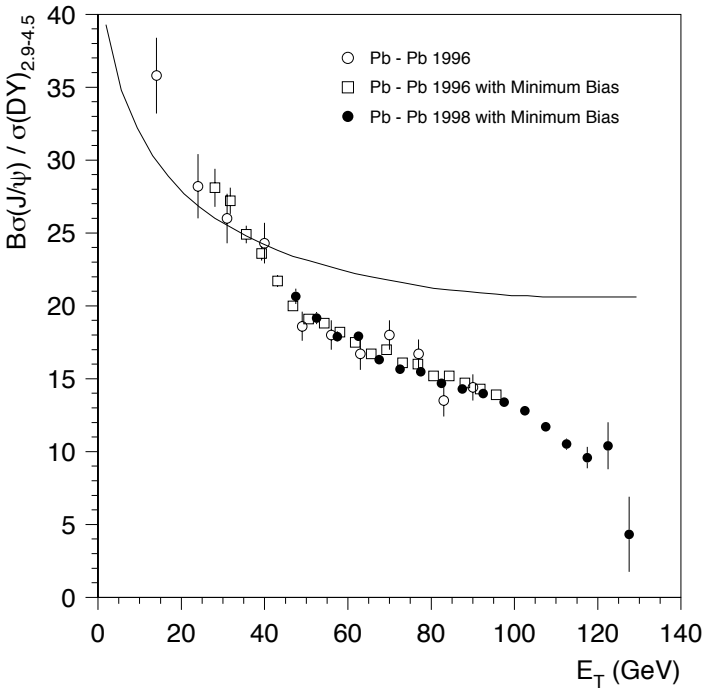

Figure 5.10. σ_ψ/σ_{DY} ratio as a function of E_T, transverse energy, obtained with the standard and minimum bias analyses of the 1996 and 1998 data samples [297]. The curve represents the J/ψ suppression due to ordinary nuclear absorption.

of the S-channel processes

$$J/\psi\ (\rho,\omega) \to X(3872) \to D^0\bar{D}^{0*} \tag{5.34}$$

to be negligible. Nevertheless they can be enhanced because the properties of open charm mesons change when propagating inside a hadron medium. In particular their masses are expected to decrease, lowering the $D^0\bar{D}^{0*}$ threshold. Also the non-resonant modes are affected by in-medium D meson properties. Hence we re-analyze some results previously obtained [307, 308, 314, 309, 310], in particular those in [308].

In Section 5.1.2.1 we will obtain an estimate for the cross section for the process of Eq. (5.34), using the couplings derived in Section 4.1. In the subsequent Section 5.1.2.2, we will briefly review how the properties of open charm mesons are expected to be modified inside the hadron medium. Finally in Sections 5.1.2.3 and 5.1.2.4 using the results found in the literature we will quantify the effect of this dissociation process and update the estimates on the non resonant channels of Eq. (5.33) with respect to those given in [308]. We will then compare the predictions obtained with the experimental data.

5.1.2.1 Cross sections

The cross section for the process of Eq. (5.34), depicted in Fig. 5.11, reads as follows (see Appendix E.3)

$$\sigma(J/\psi\ \rho \to D\bar{D}^{0*}) = \frac{1}{9}\frac{1}{2\ \lambda^{1/2}(s, m_\psi^2, m_\rho^2)}\ f(s, m_\psi^2, m_\rho^2, m_{X_{1,2}}^2, m_{_D}^2, m_{_{D^*}}^2)\ \frac{1}{16\pi}\frac{\lambda^{1/2}(s, m_{_D}^2, m_{_{D^*}}^2)}{s}, \tag{5.35}$$

where $f(s)$ is the integral over the scattering angle of the sum over polarizations of the squared matrix element

$$f(s, m_\psi^2, m_\rho^2, m_{X_{1,2}}^2, m_{_D}^2, m_{_{D^*}}^2) = \int d\cos\theta \sum_{\text{pol}} |\mathcal{M}_{\text{via } X_{1,2}}|^2(s, m_\psi^2, m_\rho^2, m_{X_{1,2}}^2, m_{_D}^2, m_{_{D^*}}^2, \theta). \tag{5.36}$$

For the matrix elements we use the couplings reported in Table 4.2. The resulting cross sections are shown in Figs. 5.12-5.15 as functions of E_ρ or E_ω, the energies of the ρ and the ω in the rest frame of the J/ψ: $s = m_{\rho,\omega}^2 + m_\psi^2 + 2m_\psi E_{\rho,\omega}$.

The functional behavior of the cross sections shown can be explained as follows. At small values of the energy of the incoming ρ, ω the "exothermic" peak appears[3]: the threshold energy of the reaction $m_{_D} + m_{_{D^*}}$ is indeed smaller than the minimum value of $\sqrt{s}$, namely $m_\rho + m_\psi$, so that the divergence in the flux factor is located at a larger value than the threshold one. At higher energies, $s >> m_X^2$, the flux factor behaves as $1/s$, whereas the phase space is approximately constant ($\lambda^{1/2}(s, 0, 0)/s \simeq 1$) so that

$$\sigma(s) \sim \frac{1}{s} \times f(s) \quad \text{as} \quad s >> m_X^2. \tag{5.37}$$

Here comes the difference between the 1^{++} and the 2^{-+} assignments. In the X_1 case at high energies $f(s) \sim s^0$ giving $\sigma(s) \sim 1/s$. If instead $X = X_2$, $f(s) \sim s^7$ giving instead $\sigma(s) \sim s^6$.

The divergence observed at high energies in the 2^{-+} assignment should be mitigated including a form factor which modifies the propagation of the virtual X_2. As commented in [323], there is 'no empirical information on form factors involving charmonia'. At any rate it is suggested that one can consider a polar expression as

$$F(\boldsymbol{q}) = \frac{1}{1 + \frac{|\boldsymbol{q}|^2}{\Lambda^2}} = \frac{1}{1 + \frac{E_\rho^2 - m_\rho^2}{\Lambda^2}}, \tag{5.38}$$

In Figs. 5.14 and 5.15 the dashed lines represent the cross sections corrected by this polar form factor with $\Lambda = m_X$. On the other hand this effect on the process mediated by a virtual X_1 can be safely neglected, since it would be effective only in the high energy region where the cross section drops down.

5.1.2.2 In-medium properties of open charm mesons

The modifications of the masses and decay widths of open charm mesons D^0 and D^{0*} inside a hot pion gas have been computed for example in [299], following the approach discussed in [324]. Indeed the presence of a gas of light hadrons, such as π's, can sustain scattering processes which involve D-mesons leading to a modification

[3] In Fig. 5.14 the peak is not resolved because of the x-scale chosen.

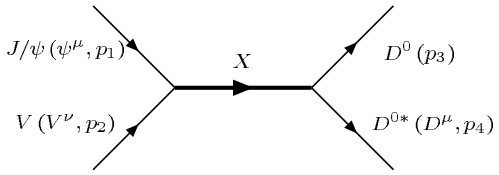

Figure 5.11. Feynman graph for $J/\psi\ (\rho, \omega) \to X(3872) \to D^0 \bar{D}^{0*}$.

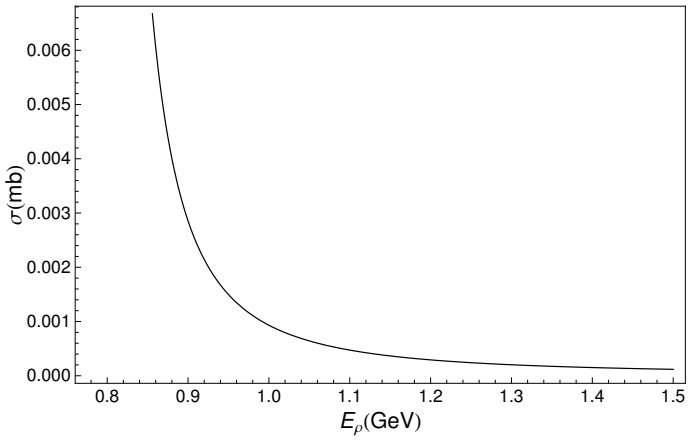

Figure 5.12. Dissociation cross section of J/ψ into open charm mesons mediated by X_1 as a function of the energy of the ρ in the rest frame of the J/ψ ($g_{_{1\psi\rho}} = 0.14$, $g_{_{1DD^*}} = 3.5$ GeV). The low energy 'exothermic' peak is present.

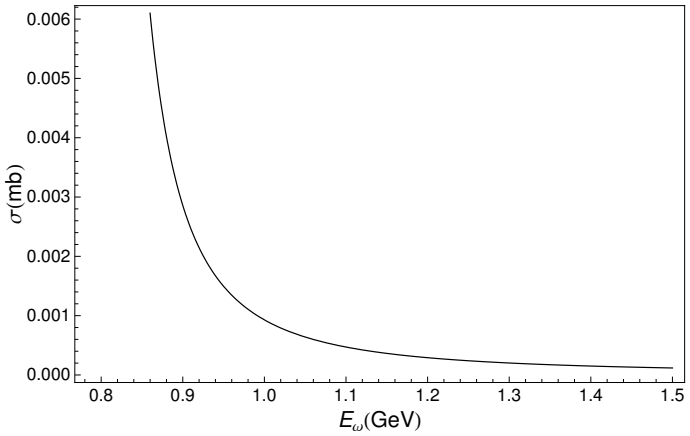

Figure 5.13. Dissociation cross section of J/ψ into open charm mesons mediated by X_1 as a function of the energy of the ω in the rest frame of the J/ψ ($g_{_{1\psi\omega}} = 0.36$, $g_{_{1DD^*}} = 3.5$ GeV). The low energy 'exothermic' peak is present.

of their masses and widths. These two quantities are both related to the self-energy diagrams, which can be written at finite temperature as the thermal averages of the resonant part of the $D\pi^{\pm,0}$ forward scattering amplitude.

The decrease of the mass and the increasing decay width for both the D-mesons found in [299] are shown in Fig. 5.16 and Fig. 5.17.

The authors of [316, 317], obtained similar results but with a different approach.

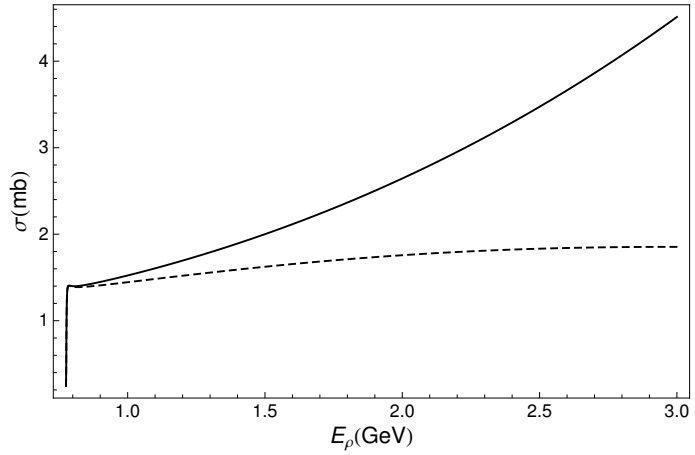

Figure 5.14. Dissociation cross section of J/ψ into open charm mesons mediated by X_2 as a function of the energy of the ρ in the rest frame of the J/ψ ($g_{_{2\psi\rho}} = -0.29$ GeV^{-1}, $g'_{_{2\psi\rho}} = 0.28$ GeV^{-1} and $g_{_{2DD^*}} = 189$). If one uses the other set of couplings for ρ the cross section is roughly the same. The dashed line includes the polar form factor of X_2, while the solid one does not.

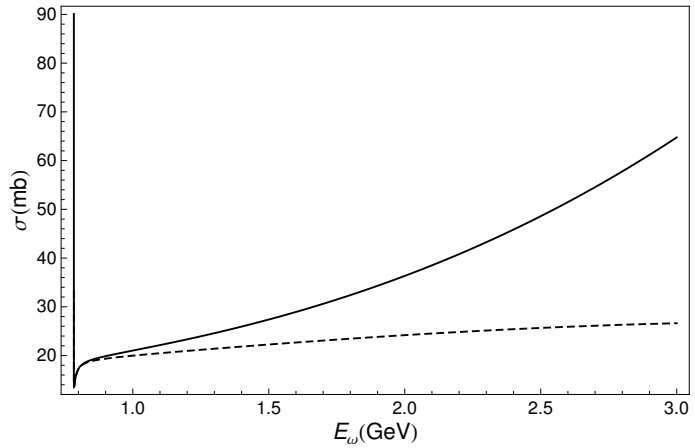

Figure 5.15. Dissociation cross section of J/ψ into open charm mesons mediated by X_2 as a function of the energy of the ω in the rest frame of the J/ψ ($g_{_{2\psi\omega}} = 1.58$ GeV^{-1}, $g'_{_{2\psi\omega}} = -0.74$ GeV^{-1} and $g_{_{2DD^*}} = 189$). Consider that we are actually concerned only with relatively low energy ρ and ω mesons in a Hagedorn gas. The dashed line includes the polar form factor of X_2, while the solid one does not.

They assume that the shape of $q'\bar{q}$ interaction potentials, responsible for the binding of mesons, is sensitive to the temperature. Thus it can happen that some discrete levels, corresponding to different $c\bar{q}$ excitations, are shifted into the continuous part of the spectrum becoming metastable states with different masses and non-vanishing widths. Each D-meson excitation undergoes this transition at a different critical temperature: $\Delta M \propto -(T - T_C)\theta(T - T_C)$.

Since we do not find any relevant differences on the J/ψ dissociation by using the two approaches, we will consider only the one in [299].

The broadening and shifting of the masses of the two open charm mesons lead

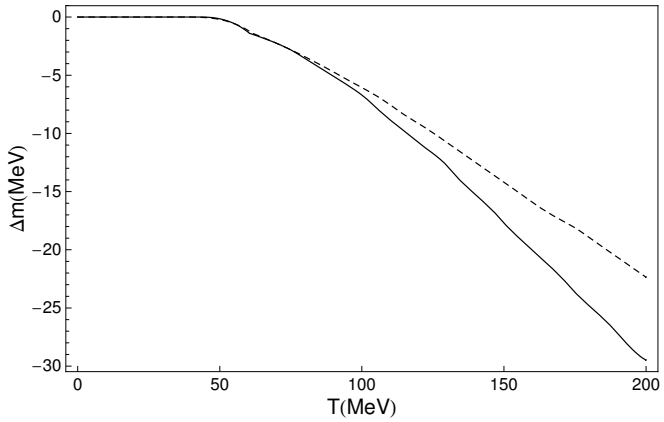

Figure 5.16. In medium mass modification computed in [299] for D^0 (solid line) and D^{0*} (dashed line).

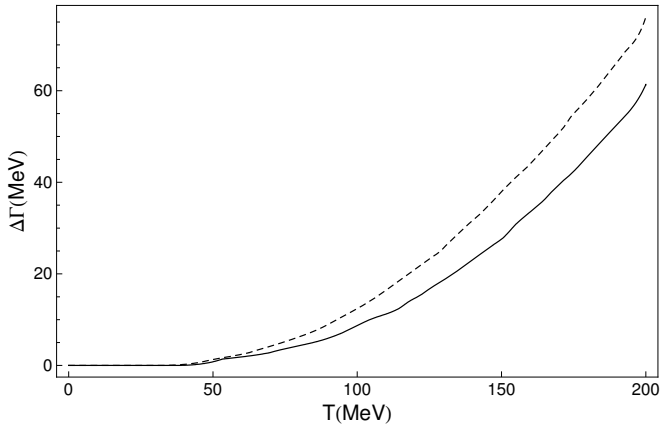

Figure 5.17. In medium total decay width computed in [299] for D^0 (solid line) and D^{0*} (dashed line).

to a modification of the decay width and mass of the $X(3872)$. Since we do not have clues on how in-medium effects would modify the mass of a $X_{1,2}$ tetraquark, we simply assume that if $X(3872) = X_1$ it is a $D^0\bar{D}^{0*}$ molecule; if $X(3872) = X_2$ it is a charmonium state. We remind here that the 1^{++} assignment is severely at odds with a $2\,^3P_1$ standard charmonium interpretation essentially because of the small radiative transition rate $X \to J/\psi\,\gamma$ with respect to what expected. In the molecular interpretation the mass of the X_1 is directly related to the sum of the masses of the D^0 and D^{0*} and thus it will decrease with the temperature. In the charmonium assignment (and likely also for tetraquarks) one might expect the mass of the X_2 to be almost stable with temperature. This is because X_2 would be the 1^1D_2 charmonium radial ground state and Debye screening is not expected to alter

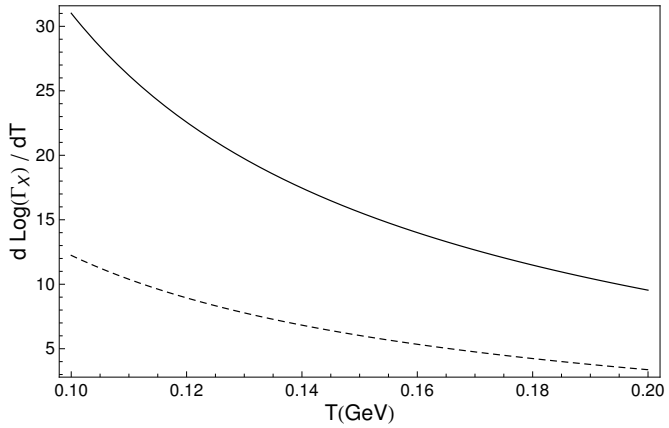

Figure 5.18. Logarithmic derivative of the total decay width of $X(3872)$ as a function of the temperature in the case $X = X_1$ and $m_{_X} = m_{_D}(T) + m_{_{D^*}}(T)$ (dashed line) and $X = X_2$ and $m_{_X} = 3872$ MeV (solid line).

the lowest lying levels [296]. The $D^0\bar{D}^{0*}$ width can be computed as

$$\Gamma(X \to D^0\bar{D}^{0*})_{_T} = \frac{1}{2s_{_X}+1}\frac{1}{8\pi m_{_X}^2}\int_{s_2^{\min}}^{s_2^{\max}} ds_2 \int_{s_1^{\min}}^{s_1^{\max}} ds_1 \sum_{\text{pol}} |\mathcal{M}_{X\to DD*}(s_1,s_2)|^2 \frac{\sqrt{\lambda(m_{_X}^2,s_1,s_2)}}{2m_{_X}} \times BW(s_1, m_{_D}(T), \Gamma_{_D}(T))\ BW(s_2, m_{_{D^*}}(T), \Gamma_{_{D^*}}(T)), \tag{5.39}$$

where by BW we mean the standard normalized Breit-Wigner function

$$BW(s,m,\Gamma) = \frac{1}{\pi}\frac{m\Gamma}{(s-m^2)^2+(m\Gamma)^2} \tag{5.40}$$

and $s^{\min}$ and $s^{\max}$ are fixed by the kinematics. We show the results in terms of the logarithmic derivative of the total width of $X_{1,2}$ with respect to the temperature, see Fig. 5.18: in-medium effects make the X_2 become much broader than X_1. This fact can be understood by taking into account the dependence of the decay width on the masses of the particles in the final state. The phase space volume is enlarged proportionally to the decay momentum p^*. As for the matrix element, if $J^{PC} = 1^{++}$ the $X \to D^0\bar{D}^{0*}$ decay has $L = 0$ and thus $|\mathcal{M}|^2 \sim$ constant, whereas if X is a 2^{-+} state it has $L = 1$ so that $|\mathcal{M}|^2 \propto p^{*2}$. Thus if $J^{PC} = 1^{++}$ then $\Gamma_X \propto p^*$, instead if $J^{PC} = 2^{-+}$ then $\Gamma_X \propto p^{*3}$.

To summarize, the fact that the charmonium X_2 mass is not affected by the medium makes the $X_2 \to D^0\bar{D}^{0*}$ P-wave decay much larger because the D^0 and D^{0*} masses are instead sensitively decreased in the finite temperature medium.

5.1.2.3 Comparison to data on J/ψ suppression at RHIC

The average absorption length (mean free path) of the J/ψ due to the presence of a ρ meson gas at temperature T is the inverse of the thermal average of the product

of the density number ρ of ρ mesons times the cross section σ (given in Eq. (5.34)):

$$\langle \rho\sigma_{J/\psi\ \rho\to D^0\bar{D}^{0*}}\rangle_T = (2s_\rho+1)\int \frac{d^3p_\rho}{(2\pi)^3}\frac{\sigma(E_\rho)}{e^{E_\rho/\kappa_B T}-1} = \frac{2s_\rho+1}{2\pi^2}\int_{E_\rho^{\min}}^{E_\rho^{\max}} dE_\rho \frac{p_\rho\, E_\rho\, \sigma(E_\rho)}{e^{E_\rho/\kappa_B T}-1}. \tag{5.41}$$

Here the kinematics imposes that

$$E_\rho^{\min} = \max\left[m_\rho, \sqrt{\frac{(m_{_D}+m_{D^*})^2 - m_\rho^2 - m_\psi^2}{2m_\psi^2}}\right]. \tag{5.42}$$

By numerical inspection we have found that it is safe to cut-off the integrals at $E^{\max}_{\rho,\omega} = 1.5$ GeV and $E^{\max}_{\rho,\omega} = 3.5$ GeV for $J^{PC} = 1^{++}$ and $J^{PC} = 2^{-+}$ respectively. The difference between the two values for $E^{\max}$ can be understood noticing that the cross section diminishes as the energy grows if $J^{PC} = 1^{++}$, while it grows with energy for $J^{PC} = 2^{-+}$.

Given that the masses of the D^0 and D^{0*} mesons are supposed to change with the temperature we need to take into account this effect in the calculation of the thermal averages. We average the absorption length over the Breit-Wigner distributions of the D and of the D^*; the formula for $\langle\rho\sigma\rangle_T$ is therefore

$$\langle \rho\sigma_{J/\psi\ \rho\to X_{1,2}\to DD^*}\rangle_T = \frac{2s_\rho+1}{2\pi^2}\int_{s_2^{\min}}^{s_2^{\max}} ds_2 \int_{s_1^{\min}}^{s_1^{\max}} ds_1 \int_{E_\rho^{\min}}^{E_\rho^{\max}} dE_\rho$$
$$\frac{p_\rho\, E_\rho\, \sigma(E_\rho, s_1, s_2, m_{_X}(T), \Gamma_{_X}(T))}{e^{E_\rho/\kappa_B T}-1} \times BW(s_1, m_{_D}(T), \Gamma_{_D}(T))\ \ BW(s_2, m_{D^*}(T), \Gamma_{D^*}(T)). \tag{5.43}$$

As already mentioned in the previous section, we report only the results obtained using the masses and widths of the D-mesons computed in [299]. If one uses the discontinuous functions for $m_{_D}(T)$ and $\Gamma_{_D}(T)$ proposed in [316, 317], the values obtained for $\langle\rho\sigma\rangle_{_T}$ are of the same magnitude. Moreover, regardless of whether the non-resonant channel is included, $\langle\rho\sigma\rangle_{_T}$ does *not* show any discontinuity that can help in fitting the observed dip in the experimental data, contrarily to what shown in [316, 317]. The same holds for the ω.

In Figs. 5.19 and 5.20 we show the results for the inverse average absorption length for the resonant J/ψ suppression mediated by X_2 and initiated by ρ and ω respectively. For the X_1 case we find the effect is negligible, since the in-medium X_1 is still too narrow for ρ and ω to effectively dissociate the J/ψ into open charm mesons.

When computing the thermal average $\langle\rho\sigma\rangle_T$ associated to X_2 one should use the cross section corrected by the form factor. Nevertheless due to the exponential $e^{-E_\rho/kT}$ in the Bose-Einstein statistics, the region in E_ρ which gives the largest contribution to $\langle\rho\sigma\rangle_T$ extends up to ~ 1.8 GeV for $T = 170$ MeV. In this region the effect of the form factor is not dramatic and thus it can be safely neglected without modifying the final picture.

We also update the estimates for the non-resonant channels enumerated in Eq. (5.33) as discussed in [308]. In Section E.4.2 of Appendix E, we give some details on the counting rules for all the J/ψ absorption processes we consider in the hadron gas.

In Table 5.2 we give a summary of the results for the inverse mean free paths. The contribution of the X_1 is negligible whereas the contribution from the X_2 resonant channel amounts to the 50% of the non-resonant channels at $T = 100$ MeV. With the growing temperature the resonant contribution is found to weight less than the non-resonant ones, reducing to a 10% of the non-resonant total at about the Hagedorn temperature $T \sim 170$ MeV. We remind the reader that we have neglected possible interferences between resonant and non resonant channels.

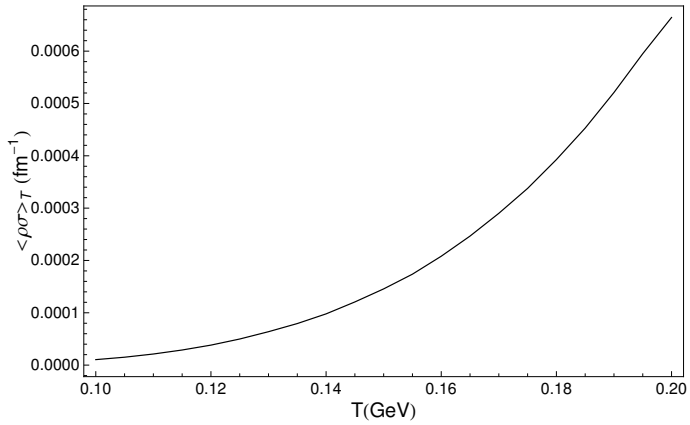

Figure 5.19. $J/\psi\ \rho \to D^0 \bar{D}^{0*}$: Inverse average absorption length for X_2 hypothesis, using $m_{_X} = 3.8723$ GeV.

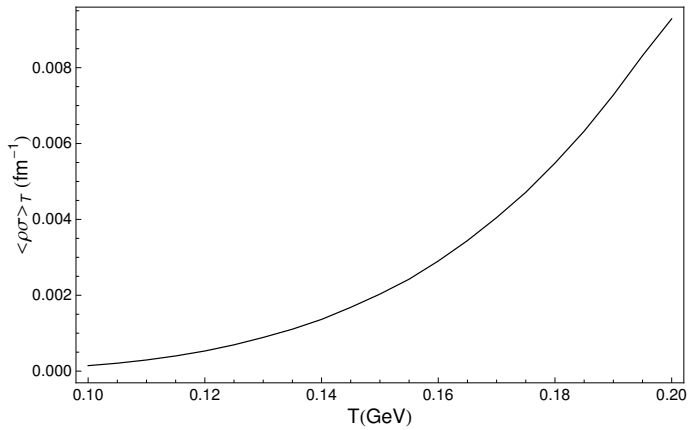

Figure 5.20. $J/\psi\ \omega \to D^0 \bar{D}^{0*}$: Inverse average absorption length for X_2 hypothesis, using $m_{_X} = 3.8723$ GeV.

We now take into account the recent RHIC data on the so called nuclear modification factor $R_{A+A}^{J/\psi}$, reported in [321] as a function of the number of participants in the collision. The quantity $R_{A+A}^{J/\psi}$ measures the ratio of the J/ψ yield in $A + A$ and pp collisions scaled by the number of nucleon-nucleon collisions. We will consider only Au-Au collisions at RHIC, due to their higher statistical significance. We will

Table 5.2. Inverse absorption lengths as defined in Eq. (5.43) for all the particles in the gas. For each temperature we show the results obtained for fixed D-mesons masses (upper entry of each cell) and for decreasing D-mesons masses as computed in [299] (lower entry of each cell). Since the ϕ decays only into $D_s\bar{D}_s$ and we assume that D_s mesons do not change their masses and widths inside a hadron medium, the upper and lower entries of each cell are equal. As for the resonant contribution due to X_2 (first column) we do not report the results with fixed D-mesons masses, since they are negligible with respect to the non-resonant ones (NR). We do not consider temperatures higher than the value we use for the Hagedorn temperature $T_H \sim 177$ MeV. (Inverse absorption length are expressed in fm^{-1}, temperatures are in GeV.)

T	$\langle\rho\sigma\rangle_T^{(\rho+\omega)X_2}$	$\langle\rho\sigma\rangle_T^{\rho+\omega}$	$\langle\rho\sigma\rangle_T^{K}$	$\langle\rho\sigma\rangle_T^{K^*}$	$\langle\rho\sigma\rangle_T^{\phi}$	$\langle\rho\sigma\rangle_T^{\pi+\eta}$	$\langle\rho\sigma\rangle_T^{\mathrm{NR}}$
0.150	–	0.00700	0.00182	0.00244	0.00052	0.00469	0.01648
	0.00218	0.00801	0.00212	0.00268	0.00052	0.00580	0.01908
0.155	–	0.00948	0.00239	0.00341	0.00074	0.00607	0.02208
	0.00260	0.01101	0.00280	0.00375	0.00074	0.00753	0.02565
0.160	–	0.01267	0.00311	0.00467	0.00102	0.00774	0.02920
	0.00311	0.01478	0.00365	0.00516	0.00102	0.00967	0.03402
0.165	–	0.01672	0.00398	0.00631	0.00138	0.00977	0.03817
	0.00369	0.01959	0.00470	0.00670	0.00138	0.01224	0.04456
0.170	–	0.02183	0.00505	0.00842	0.00186	0.01219	0.04935
	0.00434	0.02566	0.00597	0.00934	0.00186	0.01533	0.05769
0.175	–	0.02821	0.00633	0.01109	0.00247	0.01506	0.06316
	0.00505	0.03326	0.00751	0.01234	0.00247	0.01904	0.07398
0.180	–	0.03610	0.00786	0.01445	0.00324	0.01845	0.08010
	0.00588	0.04270	0.00935	0.01612	0.00324	0.02341	0.09400

also reconsider the old data on Pb-Pb collisions from NA50 [284] to show how the picture has changed in the last years.

Refs. [325, 326] have also considered the possibility that a recombination mechanism could compensate the J/ψ suppression due to QGP, making the drop in RHIC data less evident with respect to NA50, where this mechanism is expected to be weaker due to the much smaller energies involved. However in [322] it was shown that the recombination effects are of the same order of magnitude as the experimental uncertainties and thus they can be safely neglected.

The geometry of the heavy ion collision is shown schematically in Fig. 5.21, which depicts the time-evolution in the center of mass frame. We consider the J/ψ to be created with Feynman's $x \sim 0$, during the overlap of the two nuclei. These particles have to overcome absorption from the column density of nucleons of extension L. In the center of mass frame the length of the column is L/γ. In the same frame, the density of nucleons is $\rho_{\mathrm{nucl}}\gamma$, so that the absorption factor is Lorentz invariant and given by $\exp\left(-\rho_{\mathrm{nucl}}\sigma_{\mathrm{nucl}}L\right)$ (see [327]). The nuclear absorption cross section, σ_{nucl}, has been determined in [328] from the behavior of the cross section for $p + A \to J/\psi + \mathrm{All}$ and $\mathrm{d} + \mathrm{Au} \to J/\psi + \mathrm{All}$

$$\sigma_{\mathrm{nucl}}^{\mathrm{RHIC}} = (3.5 \pm 0.2)\ \mathrm{mb}. \tag{5.44}$$

As for NA50 one learns from [329] that

$$\sigma_{\rm nucl}^{\rm NA50} = (4.3 \pm 0.2)\ {\rm mb}. \tag{5.45}$$

For the density of ordinary nuclear matter we take $\rho_{\rm nucl} = 0.17\ {\rm fm}^{-3}$ [294].

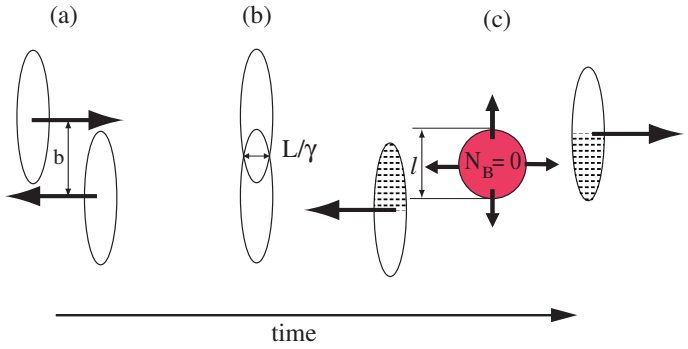

Figure 5.21. Geometry of the collision between two identical heavy nuclei with impact parameter b. After the two nuclei have traversed each other, a thermalized gas of lighter resonances is formed.

In Fig. 5.21(c) we show the hadron fireball produced by the central collisions of the interacting nucleons [283] (the *comoving particles* $\pi, \rho, \omega, ...$). The fireball has a transverse dimension, l, approximately equal to the length of the overlapping region

$$l = 2R - b. \tag{5.46}$$

The attenuation due to the interactions with the hadrons in the fireball is related to the average length that a J/ψ has to traverse before leaving it. The RHIC data in [321] are taken in two different rapidity regions: a forward rapidity region $1.2 < |y| < 2.2$ and a mid rapidity region $|y| < 0.35$. We take, for simplicity, a spherical fireball and we simulate the production of a particle at some point inside the sphere and with a given direction of the velocity. Assuming a uniform linear motion inside the fireball, the distance d given the starting point $\boldsymbol{r}$ and the direction of the velocity $\hat{\boldsymbol{v}}$, can be written in implicit form as

$$|\boldsymbol{r} + d\hat{\boldsymbol{v}}| = \frac{l}{2}. \tag{5.47}$$

The point on the spherical surface where the particle emerges from the fireball is thus $\boldsymbol{r}' = \boldsymbol{r} + d\hat{\boldsymbol{v}}$, from which one can compute the rapidity of the J/ψ observed, $y \simeq \eta = -\ln(\tan(\theta/2))$, with θ the polar angle associated to $\boldsymbol{r}'$. To obtain the average distance one needs to integrate over the two angles which identify the direction of $\hat{\boldsymbol{v}}$ and over $\boldsymbol{r}$, respecting the constraint on the polar angle of the emersion point given by the experimental bounds on the rapidity ($y_0 < |y| < y_1$ implies $\theta_0 < \theta < \theta_1$). To make our simple simulation more realistic we take into account that the distribution of the directions of the velocity is not uniform, but can be approximated by $f(\hat{\boldsymbol{v}}_T) \propto 1/p_T$, where p_T is the transverse momentum with respect to the beam axis. Finally one has

$$\bar{d} = \frac{\int d\boldsymbol{r} \int d\hat{\boldsymbol{v}}\ f(\hat{\boldsymbol{v}}_T) d(\boldsymbol{r}, \hat{\boldsymbol{v}})\ \Theta(\theta)}{\int d\boldsymbol{r} \int d\hat{\boldsymbol{v}}\ f(\hat{\boldsymbol{v}}_T)\ \Theta(\theta)}, \tag{5.48}$$

with

$$\Theta(\theta) = \begin{cases} 1 & \theta_0 < \theta < \theta_1 \\ 0 & \text{elsewhere} \end{cases} . \tag{5.49}$$

The result of this computation is $\bar{d}_{\text{fwd}} = 0.4\,l$ and $\bar{d}_{\text{mid}} = 0.3\,l$ in the forward and mid rapidity region respectively. Thus, the attenuation factor due to absorption by the comoving particles is

$$\mathcal{A}^{\text{fwd(mid)}}_{\pi,\rho,\omega,\ldots} \propto \exp\left[-\Sigma_i \langle \rho_i \sigma_i \rangle_{T(l)} \bar{d}_{\text{fwd(mid)}}\right], \tag{5.50}$$

the subscript i labels the species of hadrons making up the fireball, ρ_i the number density of the effective (i.e. above threshold) particles and σ_i the corresponding J/ψ dissociation cross section. Brackets indicate an average over the energy distribution in the fireball. This thermal average is computed at a certain temperature $T(l)$, which is given by the centrality of the collision, as we shall explain in detail in the next subsection.

The NA50 measurements on Pb-Pb collisions were inclusive. Hence one needs to integrate the distance $d(\boldsymbol{r}, \hat{\boldsymbol{v}})$ over the whole range for the polar angle, obtaining $\bar{d} = 3/8\,l$, as was done in the previous analysis contained in [308].

As noted before, we can compute the nuclear absorption length, L, as a function of b using NA50 data [330, 331] for Pb-Pb collisions. We report this function in Fig. 5.22. Exploiting Eq. (5.46), one can obtain L as a function of l. We can reasonably

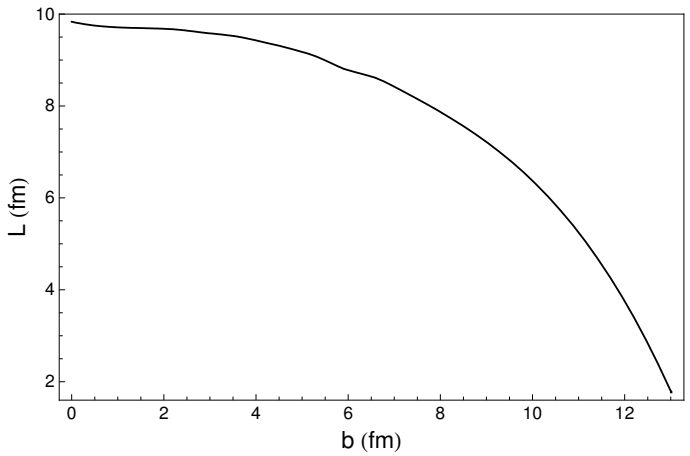

Figure 5.22. Mean length of the path that a J/ψ produced during a Pb-Pb collisions at NA50 must travel in nuclear matter as a function of the impact parameter b [330, 331].

suppose that the same function $L(b)$ can be used in the analysis of Au-Au collisions at RHIC, since Au and Pb have approximately the same radius ($R_{\text{Pb}} = 7.1$ fm and $R_{\text{Au}} = 7.0$ fm).

Putting it all together, we write the attenuation of the J/ψ, due to both comovers and nuclear effects, as a function of l according to

$$\mathcal{A}^{\text{fwd(mid)}}(l) = C_0 + C \times \exp[-\rho_{\text{nucl}} \sigma_{\text{nucl}} L(l)] \times \exp\left[-\Sigma_i \langle \rho_i \sigma_i \rangle_{T(l)} \bar{d}_{\text{fwd(mid)}}\right], \tag{5.51}$$

where C is an appropriate normalization constant and C_0 is an offset. To fit NA50 data we substitute $\bar{d}_{\text{fwd(mid)}}$ with $3/8\,l$.

To obtain the experimental data [321] as a function of l we use the expression for the number of participants as a function of b obtained in Eq. (5.10), see Fig. (5.23).

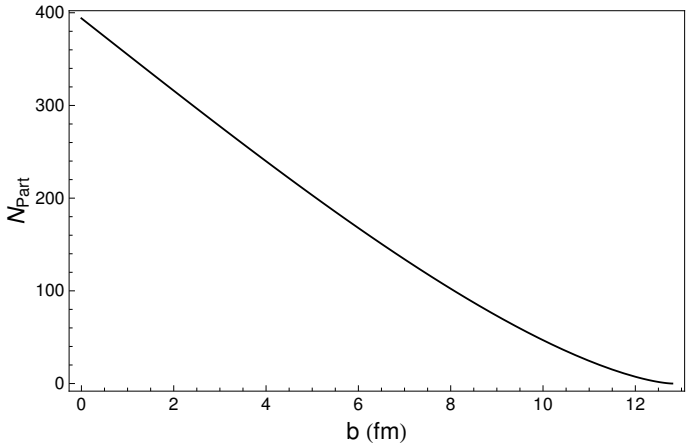

Figure 5.23. Average number of participant nucleons in a Au-Au collision as a function of the impact parameter b computed using Eq. (5.10).

5.1.2.4 Hagedorn Gas

Here we wish to determine the function $T(l)$ to be used in Eq. (5.50). We will describe the fireball as a Hagedorn gas of resonances. The partition function of a Hagedorn gas in the classical Boltzmann limit ($E >> \kappa_B T$) can be written as [294]

$$\ln(Z_H^{cl}) = \left(\frac{T}{2\pi}\right)^{3/2} \int dm\ \rho(m) m^{3/2} e^{-m/T}. \tag{5.52}$$

$\rho(m)$ is the mass spectrum of hadronic states, which has the empirical shape

$$\rho(m) = \frac{c}{(m_0^2 + m^2)^{3/2}} e^{m/T_H}, \tag{5.53}$$

with $m_0 = 0.96$ GeV, $c = 2.12$ GeV^2 and $T_H = 177$ MeV [308]. T_H is known as the Hagedorn temperature. For a recent determination see [332]. As soon as $T \geq T_H$ the integral in Eq. (5.52) diverges, hence this thermodynamical description is valid up to $T \leq T_H$. Above the Hagedorn temperature the system undergoes a phase transition, which can be interpreted as the transition from hadronic matter to QGP.

From the partition function of Eq.(5.52) one can easily obtain the energy density $\epsilon(T)$

$$\epsilon(T) = -\frac{\partial}{\partial\beta} \ln(Z_H^{cl}) = \left(\frac{T}{2\pi}\right)^{3/2} \int dm\ \frac{c}{(m_0^2 + m^2)^{3/2}} m^{5/2} \left(1 + \frac{3}{2}\frac{T}{m}\right) e^{m(1/T_H - 1/T)}. \tag{5.54}$$

On the other hand Eqs. (5.14,5.15,5.16) give the function $\epsilon(b)$ at NA50 and PHENIX. From $\epsilon(b) = \epsilon(T)$ we deduce $T(b)$ and in turn $T(l)$. We show $T(l)$ for Pb-Pb collisions at NA50 and Au-Au collisions at RHIC in Figs. 5.24 and 5.25 respectively. It is

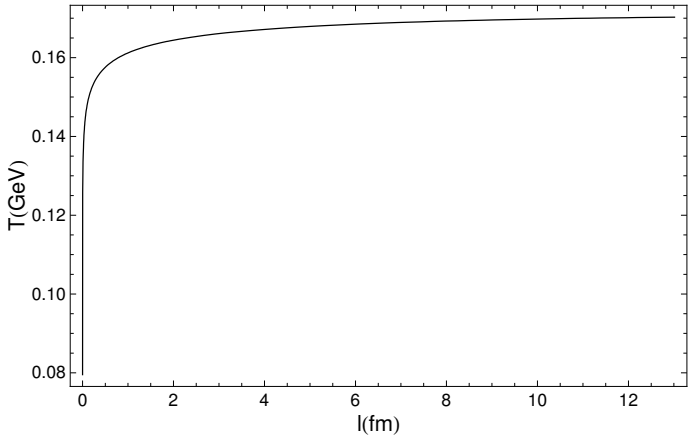

Figure 5.24. Temperature of the Hagedorn gas formed after a Pb-Pb collision at NA50 as a function of $l = 2R - b$.

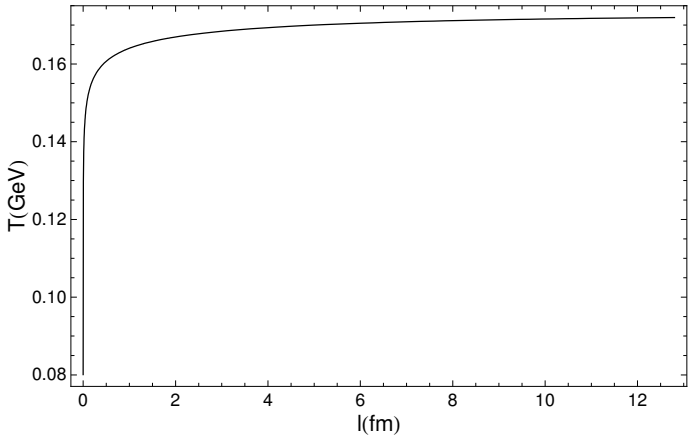

Figure 5.25. Temperature of the Hagedorn gas formed after a Au-Au collision at RHIC (right panel) as a function of $l = 2R - b$.

evident that over a wide range of l the temperature is almost constant and below T_H.

Now we have all the ingredients to perform a best fit of the experimental data using the attenuation function defined in Eq. (5.51). We show the agreement between experimental data and theoretical prediction in Fig. 5.26 for NA50 data, and in Figs. 5.27 and 5.28 for RHIC data. We remind here that C and C_0 are fit parameters which include bulk effects we do not dwell upon. Moreover the differences we find in these parameters between RHIC and NA50 are not statistically significant within the errors.

5.1.2.5 Discussion and conclusions

We use the coupling strengths we found in Section 4.1 to explore the potential role of $X_{1,2}$ in J/ψ absorption processes like $J/\psi\ (\rho, \omega) \to X_{1,2} \to D^0 \bar{D}^{0*}$. Such processes might occur in a hot resonance gas produced in heavy ion collisions. Regardless of the detail mechanism by which the resonance gas is formed, processes as the ones

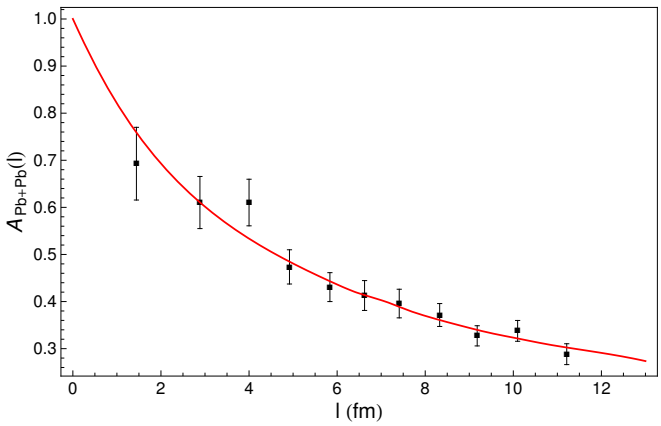

Figure 5.26. Attenuation function for the J/ψ yield in Pb-Pb collisions as measured at NA50 (Squares) and as predicted by the hadron gas description (Red Line). The best fit is obtained for $C_0 = -0.2$ and $C = 1.4$ giving a $\chi^2/\mathrm{DOF} = 4.9/9$. In absence of the resonant contribution from X_2 and of the in-medium effects on the D mesons we obtain $\chi^2/\mathrm{DOF} = 5.1/9$.

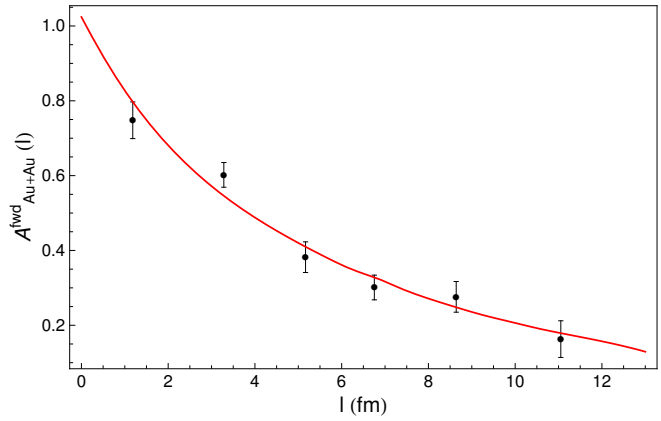

Figure 5.27. Attenuation function for the J/ψ yield in Au-Au collisions in the forward rapidity region $1.2 < |y| < 2.2$ as measured at RHIC (Disks) and as predicted by the hadron gas description (Red Line). The best fit is obtained for $C_0 = -0.6$ and $C = 1.9$ giving a $\chi^2/\mathrm{DOF} = 5.6/4$. In absence of the resonant contribution from X_2 and of the in-medium effects on the D mesons we obtain $\chi^2/\mathrm{DOF} = 6/4$. In this rapidity region the J/ψ is reconstructed in the $\mu^+\mu^-$ mode.

mentioned above are mimicking the in-plasma J/ψ suppression hypothetically due to the Debye screening of the $c\bar{c}$ confining potential. Therefore this is a background to the Debye J/ψ suppression signal. How far can we go with a hadron gas picture in fitting data on J/ψ suppression at RHIC? A limitation to the hadron gas description might come from the excessively high temperature needed for the gas to account for the observed J/ψ suppression effect. This was discussed in [307, 308]: a hadron gas description fails above the critical Hagedorn temperature, the highest temperature for hadron matter.

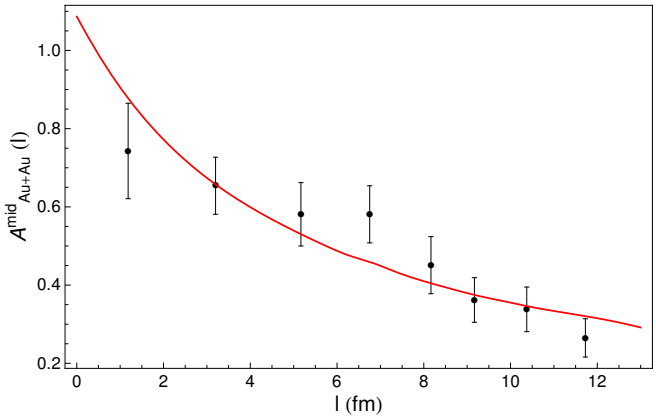

Figure 5.28. Attenuation function for the J/ψ yield in Au-Au collisions in the mid rapidity region $|y| < 0.35$ as measured at RHIC (Disks) and as predicted by the hadron gas description (Red Line). The best fit is obtained for $C_0 = -0.5$ and $C = 1.8$ giving a $\chi^2/\mathrm{DOF} = 6.1/6$. In absence of the resonant contribution from X_2 and of the in-medium effects on the D mesons we obtain $\chi^2/\mathrm{DOF} = 6.5/6$. In this rapidity region the J/ψ is reconstructed in the e^+e^- mode.

The analysis in [307, 308] was based on NA50 data on Pb-Pb collisions, see Fig. 5.26, where at a centrality of about 4 fm in units of $l = 2R - b$, a drop was observed (actually a one sigma effect) in the J/ψ yield in going from the three leftmost points towards higher centralities. In the low l region ($l \leq 4$ fm) the authors of [307, 308] used also data on S-U collisions and the approach was to perform a best fit in that region (where the hadron gas picture is more reliable, the energy density being smaller) with an exponential attenuation function at some temperature T. An unreasonably large T was then needed to fit data also at $l \geq 4$ fm. Using a Hagedorn gas model the fit was simply very poor. Moreover in [333] it was pointed out a correlation in the l dependence of the J/ψ suppression and the enhancement of strange particle production observed in NA50 data.

Here we took a different approach. We note that the drop at $l = 4$ fm observed by NA50 (Fig. 5.26), is much less evident in the recent Au-Au RHIC data in Fig. 5.27 and absent in Fig. 5.28. Therefore we fit the whole data set (and not only the $l \leq 4$ fm region) with an attenuation function computed in a Hagedorn gas having a limiting temperature $T_H = 177$ MeV. As stated in Section 5.1.2.3 we are neglecting possible charm recombination effects.

Actually we find a very good fit to data just using the attenuation functions computed in [308]. This is so because the nuclear part of the attenuation function in Au-Au collisions at RHIC is expected to be almost the same as that in Pb-Pb collisions at NA50, because Pb and Au nuclei are very similar in size and the J/ψ nuclear absorption cross sections turns out to be very similar at RHIC and NA50. Moreover to define the dependence of the temperature on centrality, we use the energy density produced in the RHIC collisions according to the Bjorken description, and we found it to be almost equal to the one computed for NA50.

Including some hypothetical in-medium effects on mass decreasing and broadening of open charm mesons [298, 299, 300, 301, 302, 303, 304, 305, 306] and a resonant

contribution from the J/ψ $(\rho,\omega) \to X_2 \to D^0\bar{D}^{0*}$ channel (about the 10% of the non-resonant one) we get slightly larger inverse absorption lengths as shown in Table 5.2 which altogether slightly improve the fit to data, decreasing the χ^2/DOF from 6/4 to 5.6/4; see Figs. 5.27 and 5.28. In the calculation of J/ψ absorption we assume that $X = X_2$ has more likely a 2^{-+} charmonium interpretation, whereas $X = X_1$ has a 1^{++} molecule assignment if only because we have no clues on how a finite temperature hadron medium would alter mass and width of a tetraquark particle. In this respect a charmonium X_2 gets a much larger width because its mass is not modified by the medium, while the masses of its decay products D^0 and D^{0*} are. The larger width of X_2 is in turn responsible for the most effective J/ψ $(\rho,\omega) \to X_2$ conversion which has a very low rate for a narrow X_1. The X_1 is expected to stay narrow even in medium because: *i*) its mass lowers as the sum of D^0 and D^{0*} masses, *ii*) $X_1 \to D^0\bar{D}^{0*}$ is an S-wave decay.

The conclusion which can be drawn from this analysis is that, given the hypotheses we use, data on J/ψ yield in heavy ion collisions are likely the less compelling ones in the search of a deconfined quark-gluon state of matter because they are affected by a large hadronic background in the sense explained above.

In order to have a clearer picture, it would be very important to have RHIC data on J/ψ suppression for a larger number of impact parameter bins, in particular in the intermediate centrality range.

This analysis shows also how the XYZ mesons being discovered in the last few years might have impact on a wide class of elementary processes: we find here that if the $X(3872)$ were confirmed to be a 2^{-+} state, under certain hypotheses on the behavior of open charm mesons in a hot hadron gas, it would give a non-negligible contribution to the hadron J/ψ dissociation mechanism.

5.2 J/ψ inclusive production from B-decays [7]

5.2.1 State of the art

Let us consider the inclusive J/ψ production from B decays: $B \to J/\psi + \text{All}$. On very general grounds we can distinguish two regions of the J/ψ decay momentum (p_ψ) spectrum. The high p_ψ range is fed by events in which the $c\bar{c}$ pair coming from the weak b-quark decay is produced in *color-singlet* configuration, Fig. 5.29. The $c\bar{c}$ hadronize directly into a J/ψ without loosing energy for the emission of gluons which otherwise would be necessary to carry away the color charge of the pair. The resulting process is a two body decay with some kaonic state $\mathcal{K}$: $B \to J/\psi\,\mathcal{K}$.

The slower J/ψ's appear instead when the $c\bar{c}$ pair is produced in *color octet* configuration, Fig. 5.30. In this case the emitted gluons carry part of the $c\bar{c}$ energy and then materialize into light hadrons in the final state. The resulting process is a multi-body decay in which the light hadrons produced do not come from any resonant state: $B \to J/\psi + \text{All}_{\text{non resonant}}$.

One of the first analyses of the decay momentum distribution of J/ψ from B decays was performed by the CLEO collaboration [334], Fig. 5.31. As expected they observed that the J/ψ momentum distribution $d\Gamma/dp_\psi$ is well described at large p_ψ by the sum of the exclusive modes $B \to KJ/\psi$ and $B \to K^*J/\psi$ [335]. At lower momenta there are significant contributions from feed-down processes

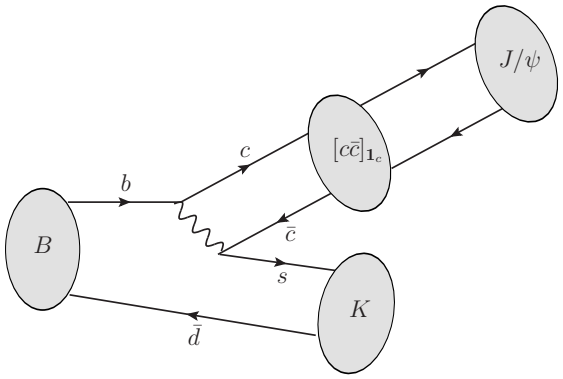

Figure 5.29. $b \to [c\bar{c}]_{\mathbf{1}_c} s$.

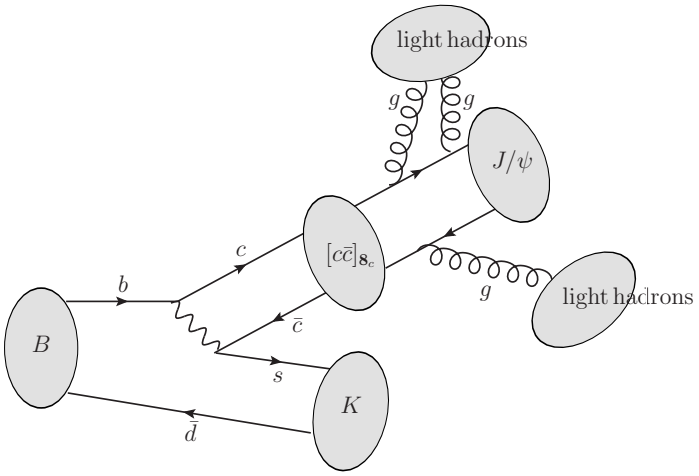

Figure 5.30. $b \to [c\bar{c}]_{\mathbf{8}_c} s$.

$B \to \chi_c X, \chi_c \to J/\psi\ \gamma$ and $B \to \psi' X, \psi' \to J/\psi\ \pi^+\pi^-$. After combining these contributions with the two-body modes, there naturally remains a shortfall across a large range of p_ψ, having not counted contributions from higher kaon resonances and non-resonant multi-particle final states.

Beneke *et al.* [340] proposed that the remaining part of spectrum could be explained by a large $c\bar{c}$ color octet contribution which feeds non-resonant multi-body final states; the calculation is performed within the framework of non-relativistic-QCD (NRQCD). They confront their results with the inclusive J/ψ spectrum after having subtracted from it the $B \to KJ/\psi$ and $B \to K^*J/\psi$ components. The agreement found with data is rather good using reasonable values for the physical parameters involved in the computation, essentially $\Lambda_{\rm QCD}$ and the Fermi momentum p_F of the b quark inside the B meson.

Belle [338] subsequently observed the decay $B \to K_1(1270)J/\psi$ with a branching fraction larger than $B \to KJ/\psi$ and $B \to K^*J/\psi$. In an improved analysis of the

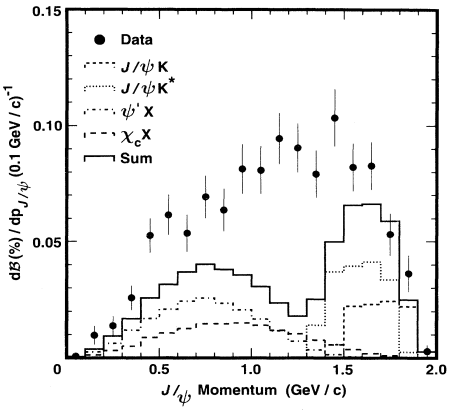

Figure 5.31. Momentum spectrum for inclusive J/ψ production from B decays from CLEO [334]. The expected momentum spectra for the exclusive processes $B \to J/\psi\, K$ and $B \to J/\psi\, K^{\star}$, as well as the feed down from $B \to \chi_c\, X$ and $B \to \psi' X$ are overlaid.

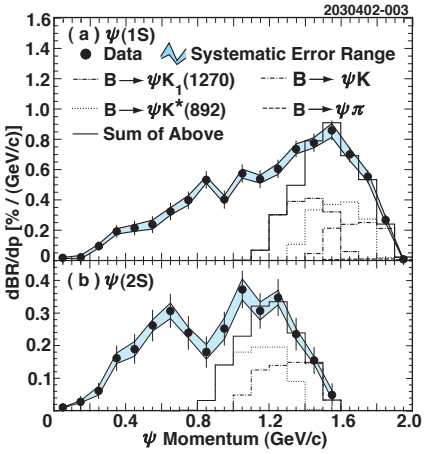

Figure 5.32. Momentum distributions of (a) J/ψ and (b) $\psi(2S)$ produced directly from B decays from CLEO [336]. The histograms show the contributions of two-body $B \to J/\psi\, X$ decays, where the line shapes are obtained from Monte Carlo simulation and the normalizations are from previous determinations of exclusive branching fractions [337, 338, 339].

inclusive J/ψ spectrum, CLEO found that by summing all three of the two-body modes, Fig. 5.32 a good fit to the inclusive spectra is obtained for $p_\psi > 1.5$ GeV [336], which implies that the color octet contribution should be refitted.

In a higher statistics analysis by BaBar [341], in which many feed-down modes from higher charmonia were directly measured and subtracted, the inclusive spectrum is confronted with the results of Beneke *et al.*, and it is noted that even after including color octet contributions, there remains an excess of events at low momenta: see Fig. 5.33 red-dashed line in the region $0 < p_\psi < 0.8$ GeV.

This excess has provoked, since its observation, a variety of exotic interpretations. In [342] the discrepancy has been explained assuming that the J/ψ recoils against a $\Lambda - \bar{p}$ strange baryonium state, while in [343, 344] the existence of *intrinsic charm* inside the B-meson has been considered. Nevertheless the most explored possibility is the production of a strange hybrid meson $K_H = s\bar{d}g$ together with the J/ψ in the B-meson decay. First proposed in [344], its contribution has been later quantified in [345, 346, 347]. The BaBar analysis, however, does not include the large $K_1(1270) J/\psi$ mode, thus, for the reasons outlined above, it does not yield the full picture.

In [7] we updated the theoretical prediction on three different aspects.

Heavy Kaons. We update the color singlet contribution. The Belle collaboration recently [348] analyzed the $B^+ \to J/\psi\ K^+\pi^+\pi^-$ decay and performed an amplitude analysis to determine the resonant structure of the $K^+\pi^+\pi^-$ system, identifying several heavy kaon resonances $\mathcal{K} = K_1(1270)$, $K_1(1400)$, $K^*(1410)$,

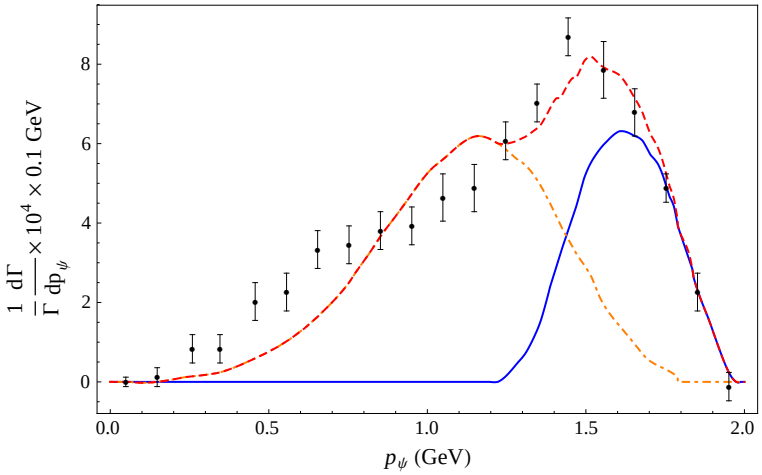

Figure 5.33. $d\Gamma/dp_\psi$ for J/ψ mesons produced *directly*, *i.e.* not from higher charmonium resonances, in B decays (points) from BaBar [341]. The red-dashed line is the sum of the color octet component from [340] (orange-dotdashed line) and the color singlet ($J/\psi K$ and $J/\psi K^*$) component from simulation (blue-solid line).

$K_2^*(1430)$, $K_2(1600)$, $K_2(1770)$, $K_2(1980)$. Given that these newly identified kaons have large masses, they are expected to make significant contributions to the lower side of the momentum spectrum of J/ψ (Section 5.2.2).

XYZ. We also include the XYZ exotic resonances contribution. Some of these resonances are produced in B decays and then decay into final state containing the J/ψ. As first suggested in [349] they are expected to fill the low p_ψ bins, so that even if their weight in terms of branching ratio turns out to be modest, their distribution peaks in the region where the discrepancy is observed (Section 5.2.3).

Color Octet. The two-body modes $B \to \mathcal{K} J/\psi$ and XYZ contributions $B \to XK \to J/\psi + \ldots$ further constrain the contribution from non-resonant (color octet) final states. We thus reconsider the role of the NRQCD based model by Beneke *et al.* [340] with the aim of fully reconstructing the entire $d\Gamma/dp_\psi$ distribution. We essentially perform a new fit of the color octet component in light of the new color-singlet and XYZ components (Section 5.2.4).

5.2.2 Color singlet contribution: $B \to \mathcal{K} J/\psi$

Belle [348] measures the branching ratio

$$\mathcal{B}_{\rm tot} = \mathcal{B}(B^+ \to J/\psi\, K^+\pi^+\pi^-) = (71.6 \pm 1 \pm 6) \times 10^{-5}. \tag{5.55}$$

Looking at the invariant mass spectrum of $K^+\pi^+\pi^-$, they are able to isolate the resonant contributions in which $K^+\pi^+\pi^-$ originate from the decay of a heavy kaon $\mathcal{K}_j$ through some intermediate resonant state $\mathcal{R}_i$ as in

$$\mathcal{B}(B^+ \to \mathcal{K}_j J/\psi \to \mathcal{R}_i J/\psi \to J/\psi\, K^+\pi^+\pi^-) = \mathcal{B}_{\rm tot} f_i^j \tag{5.56}$$

with f_i^j the measured fractions. The intermediate resonant states $\mathcal{R}_i$ are the following

$$\mathcal{R}_i = K\rho,\ \ K\omega,\ \ K^*\pi,\ \ K_0^*(1430)\pi,\ \ K_2^*(1430)\pi \ \text{ and } \ Kf_{0,2}. \tag{5.57}$$

Since the interference between different heavy kaons is neglected, the sum of the measured fractions is larger than one. The neglected interference contributions are expected to be irrelevant when $\Gamma_{\mathcal{K}_j}/m_{\mathcal{K}_j} << 1$, so we rescale each fraction f_i^j proportionally to the width of the heavy kaon $\mathcal{K}_j$

$$\tilde{f}_i^j = C \times \left(1 - \frac{\Gamma_j}{m_j}\right) f_i^j, \tag{5.58}$$

where $C = 1/\sum_j \sum_i (1 - \frac{\Gamma_j}{m_j}) f_i^j$, so that $\sum_j \sum_i \tilde{f}_i^j = 1$. Now we observe that

$$\begin{aligned}\mathcal{B}(B^+ \to \mathcal{K}_j J/\psi \to \mathcal{R}_i J/\psi \to J/\psi\ K^+\pi^+\pi^-) \\ = \mathcal{I}_i \times \mathcal{B}(B^+ \to \mathcal{K}_j J/\psi) \times \mathcal{B}(\mathcal{K}_j \to \mathcal{R}_i) \times \mathcal{B}(\mathcal{R}_i \to K\pi\pi),\end{aligned} \tag{5.59}$$

where $\mathcal{I}_i$ are isospin factors

$$\mathcal{I}(K\rho) = 1/3, \quad \mathcal{I}(K^*\pi) = \mathcal{I}(K_{0,2}^*(1430)\pi) = 4/9, \tag{5.60}$$

$$\mathcal{I}(K\omega) = 1, \quad \mathcal{I}(Kf_0) = \mathcal{I}(Kf_2) = 2/3 \tag{5.61}$$

and $\mathcal{B}(\mathcal{R}_i \to K\pi\pi)$ are all unity except for $\mathcal{B}(K\omega \to K\pi\pi) = 0.0153$ and $\mathcal{B}(Kf_2 \to K\pi\pi) = 0.848$. For some of the heavy kaons, namely $K_2(1600)$, $K_2(1770)$ and $K_2(1980)$, the values of $\mathcal{B}(\mathcal{K}_j \to \mathcal{R}_i)$ are not known experimentally and we thus extract a maximum value for them and in turn a minimum value for the relative $\mathcal{B}(B \to \mathcal{K}_j J/\psi)$. The results obtained are summarized in Table 5.3.

Table 5.3. Branching ratios for the decays $B \to \mathcal{K}_j J/\psi$ extracted from Belle [348].

$\mathcal{K}_j$	$m_{\mathcal{K}_j}$ (GeV)	$\Gamma_{\mathcal{K}_j}$ (GeV)	$\mathcal{B}(B^+ \to \mathcal{K}_j J/\psi) \times 10^5$
$K_1(1270)$	1.270	0.090	144.0 ± 29.3
$K_1(1400)$	1.403	0.174	25.1 ± 5.7
$K^*(1410)$	1.414	0.232	$> 5.1 \pm 2.4$ and $< 11.8 \pm 5.7$
$K_2^*(1430)$	1.430	0.100	40.2 ± 24.0
$K_2(1600)$	1.605	0.115	$> 8.4 \pm 2.9$
$K_2(1770)$	1.773	0.186	$> 4.4 \pm 1.5$
$K_2(1980)$	1.973	0.373	$> 15.2 \pm 2.5$

The branching ratios in Table 5.3 are used to perform a Monte Carlo simulation of the decay chain. The two-body differential decay width in the rest frame of the decaying particle, namely the B-meson rest frame, is

$$d\Gamma(B \to \mathcal{K}_j J/\psi) = \frac{1}{2m_B}(2\pi)^4 \delta^{(4)}(p_B - p_{\mathcal{K}_j} - p_\psi) \sum_{\text{pol}} |\langle \psi \mathcal{K}_j | B \rangle|^2 \frac{d^3 p_{\mathcal{K}_j}}{(2\pi)^3 2E_{\mathcal{K}_j}} \frac{d^3 p_\psi}{(2\pi)^3 2E_\psi}. \tag{5.62}$$

We weight vertices with the appropriate powers of momenta required by the decay partial wave

$$\begin{aligned} &\text{spin 0 kaon} \;:\; \langle\psi(\epsilon,p)\mathcal{K}_j(q)|B(p_B)\rangle \propto \epsilon\cdot q, \\ &\text{spin 1 kaon} \;:\; \langle\psi(\epsilon,p)\mathcal{K}_j(\eta,q)|B(p_B)\rangle \propto \epsilon\cdot\eta, \\ &\text{spin 2 kaon} \;:\; \langle\psi(\epsilon,p)\mathcal{K}_j(\pi,q)|B(p_B)\rangle \propto \epsilon^\mu\pi_{\mu\nu}p^\nu, \end{aligned} \tag{5.63}$$

where ϵ and p are the polarization and momentum of the J/ψ, p_B is the momentum of the B-meson, η and π are polarization vector and polarization tensor of the spin 1 or spin 2 heavy kaon, q is the heavy kaon momentum. It is important here to observe that since the heaviest kaons are spin 2 states the decay occurs in P-wave and thus events are naturally pushed towards higher values of p_ψ in the allowed kinematic region.

To integrate Eq. (5.62) in phase space and obtain $d\Gamma(B\to\mathcal{K}_jJ/\psi)/dp_\psi$ we use Monte Carlo methods. We simulate a two body decay $B\to\mathcal{K}_jJ/\psi$ sorting randomly an angular configuration for the decay products in the B-meson rest frame. Then we apply a Lorentz transformation to the four-momenta of the final state particles and compute p_ψ in the laboratory frame [4], the $\Upsilon(4s)$ rest frame where $|\boldsymbol{p}_B| = \sqrt{\lambda(m^2_{\Upsilon(4S)}, m^2_B, m^2_B)} \simeq 0.341$ GeV.

To account for the $\mathcal{K}_j$ decay width we extract their squared mass $\sqrt{s}$ andomly from a Breit-Wigner distribution with comoving width

$$\frac{\frac{s}{m_{\mathcal{K}_j}}\Gamma_{\mathcal{K}_j}}{(s-m^2_{\mathcal{K}_j})^2 + (\frac{s}{m_{\mathcal{K}_j}}\Gamma_{\mathcal{K}_j})^2}, \tag{5.65}$$

where $m_{\mathcal{K}_j}$ and $\Gamma_{\mathcal{K}_j}$ are the on-shell measured mass and width of the heavy kaon.

The red-solid line in Fig. 5.34 is our picture of all the exclusive two-body contributions listed in Table 5.3: the agreement with data we found extends down to $p_\psi \sim 1.2$ GeV.

5.2.3 Exotic mesons contributions: $B\to\mathcal{K}\mathcal{X}$

As detailed in Chapter 2 some of the recently discovered XYZ mesons have been observed in B decays produced together with the pseudoscalar kaon K and/or the vector kaon $K^*(892)$. Furthermore they all decay into final states containing a charmonium state, a J/ψ or a ψ', together with light hadrons. They thus contribute to the inclusive J/ψ production from B decays. The relative branching ratios are reported in Table 5.4. For the decay $\mathcal{B}(B\to K^*X(3872))$ only an upper limit is known [57]

$$\mathcal{B}(B\to K^*X(3872))\times\mathcal{B}(X(3872)\to J/\psi\,\pi^+\pi^-) < 0.34\times10^{-5} \tag{5.66}$$

[4] If one assumes that the B-meson is moving along the $\hat{z}$ direction and indicates the four-momentum of the J/ψ in the B-meson rest frame with $p^\star_\psi = (\sqrt{m^2_\psi+|\boldsymbol{p}^\star|^2}, |\boldsymbol{p}^\star|s_{\theta^\star}, 0, |\boldsymbol{p}^\star|c_{\theta^\star})$ then

$$|\boldsymbol{p}_\psi|^2 = (|\boldsymbol{p}^\star|s_{\theta^\star})^2 + \left(\gamma|\boldsymbol{p}^\star|c_{\theta^\star} + \beta\gamma\sqrt{m^2_\psi+|\boldsymbol{p}^\star|^2}\right)^2, \tag{5.64}$$

where $|\boldsymbol{p}^\star| = \sqrt{\lambda(m^2_B, m_\psi, s)}/(2m_B)$, $c_{\theta^\star}$ is extracted randomly from a uniform distribution in the interval $[-1,1]$, $\beta = p_B/E_B$ and $\gamma = 1/\sqrt{1-\beta^2}$.

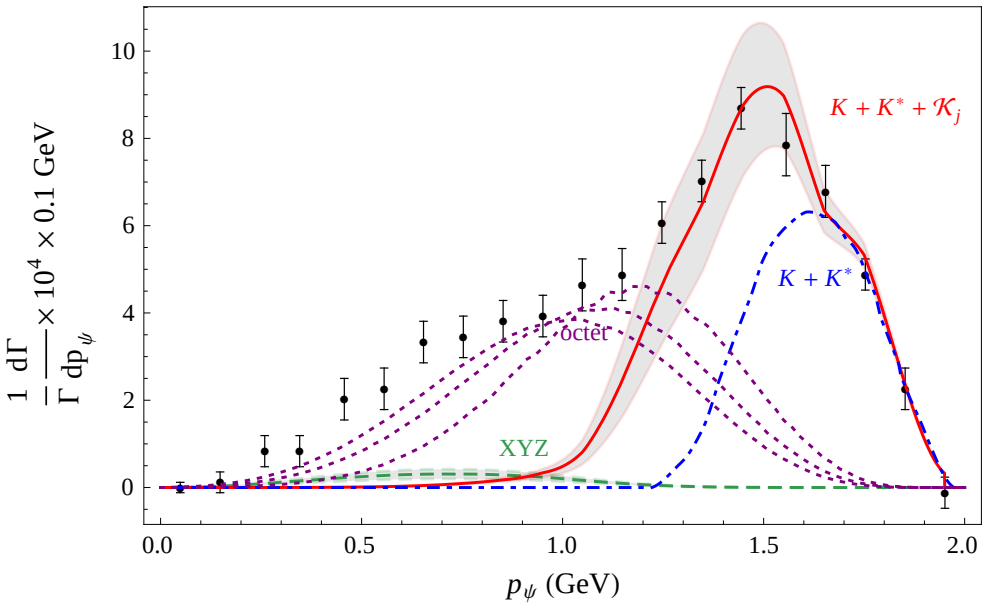

Figure 5.34. Different contributions to the inclusive spectrum of $B \to J/\psi +$ All decays. The red-solid line accounts for the two-body decays of the type $B \to \mathcal{K}J/\psi$; the blue dot-dashed line shows the contributions from $B \to KJ/\psi$ and $B \to K^*J/\psi$ decays considered in [341]; the green-dashed line represents the decays mediated by the exotic mesons $B \to \mathcal{K}\mathcal{X} \to \mathcal{K}J/\psi +$ light hadrons; the purple-dotted lines come from the non-resonant multi-particle final states, *i.e.*, the color octet component, for three values of $\Lambda_{\rm QCD} = 300, 500, 800$ MeV (and $p_F = 300$ MeV) from right to left respectively, according to [340]. Data points, black disks, are taken from BaBar [341].

Table 5.4. Measured branching ratios for the decay $B \to K\mathcal{X}_j$. Where data is available for both neutral and charged B we take the average. (Masses and widths are in GeV).

$\mathcal{X}_j$	$m_{\mathcal{X}_j}$	$\Gamma_{\mathcal{X}_j}$	Final State	$\mathcal{B}(B \to K\mathcal{X}_j \to KJ/\psi + \ldots) \times 10^5$
$X(3872)$	3.872	0.003	$J/\psi\ \rho \to J/\psi\ \pi^+\pi^-$	0.72 ± 0.22 [66]
			$J/\psi\ \omega$	0.6 ± 0.3 [68]
$Y(3940)$	3.940	0.087	$J/\psi\ \omega$	3.70 ± 1.14 [350]
$Y(4140)$	4.140	0.012	$J/\psi\ \phi$	0.9 ± 0.4 [90]
$Y(4260)$	4.260	0.095	$J/\psi\ f_0 \to J/\psi\ \pi^+\pi^-$	2.00 ± 0.73 [350]

In addition to these decays one can suppose that XYZ are produced with heavier kaons, when allowed by kinematics, even if these processes have not yet been revealed.

The differential decay widths in the B-meson rest frame for three or four bodies in the final state read respectively

$$d\Gamma(B \to \mathcal{K}J/\psi\ \omega) = \frac{1}{2m_B}(2\pi)^4\delta^{(4)}(p_B - p_{\mathcal{K}} - p_\psi - p_\omega)\sum_{\rm pol}|\langle \mathcal{K}J/\psi\ \omega|B\rangle|^2 d\Phi^{(3)} \qquad (5.67)$$

and

$$d\Gamma(B \to \mathcal{K}J/\psi\ \pi^+\pi^-) = \frac{1}{2m_{_B}}(2\pi)^4\delta^{(4)}(p_{_B}-p_{_\mathcal{K}}-p_\psi-p_{\pi^+}-p_{\pi^-})\sum_{\rm pol}|\langle\mathcal{K}J/\psi\ \pi^+\pi^-|B\rangle|^2 d\Phi^{(4)}, \tag{5.68}$$

where $d\Phi^{(3,4)}$ are the three and four body phase space defined in Appendix E. To integrate the phase space we use the same Monte Carlo method described for the heavy kaons, Section 5.2.2. As for the transition matrix elements we use the narrow width approximation for the $\mathcal{X}$ so that

$$\sum_{\rm pol}|\langle\mathcal{K}J/\psi\ \omega|B\rangle|^2 = \frac{1}{3}\sum_{\rm pol}|\langle\mathcal{K}\mathcal{X}|B\rangle|^2\frac{1}{(s-m_{_\mathcal{X}}^2)^2+(m_{_\mathcal{X}}\Gamma_{_\mathcal{X}})^2}\sum_{\rm pol}|\langle\psi\omega|\mathcal{X}\rangle|^2. \tag{5.69}$$

or

$$\begin{aligned}\sum_{\rm pol}|\langle\mathcal{K}J/\psi\ \pi^+\pi^-|B\rangle|^2 =& \frac{1}{3}\sum_{\rm pol}|\langle\mathcal{K}\mathcal{X}|B\rangle|^2\frac{1}{(s-m_{_\mathcal{X}}^2)^2+(m_{_\mathcal{X}}\Gamma_{_\mathcal{X}})^2}\\ &\times\frac{1}{3}\sum_{\rm pol}|\langle\psi\rho|\mathcal{X}\rangle|^2\frac{1}{(s-m_\rho^2)^2+(m_\rho\Gamma_\rho)^2}\sum_{\rm pol}|\langle\pi^+\pi^-|\rho\rangle|^2\end{aligned} \tag{5.70}$$

if the dipion comes from a ρ, while

$$\begin{aligned}\sum_{\rm pol}|\langle\mathcal{K}J/\psi\ \pi^+\pi^-|B\rangle|^2 =& \frac{1}{3}\sum_{\rm pol}|\langle\mathcal{K}\mathcal{X}|B\rangle|^2\frac{1}{(s-m_{_\mathcal{X}}^2)^2+(m_{_\mathcal{X}}\Gamma_{_\mathcal{X}})^2}\\ &\times\sum_{\rm pol}|\langle\psi f_0|\mathcal{X}\rangle|^2\frac{1}{(s-m_{f_0}^2)^2+(m_{f_0}\Gamma_{f_0})^2}\sum_{\rm pol}|\langle\pi^+\pi^-|f_0\rangle|^2\end{aligned} \tag{5.71}$$

if the dipion comes from an f_0. For a reason which we will explain hereafter we need to assume that all the exotics $\mathcal{X}$ are spin one mesons.

The sum over polarizations of the transition matrix elements is written in the form $\sim const.\times(|\boldsymbol{p}^*|^2)^L$, where L is the partial decay wave of the process and $|\boldsymbol{p}^*|$ is the decay momentum in the rest frame of the decaying particle. The values of the branching ratios in Table 5.4 are used to normalize the distributions for the processes involving the lightest scalar kaon $K(500)$.

On the other hand no data are currently available for the heavier kaons . To have an estimate of the branching ratios we parametrize as follows the transition matrix elements for scalar and vector kaons

$$\begin{aligned}&\text{spin 0 kaon}\ :\ \langle\mathcal{X}(\epsilon,p)\mathcal{K}(q)|B(P)\rangle = g\ \epsilon\cdot q,\\ &\text{spin 1 kaon}\ :\ \langle\mathcal{X}(\epsilon,p)\mathcal{K}(\eta,q)|B(P)\rangle = g'\ \epsilon\cdot\eta.\end{aligned} \tag{5.72}$$

From a dimensional analysis $[g]=M^0$, $[g']=M$. We now suppose that $g'=\Lambda\ g$, with Λ some mass scale. Using the upper limit in Eq. (5.66) together with the value of $\mathcal{B}(B\to KX(3872))$ reported in Table 5.4, we obtain $\Lambda\lesssim 600$ MeV. We thus decide to extract g from the known branching ratios reported in Table 5.4 and fix $g'=m_{\mathcal{K}_{J=1}}g$, where $\mathcal{K}_{J=1}$ is the generic vector kaon. We cannot consider here the decay $B\to\mathcal{K}\mathcal{X}$ with a spin 2 kaon, since we do not have any experimental data to compare with.

The green-dashed line in Fig. 5.34 shows the sum of all XYZ contributions along with all kaons allowed by kinematics.

5.2.4 Color octet contribution: $B \to J/\psi + X_{\text{non res}}$

Non relativistic QCD. Non relativistic QCD (NRQCD) is an effective field theory which approximates full QCD when applied to a bound state containing more than one heavy quark. It was first introduced in [351], for a review see [352]. NRQCD approximation is motivated by the fact that the relative velocity between quark and antiquark inside a heavy quarkonium state is *small*. This is actually due to asymptotic freedom, since, as we have already discussed in Section 1.2.3, $v \sim \alpha_s(m_Q)$. Since $m_Q >> \Lambda_{\text{QCD}}$, the scale at which the strong coupling behavior of QCD sets in, then $\alpha_s(m_Q) << 1$ and in turn $v << 1$. As a consequence there are three well separated anergy scales

$$m_Q^2 >> (m_Q v)^2 >> (m_Q v^2)^2. \tag{5.73}$$

This hierarchy allows a perturbative expansion in the velocity v^2. The NRQCD Lagrangian can be divided into three terms

$$\mathcal{L} = \mathcal{L}_{heavy} + \mathcal{L}_{light} + \delta\mathcal{L}, \tag{5.74}$$

where $\mathcal{L}_{heavy}$ describes the interactions between heavy quarks, $\mathcal{L}_{light}$ accounts instead for the light degrees of freedom, $\delta\mathcal{L}$ includes the relativistic corrections in the form of an expansion in v^2. Combining perturbative factorization with NRQCD is possible to make rigorous predictions of quarkonium production. A general production process may indeed be written as

$$d\sigma = \sum_n d\sigma_{i+j\to Q\bar{Q}[n]+X} \langle O_n^H \rangle. \tag{5.75}$$

$d\sigma_{i+j\to Q\bar{Q}[n]+X}$ accounts for the short-distance interaction, which converts two partons i and j into a $Q\bar{Q}$ pair in spin, color and orbital configuration n plus anything else. It is calculable using perturbative QCD as an expansion in powers of α_s. On the other hand $\langle O_n^H \rangle$ describes the long-distance part, *i.e.* the hadronization of the heavy quark pair $Q\bar{Q}[n]$ into the hadron H, and can be computed as expansion in v^2. $\langle O_n^H \rangle$ is defined as

$$\langle O_n^H \rangle \equiv \langle 0|O_n^H|0\rangle = \sum_X \langle 0|\psi^\dagger \Gamma^n \chi|H+X\rangle\langle H+X|\chi^\dagger\Gamma^n\psi|0\rangle, \tag{5.76}$$

where ψ and χ are the quark and antiquark field respectively, and Γ^n determine the color, spin and orbital configuration and thus is the product of a color matrix (either the unit matrix or T^A), a spin matrix (either the unit matrix or σ^i), and a polynomial in the covariant derivative. Eq. (5.76) follows from the fact that $\langle O_n^H \rangle$ is the square of the amplitude summed over final states ($\sum_X |\langle H+X|Q\bar{Q}[n]\rangle|^2$) and thus involves the creation of a $Q\bar{Q}$ pair at a space-time point, its propagation into the asymptotic future, where the out state includes the quarkonium H, and, finally, the propagation of the $Q\bar{Q}$ pair back in time to the creation point. The power of the NRQCD + factorization formalism for production lies in the universality of the matrix elements $\langle O_n^H \rangle$. Thus to make a prediction for a given process one must first extract the appropriate matrix elements from another process. The dimension in v of the matrix elements $\langle O_n^H \rangle$ depends on the configuration n and on the quantum

numbers of the hadron H.

$\boldsymbol{B \to J/\psi + X_{\text{non res}}}$. We are considering the process

$$B \to c\bar{c}[n] + X_i \to J/\psi + Y_j, \tag{5.77}$$

where the hard process produces $c\bar{c}[n]$ plus other resonances X_i, whereas the long-distance hadronization converts the $c\bar{c}[n]$ pair into a J/ψ emitting soft particles which, together with X_i, form Y_j. At the leading order the $c\bar{c}$ pair must be produced in the same color spin and orbital configuration of the J/ψ, *i.e.* $1^3S_1^{(1)}$ [5]. The associated matrix element is $\langle O^{J/\psi}_{(1)}(1^3S_1)\rangle$. Going at the order v^4 three additional configurations must be included: $1^3P_J^{(8)}$, $1^3S_1^{(8)}$ and $1^1S_0^{(8)}$. These contributions are suppressed by a factor $v^4 \sim 1/15$ with respect to the color singlet one, but if one expands the hard partonic cross section to the first order in α_s, one realizes that the probability to produce the $c\bar{c}$ pair in color octet from the decay of a b-quark is ~ 15 times larger than that to produce the $c\bar{c}$ in color singlet. Thus the color octet channel is as important as the color singlet one in this specific process.

Since we aim at the p_ψ spectrum we need to consider the kinematic effect of the emission of soft gluons, which are expected to be relevant especially near the kinematic end-point of the distribution. To do this Beneke and collaborators in [340], associated with each of the color-spin-orbital configurations a non-perturbative shape function for the energy and the invariant mass distribution of the radiated system with a characteristic energy scale of $m_c v^2 \approx \Lambda_{\text{QCD}}$. Using the factorization formula they write

$$\begin{aligned}(2\pi)^3 2E_{p_\psi}\frac{d\Gamma}{d^3p_\psi} =& \frac{1}{2m_B}\sum_n \int \frac{d^4l}{(3\pi^4)} \\ & \int dPS(p_i)(2\pi)^4\delta^{(4)}(p_B - P_L - l - \sum_i p_i)\, H_n(p_B, P_L, l, p_i) \\ & \times \int dPS(k_j)(2\pi)^4\delta^{(4)}(P + \sum_j k_j - P_L - l) S_n(p_\psi, P_L, k_j),\end{aligned} \tag{5.78}$$

where P_L is the $c\bar{c}$ pair longitudinal momentum, l its transverse momentum, p_i are the momenta of the partons produced in the hard process, k_j those of the soft partons and p_B is the momentum of the decaying B-meson. PS here indicates the phase space factor. S_n accounts for the hadronization of $c\bar{c}$ into a J/ψ, whereas H_n is the hard scattering amplitude.

In this approach the color octet channel leads to non-resonant multi-body final states since the probability that the emitted soft gluons reassemble with the spectators (the partons produced in the hard scattering) to form a single hadron is assumed to be very small (factorization hypothesis). The two-body modes are due to the color singlet channel and must be considered separately.

Let us analyze each factor of Eq. (5.78) one by one. The hard scattering amplitude H_n for $b \to c\bar{c}s$ can be computed using perturbation theory and the results are

[5] The superscript within parentheses denotes the color configuration.

reported in [340]. As for the soft part, a radiation function is defined

$$\Phi_n(k; p_\psi, P_L) = \int dPS(k_j)(2\pi)^4 \delta^{(4)}(k - \sum_j k_j) S_n(p_\psi, P_L, k_j), \tag{5.79}$$

which is related to the NRQCD matrix element by

$$\frac{1}{(2\pi)^3} \int dk^2 \int_{\sqrt{k^2}}^{\infty} dk_0 \sqrt{k_0^2 - k^2}\, \Phi_n(k; p_\psi, P_L) = \langle O_n^{J/\psi} \rangle. \tag{5.80}$$

To fix to the scale Λ_n the typical energy of the radiated particles and its invariant mass, the shape function Φ_n is approximated with a gaussian

$$\Phi_n(k) = a_n |\boldsymbol{k}|^{b_n} \exp(-\frac{k_0^2}{\Lambda_n^2}) k^2 \exp(-\frac{k^2}{\Lambda_n^2}), \tag{5.81}$$

where $b_n = 2$ if $n =^1 S_0^{(8)}$ and $b_n = 0$ if $n =^3 P_0^{(8)}, ^3 S_1^{(8)}$, whereas Λ_n are all of the oder of $\Lambda_{\rm QCD}$. The constants a_n must be deduce using the normalization condition of Eq. (5.80). The $\langle \mathcal{O}_n^{J/\psi} \rangle$ can be determined by fits to J/ψ production in a variety of processes. Nevertheless, enforcing these normalization conditions underestimates data, because the phenomenological values of the matrix elements are computed from integrated quantities in leading order calculations, while the shape functions contain higher order corrections in the velocity expansion. To overcome this difficulty one chooses to fix the absolute normalization by adjusting the sum of all contributions to data.

Eq. (5.78) is computed in the b-quark rest frame. The Fermi motion of the b-quark inside the B meson is taken into account giving to the b-quark a floating mass ($p_B = p_b + p_{\rm sp}$ in the B-rest frame)

$$m_b^2(p) = m_B^2 + m_{\rm sp}^2 - 2M_B \sqrt{p^2 + m_{\rm sp}^2}, \tag{5.82}$$

where $m_{\rm sp}^2$ is the invariant mass of the light degrees of freedom (quarks and gluons) inside the B meson and p is the b-quark three-momentum modulus. Relying on the ACCMM model [353] one assumes that the probability to find a b-quark with three momentum squared p^2 inside a B meson is a gaussian with spread equal to the Fermi momentum p_F:

$$\Phi_{\rm ACCMM} = \frac{4\pi}{\sqrt{\pi} p_F^3} \exp(-\frac{p^2}{p_F^2}). \tag{5.83}$$

We use Monte Carlo methods to obtain the final p_ψ distribution. The tunable parameters of the model are essentially $\Lambda_{\rm QCD}$ and the Fermi momentum p_F. In Fig. 5.34 we report three color-octet distributions (purple-dotted lines) for three different values of $\Lambda_{\rm QCD} = 300, 500, 800$ MeV, having fixed the Fermi momentum to $p_F = 300$ MeV. We observe that for higher values of $\Lambda_{\rm QCD}$ the distribution peaks at lower p_ψ.

In [340] the comparison is made with data where the two-body modes with K and K^* are subtracted. The agreement with the experimental spectrum, having fixed $\Lambda_{\rm QCD} = 300$ MeV and $p_F = 300$ MeV, is shown in Fig. 5.35, red-dashed curve.

An observation is in order: possible interference effects between the octet final states, which at least contain two pions in addition to $\mathcal{K}J/\psi$, and the multi-body final states originated from the exclusive modes with heavier kaons decaying to $\mathcal{K}+$ pions and XYZ resonances can be safely neglected as $\Gamma_{\mathcal{K}_j}/m_{\mathcal{K}_j} < 0.2$ and $\Gamma_{\mathcal{X}_j}/m_{\mathcal{X}_j} << 1$. This would be a stronger assumption for hypothetical new broad resonances.

5.2.5 Results and outlook

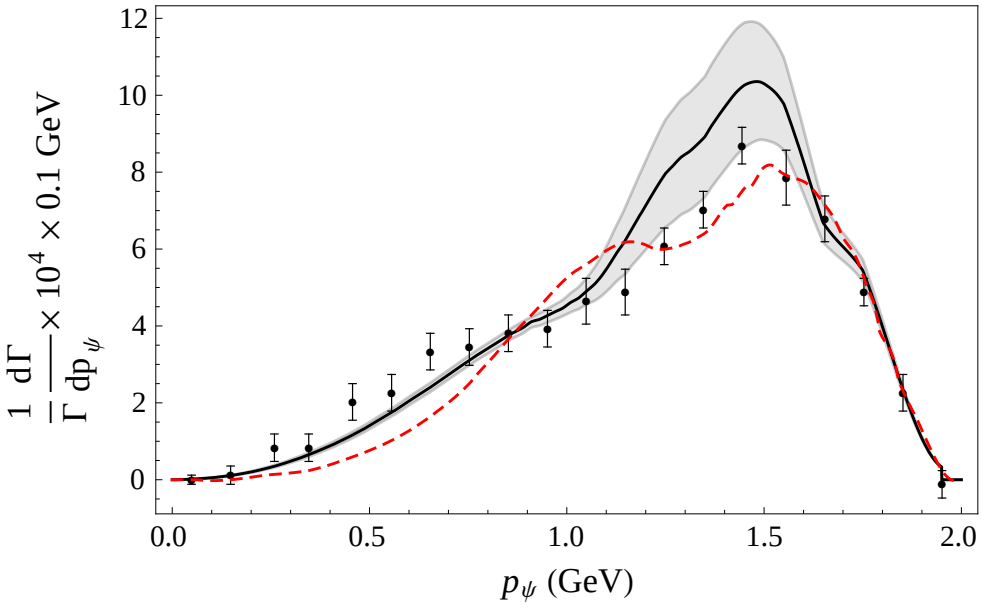

Figure 5.35. The black-solid line represents the sum of all the contributions reported in Fig. 5.34, namely $B \to \mathcal{K}J/\psi$, $B \to \mathcal{K}\mathcal{X}$ and the octet contribution for $\Lambda_{\rm QCD} = 500$ MeV and $p_F = 500$ MeV, compared to the old theoretical prediction [341] (red-dashed line) computed as the sum of $B \to KJ/\psi$, $B \to K^*J/\psi$ and the color octet component with $\Lambda_{\rm QCD} = 300$ MeV and $p_F = 300$ MeV. Going from the red-dashed line to the black-solid one the χ^2/DOF improves from 60/19 to 22/19, having included also the theoretical errors. If one choses $\Lambda_{\rm QCD} = 800$ MeV and $p_F = 300$ MeV the best fit further improves (χ^2/DOF = 19/19). Data points, black disks, are taken from BaBar [341].

The black-solid curve in Fig. 5.35 is obtained as a sum of the standard two-body contributions from kaons (red-solid curve in Fig. 5.34) with the XYZ contributions (green-dashed) plus one of the color octet components (purple-dotted). The latter are three curves obtained with $\Lambda_{\rm QCD} = 300, 500, 800$ MeV (and $p_F = 300$ MeV) from right to left respectively. To best fit data in Fig. 5.35 we choose the octet component with $\Lambda_{\rm QCD} = 500$ MeV and also need to push p_F up to $p_F = 500$ MeV. The values chosen for $\Lambda_{\rm QCD}$ and p_F are critically on the high sides of the allowed ranges which are supposed to be $\Lambda_{\rm QCD} \in [200, 450]$ MeV [351] and $p_F \in [300, 450]$ MeV. Yet the black-solid curve in Fig. 5.35 represents a considerable improvement with respect to the old one (red-dashed). Relying on the validity of the NRQCD approach, our results seem to indicate that the addition of new resonances of the XYZ kind feeding the low p_ψ region would effectively improve the agreement with data. Indeed if the total

branching ratio due to the XYZ turns out to be three times the currently observed value, a good description of data, namely $\chi^2/\mathrm{DOF} = 28/19$, would be obtained including a color octet component with $\Lambda_{\mathrm{QCD}} = 300$ MeV and $p_{_F} = 500$ MeV. In this respect our results could be suggestive of the existence of a number of not yet discovered exotic mesons: new outcomes may arrive from Belle and LHCb.

Conclusions

The comprehension of strong interactions in the non perturbative region of energy is tightly related to the understanding of the internal structure of hadrons. The appearance of exotic mesons XYZ in the heavy charmonium and bottomonium sector clearly indicates that new structures, beyond the standard $q\bar{q}$ one, do exist.

In this thesis we aimed at making some steps forward in the interpretation of the XYZ spectrum, relying on a phenomenological approach.

In the first part of our work, we have focused on the multiquark states, mesons made up by two quarks and two antiquarks $Q\bar{Q}q\bar{q}$, in two different configurations: tetraquarks (diquark-antidiquark bound states) and meson-meson molecules.

For what concerns tetraquarks, we have developed a string model for orbitally excited $[Qq][\bar{Q}\bar{q}]$ bound states [2], in order to obtain predictions for the masses of two 1^{--} exotic resonances, $Y(4350)$ and $Y(4630)/Y(4660)$, which we interpret as P-wave tetraquarks. Indeed we found that $Y(4630)$ and $Y(4660)$ can be described as a single resonance, named Y_B, which exhibits the distinctive feature of tetraquark states: it decays predominantly into baryon-antibaryon $(\Lambda_c^+\Lambda_c^-)$ [3].

Our string model has been first tested on standard charmonium and bottomonium states, relying on the fact that from the point of view of color $[Qq] \sim \bar{Q}$ and $[\bar{Q}\bar{q}] \sim Q$. Including relativistic corrections, spin-orbit and tensor interactions, we have obtained the spectrum of P and D-wave charmonia and bottomonia, fitting few model parameters to data. We found that the string tension σ is not universal, in the sense that we obtain two different values for charm and bottom. The universal quantity comes out to be the ratio σ^2/m_Q (m_Q is the heavy quark mass) which governs the shape of the Regge trajectories for heavy quarkonia $\mathcal{E} \simeq (\sigma^2/m_Q)^{1/3}\, L^{2/3}$, characteristically different from the one of light mesons $\mathcal{E} \simeq \sqrt{\sigma L}$. Furthermore we obtain a prediction of the mass of the 1^1D_2 charmonium state $M(^1D_2) \simeq 3794$ MeV. This value can be compared with the mass of $X(3872)$, which in the 2^{-+} quantum numbers assignment could be identified with the standard 1^1D_2.

We have then considered the spectrum of P-wave $[cq][\bar{c}\bar{q}]$ tetraquarks, using the same string tension obtained for standard $c\bar{c}$. The other input value of the model is the $[cq]$ diquark mass, which we have computed identifying the $X(3872)$ with an S or P-wave tetraquark, depending on weather its J^{PC} quantum numbers are 1^{++} or 2^{-+} respectively. In the first assignment, $X(3872)$ with $J^{PC} = 1^{++}$, the mass of the diquark is $m_{[cq]} = 1933$ MeV and we identify $Y(4350)$ with the radial ground state of a P-wave tetraquark and the Y_B with its first radial excitation. In the second case, $X(3872)$ with $J^{PC} = 2^{-+}$, the diquark is quite lighter $m_{[cq]} = 1716$ MeV and thus $Y(4350)$ and Y_B match the masses of the first and second radially excited P-wave tetraquarks. Nevertheless a $[cq]$ diquark as light as 1716 MeV implies the existence

of S-wave tetraquark states with mass in the range $3.4 \div 3.5$ GeV, which is populated by the well established χ_{cJ} and h_c. The non observation of additional resonances in that mass window represents a problem for our interpretation. Relying on the conservation of the heavy quark pair spin in the decay of tetraquarks into hidden or open charm, we have given some selection rules which could explain the absence of some of the predicted S-wave states. Some of them could indeed be too broad to be observable.

As for molecules, our results concern the prompt production cross section of $X(3872)$ in $p\bar{p}$ collisions [5], in the hypothesis that it is a $D^0\bar{D}^{0*}$ S-wave molecule, which is valid only in the 1^{++} assignment. Being a loosely bound molecule with nearly zero binding energy, the D mesons inside the $X(3872)$ must be almost collinear. We estimated that the relative three-momentum k cannot exceed ~ 35 MeV. Using standard Monte Carlo event generators, we compute the theoretical cross section for the production of a $D^0\bar{D}^{0*}$ pair with fixed k and we then integrate up to $k \lesssim 35$ MeV. We obtain a value which is nearly *300 times smaller* than the one measured by CDF. This result put in some trouble the molecular interpretation of the $X(3872)$ and thus prompted the study of other authors, which claimed that Final State Interactions (FSI) between D^0 and $\bar{D}^{0*}$ enhance the cross section and reconcile the theoretical prediction with the experimental data [279]. Nevertheless in a subsequent paper [6] we casted some doubts on the possibility that FSI could play such a pivotal role.

If the $X(3872)$ were instead a 2^{-+} resonance, the molecular hypothesis would be ruled out, whereas both the charmonium and tetraquark interpretations remain possible. We thus tested the charmonium 1^1D_2 option on the prompt production mechanism, exploiting a previous work by Cho and Wise [281] on the production of D-wave charmonia in hadronic collisions. Also in this case the expected value is much smaller than the observed one.

Both the molecular and charmonium descriptions fail to reproduce the measured prompt production cross section. A theoretical estimate of this value in the case of $X(3872)$ being a tetraquark cannot be computed at the present time, since Monte Carlo event generators, which represent the only reliable model for hadronic production, do not include tetraquarks among their final states.

The second part of our work have been devoted to indirect searches of XYZ, studying processes in which the exotic mesons act as intermediate states.

The first process we have considered is the J/ψ suppression in ultra-relativistic heavy ions collisions [4]. This signal has been indicated since a long time as the most compelling evidence of the existence of Quark Gluon Plasma (QGP). However several authors observed that the interaction of the J/ψ's produced in the collisions inside the hot hadron gas (fireball) which is formed in place or after the QGP, could cause its dissociation and thus constitutes a background signal to the screening due to QGP. The hot hadron gas is filled mainly with light mesons (π, ρ, ω) and the J/ψ can be dissociated by the interaction with these mesons. Besides the non resonant scattering processes, as $J/\psi\,\pi \to D\bar{D}$, also the resonant ones, like $J/\psi\,\rho(\omega) \to X(3872) \to D^0\bar{D}^{0*}$, are at work inside the fireball. After having determined the strong couplings of $X(3872)$ [4] in the 1^{++} and 2^{-+} cases without making any assumptions on the nature of the resonance, we have computed the inverse mean free path of a J/ψ inside the fireball, also including the in medium effects on open-charm mesons. We found that while the role of $X(3872)$ is negligible

if it has $J^{PC} = 1^{++}$, its contribution amounts to nearly the 10% of the non resonant one at the typical temperatures of heavy ions collisions at RHIC, $T \sim 170$ MeV. Comparing our results with the PHENIX experimental data, we concluded that the J/ψ suppression signal can be satisfactorily explained by the dissociation effect due to a hot hadron gas.

In the last section we studied the decay momentum distribution of the J/ψ's inclusively produced in B-decays [7]. A discrepancy between data and theory appears in the low-energy momentum region. Up to now two channels were considered: the two-body modes ($B \to J/\psi\, \mathcal{K}$) which fill the upper part of the spectrum, and the non resonant multi-body modes which can be considered in the framework of Non Relativistic QCD (NRQCD) and are responsible for the production of slow J/ψ's. Based on a recent analysis by Belle, which identifies many new two-body decays, in which a J/ψ is produced in pair with a heavy kaon, we have updated the theoretical prediction of the two-body contributions, finding a good agreement with data for $p_\psi \geq 1.2$ GeV. Also, we included the contribution of XYZ mesons $B \to \mathcal{X}\mathcal{K} \to J/\psi + \text{light hadrons}$, since it is expected to peak in the low momentum region, as first suggested in [349]. We found that even if the weight in terms of branching ratio is very poor, the XYZ distribution peaks in the region of the discrepancy. To obtain the full picture we have reconsidered the NRQCD estimate of the non resonant multi-body modes, in which the $c\bar{c}$ pair is produced in color octet configuration. We fit the sum of the two-body channels, the XYZ contribution and the color octet component to data, obtaining an improvement in the theory/data agreement. Nevertheless to obtain the best fit we are forced to choose unnatural values for the two parameters ($\Lambda_{\rm QCD}$ and p_F) which govern the shape of the color octet distribution. This could be an indication that if new mesons of the XYZ kind happen to be discovered, we could obtain a good fit of the experimental data for reasonable values of $\Lambda_{\rm QCD}$ and of p_F.

Appendix A

Relativistic corrections

Spin Orbit Interaction. The spin-orbit interaction can be rewritten as:

$$\boldsymbol{S}\cdot\boldsymbol{L}=\frac{|\boldsymbol{J}|^2-|\boldsymbol{S}|^2-|\boldsymbol{L}|^2}{2}, \tag{A.1}$$

which becomes

$$\langle J,L,S|\boldsymbol{S}\cdot\boldsymbol{L}|J,L,S\rangle=\frac{J(J+1)-S(S+1)-L(L+1)}{2}. \tag{A.2}$$

on a state of definite total angular momentum, spin angular momentum and orbital angular momentum.

Spin Spin Interaction. As for the tensor term one has to evaluate the expectation value of the tensor operator $|\boldsymbol{S}|^2-3(\boldsymbol{S}\cdot\boldsymbol{n})^2$ between $|J,J_z;L,S\rangle$ eigenstates:

$$\langle J,J_z;L,S||\boldsymbol{S}|^2-3(\boldsymbol{S}\cdot\boldsymbol{n})^2|J,J_z;L,S\rangle=S(S+1)-3\cdot\langle J,J_z;L,S|(\boldsymbol{S}\cdot\boldsymbol{n})^2|J,J_z;L,S\rangle. \tag{A.3}$$

The operator $(\boldsymbol{S}\cdot\boldsymbol{n})^2$ (remember that $\boldsymbol{S}$ is the total spin of the $c\bar{c}$ pair) can be decomposed in cartesian coordinates in the following way:

$$(\boldsymbol{S}\cdot\boldsymbol{n})^2=\left(\hat{S}_x x+\hat{S}_y y+\hat{S}_z z\right)^2. \tag{A.4}$$

Since $\boldsymbol{S}$ is an angular momentum operator we can built the whole spectrum of the $\hat{S}_z$ eigenstates introducing the lowering and raising operators $\hat{S}_+$ and $\hat{S}_-$ using $\hat{S}_x$ and $\hat{S}_y$ in the usual way:

$$\begin{aligned}\hat{S}_+&=\hat{S}_x+i\hat{S}_y,\\ \hat{S}_-&=\hat{S}_x-i\hat{S}_y,\end{aligned} \tag{A.5}$$

which in turn means

$$\begin{aligned}\hat{S}_x&=\frac{\hat{S}_++\hat{S}_-}{2},\\ \hat{S}_y&=\frac{\hat{S}_+-\hat{S}_-}{2i}.\end{aligned} \tag{A.6}$$

One can thus write the operator in Eq. (A.4) as

$$(\boldsymbol{S}\cdot\boldsymbol{n})^2 = \left(\frac{\hat{S}_+^2+\hat{S}_-^2+\hat{S}_+\hat{S}_-+\hat{S}_-\hat{S}_+}{4}\right)x^2 - \left(\frac{\hat{S}_+^2+\hat{S}_-^2-\hat{S}_+\hat{S}_--\hat{S}_-\hat{S}_+}{4}\right)y^2 + \hat{S}_z^2\,z^2 + \left(\frac{\hat{S}_+^2-\hat{S}_-^2}{4i}\right)xy + \left(\frac{\hat{S}_+\hat{S}_z+\hat{S}_z\hat{S}_+ + \hat{S}_-\hat{S}_z+\hat{S}_z\hat{S}_-}{2}\right)xz + \left(\frac{\hat{S}_+\hat{S}_z+\hat{S}_z\hat{S}_+ - \hat{S}_-\hat{S}_z-\hat{S}_z\hat{S}_-}{2}\right)yz. \tag{A.7}$$

To compute the expectation value in Eq. (A.3) one has to rewrite the eigenstate $|J, J_z; L, S\rangle$ in terms of eigenstates of S_z and L_z which means:

$$|J, J_z; L, S\rangle = \sum_{L_z,S_z} C_{L_z,S_z}|L, L_z; S, S_z\rangle, \tag{A.8}$$

where C_{L_z,S_z} are the Clebsch-Gordan coefficients and depend also on J, J_z, L and S.

The action of $(\boldsymbol{S}\cdot\boldsymbol{n})^2$ on a $|L, L_z; S, S_z\rangle$ eigenstate is known once the action of $\hat{S}_+$, $\hat{S}_-$ and $\hat{S}_z$ is known. We remind some few useful relations:

$$\begin{aligned}
\hat{S}_+|L, L_z; S, S_z-1\rangle &= \sqrt{(S+S_z)(S-S_z+1)}|L, L_z; S, S_z\rangle \\
\hat{S}_-|L, L_z; S, S_z+1\rangle &= \sqrt{(S+S_z)(S-S_z+1)}|L, L_z; S, S_z\rangle \\
\hat{S}_z|L, L_z; S, S_z\rangle &= S_z|L, L_z; S, S_z\rangle
\end{aligned} \tag{A.9}$$

and of course

$$\begin{aligned}
\hat{S}_+|L, L_z; S, S\rangle &= 0 \\
\hat{S}_-|L, L_z; S, -S\rangle &= 0.
\end{aligned} \tag{A.10}$$

We are left with the orbital part, which consist only in the computation of the expectation value of product of coordinates between the spherical harmonics Y_{L,L_z} associated with the eigenstate $|L, L_z\rangle$. Explicitly we have:

$$\begin{aligned}
&\langle J, J_z; L, S|\left(\frac{\hat{S}_+^2-\hat{S}_-^2}{4i}\right)xy|J, J_z; L, S\rangle = \\
&= \frac{1}{4i}\sum_{L_z',S_z'}\sum_{L_z,S_z} C^*_{L_z',S_z'}C_{L_z,S_z}\langle L, L_z'; S, S_z'|(\hat{S}_+^2-\hat{S}_-^2)xy|L, L_z; S, S_z\rangle \\
&= \frac{1}{4i}\sum_{L_z',S_z'}\sum_{L_z,S_z} C^*_{L_z',S_z'}C_{L_z,S_z}\langle L, L_z'|xy|L, L_z\rangle\langle S, S_z'|\hat{S}_+^2-\hat{S}_-^2|S, S_z\rangle.
\end{aligned} \tag{A.11}$$

To complete the computation we have to carry out the following integral:

$$\langle L, L_z'|xy|L, L_z\rangle = \int_0^{2\pi} d\phi \int_{-1}^{1} d\cos\theta\, Y^*_{L,L_z'}\,\cos\phi\,\sin\phi\sin^2\theta\, Y_{L,L_z}, \tag{A.12}$$

whereas the spin term $\langle S, S_z'|\hat{S}_+^2 - \hat{S}_-^2|S, S_z\rangle$ can be computed using the rules in Eq. (A.9,A.10).

The same will happen for all the terms in Eq. (A.7).

Here are the results for the $\{L = 1, S = 1\}$ system of the 1^3P_J and for the $\{L = 2, S = 1\}$ system of the 1^3D_J (notation as in Eq. (A.3)):

$$\begin{aligned}
\langle 0, 0; 1, 1||\boldsymbol{S}|^2 - 3(\boldsymbol{S}\cdot\boldsymbol{n})^2|0, 0; 1, 1\rangle &= +2 \\
\frac{1}{3}\sum_{J_z=-1,0,1}\langle 1, J_z; 1, 1||\boldsymbol{S}|^2 - 3(\boldsymbol{S}\cdot\boldsymbol{n})^2|1, J_z; 1, 1\rangle &= -1 \\
\frac{1}{5}\sum_{J_z=-2,\ldots,2}\langle 2, J_z; 1, 1||\boldsymbol{S}|^2 - 3(\boldsymbol{S}\cdot\boldsymbol{n})^2|2, J_z; 1, 1\rangle &= +\frac{1}{5}
\end{aligned} \tag{A.13}$$

$$\begin{aligned}
\frac{1}{3}\sum_{J_z=-1,0,1}\langle 1, J_z; 2, 1||\boldsymbol{S}|^2 - 3(\boldsymbol{S}\cdot\boldsymbol{n})^2|1, J_z; 2, 1\rangle &= +1 \\
\frac{1}{5}\sum_{J_z=-2,\ldots,2}\langle 2, J_z; 2, 1||\boldsymbol{S}|^2 - 3(\boldsymbol{S}\cdot\boldsymbol{n})^2|2, J_z; 2, 1\rangle &= -1 \\
\frac{1}{7}\sum_{J_z=-3,\ldots,3}\langle 3, J_z; 2, 1||\boldsymbol{S}|^2 - 3(\boldsymbol{S}\cdot\boldsymbol{n})^2|3, J_z; 2, 1\rangle &= +\frac{2}{7}
\end{aligned} \tag{A.14}$$

Appendix B

Lie groups

Few definitions taken from [354, 355].

Lie group. A Lie group is a group whose elements g depend in a continuos and differentiable way on a set of real parameters $\boldsymbol{\alpha} = \left\{\alpha^A\right\}_{A=1,\ldots,N}$. The generic element of the group is indicated by $g(\boldsymbol{\alpha})$, with $\boldsymbol{\alpha}$ chosen in such a way that the identity element of the group e corresponds to $\boldsymbol{\alpha} = \mathbf{0}$, *i.e.* $g(\mathbf{0}) = e$.

Representation. A representation R of the group is an operation that assigns to a generic element g a linear operator $D_R(g)$ defined on a linear space

$$g \to D_R(g) \tag{B.1}$$

with the following properties

$$D_R(e) = \mathbf{1} \tag{B.2}$$
$$D_R(g_1)D_R(g_2) = D_R(g_1 g_2) \tag{B.3}$$
$$\tag{B.4}$$

The space on which the operators D_R act is called the *basis of the representation* R. In what follows we will deal with *matrix representations*, that is representation in which the basis is a vector space of finite dimension n, and to the generic element g of the group is associated a $n \times n$ matrix $(D_R(g))_{ij}$, with $i, j = 1, \ldots, n$. The *dimension of the representation* is given by the dimension of the basis space. If we indicate with $\boldsymbol{\phi} = \{\phi^i\}_{i=1,\ldots,n}$ the generic element of the basis space, the element g of the group induces the following transformation of the vector space

$$\boldsymbol{\phi} \to D_R(g)\boldsymbol{\phi} \tag{B.5}$$

Reducible/Irreducible Representation. A representation R is called *reducible* if it has an invariant subspace, *i.e.* if the action of any $D_R(g)$ on the vectors in the subspace gives another vector of the subspace. Conversely, a representation with no invariant subspace is called irreducible.

Group generators. If the α^a are infinitesimal we are in the vicinity of the identity element thus, by the assumptions of smoothness, we have

$$D_R(g(\alpha)) \equiv D_R(\alpha) \sim \mathbf{1} + i\alpha^A T_R^A, \tag{B.6}$$

with

$$T_R^A \equiv -i \left.\frac{\partial D_R}{\partial \alpha^A}\right|_{\boldsymbol{\alpha}=\mathbf{0}} \tag{B.7}$$

The T_R^A are called the *generators* of the group in the representation R.

It can be shown that the generic element of the group $g(\boldsymbol{\alpha})$ can always be written as

$$D_R(g(\boldsymbol{\alpha})) = \exp\left(i\alpha^A T_R^A\right), \tag{B.8}$$

Given two matrices $D_R(g_1) = \exp\left(i\alpha^A T_R^A\right)$ and $D_R(g_2) = \exp\left(i\beta^A T_R^A\right)$ their product is equal to $D_R(g_1 g_2)$ which can itself be parametrized as $\exp\left(i\delta^A T_R^A\right)$. The condition of Eq. (B.3) implies that

$$\exp\left(i\alpha^A T_R^A\right) \exp\left(i\beta^A T_R^A\right) = \exp\left(i\delta^A T_R^A\right) \tag{B.9}$$

Taking the logarithm and expanding up to second order in α and β one gets

$$\alpha^A \beta^A \left[T_R^A, T_R^B\right] = i\gamma^C T_R^C \tag{B.10}$$

with $\gamma^C = 2(\alpha^C + \beta^C - \delta^C(\boldsymbol{\alpha}, \boldsymbol{\beta}))$. Since it must be true for all $\boldsymbol{\alpha}$ and $\boldsymbol{\beta}$, γ^C must be linear in α^C and β^C, so that one can write in general $\gamma^C = f^{ABC}\alpha^C\beta^C$, for some constants f^{ABC}, called *structure constants*. Therefore

$$\left[T^A, T^B\right] = i\, f^{ABC} T_R^C. \tag{B.11}$$

This is called the *Lie algebra* of the group under consideration. It is important to observed that even if the explicit form of the generators T_R^A does depend on the representation used, the structure constants f^{ABC} are independent of it.

Adjoint representation. The structure constants themselves generate a representation of the algebra called the *adjoint representation*. Using the Lie Algebra of the group we can compute

$$\left[T^A, \left[T^B, T^C\right]\right] = i f^{BCD}\left[T^A, T^D\right] = -f^{BCD} f^{ADE} T^E. \tag{B.12}$$

Since the generators satisfy the Jacobi identity

$$\left[T^A, \left[T^B, T^C\right]\right] + \text{cyclic permutations} = 0, \tag{B.13}$$

then

$$f^{BCD} f^{ADE} + f^{ABD} f^{CDE} + f^{CAD} f^{BDE} = 0, \tag{B.14}$$

which implies that we can define a set of matrices X^A

$$\left(X^A\right)_{BC} = f^A_{BC}, \tag{B.15}$$

which satisfy the Lie Algebra of the group. They are the generators in the *adjoint representation*.

Scalar product between generators. As a definition of scalar product between generators in the adjoint representation one can choose the trace operator

$$\mathrm{tr}(X^A X^B). \tag{B.16}$$

This is a real symmetric matrix. One can show that making a linear transformation on the generic generators T^A through the matrix L, induces a linear transformation on the structure constants and thus on the generators in the adjoint representation. The trace is modified as follows

$$\mathrm{tr}(X^A X^B) \to L^{AC} L^{BD}\, \mathrm{tr}(X^C X^D) \tag{B.17}$$

We can thus choose an orthogonal matrix to diagonalize the trace

$$\mathrm{tr}(X^A X^B) = k^A \delta^{AB} \tag{B.18}$$

For the class of Lie Algebras called *Compact Lie Algebras* $k^A > 0$ and $k^A = k$, $\forall A$

$$\mathrm{tr}(X^A X^B) = k \delta^{AB} \tag{B.19}$$

In this basis the structure constants f^{ABC} are *completely antisymmetric*

$$f^{ABC} = f^{BCA} = f^{CAB} = -f^{BAC} = -f^{ACB} = -f^{CBA}. \tag{B.20}$$

Eq. (B.19) can be extended to all the representations

$$\mathrm{tr}(T^A_R T^B_R) = k(R) \delta^{AB} \tag{B.21}$$

Casimir operators. A *Casimir operator* C commutes with all the generators of the group

$$[C, T^A_R] = 0, \qquad \forall A. \tag{B.22}$$

Starting from two representation R_1 and R_2, each of which defined by a basis space, one can build the tensor product space $R_1 \otimes R_2$. The generators on the tensor product space are thus

$$T^A_{R_1 \otimes R_2} \equiv T^A_{R_1} \otimes \mathbf{1}_{R_2} + \mathbf{1}_{R_1} \otimes T^A_{R_2}. \tag{B.23}$$

We now show that $\sum_A \left(T^A_{R_1\otimes R_2}\right)^2$ is a Casimir Operator. To do so we need to check that it commutes with all the generators of the group

$$\begin{aligned}
&\left[\sum_A \left(T^A_{R_1\otimes R_2}\right)^2, T^B_{R_1}\right] \\
&= \sum_A \left[\left(T^A_{R_1}\otimes \mathbf{1}_{R_2} + \mathbf{1}_{R_1}\otimes T^A_{R_2}\right)\left(T^A_{R_1}\otimes \mathbf{1}_{R_2} + \mathbf{1}_{R_1}\otimes T^A_{R_2}\right), T^B_{R_1}\right] \\
&= \sum_A \left(T^A_{R_1}\otimes \mathbf{1}_{R_2} + \mathbf{1}_{R_1}\otimes T^A_{R_2}\right)\left[T^A_{R_1}\otimes \mathbf{1}_{R_2} + \mathbf{1}_{R_1}\otimes T^A_{R_2}, T^B_{R_1}\right] \\
&+ \sum_A \left[T^A_{R_1}\otimes \mathbf{1}_{R_2} + \mathbf{1}_{R_1}\otimes T^A_{R_2}, T^B_{R_1}\right]\left(T^A_{R_1}\otimes \mathbf{1}_{R_2} + \mathbf{1}_{R_1}\otimes T^A_{R_2}\right)
\end{aligned} \tag{B.24}$$

Now we use the standard commutation relation for a Lie Group

$$\left[T^A_{R_1}, T^B_{R_1}\right] = if^{ABC}T^C_{R_1} \tag{B.25}$$

to obtain

$$\begin{aligned}
&\left[\sum_A \left(T^A_{R_1\otimes R_2}\right)^2, T^B_{R_1}\right] \\
&= \sum_{A,C}\left(T^A_{R_1}\otimes \mathbf{1}_{R_2} + \mathbf{1}_{R_1}\otimes T^A_{R_2}\right) if^{ABC}T^C_{R_1} + \sum_{A,C} if^{ABC}T^C_{R_1}\left(T^A_{R_1}\otimes \mathbf{1}_{R_2} + \mathbf{1}_{R_1}\otimes T^A_{R_2}\right) \\
&= \sum_{A,C} if^{ABC}\left(T^A_{R_1}T^C_{R_1}\otimes \mathbf{1}_{R_2} + T^C_{R_1}T^A_{R_1}\otimes \mathbf{1}_{R_2}\right) = 0,
\end{aligned} \tag{B.26}$$

since f^{ABC} is a completely antisymmetric tensor. The same holds for the commutation relations with $T^A_{R_2}$. We can thus use the Schur's lemma to write

$$\sum_A \left(T^A_R\right)^2 = C(R)\mathbf{1}, \tag{B.27}$$

where $R = R_1 \otimes R_2$.

We now derive the expression of $C(R)$ in terms of the constant $k(R)$ defined in Eq. (B.21). Summing over A in Eq. (B.21) we obtain

$$\sum_A \mathrm{Tr}\left(T^A_R T^A_R\right) = k(R)\sum_A \delta^{AB} = k(R)\dim(G). \tag{B.28}$$

where $\dim(G)$ is the dimension of the group, that is the number of generators. On the other hand we can take the trace of Eq.(B.27)

$$\sum_A \mathrm{Tr}\left(T^A_R T^A_R\right) = C(R)\mathrm{Tr}(\mathbf{1}) = C(R)\dim(R), \tag{B.29}$$

where $\dim(R)$ is the dimension of the R representation. Equating Eq. (B.28) and Eq. (B.29) we get to

$$C(R) = k(R)\frac{\dim(G)}{\dim(R)}. \tag{B.30}$$

Finally we derive two equations which relate the constant $k(R_1 \otimes R_2)$ and $k(R_1 \oplus R_2)$ with $k(R_1)$ and $k(R_2)$:

$$\begin{cases} k(R_1 \otimes R_2) = k(R_1)\dim(R_2) + \dim(R_1)k(R_2) \\ k(R_1 \oplus R_2) = k(R_1) + k(R_2) \end{cases} \tag{B.31}$$

To prove these two equations we use the definition of $k(R)$, Eq. (B.21), and the expression for $T^A_{R_1 \otimes R_2}$, Eq. (B.23). Let us start from the first one

$$\begin{aligned} &\mathrm{Tr}\left(T^A_{R_1\otimes R_2} T^B_{R_1\otimes R_2}\right) = \\ &= \mathrm{Tr}\left(\left(T^A_{R_1} \otimes \mathbf{1}_{R_2} + \mathbf{1}_{R_1} \otimes T^A_{R_2}\right)\left(T^B_{R_1} \otimes \mathbf{1}_{R_2} + \mathbf{1}_{R_1} \otimes T^B_{R_2}\right)\right) \\ &= \mathrm{Tr}\left(T^A_{R_1} T^B_{R_1} \otimes \mathbf{1}_{R_2} + T^B_{R_1} \otimes T^A_{R_2} + T^A_{R_1} \otimes T^B_{R_2} + \mathbf{1}_{R_1} \otimes T^A_{R_2} T^B_{R_2}\right) \\ &= \mathrm{Tr}\left(T^A_{R_1} T^B_{R_1}\right)\mathrm{Tr}\left(\mathbf{1}_{R_2}\right) + \mathrm{Tr}\left(T^B_{R_1}\right)\mathrm{Tr}\left(T^A_{R_2}\right) + \mathrm{Tr}\left(T^A_{R_1}\right)\mathrm{Tr}\left(T^B_{R_2}\right) + \mathrm{Tr}\left(\mathbf{1}_{R_1}\right)\mathrm{Tr}\left(T^A_{R_2} T^B_{R_2}\right) \\ &= k(R_1)\delta^{AB}\dim(R_2) + \dim(R_1)k(R_2)\delta^{AB} \equiv k(R_1 \otimes R_2)\delta^{AB} \end{aligned} \tag{B.32}$$

As for the second equation we start from the definition of direct sum of representations

$$R_1 \oplus R_2 = \begin{pmatrix} R_1 & 0 \\ 0 & R_2 \end{pmatrix} \tag{B.33}$$

and we take the trace of the product of two generators of this representation

$$\begin{aligned} \mathrm{Tr}\left(T^A_{R_1\oplus R_2} T^B_{R_1\oplus R_2}\right) &= \mathrm{Tr}\begin{pmatrix} T^A_{R_1} T^B_{R_1} & 0 \\ 0 & T^A_{R_2} T^B_{R_2} \end{pmatrix} = \mathrm{Tr}\left(T^A_{R_1} T^B_{R_1}\right) + \mathrm{Tr}\left(T^A_{R_2} T^B_{R_2}\right) \\ &= k(R_1)\delta^{AB} + k(R_2)\delta^{AB} \equiv k(R_1 \otimes R_2)\delta^{AB} \end{aligned} \tag{B.34}$$

Let us consider the quantity

$$Q(R_1 \otimes R_2) = \sum_A T^A_{R_1} T^A_{R_2}. \tag{B.35}$$

We can exploit the definition of $T^A_{R_1\otimes R_2}$ in Eq. (B.23) to write

$$\begin{aligned} \left(T^A_{R_1\otimes R_2}\right)^2 &= \left(T^A_{R_1} \otimes \mathbf{1}_{R_2} + \mathbf{1}_{R_1} \otimes T^A_{R_2}\right)\left(T^A_{R_1} \otimes \mathbf{1}_{R_2} + \mathbf{1}_{R_1} \otimes T^A_{R_2}\right) \\ &= \left(T^A_{R_1}\right)^2 \otimes \mathbf{1}_{R_2} + \mathbf{1}_{R_1} \otimes \left(T^A_{R_2}\right)^2 + 2\, T^A_{R_1} \otimes T^A_{R_2}. \end{aligned} \tag{B.36}$$

In this way, using the result of Eq. (B.27), $Q(R_1 \otimes R_2)$ comes out to be

$$Q(R_1 \otimes R_2) = \frac{1}{2}\left[\sum_A \left(T^A_{R_1\otimes R_2}\right)^2 - \sum_A \left(T^A_{R_1}\right)^2 - \sum_A \left(T^A_{R_2}\right)^2\right]. \tag{B.37}$$

Appendix C

Quark bilinears

C.1 J^{PC} quantum numbers of $q\bar{q}$ states

In this section we classify the $q\bar{q}$ structures depending on their J^{PC} quantum numbers. With q we indicate a Dirac spinor. Using a complete basis for the Dirac matrices

$$\left\{\mathbf{1}, \gamma^5, \gamma^\mu, \gamma^\mu\gamma^5, \sigma^{\mu\nu}\right\}, \tag{C.1}$$

we can build the following Fermi bilinears

$$\bar{q}q,\ \bar{q}\,\gamma^5 q,\ \bar{q}\gamma^\mu q,\ \bar{q}\gamma^\mu\gamma^5 q,\ \bar{q}\sigma^{\mu\nu}q. \tag{C.2}$$

To compute the J^{PC} quantum numbers of these Fermi bilinears we need first to define the transformation of a Dirac spinor under Lorentz transformation (Λ), parity ($\mathcal{P}$) and charge conjugation ($\mathcal{C}$). In the Weyl basis, where

$$\gamma^0 = \begin{pmatrix} 0 & \mathbf{1} \\ \mathbf{1} & 0 \end{pmatrix}, \qquad \gamma^i = \begin{pmatrix} 0 & \sigma^i \\ -\sigma^i & 0 \end{pmatrix}, \qquad \gamma^5 = \begin{pmatrix} -\mathbf{1} & 0 \\ 0 & \mathbf{1} \end{pmatrix} \tag{C.3}$$

$$\text{and } q = \begin{pmatrix} q_L \\ q_R \end{pmatrix}, \tag{C.4}$$

q and $\bar{q}$ transform as

$$\begin{cases} q \xrightarrow{\Lambda} S(\Lambda)q \\ q \xrightarrow{\mathcal{P}} \gamma^0 q \\ q \xrightarrow{\mathcal{C}} C\bar{q}^T \end{cases} \qquad \begin{cases} \bar{q} \xrightarrow{\Lambda} \bar{q}S(\Lambda)^{-1} \\ \bar{q} \xrightarrow{\mathcal{P}} \bar{q}\gamma^0 \\ \bar{q} \xrightarrow{\mathcal{C}} q^T C \end{cases} \tag{C.5}$$

with

$$C = \begin{pmatrix} i\sigma^2 & 0 \\ 0 & -i\sigma^2 \end{pmatrix} = -i\sigma^2 \otimes \gamma^5. \tag{C.6}$$

Some properties of C will be useful in what follows

$$\begin{aligned} &C^2 = -\mathbf{1}, \\ &CC^\dagger = C^\dagger C = \mathbf{1}, \\ &C^\dagger = C^{-1}, \\ &C^\dagger = -C, \\ &C^T = -C. \end{aligned} \tag{C.7}$$

Let us consider the bilinears one by one.

$\bar{q}q$: $J^{PC} = 0^{++}$

- $\bar{q}q \xrightarrow{\Lambda} \bar{q}S(\Lambda)^{-1}S(\Lambda)q = \bar{q}q$
- $\bar{q}q \xrightarrow{\mathcal{P}} \bar{q}\gamma^0\gamma^0 q = \bar{q}q$
- $\bar{q}q \xrightarrow{\mathcal{C}} q^T C C\bar{q}^T = -q^T\bar{q}^T = \bar{q}q$

$\bar{q}\gamma^5 q$: $J^{PC} = 0^{-+}$

- $\bar{q}\gamma^5 q \xrightarrow{\Lambda} \bar{q}S(\Lambda)^{-1}\gamma^5 S(\Lambda)q = \det(\Lambda)\bar{q}\gamma^5 q = \bar{q}\gamma^5 q$
- $\bar{q}\gamma^5 q \xrightarrow{\mathcal{P}} \bar{q}\gamma^0\gamma^5\gamma^0 q = -\bar{q}\gamma^5 q$
- $\bar{q}\gamma^5 q \xrightarrow{\mathcal{C}} q^T C\gamma^5 C\bar{q}^T = -q^T C\gamma^5 C^{-1}\bar{q}^T = -q^T\gamma^{5T}\bar{q}^T = \bar{q}\gamma^5 q$

$\bar{q}\gamma^\mu q$: $J^{PC} = 0^{+-}$ and $J^{PC} = 1^{--}$

- $\bar{q}\gamma^\mu q \xrightarrow{\Lambda} \Lambda^\mu_\nu \bar{q}\gamma^\nu q$

- $\bar{q}\gamma^0 q \xrightarrow{\mathcal{P}} \bar{q}\gamma^0\gamma^0\gamma^0 q = \bar{q}\gamma^0 q$
- $\bar{q}\gamma^0 q \xrightarrow{\mathcal{C}} q^T C\gamma^0 C\bar{q}^T = -q^T C\gamma^0 C^{-1}\bar{q}^T = q^T\gamma^{0T}\bar{q}^T = -\bar{q}\gamma^0 q$

- $\bar{q}\gamma^i q \xrightarrow{\mathcal{P}} \bar{q}\gamma^0\gamma^i\gamma^0 q = -\bar{q}\gamma^i q$
- $\bar{q}\gamma^i q \xrightarrow{\mathcal{C}} q^T C\gamma^i C\bar{q}^T = -q^T C\gamma^i C^{-1}\bar{q}^T = q^T\gamma^{iT}\bar{q}^T = -\bar{q}\gamma^i q$

$\bar{q}\gamma^\mu\gamma^5 q$: $J^{PC} = 0^{-+}$ and $J^{PC} = 1^{++}$

- $\bar{q}\gamma^\mu\gamma^5 q \xrightarrow{\Lambda} \Lambda^\mu_\nu \bar{q}\gamma^\nu\gamma^5 q$

- $\bar{q}\gamma^0\gamma^5 q \xrightarrow{\mathcal{P}} \bar{q}\gamma^0\gamma^0\gamma^5\gamma^0 q = -\bar{q}\gamma^0\gamma^5 q$
- $\bar{q}\gamma^0\gamma^5 q \xrightarrow{\mathcal{C}} q^T C\gamma^0\gamma^5 C\bar{q}^T = -q^T C\gamma^0\gamma^5 C^{-1}\bar{q}^T = -q^T C\gamma^0 C^{-1} C\gamma^5 C^{-1}\bar{q}^T$
  $= q^T\gamma^{0T}\gamma^{5T}\bar{q}^T = \bar{q}\gamma^0\gamma^5 q$

- $\bar{q}\gamma^i\gamma^5 q \xrightarrow{\mathcal{P}} \bar{q}\gamma^0\gamma^i\gamma^5\gamma^0 q = \bar{q}\gamma^i\gamma^5 q$
- $\bar{q}\gamma^i\gamma^5 q \xrightarrow{\mathcal{C}} q^T C\gamma^i\gamma^5 C\bar{q}^T = -q^T C\gamma^i\gamma^5 C^{-1}\bar{q}^T = -q^T C\gamma^i C^{-1} C\gamma^5 C^{-1}\bar{q}^T$
  $= q^T\gamma^{iT}\gamma^{5T}\bar{q}^T = \bar{q}\gamma^i\gamma^5 q$

$\bar{q}\sigma^{\mu\nu}q$: $J^{PC} = 1^{--}$ and $J^{PC} = 1^{+-}$

$$\sigma^{\mu\nu} = \frac{i}{2}\left[\gamma^\mu, \gamma^\nu\right] \tag{C.8}$$

$\sigma^{0i} = i\gamma^0\gamma^i$ or $\sigma^{ij} = i\gamma^i\gamma^j$ each of which accounts for 3 degrees of freedom.

- $\bar{q}\gamma^0\gamma^i q \xrightarrow{\mathcal{P}} \bar{q}\gamma^0\gamma^0\gamma^i\gamma^0 q = -\bar{q}\gamma^0\gamma^i q$
- $\bar{q}\gamma^0\gamma^i q \xrightarrow{\mathcal{C}} q^T C\gamma^0\gamma^i C\bar{q}^T = -q^T C\gamma^0\gamma^i C^{-1}\bar{q}^T = -q^T C\gamma^0 C^{-1} C\gamma^i C^{-1}\bar{q}^T$
  $= -q^T\gamma^{0T}\gamma^{iT}\bar{q}^T = -\bar{q}\gamma^0\gamma^i q$

- $\bar{q}\gamma^i\gamma^j q \xrightarrow{\mathcal{P}} \bar{q}\gamma^0\gamma^i\gamma^j\gamma^0 q = \bar{q}\gamma^i\gamma^j q$
- $\bar{q}\gamma^i\gamma^j q \xrightarrow{\mathcal{C}} q^T C\gamma^i\gamma^j C\bar{q}^T = -q^T C\gamma^i\gamma^j C^{-1}\bar{q}^T = -q^T C\gamma^i C^{-1} C\gamma^j C^{-1}\bar{q}^T$
  $= -q^T\gamma^{iT}\gamma^{jT}\bar{q}^T = -\bar{q}\gamma^i\gamma^j q$

The results are summarized in Table C.1. Beside the spin wave function, we need to describe the color wave function. When dealing with standard mesons, the colors of the quark and the antiquark inside the meson need to neutralize with each other

$$\bar{q}^\alpha \Gamma q^\beta \delta_{\alpha\beta} \tag{C.9}$$

As shown in Section 3.1 and summarized in Table 3.1, this the favorite configuration as for the color charge computed in the One Gluon Exchange model.

Table C.1. J^{PC} classification of $\bar{q}\Gamma q$ states.

J^{PC}	Bilinear
0^{++}	$\bar{q}q$
0^{-+}	$\bar{q}\gamma^5 q$, $\bar{q}\gamma^0\gamma^5 q$
0^{+-}	$\bar{q}\gamma^0 q$
1^{--}	$\bar{q}\gamma^i q$, $\bar{q}\sigma^{0i} q$
1^{++}	$\bar{q}\gamma^i\gamma^5 q$
1^{+-}	$\bar{q}\sigma^{ij} q$

C.2 J^{PC} quantum numbers of qq states

In this section we classify the qq structures depending on their J^{PC} quantum numbers. A qq state can be rewritten in the form of a Fermi bilinear as follows

$$qq \to \bar{q}_{\rm C} q, \tag{C.10}$$

where $q_{\rm C} = C\bar{q}^T$ and thus $\bar{q}_{\rm C} = q^T C$. Using the usual basis for gamma matrices we build the following structures

$$\bar{q}_{\rm C} q,\ \bar{q}_{\rm C}\gamma^5 q,\ \bar{q}_{\rm C}\gamma^\mu q,\ \bar{q}_{\rm C}\gamma^\mu\gamma^5 q,\ \bar{q}_{\rm C}\sigma^{\mu\nu} q \tag{C.11}$$

and study their properties with respect to Lorentz transformation and parity. Since a qq state is not an eigenstate of charge conjugation, the bilinears $\bar{q}_{\rm C}\Gamma q$ can be classified according to J^P and not J^{PC}.

Under Lorentz transformation Λ the charge conjugate spinors transform as

$$\begin{cases} \bar{q}_{\rm C} \xrightarrow{\Lambda} q^T S(\Lambda)^T C = q^T C S(\Lambda)^{-1} C^{-1} C = \bar{q}_{\rm C} S(\Lambda)^{-1} \\ \bar{q}_{\rm C} \xrightarrow{\mathcal{P}} q^T\gamma^0 C = -\bar{q}_{\rm C}\gamma^0 \end{cases} \tag{C.12}$$

$\bar{q}_{\rm C} q$: $J^P = 0^-$

- $\bar{q}_{\rm C} q \xrightarrow{\Lambda} \bar{q}_{\rm C} S(\Lambda)^{-1} S(\Lambda) q = \bar{q}_{\rm C} q$

- $\bar{q}_{\rm C} q \xrightarrow{\mathcal{P}} -\bar{q}_{\rm C}\gamma^0\gamma^0 q = -\bar{q}_{\rm C} q$

$\bar{q}_{\rm C}\gamma^5 q$: $J^P = 0^+$

- $\bar{q}_{\rm C}\gamma^5 q \xrightarrow{\Lambda} \bar{q}_{\rm C} S(\Lambda)^{-1}\gamma^5 S(\Lambda) q = \det(\Lambda)\bar{q}_{\rm C} q$
- $\bar{q}_{\rm C}\gamma^5 q \xrightarrow{\mathcal{P}} -\bar{q}_{\rm C}\gamma^0\gamma^5\gamma^0 q = \bar{q}_{\rm C}\gamma^5 q$

$\bar{q}_{\rm C}\gamma^\mu q$: $J^P = 0^-$ and $J^P = 1^+$

- $\bar{q}_{\rm C}\gamma^\mu q \xrightarrow{\Lambda} \Lambda^\mu_\nu \bar{q}_{\rm C}\gamma^\nu q$
- $\bar{q}_{\rm C}\gamma^0 q \xrightarrow{\mathcal{P}} -\bar{q}_{\rm C}\gamma^0\gamma^0\gamma^0 q = -\bar{q}_{\rm C}\gamma^0 q$
- $\bar{q}_{\rm C}\gamma^i q \xrightarrow{\mathcal{P}} -\bar{q}_{\rm C}\gamma^0\gamma^i\gamma^0 q = \bar{q}_{\rm C}\gamma^i q$

$\bar{q}_{\rm C}\gamma^\mu\gamma^5 q$: $J^P = 0^+$ and $J^P = 1^-$

- $\bar{q}_{\rm C}\gamma^\mu\gamma^5 q \xrightarrow{\Lambda} \Lambda^\mu_\nu \bar{q}_{\rm C}\gamma^\nu\gamma^5 q$
- $\bar{q}_{\rm C}\gamma^0\gamma^5 q \xrightarrow{\mathcal{P}} -\bar{q}_{\rm C}\gamma^0\gamma^0\gamma^5\gamma^0 q = \bar{q}_{\rm C}\gamma^0 q$
- $\bar{q}_{\rm C}\gamma^i\gamma^5 q \xrightarrow{\mathcal{P}} -\bar{q}_{\rm C}\gamma^0\gamma^i\gamma^5\gamma^0 q = -\bar{q}_{\rm C}\gamma^i q$

$\bar{q}_{\rm C}\sigma^{\mu\nu} q$: $J^P = 1^+$ and $J^P = 1^-$

$\sigma^{0i} = i\gamma^0\gamma^i$ or $\sigma^{ij} = i\gamma^i\gamma^j$ each of which accounts for 3 degrees of freedom.

- $\bar{q}_{\rm C}\gamma^0\gamma^i q \xrightarrow{\mathcal{P}} -\bar{q}_{\rm C}\gamma^0\gamma^0\gamma^i\gamma^0 q = \bar{q}_{\rm C}\gamma^0\gamma^i q$
- $\bar{q}_{\rm C}\gamma^i\gamma^j q \xrightarrow{\mathcal{P}} -\bar{q}_{\rm C}\gamma^0\gamma^i\gamma^j\gamma^0 q = -\bar{q}_{\rm C}\gamma^i\gamma^j q$

The results are summarized in Table C.2. As for the color part of the wave function, we have shown in Section 3.1 that the favored configuration is the antisymmetric one

$$\bar{q}^\alpha_{\rm C}\Gamma q^\beta \epsilon_{\alpha\beta\gamma}. \tag{C.13}$$

Table C.2. J^P classification of qq states.

J^P	Bilinear
0^-	$\bar{q}_{\rm C} q$, $\bar{q}_{\rm C}\gamma^0 q$
0^+	$\bar{q}_{\rm C}\gamma^5 q$, $\bar{q}_{\rm C}\gamma^0\gamma^5 q$
1^-	$\bar{q}_{\rm C}\gamma^i\gamma^5 q$, $\bar{q}_{\rm C}\sigma^{ij} q$
1^+	$\bar{q}_{\rm C}\gamma^i q$, $\bar{q}_{\rm C}\sigma^{0i} q$

Appendix D

Fierz transformations

D.1 Fierz transformations for Pauli matrices

Let us start from the following identity:

$$\delta_b^a \delta_d^c = \frac{1}{2}\delta_d^a \delta_b^c + \frac{1}{2}\boldsymbol{\sigma}_d^a \cdot \boldsymbol{\sigma}_b^c. \tag{D.1}$$

The previous relation can be easily verified tracing over the two couples of indices (remember $a = 1, 2$):

$$\begin{aligned} \sum_{a=b}\sum_{c=d} \delta_b^a \delta_d^c \quad &= \frac{1}{2}\sum_{a=b}\sum_{c=d} \delta_d^a \delta_b^c + \frac{1}{2}\sum_{a=b}\sum_{c=d} \boldsymbol{\sigma}_d^a \cdot \boldsymbol{\sigma}_b^c \\ 2 \times 2 \quad &= \frac{1}{2}\sum_{a}\sum_{c} \delta_c^a \delta_a^c + \frac{1}{2}\sum_{a}\sum_{c} \boldsymbol{\sigma}_c^a \cdot \boldsymbol{\sigma}_a^c \\ 2 \times 2 \quad &= \frac{1}{2} \times 2 + \frac{1}{2}\mathrm{Tr}\left(\boldsymbol{\sigma} \cdot \boldsymbol{\sigma}\right). \end{aligned} \tag{D.2}$$

To compute $\mathrm{Tr}\left(\boldsymbol{\sigma} \cdot \boldsymbol{\sigma}\right)$ remember the commutation and anticommutation relations for Pauli matrices

$$\begin{aligned} \left[\sigma^i, \sigma^j\right] &= 2i\epsilon^{ijk}\sigma^k, \\ \left\{\sigma^i, \sigma^j\right\} &= 2\delta^{ij}\mathbf{1}, \end{aligned} \tag{D.3}$$

which in turn imply that

$$\sigma^i \sigma^j = \delta^{ij}\mathbf{1} + i\epsilon^{ijk}\sigma^k. \tag{D.4}$$

Thus

$$\mathrm{Tr}\left(\boldsymbol{\sigma} \cdot \boldsymbol{\sigma}\right) = \sum_i \mathrm{Tr}\left(\sigma^i \sigma^i\right) = \sum_i \delta^{ii}\mathrm{Tr}(\mathbf{1}) + i\sum_i \epsilon^{ijk}\mathrm{Tr}(\sigma^k) = 3 \times 2, \tag{D.5}$$

which gives the result of Eq. (D.2). We now define $\sigma^A = \left(\mathbf{1}, \sigma^i\right)$ and the generic linear combination σ

$$\sigma = \frac{1}{2}\sum_A c_A \sigma^A. \tag{D.6}$$

Now observe that

$$\mathrm{Tr}\left(\sigma\sigma^A\right) = \frac{1}{2}\mathrm{Tr}\left[\left(\sum_B c_B\sigma^B\right)\sigma^A\right] = \sum_B c_B\mathrm{Tr}\left(\sigma^B\sigma^A\right) = c_A, \tag{D.7}$$

where we have used in the last identity $\mathrm{Tr}\left(\sigma^B\sigma^A\right) = 2\delta^{AB}$. We can thus rewrite σ as follows

$$\sigma = \sum_A \mathrm{Tr}\left(\sigma\sigma^A\right)\sigma^A \tag{D.8}$$

or equivalently

$$\sigma^i_j = \sum_A \sigma^l_m \left(\sigma^A\right)^m_l \left(\sigma^A\right)^i_j = \frac{1}{2}\sigma^l_m \sum_A \left(\sigma^A\right)^m_l \left(\sigma^A\right)^i_j. \tag{D.9}$$

The previous relation holds if and only if

$$\delta^i_l\delta^m_j = \sum_A \left(\sigma^A\right)^m_l \left(\sigma^A\right)^i_j \tag{D.10}$$

Multiplying both sides of Eq. (D.10) by $F^{m'}_m G^l_{l'}$, where F and G are two generic 2×2 matrices, one obtains

$$\begin{aligned} F^{m'}_m G^l_{l'}\delta^i_l\delta^m_j &= F^{m'}_m G^l_{l'}\sum_A \left(\sigma^A\right)^m_l \left(\sigma^A\right)^i_j \\ F^{m'}_j G^i_{l'} &= \sum_A \left(F\sigma^A G\right)^{m'}_{l'} \\ \left(\bar{a}_m F^m_j b^j\right)\left(\bar{c}_i G^i_l d^l\right) &= \sum_A \left[\bar{a}_m \left(F\sigma^A G\right)^m_l d^l\right]\left[\bar{c}_i \left(\sigma^A\right)^i_j b^j\right], \end{aligned} \tag{D.11}$$

which is the Fierz identity for Pauli matrices.

D.1.1 Diquark-antidiquark spin wave functions

The diquark-antidiquark spin wave functions in the $(S_{cq}\times S_{\bar{c}\bar{q}})_S$ basis can be rewritten in the bases $(S_{c\bar{q}}\times S_{q\bar{c}})_S$ and $(S_{c\bar{c}}\times S_{q\bar{q}})_S$ of the open- and closed-flavor final states, respectively. Making use of the Fierz identity of Eq. (D.11), we derive the matrix elements $\langle(S_{c\bar{c}}\times S_{q\bar{q}})_S|(S_{cq}\times S_{\bar{c}\bar{q}})_S\rangle$ for closed flavor decay:

	$\lvert(0\times 0)_0\rangle$	$\lvert(1\times 1)_0\rangle$
$\langle(0\times 0)_0\rvert$	$1/2$	$\sqrt{3}/2$
$\langle(1\times 1)_0\rvert$	$\sqrt{3}/2$	$-1/2$

(D.12)

	$\lvert(1\times 1)_1\rangle$	$\sqrt{1/2}\left(\lvert(1\times 0)_1\rangle + \lvert(0\times 1)_1\rangle\right)$	$\sqrt{1/2}\left(\lvert(1\times 0)_1\rangle - \lvert(0\times 1)_1\rangle\right)$
$\langle(1\times 1)_1\rvert$	0	1	0
$\langle(1\times 0)_1\rvert$	$\sqrt{1/2}$	0	$\sqrt{1/2}$
$\langle(0\times 1)_1\rvert$	$\sqrt{1/2}$	0	$-\sqrt{1/2}$

(D.13)

	$\lvert(1\times 1)_2\rangle$
$\langle(1\times 1)_2\rvert$	1

(D.14)

The corresponding matrix elements $\langle (S_{c\bar{q}} \times S_{q\bar{c}})_S | (S_{cq} \times S_{\bar{c}\bar{q}})_S \rangle$ for open flavor decay are:

$$\begin{array}{ccc} & |(0\times 0)_0\rangle & |(1\times 1)_0\rangle \\ \langle (0\times 0)_0| & -1/2 & \sqrt{3}/2 \\ \langle (1\times 1)_0| & -\sqrt{3}/2 & -1/2 \end{array} \tag{D.15}$$

$$\begin{array}{ccccc} & |(1\times 1)_1\rangle & \sqrt{1/2}\left(|(1\times 0)_1\rangle + |(0\times 1)_1\rangle\right) & \sqrt{1/2}\left(|(1\times 0)_1\rangle - |(0\times 1)_1\rangle\right) \\ \langle (1\times 1)_1| & 0 & 0 & -1 \\ \langle (1\times 0)_1| & \sqrt{1/2} & -\sqrt{1/2} & 0 \\ \langle (0\times 1)_1| & \sqrt{1/2} & \sqrt{1/2} & 0 \end{array} \tag{D.16}$$

$$\begin{array}{cc} & |(1\times 1)_2\rangle \\ \langle (1\times 1)_2| & 1 \end{array} \tag{D.17}$$

D.2 Fierz transformations for Gell-Mann matrices

We want to show that

$$\delta^a_b \delta^c_d = \frac{1}{3}\delta^a_d \delta^c_b + \frac{1}{2}\boldsymbol{\lambda}^a_d \cdot \boldsymbol{\lambda}^c_b. \tag{D.18}$$

As we did for Pauli matrices, we compute the trace over the two couples of indices (remember $a = 1, 2, 3$):

$$\begin{aligned} \sum_{a=b}\sum_{c=d} \delta^a_b \delta^c_d \quad &= \frac{1}{3}\sum_{a=b}\sum_{c=d} \delta^a_d \delta^c_b + \frac{1}{2}\sum_{a=b}\sum_{c=d} \boldsymbol{\lambda}^a_d \cdot \boldsymbol{\lambda}^c_b \\ 3\times 3 \quad &= \frac{1}{3}\sum_{a}\sum_{c} \delta^a_c \delta^c_a + \frac{1}{2}\sum_{a}\sum_{c} \boldsymbol{\lambda}^a_c \cdot \boldsymbol{\lambda}^c_a \\ 3\times 3 \quad &= \frac{1}{3}\times 3 + \frac{1}{2}\mathrm{Tr}\left(\boldsymbol{\lambda}\cdot\boldsymbol{\lambda}\right). \end{aligned} \tag{D.19}$$

To compute $\mathrm{Tr}\left(\boldsymbol{\lambda}\cdot\boldsymbol{\lambda}\right)$ remember the commutation and anticommutation relations for Gell-Mann matrices

$$\begin{aligned} \left[\lambda^i, \lambda^j\right] &= 2\, i f^{ijk}\lambda^k, \\ \left\{\lambda^i, \lambda^j\right\} &= 4\times\left(\frac{1}{3}\delta^{ij}\mathbf{1} + \frac{1}{2}d^{ijk}\lambda^k\right), \end{aligned} \tag{D.20}$$

which in turn imply that

$$\lambda^i\lambda^j = \frac{2}{3}\delta^{ij}\mathbf{1} + 2d^{ijk}\lambda^k + i f^{ijk}\lambda^k. \tag{D.21}$$

Thus

$$\mathrm{Tr}\left(\boldsymbol{\lambda}\cdot\boldsymbol{\lambda}\right) = \sum_i \frac{2}{3}\delta^{ii}\mathrm{Tr}\left(\mathbf{1}\right) + \sum_i 2d^{iik}\mathrm{Tr}\left(\lambda^k\right) + i\sum_i f^{iik}\mathrm{Tr}\left(\lambda^k\right) = 16, \tag{D.22}$$

which gives the result of Eq. (D.19).

Appendix E

Cross section and decay widths

E.1 $X \to J/\psi\ \rho$

Here we report the formulae used for the computation of the width of $X \to J/\psi\ \rho$.

$$d\Gamma(X \to J/\psi\ \pi^+\pi^-) = \frac{1}{2s_X+1}\frac{1}{2m_X}\sum_{\text{pol}}|\langle J/\psi\ \pi^+\pi^-|X\rangle|^2\, d\Phi^{(3)}, \tag{E.1}$$

where

$$d\Phi^{(3)} = (2\pi)^4\delta^{(4)}(P-p_\psi-p_1-p_2)\frac{d^3p_\psi}{(2\pi)^3 2E_\psi}\frac{d^3p_1}{(2\pi)^3 2E_1}\frac{d^3p_2}{(2\pi)^3 2E_2}. \tag{E.2}$$

Using the narrow width approximation for the ρ and the unstable particle propagator

$$\sum_{\text{pol}}|\langle J/\psi\ \pi^+\pi^-|X\rangle|^2 = \frac{1}{3}\sum_{\text{pol}}|\langle J/\psi\ \rho|X\rangle|^2\frac{1}{(s-m_\rho^2)^2+(m_\rho\Gamma_\rho)^2}\sum_{\text{pol}}|\langle\pi^+\pi^-|\rho\rangle|^2, \tag{E.3}$$

where $\sum_{\text{pol}}|\langle\pi^+\pi^-|\rho\rangle|^2 = g_{\rho\pi}^2$, with $g_{\rho\pi}$ a constant number. The phase space factor can be rewritten as

$$\begin{aligned}
\mathrm{d}\bar{\Phi}^{(3)} &= (2\pi)^4\int d^4p_\rho\,\delta^{(4)}(P-p_\psi-p_\rho)\delta^{(4)}(p_\rho-p_1-p_2)\frac{d^3p_\psi}{(2\pi)^3 2E_\psi}\frac{d^3p_1}{(2\pi)^3 2E_1}\frac{d^3p_2}{(2\pi)^3 2E_2}\\
&= \frac{1}{2\pi}\int ds\,(2\pi)^4\delta^{(4)}(P-p_\psi-p_\rho)\frac{d^3p_\rho}{(2\pi)^3 2\sqrt{s+|\boldsymbol{p}_\rho|^2}}\frac{d^3p_\psi}{(2\pi)^3 2E_\psi}\\
&\quad\times(2\pi)^4\delta^{(4)}(p_\rho-p_1-p_2)\frac{d^3p_1}{(2\pi)^3 2E_1}\frac{d^3p_2}{(2\pi)^3 2E_2}.
\end{aligned} \tag{E.4}$$

The notation $d\bar{\Phi}^{(3)}$ is to indicate that we have an intermediate ρ. Now we observe that [1]

$$\int(2\pi)^4\delta^{(4)}(P-p_\psi-p_\rho)\frac{d^3p_\rho}{(2\pi)^3 2\sqrt{s+|\boldsymbol{p}_\rho|^2}}\frac{d^3p_\psi}{(2\pi)^3 2E_\psi} \equiv \Phi^{(2)}(m_X, m_\psi, \sqrt{s}) = \frac{1}{4\pi}\frac{p^*(m_X^2, m_\psi^2, s)}{m_X} \tag{E.5}$$

[1] $\Phi^{(2)}$ is the two body phase space.

and

$$\int (2\pi)^4 \delta^{(4)}(p_\rho - p_1 - p_2) \frac{d^3p_1}{(2\pi)^3 2E_1} \frac{d^3p_2}{(2\pi)^3 2E_2} = \Phi^{(2)}(\sqrt{s}, m_{\pi^+}, m_{\pi^-}) = \frac{1}{4\pi} \frac{p^*(s, m_{\pi^+}^2, m_{\pi^-}^2)}{\sqrt{s}}, \tag{E.6}$$

with p^* the decay momentum in the decaying particle rest frame

$$p^*(x, y, z) = \frac{\sqrt{\lambda(x, y, z)}}{2\sqrt{x}}, \tag{E.7}$$

where the Källén function is

$$\lambda(x, y, z) = x^2 + y^2 + z^2 - 2xy - 2yz - 2xz. \tag{E.8}$$

Thus it results that

$$\bar{\Phi}^{(3)}(m_X, m_\psi, m_{\pi^+}, m_{\pi^-}) = \frac{1}{2\pi} \int ds \, \frac{1}{4\pi} \frac{p^*(m_X^2, m_\psi^2, s)}{m_X} \frac{1}{4\pi} \frac{p^*(s, m_{\pi^+}^2, m_{\pi^-}^2)}{\sqrt{s}}. \tag{E.9}$$

The full decay width is then

$$\begin{aligned} \Gamma(X \to J/\psi \, \pi^+\pi^-) =& \frac{1}{2s_X + 1} \frac{1}{2m_X} \frac{1}{6\pi} \int ds \, \sum_{\text{pol}} |\langle J/\psi \, \rho(s) | X \rangle|^2 \\ & \times \frac{1}{4\pi} \frac{p^*(m_X^2, m_\psi^2, s)}{m_X} \frac{g_{\rho\pi}^2}{(s - m_\rho^2)^2 + (m_\rho \Gamma_\rho)^2} \frac{1}{4\pi} \frac{p^*(s, m_{\pi^+}^2, m_{\pi^-}^2)}{\sqrt{s}}. \end{aligned} \tag{E.10}$$

$g_{\rho\pi}^2$ is related to $\Gamma(\rho \to \pi\pi)$ by

$$g_{\rho\pi}^2 = 6 m_\rho^2 \Gamma(\rho \to \pi\pi) \frac{4\pi}{p^*(m_\rho^2, m_\pi^2, m_\pi^2)} \tag{E.11}$$

Plugging the above expression in Eq. (E.10) we obtain

$$\begin{aligned} \Gamma(X \to J/\psi \, \pi^+\pi^-) =& \frac{1}{2s_X + 1} \frac{1}{8\pi m_X^2} \int ds \, \sum_{\text{pol}} |\langle J/\psi \, \rho(s) | X \rangle|^2 \\ & \times p^*(m_X^2, m_\psi^2, s) \frac{1}{\pi} \frac{m_\rho \Gamma_\rho \, \mathcal{B}(\rho \to \pi\pi)}{(s - m_\rho^2)^2 + (m_\rho \Gamma_\rho)^2} \frac{m_\rho}{\sqrt{s}} \frac{p^*(s, m_{\pi^+}^2, m_{\pi^-}^2)}{p^*(m_\rho^2, m_\pi^2, m_\pi^2)}. \end{aligned} \tag{E.12}$$

In the limit of narrow width for the ρ

$$\lim_{\Gamma \to 0} \frac{m\Gamma}{(s - m^2)^2 + (m\Gamma)^2} = \pi \delta(s - m^2). \tag{E.13}$$

Eq. (E.12) is equal to the average of

$$\sum_{\text{pol}} |\langle J/\psi \, \rho(s) | X \rangle|^2 p^*(m_X^2, m_\psi^2, s)$$

taken over the Breit-Wigner distribution for the ρ meson

$$\begin{aligned}\Gamma(X \to J/\psi\ \pi^+\pi^-) =& \frac{1}{2s_X+1}\frac{1}{8\pi m_X^2}\int ds\ \frac{1}{\pi}\frac{m_\rho\Gamma_\rho\ \mathcal{B}(\rho\to\pi\pi)}{(s-m_\rho^2)^2+(m_\rho\Gamma_\rho)^2} \\ &\times \sum_{\text{pol}} |\langle J/\psi\ \rho(s)|X\rangle|^2\ p^*(m_X^2, m_\psi^2, s).\end{aligned} \tag{E.14}$$

In actual calculations we use the so-called *comoving width*

$$m_\rho\Gamma_\rho \to \frac{s}{m_\rho}\Gamma_\rho. \tag{E.15}$$

To understand the origin of the comoving width let us consider the square modulus of the propagator of an unstable particle A with four-momentum p and decaying into two particles B and C. It can be written in the form ($p^2 = s$) [356]:

$$\frac{1}{(p^2-m^2)^2+(\sqrt{p^2}\,\Gamma(p^2))^2}, \tag{E.16}$$

where $\Gamma(p^2) = \Gamma(A(p^2) \to BC)$ is

$$\Gamma(A(p^2)\to BC) \equiv \Gamma(p^2) = \frac{g^2(p^2, m_B^2, m_C^2)}{16\pi(\sqrt{p^2})^3}\sqrt{\lambda(p^2, m_B^2, m_C^2)}. \tag{E.17}$$

Even if an unstable state cannot be properly put on the mass-shell, the mass of a narrow resonance is still well defined and for p^2 equal to its mass its decay width is

$$\Gamma(A(m^2)\to BC) \equiv \Gamma(m_A^2) = \frac{g^2(m_A^2, m_B^2, m_B^2)}{16\pi m_A^3}\sqrt{\lambda(m_A^2, m_B^2, m_C^2)}. \tag{E.18}$$

It is then straightforward to see that

$$\Gamma(p^2) = \frac{m_A^3}{(\sqrt{p^2})^3}\ \frac{g^2(p^2, m_B^2, m_C^2)}{g^2(m_A^2, m_B^2, m_C^2)}\ \frac{\sqrt{\lambda(p^2, m_B^2, m_C^2)}}{\sqrt{\lambda(m_A^2, m_B^2, m_C^2)}}\ \Gamma(m_A^2). \tag{E.19}$$

The coupling constant g has the dimension of a mass, to give the right dimension to the width ($[g] = M$).

Now let us consider two limits which are relevant to our analysis.

- Both the particles in the final state are massless, *i.e.* much lighter than A, $m_B = m_C = 0$. In this case the only mass scale of the problem is p^2 or m_A^2, and thus the only possibility is that $g^2(p^2, 0, 0) = \alpha p^2$ and thus $g^2(m_A^2, 0, 0) = \alpha m_A^2$, where α is some adimensional constant. The relation (E.19) reduces to

$$\Gamma(p^2) = \frac{\sqrt{p^2}}{m_A}\Gamma(m_A^2). \tag{E.20}$$

  This relation can be used when the unstable propagating particle has a mass much larger than that of its decay products, as in the case of the ρ.

- Only one of the decay products is massless $m_C = 0$. This is indeed the case for an intermediate D^* which decays to $D\pi$. Since $\sqrt{\lambda(p^2, m_B^2, 0)} = (p^2 - m_B^2)$ one obtains:

$$\Gamma(p^2) = \frac{m_A}{\sqrt{p^2}} \frac{(p^2 - m_B^2)}{(m_A^2 - m_B^2)} \Gamma(m_A^2). \tag{E.21}$$

  We have checked that using either Eq. (E.21) or Eq. (E.15) for the D^* propagator makes no difference. Thus we use the rule Eq. (E.15) for all the intermediate states.

E.2 $X \to J/\psi\, \omega$

Here we report the basic formulae for the computation of the width of $X \to J/\psi\, \omega$.

$$d\Gamma(X \to J/\psi\, \pi^+\pi^-\pi^0) = \frac{1}{2s_X + 1} \frac{1}{2m_X} \sum_{\text{pol}} |\langle J/\psi\, \pi^+\pi^-\pi^0 | X\rangle|^2 d\Phi^{(4)}, \tag{E.22}$$

where $d\Phi^{(4)}$ is

$$d\Phi^{(4)} = (2\pi)^4 \delta^{(4)}(P - p_\psi - \sum_{i=1}^{4} p_i) \frac{d^3p_\psi}{(2\pi)^3 2E_\psi} \prod_{i=1}^{4} \frac{d^3p_i}{(2\pi)^3 2E_i}. \tag{E.23}$$

Using narrow width approximation

$$\sum_{\text{pol}} |\langle J/\psi\, \pi^+\pi^-\pi^0 | X\rangle|^2 = \frac{1}{3} \sum_{\text{pol}} |\langle J/\psi\, \omega | X\rangle|^2 \frac{1}{(s - m_\omega^2)^2 + (m_\omega \Gamma_\omega)^2} \sum_{\text{pol}} |\langle \pi^+\pi^-\pi^0 | \omega\rangle|^2 \tag{E.24}$$

and we further assume that $\sum_{\text{pol}} |\langle \pi^+\pi^-\pi^0 | \rho\rangle|^2 = g_{\omega\pi}^2$, with $g_{\omega\pi}$ a constant number. The phase space factor can be rewritten as

$$\begin{aligned} d\bar{\Phi}^{(4)} &= (2\pi)^4 \int d^4p_\omega \delta^{(4)}(P - p_\psi - p_\omega) \delta^{(4)}(p_\omega - \sum_i p_i) \frac{d^3p_\psi}{(2\pi)^3 2E_\psi} \prod_i \frac{d^3p_i}{(2\pi)^3 2E_i} \\ &= \frac{1}{2\pi} \int ds\, (2\pi)^4 \delta^{(4)}(P - p_\psi - p_\omega) \frac{d^3p_\omega}{(2\pi)^3 2\sqrt{s + |\boldsymbol{p}_\omega|^2}} \frac{d^3p_\psi}{(2\pi)^3 2E_\psi} \\ &\quad \times (2\pi)^4 \delta^{(4)}(p_\omega - \sum_i p_i) \prod_i \frac{d^3p_i}{(2\pi)^3 2E_i}, \end{aligned} \tag{E.25}$$

where the notation $d\bar{\Phi}^{(4)}$ is to indicate that we have an intermediate ω. Now

$$\int (2\pi)^4 \delta^{(4)}(P - p_\psi - p_\omega) \frac{d^3p_\omega}{(2\pi)^3 2\sqrt{s + |\boldsymbol{p}_\omega|^2}} \frac{d^3p_\psi}{(2\pi)^3 2E_\psi} = \frac{1}{4\pi} \frac{p^*(m_X^2, m_\psi^2, s)}{m_X} \tag{E.26}$$

and

$$\int (2\pi)^4 \delta^{(4)}(p_\omega - \sum_i p_i) \prod_i \frac{d^3p_i}{(2\pi)^3 2E_i} = \Phi^{(3)}(\sqrt{s}, m_{\pi^+}, m_{\pi^-}, m_{\pi^0}). \tag{E.27}$$

The expression for the three body phase space is the following

$$\Phi^{(3)}(\sqrt{s}, m_1, m_2, m_3) = \frac{1}{32\pi^3}\int d\omega\left(x_+(\sqrt{s}, m_1, m_2, m_3, \omega) - x_-(\sqrt{s}, m_1, m_2, m_3, \omega)\right), \tag{E.28}$$

where

$$\begin{aligned} x_\pm(\sqrt{s}, m_1, m_2, m_3, \omega) = \\ = \frac{\frac{\left(m_2^2-m_3^2\right)(\sqrt{s}-\omega)}{4\sqrt{s}} \pm \frac{1}{2}\sqrt{\left(\omega^2-m_1^2\right)\left(\omega_m\left(\sqrt{s}, m_1, m_2, m_3\right)-\omega\right)\left(\frac{2m_2m_3}{\sqrt{s}} - \omega + \omega_m\left(\sqrt{s}, m_1, m_2, m_3\right)\right)}}{\frac{(m_2+m_3)^2}{2\sqrt{s}} - \omega + \omega_m\left(\sqrt{s}, m_1, m_2, m_3\right)} \end{aligned} \tag{E.29}$$

with

$$\omega_m(\sqrt{s}, m_1, m_2, m_3) = \frac{m_1^2 - (m_2+m_3)^2 + s}{2\sqrt{s}}. \tag{E.30}$$

Finally

$$\Phi^{(4)}(m_X, m_\psi, m_{\pi^+}, m_{\pi^-}, m_{\pi^0}) = \frac{1}{2\pi}\int ds\,\frac{1}{4\pi}\frac{p^*(m_X^2, m_\psi^2, s)}{m_X}\Phi^{(3)}(\sqrt{s}, m_{\pi^+}, m_{\pi^-}, m_{\pi^0}). \tag{E.31}$$

The full decay width is then

$$\begin{aligned} \Gamma(X \to J/\psi\,\pi^+\pi^-\pi^0) = \frac{1}{2s_X+1}\frac{1}{2m_X}\frac{1}{6\pi}\int ds\sum_{\text{pol}}|\langle J/\psi\,\omega(s)|X\rangle|^2 \\ \times\frac{1}{4\pi}\frac{p^*(m_X^2, m_\psi^2, s)}{m_X}\frac{g_{\omega\pi}^2}{(s-m_\omega^2)^2+(m_\omega\Gamma_\omega)^2}\,\Phi^{(3)}(\sqrt{s}, m_{\pi^+}, m_{\pi^-}, m_{\pi^0}). \end{aligned} \tag{E.32}$$

We can relate $g_{\omega\pi}^2$ to $\Gamma(\omega \to 3\pi)$

$$g_{\omega\pi}^2 = 6m_\omega\Gamma(\omega\to\pi\pi\pi)\frac{1}{\Phi^{(3)}(m_\omega, m_{\pi^+}, m_{\pi^-}, m_{\pi^0})}, \tag{E.33}$$

thus giving

$$\begin{aligned} \Gamma(X \to J/\psi\,\pi^+\pi^-\pi^0) = \frac{1}{2s_X+1}\frac{1}{8\pi m_X^2}\int ds\sum_{\text{pol}}|\langle J/\psi\,\omega(s)|X\rangle|^2 \\ \times p^*(m_X^2, m_\psi^2, s)\frac{1}{\pi}\frac{m_\omega\Gamma_\omega\,\mathcal{B}(\omega\to 3\pi)}{(s-m_\omega^2)^2+(m_\omega\Gamma_\omega)^2}\times\frac{\Phi^{(3)}(\sqrt{s}, m_{\pi^+}, m_{\pi^-}, m_{\pi^0})}{\Phi^{(3)}(m_\omega, m_{\pi^+}, m_{\pi^-}, m_{\pi^0})}. \end{aligned} \tag{E.34}$$

In the limit of narrow width for the ω, Eq. (E.34) is equal to the average of

$$\sum_{\text{pol}}|\langle J/\psi\,\omega(s)|X\rangle|^2 p^*(m_X^2, m_\psi^2, s) \tag{E.35}$$

taken over the Breit-Wigner distribution of the ω meson (using the comoving width of the ω)

$$\begin{aligned} \Gamma(X \to J/\psi\,\pi^+\pi^-\pi^0) = \frac{1}{2s_X+1}\frac{1}{8\pi m_X^2}\int ds\sum_{\text{pol}}|\langle J/\psi\,\omega(s)|X\rangle|^2 \\ \times p^*(m_X^2, m_\psi^2, s)\frac{1}{\pi}\frac{m_\omega\Gamma_\omega\,\mathcal{B}(\omega\to\pi\pi)}{(s-m_\omega^2)^2+(m_\omega\Gamma_\omega)^2}. \end{aligned} \tag{E.36}$$

In actual calculations we use $m_\omega\Gamma_\omega \to \frac{s}{m_\omega}\Gamma_\omega$.

E.3 $J/\psi\ (\rho,\omega) \to X(3872) \to D^0\bar{D}^{0*}$ cross section

The differential cross section for $J/\psi\ \rho \to D^0\bar{D}^{0*}$ is

$$\begin{aligned} d\sigma(J/\psi\ \rho \to D^0\bar{D}^{0*}) =& \frac{1}{9}\frac{1}{4\phi}(2\pi)^4\delta^{(4)}\left(p_{_D} + p_{_{D^*}} - p_\psi - p_\rho\right) \\ & \times \sum_{\text{pol}} \left|\mathcal{M}_{J/\psi\ \rho\to D^0\bar{D}^{0*}}\right|^2 \frac{d^3p_{_D}}{(2\pi)^3 2\omega_{_D}} \frac{d^3p_{_D}}{(2\pi)^3 2\omega_{_{D^*}}}, \end{aligned} \tag{E.37}$$

with the flux ϕ defined by

$$\phi = \sqrt{(p_\psi \cdot p_\rho)^2 - m_\psi^2 m_\rho^2} = \frac{1}{2}\sqrt{\lambda(s, m_\psi^2, m_\rho^2)}. \tag{E.38}$$

We use also

$$\begin{aligned} &\int (2\pi)^4\delta\left(\omega_{_D} + \omega_{_{D^*}} - \sqrt{s}\right)\delta^{(3)}(\boldsymbol{p}_{_D} + \boldsymbol{p}_{_{D^*}}) \frac{d^3p_{_D}}{(2\pi)^3 2\omega_{_D}} \frac{d^3p_{_D}}{(2\pi)^3 2\omega_{_{D^*}}} \\ &\qquad = \frac{1}{16\pi}\frac{\sqrt{\lambda(s, m_{_D}^2, m_{_{D^*}}^2)}}{s}\, d\cos\theta. \end{aligned} \tag{E.39}$$

The above formulae leads to Eq. (5.35) and similarly for ω.

E.4 Multiplicity rules

E.4.1 $X(3872) \to D^0\bar{D}^{0*}$

Let us consider the decay $X(3872) \to D^0\bar{D}^{0*}$. Since X has even charge conjugation, whatever its spin is, the final state into open charm mesons needs to be

$$|f\rangle = \frac{|D^0\bar{D}^{0*}\rangle + |\bar{D}^0 D^{0*}\rangle}{\sqrt{2}}. \tag{E.40}$$

Assuming that

$$\langle D^0\bar{D}^{0*}|X\rangle = \langle \bar{D}^0 D^{0*}|X\rangle, \tag{E.41}$$

the sum over polarizations of the squared matrix element is

$$\sum_{\text{pol}} |\langle f|X\rangle|^2 = 2\sum_{\text{pol}} |\langle D^0\bar{D}^{0*}|X\rangle|^2. \tag{E.42}$$

When we compute the cross section for $J/\psi(\rho,\omega) \to X_J \to D^0\bar{D}^{0*}$ we actually consider the transition $J/\psi(\rho,\omega) \to f$. The flavor wave function for the ρ meson is

$$|\rho\rangle = \frac{|u\bar{u}\rangle - |d\bar{d}\rangle}{\sqrt{2}}. \tag{E.43}$$

Since the neutral D mesons contain only the u quark ($|D^0\rangle = |c\bar{u}\rangle$ e $|\bar{D}^0\rangle = |\bar{c}u\rangle$) only the $u\bar{u}$ component will contribute to the transition matrix element

$$\mathcal{M} = \frac{1}{\sqrt{2}}\langle f|\psi\rho\rangle. \tag{E.44}$$

Summing over polarization the squared matrix element one obtains

$$\sum_{\text{pol}} |\mathcal{M}|^2 = \sum_{\text{pol}} \frac{1}{2} |\langle f|\psi\rho\rangle|^2 = \sum_{\text{pol}} \frac{1}{2} \times 2 |\langle D^0 \bar{D}^{0*}|\psi\rho\rangle|^2 = \sum_{\text{pol}} |\langle D^0 \bar{D}^{0*}|\psi\rho\rangle|^2. \quad \text{(E.45)}$$

Thus one needs to replace g_{JDD^*} with $\sqrt{2}\, g_{JDD^*}$ in Eq. (4.4,4.17).

E.4.2 Non resonant processes

We consider the t - channel processes of Eq. (5.33). We computed the average absorption lengths for each of the particles in the initial state, $A = \pi,\ \eta,\ \rho,\ \omega,\ \phi,\ K^{(*)}$ using the couplings defined in [308]

$$\langle \rho \sigma_{J/\psi\, A \to D\bar{D}} \rangle_T = (2 s_A + 1) \int \frac{d^3 p_A}{(2\pi)^3} \frac{\sigma_A}{e^{E_A/\kappa_B T} - 1}. \quad \text{(E.46)}$$

Depending on the flavor content of each meson in the initial state one can define the possible open-charm mesons configuration in the final state. The flavor wave functions of the mesons we considered are the following [20] (we neglect the $s\bar{s}$ component of the η meson, since the contribution of the associated final state, $D_s^{+(*)} D_s^{-(*)}$, is small compared to the one coming from the $(u\bar{u} + d\bar{d})/\sqrt{2}$ component, *i.e.*, $D^{0(*)} \bar{D}^{0(*)}$ or $D^{\pm(*)} D^{\mp(*)}$)

$$\begin{aligned}
&\pi^+(\rho^+) = u\bar{d},\ \pi^-(\rho^-) = \bar{u}d,\ \pi^0(\rho^0) = \frac{u\bar{u} - d\bar{d}}{\sqrt{2}} \\
&\eta \simeq \frac{u\bar{u} + d\bar{d}}{\sqrt{2}} \\
&\omega \simeq \frac{u\bar{u} + d\bar{d}}{\sqrt{2}} \\
&\phi \simeq s\bar{s} \\
&K^0 = s\bar{d},\ \bar{K}^0 = \bar{s}d,\ K^+ = u\bar{s},\ K^- = \bar{u}s.
\end{aligned} \quad \text{(E.47)}$$

The multiplicity coefficients c_i^A associated to the possible final states f_i for each initial particle A are summarized in Table E.1. Given these coefficients the total dissociation cross section for the initial particle A can be written as

$$\sigma_A = \sum_i c_i^A\, \sigma_{AJ/\psi \to f_i}. \quad \text{(E.48)}$$

We can summarize all the contributions as follows

$$\begin{aligned}
\sigma_\pi &= 3 \times \Big[\sigma(J/\psi\ \pi \to D\bar{D}) + 2\sigma(J/\psi\ \pi \to D\bar{D}^*) + \sigma(J/\psi\ \pi \to D^*\bar{D}^*)\Big], \\
\sigma_{\rho+\omega} &= 4 \times \Big[\sigma(J/\psi\ \rho \to D\bar{D}) + 2\sigma(J/\psi\ \rho \to D\bar{D}^*) + \sigma(J/\psi\ \rho \to D^*\bar{D}^*)\Big] \\
\sigma_\eta &= \sigma(J/\psi\ \eta \to D\bar{D}) + 2\sigma(J/\psi\ \eta \to D\bar{D}^*) + \sigma(J/\psi\ \eta \to D^*\bar{D}^*), \\
\sigma_\phi &= \sigma(J/\psi\ \phi \to D_s^- D_s^+) + 2\sigma(J/\psi\ \phi \to D_s^- D_s^{+*}) + \sigma(J/\psi\ \phi \to D_s^{-*} D_s^{+*}), \\
\sigma_K &= 4 \times \Big[\sigma(J/\psi\ K \to D_s\bar{D}) + \sigma(J/\psi\ K \to D_s^*\bar{D}) \\
&\qquad + \sigma(J/\psi\ K \to D_s\bar{D}^*) + \sigma(J/\psi\ K \to D_s^*\bar{D}^*)\Big].
\end{aligned}$$

Table E.1. Multiplicity coefficients for the processes $J/\psi\ A \to D\bar{D}$. Notice that $D^{(*)}\bar{D}^{(*)} \equiv D\bar{D},\ D^*\bar{D}^*$.

A	$\bar{D}^{0(*)}D^{\pm(*)}$	$\bar{D}^0 D^{\pm *}$	$D^{0(*)}\bar{D}^{0(*)}$	$D^0\bar{D}^{0*}$	$D^{+(*)}D^{-(*)}$	D^+D^{-*}	$D_s^{+(*)}D_s^{-(*)}$	$D_s^+D_s^{-*}$	$D_s^{(*)}\bar{D}^{(*)}$	$D_s\bar{D}^*$	$D_s^*\bar{D}$
$\pi^\pm$	1	2	0	0	0	0	0	0	0	0	0
$\rho^\pm$	1	2	0	0	0	0	0	0	0	0	0
π^0	0	0	1/2	1	1/2	1	0	0	0	0	0
ρ^0, ω	0	0	1/2	1	1/2	1	0	0	0	0	0
η	0	0	1/2	1	1/2	1	0	0	0	0	0
ϕ	0	0	0	0	0	0	1	2	0	0	0
K^0	0	0	0	0	0	0	0	0	1	1	1
$\bar{K}^0$	0	0	0	0	0	0	0	0	1	1	1
$K^\pm$	0	0	0	0	0	0	0	0	1	1	1

Bibliography

[1] D. J. Gross, Nucl.Phys.Proc.Suppl. **74**, 426 (1999), hep-th/9809060.

[2] T. Burns, F. Piccinini, A. Polosa, and C. Sabelli, Phys.Rev. **D82**, 074003 (2010), 1008.0018.

[3] G. Cotugno, R. Faccini, A. Polosa, and C. Sabelli, Phys.Rev.Lett. **104**, 132005 (2010), 0911.2178.

[4] F. Brazzi, B. Grinstein, F. Piccinini, A. D. Polosa, and C. Sabelli, Phys.Rev. **D84**, 014003 (2011), 1103.3155.

[5] C. Bignamini, B. Grinstein, F. Piccinini, A. Polosa, and C. Sabelli, Phys.Rev.Lett. **103**, 162001 (2009), 0906.0882.

[6] C. Bignamini *et al.*, Phys.Lett. **B684**, 228 (2010), 0912.5064.

[7] T. Burns, F. Piccinini, A. Polosa, V. Prosperi, and C. Sabelli, Phys.Rev. **D83**, 114029 (2011), 1104.1781.

[8] N. A. Tornqvist, Phys.Rev.Lett. **67**, 556 (1991), Revised version.

[9] N. A. Tornqvist, Z.Phys. **C61**, 525 (1994), hep-ph/9310247.

[10] M. Gell-Mann, Phys.Lett. **8**, 214 (1964).

[11] R. P. Feynman, Phys.Rev.Lett. **23**, 1415 (1969).

[12] G. 't Hooft, Nucl.Phys. **B33**, 173 (1971).

[13] G. 't Hooft, Nucl.Phys. **B35**, 167 (1971).

[14] D. Gross and F. Wilczek, Phys.Rev.Lett. **30**, 1343 (1973).

[15] D. Politzer, Phys.Rev.Lett. **30**, 1346 (1973).

[16] S. Okubo, Prog.Theor.Phys. **27**, 949 (1962).

[17] E. D. Bloom *et al.*, Phys.Rev.Lett. **23**, 930 (1969).

[18] J. Bjorken, Phys.Rev. **179**, 1547 (1969).

[19] J. Callan, Curtis G. and D. J. Gross, Phys.Rev.Lett. **22**, 156 (1969).

[20] Particle Data Group, K. Nakamura *et al.*, J.Phys.G **G37**, 075021 (2010).

[21] N. Nielsen, Am.J.Phys. **49**, 1171 (1981).

[22] S. Glashow, J. Iliopoulos, and L. Maiani, Phys.Rev. **D2**, 1285 (1970).

[23] E598 Collaboration, J. Aubert *et al.*, Phys.Rev.Lett. **33**, 1404 (1974).

[24] SLAC-SP-017 Collaboration, J. Augustin *et al.*, Phys.Rev.Lett. **33**, 1406 (1974).

[25] G. Goldhaber *et al.*, Phys.Rev.Lett. **37**, 255 (1976).

[26] I. Peruzzi *et al.*, Phys.Rev.Lett. **37**, 569 (1976).

[27] S. L. Glashow, Nucl. Phys. **22**, 579 (1961).

[28] S. Weinberg, Phys.Rev.Lett. **19**, 1264 (1967).

[29] A. Salam, Originally printed in Svartholm: Elementary Particle Theory, Proceedings Of The Nobel Symposium Held 1968 At Lerum, Sweden, Stockholm 1968, 367-377.

[30] S. Weinberg, Phys.Rev. **D5**, 1962 (1972).

[31] S. Herb *et al.*, Phys.Rev.Lett. **39**, 252 (1977).

[32] CDF Collaboration, F. Abe *et al.*, Phys.Rev.Lett. **74**, 2626 (1995), hep-ex/9503002.

[33] D0 Collaboration, S. Abachi *et al.*, Phys.Rev.Lett. **74**, 2422 (1995), hep-ex/9411001.

[34] E. Eichten and F. Feinberg, Phys.Rev. **D23**, 2724 (1981).

[35] Quarkonium Working Group, N. Brambilla *et al.*, (2004), hep-ph/0412158.

[36] E. Eichten, S. Godfrey, H. Mahlke, and J. L. Rosner, Rev. Mod. Phys. **80**, 1161 (2008), hep-ph/0701208.

[37] J. Pumplin, W. Repko, and A. Sato, Phys.Rev.Lett. **35**, 1538 (1975).

[38] H. J. Schnitzer, Phys.Rev.Lett. **35**, 1540 (1975).

[39] D. Ebert, R. Faustov, and V. Galkin, Phys.Rev. **D67**, 014027 (2003), hep-ph/0210381.

[40] M. Voloshin, Prog.Part.Nucl.Phys. **61**, 455 (2008), 0711.4556.

[41] T. Barnes, AIP Conf. Proc. **1257**, 11 (2010), 1003.2644.

[42] J. L. Rosner, Phys.Rev. **D64**, 094002 (2001), hep-ph/0105327.

[43] J. L. Rosner, Ann. Phys. **319**, 1 (2005), hep-ph/0411003.

[44] V. Novikov *et al.*, Phys.Rept. **41**, 1 (1978).

[45] M. A. Shifman, Z.Phys. **C4**, 345 (1980).

[46] V. A. Novikov, M. A. Shifman, A. I. Vainshtein, and V. I. Zakharov, Nucl. Phys. **B191**, 301 (1981).

[47] K. Gottfried, Phys.Rev.Lett. **40**, 598 (1978).

[48] M. B. Voloshin and V. I. Zakharov, Phys.Rev.Lett. **45**, 688 (1980).

[49] V. Novikov and M. A. Shifman, Z.Phys. **C8**, 43 (1981).

[50] D. J. Gross, S. Treiman, and F. Wilczek, Phys.Rev. **D19**, 2188 (1979).

[51] L. S. Brown and R. N. Cahn, Phys.Rev.Lett. **35**, 1 (1975).

[52] M. Voloshin and Y. Zaitsev, Sov.Phys.Usp. **30**, 553 (1987).

[53] N. Brambilla *et al.*, Eur.Phys.J. **C71**, 1534 (2011), 1010.5827.

[54] Belle Collaboration, I. Adachi *et al.*, (2011), 1103.3419.

[55] S. Godfrey and N. Isgur, Phys.Rev. **D32**, 189 (1985).

[56] Belle Collaboration, S. Choi *et al.*, Phys.Rev.Lett. **91**, 262001 (2003), hep-ex/0309032.

[57] Belle Collaboration, I. Adachi *et al.*, (2008), 0809.1224.

[58] CDF II Collaboration, D. Acosta *et al.*, Phys.Rev.Lett. **93**, 072001 (2004), hep-ex/0312021.

[59] CDF Collaboration, A. Abulencia *et al.*, Phys.Rev.Lett. **96**, 102002 (2006), hep-ex/0512074.

[60] CDF Collaboration, A. Abulencia *et al.*, Phys.Rev.Lett. **98**, 132002 (2007), hep-ex/0612053.

[61] CDF Collaboration, T. Aaltonen *et al.*, Phys.Rev.Lett. **103**, 152001.

[62] D0 Collaboration, V. Abazov *et al.*, Phys.Rev.Lett. **93**, 162002 (2004), hep-ex/0405004.

[63] BABAR Collaboration, B. Aubert *et al.*, Phys.Rev. **D73**, 011101 (2006), hep-ex/0507090.

[64] BABAR Collaboration, G. B. Mohanty, Frascati Phys.Ser. **40**, 137 (2006), hep-ex/0509039.

[65] BABAR Collaboration, B. Aubert *et al.*, Phys.Rev.Lett. **96**, 052002 (2006), hep-ex/0510070.

[66] BABAR Collaboration, B. Aubert *et al.*, Phys.Rev. **D77**, 111101 (2008), 0803.2838.

[67] Belle Collaboration, K. Abe *et al.*, (2005), hep-ex/0505037.

[68] BABAR Collaboration, P. del Amo Sanchez *et al.*, Phys.Rev. **D82**, 011101 (2010), 1005.5190.

[69] Belle Collaboration, V. Bhardwaj *et al.*, Phys.Rev.Lett. **107**, 9 (2011), 1105.0177.

[70] BABAR Collaboration, B. Aubert *et al.*, Phys.Rev. **D74**, 071101 (2006), hep-ex/0607050.

[71] BABAR Collaboration, B. Aubert *et al.*, Phys.Rev.Lett. **102**, 132001 (2009), 0809.0042.

[72] Belle Collaboration, G. Gokhroo *et al.*, Phys.Rev.Lett. **97**, 162002 (2006), hep-ex/0606055.

[73] Belle Collaboration, I. Adachi *et al.*, (2008), 0810.0358.

[74] BABAR Collaboration, B. Aubert *et al.*, Phys.Rev. **D77**, 011102 (2008), 0708.1565.

[75] N. Drenska *et al.*, Riv.Nuovo Cim. **033**, 633 (2010), 1006.2741.

[76] Belle Collaboration, K. Abe *et al.*, (2005), hep-ex/0505038.

[77] Belle, K. Abe *et al.*, Phys. Rev. Lett. **98**, 082001 (2007), hep-ex/0507019.

[78] Belle Collaboration, P. Pakhlov *et al.*, Phys.Rev.Lett. **100**, 202001 (2008), 0708.3812.

[79] Belle, K. Abe *et al.*, Phys. Rev. Lett. **94**, 182002 (2005), hep-ex/0408126.

[80] BaBar, B. Aubert *et al.*, Phys. Rev. Lett. **101**, 082001 (2008), 0711.2047.

[81] Belle Collaboration, S. Uehara *et al.*, Phys.Rev.Lett. **104**, 092001 (2010), 0912.4451.

[82] Belle, S. Uehara *et al.*, Phys. Rev. Lett. **96**, 082003 (2006), hep-ex/0512035.

[83] BABAR, B. Aubert *et al.*, Phys. Rev. **D81**, 092003 (2010), 1002.0281.

[84] BABAR Collaboration, B. Aubert *et al.*, Phys.Rev. **D76**, 111105 (2007), hep-ex/0607083.

[85] Belle Collaboration, G. Pakhlova *et al.*, Phys.Rev. **D77**, 011103 (2008), 0708.0082.

[86] Belle Collaboration, C. Yuan *et al.*, Phys.Rev.Lett. **99**, 182004 (2007), 0707.2541.

[87] BaBar Collaboration, B. Aubert *et al.*, (2008), 0808.1543.

[88] CDF Collaboration, T. Aaltonen *et al.*, Phys.Rev.Lett. **102**, 242002 (2009), 0903.2229.

[89] CDF Collaboration, K. Yi, PoS **ICHEP2010**, 182 (2010), 1010.3470.

[90] CDF Collaboration, K. Yi, (2009), 0910.3163.

[91] Belle Collaboration, C.-Z. Yuan, (2009), 0910.3138.

[92] Belle Collaboration, C. Shen *et al.*, Phys.Rev.Lett. **104**, 112004 (2010), 0912.2383.

[93] BABAR Collaboration, B. Aubert *et al.*, Phys.Rev.Lett. **95**, 142001 (2005), hep-ex/0506081.

[94] Belle Collaboration, K. Abe *et al.*, (2006), hep-ex/0612006.

[95] CLEO Collaboration, T. Coan *et al.*, Phys.Rev.Lett. **96**, 162003 (2006), hep-ex/0602034.

[96] CLEO Collaboration, D. Cronin-Hennessy *et al.*, Phys.Rev. **D80**, 072001 (2009), 0801.3418.

[97] CLEO Collaboration, Q. He *et al.*, Phys.Rev. **D74**, 091104 (2006), hep-ex/0611021.

[98] Belle Collaboration, K. Abe *et al.*, Phys.Rev.Lett. **98**, 092001 (2007), hep-ex/0608018.

[99] BABAR Collaboration, B. Aubert *et al.*, (2008), 0710.1371.

[100] BABAR Collaboration, B. Aubert *et al.*, Phys.Rev. **D79**, 092001 (2009), 0903.1597.

[101] BABAR Collaboration, P. del Amo Sanchez *et al.*, Phys.Rev. **D82**, 052004 (2010), 1008.0338.

[102] Belle Collaboration, G. Pakhlova *et al.*, Phys.Rev. **D83**, 011101 (2011), 1011.4397.

[103] BABAR Collaboration, B. Aubert *et al.*, Phys.Rev.Lett. **98**, 212001 (2007), hep-ex/0610057.

[104] Belle Collaboration, X. Wang *et al.*, Phys.Rev.Lett. **99**, 142002 (2007), 0707.3699.

[105] Belle Collaboration, G. Pakhlova *et al.*, Phys.Rev.Lett. **101**, 172001 (2008), 0807.4458.

[106] BELLE Collaboration, S. Choi *et al.*, Phys.Rev.Lett. **100**, 142001 (2008), 0708.1790.

[107] BELLE Collaboration, R. Mizuk *et al.*, Phys.Rev. **D80**, 031104 (2009), 0905.2869.

[108] BABAR Collaboration, B. Aubert *et al.*, Phys.Rev. **D79**, 112001 (2009), 0811.0564.

[109] Belle Collaboration, R. Mizuk *et al.*, Phys.Rev. **D78**, 072004 (2008), 0806.4098.

[110] Belle Collaboration, K. Chen *et al.*, Phys.Rev.Lett. **100**, 112001 (2008), 0710.2577.

[111] Belle Collaboration, I. Adachi *et al.*, (2008), 0808.2445.

[112] R. Mitchell, (2011), 1102.3424.

[113] Belle Collaboration, I. Adachi *et al.*, (2011), 1105.4583.

[114] M. B. Voloshin and L. B. Okun, JETP Lett. **23**, 333 (1976).

[115] H. G. A. De Rujula and S. L. Glashow, Phys. Rev. Lett. **38**, 317 (1997).

[116] T. Barnes, (1994), hep-ph/9406215.

[117] F. Close and C. Downum, Phys.Rev.Lett. **102**, 242003 (2009), 0905.2687.

[118] J. D. Weinstein and N. Isgur, Phys.Rev. **D41**, 2236 (1990).

[119] E. S. Swanson, Annals Phys. **220**, 73 (1992).

[120] E. S. Swanson, Phys. Lett. **B588**, 189 (2004), hep-ph/0311229.

[121] N. A. Tornqvist, Phys.Rev.Lett. **67**, 556 (1991).

[122] F. Close, C. Downum, and C. E. Thomas, Phys. Rev. **D81**, 074033 (2010), 1001.2553.

[123] A. V. Manohar and M. B. Wise, Nucl.Phys. **B399**, 17 (1993), hep-ph/9212236.

[124] N. A. Tornqvist, Z.Phys. **C61**, 525 (1994), hep-ph/9310247.

[125] J. D. Weinstein and N. Isgur, Phys.Rev.Lett. **48**, 659 (1982).

[126] J. D. Weinstein and N. Isgur, Phys.Rev. **D27**, 588 (1983).

[127] D. O. Caldwell, Mod.Phys.Lett. **A2**, 771 (1987).

[128] R. S. Longacre, Phys.Rev. **D42**, 874 (1990).

[129] E. S. Swanson, Phys.Rept. **429**, 243 (2006), hep-ph/0601110.

[130] N. A. Tornqvist, Phys.Lett. **B590**, 209 (2004), hep-ph/0402237.

[131] D. Gamermann and E. Oset, Phys.Rev. **D80**, 014003 (2009), 0905.0402.

[132] D. Gamermann, J. Nieves, E. Oset, and E. Ruiz Arriola, Phys.Rev. **D81**, 014029 (2010), 0911.4407.

[133] D. Gamermann, J. Nieves, E. Oset, and E. Arriola, AIP Conf.Proc. **1257**, 326 (2010), 1001.3254.

[134] M. Suzuki, Phys.Rev. **D72**, 114013 (2005), hep-ph/0508258.

[135] E. Braaten and M. Kusunoki, Phys.Rev. **D69**, 074005 (2004), hep-ph/0311147.

[136] E. Braaten and M. Kusunoki, Phys.Rev. **D72**, 054022 (2005), hep-ph/0507163.

[137] C. Hanhart, Y. Kalashnikova, A. E. Kudryavtsev, and A. Nefediev, Phys.Rev. **D76**, 034007 (2007), 0704.0605.

[138] E. Braaten and J. Stapleton, Phys.Rev. **D81**, 014019 (2010), 0907.3167.

[139] Y. Kalashnikova and A. Nefediev, Phys.Rev. **D80**, 074004 (2009), 0907.4901.

[140] C. Hanhart, Y. Kalashnikova, and A. Nefediev, Phys.Rev. **D81**, 094028 (2010), 1002.4097.

[141] V. Baru, C. Hanhart, Y. Kalashnikova, A. Kudryavtsev, and A. Nefediev, Eur.Phys.J. **A44**, 93 (2010), 1001.0369.

[142] P. Artoisenet, E. Braaten, and D. Kang, Phys.Rev. **D82**, 014013 (2010), 1005.2167.

[143] M. Voloshin, Phys.Lett. **B604**, 69 (2004), hep-ph/0408321.

[144] S. Dubynskiy and M. B. Voloshin, Phys.Rev. **D77**, 014013 (2008), 0709.4474.

[145] M. Voloshin, Int.J.Mod.Phys. **A21**, 1239 (2006), hep-ph/0509192.

[146] E. Braaten, M. Kusunoki, and S. Nussinov, Phys.Rev.Lett. **93**, 162001 (2004), hep-ph/0404161.

[147] E. Braaten and M. Kusunoki, Phys.Rev. **D71**, 074005 (2005), hep-ph/0412268.

[148] X. Liu and S.-L. Zhu, Phys.Rev. **D80**, 017502 (2009), 0903.2529.

[149] T. Branz, T. Gutsche, and V. E. Lyubovitskij, Phys. Rev. **D80**, 054019 (2009), 0903.5424.

[150] J. R. Zhang and M. Q. Huang, Phys. Rev. D **80**, 056004 (2009).

[151] T. Branz, T. Gutsche, and V. E. Lyubovitskij, (2010), 1001.3959.

[152] R. M. Albuquerque, M. E. Bracco, and M. Nielsen, Phys. Lett. B **678**, 186 (2009), 0903.5540.

[153] G. J. Ding, Eur.Phys.J. **C64**, 297 (2009), 0904.1782.

[154] J. R. Zhang and M. Q. Huang, J. Phys. G **37**, 025005 (2010), 0905.4178.

[155] M. Nielsen, F. S. Navarra, and S. H. Lee, (2009), 0911.1958.

[156] T. G. T. Branz and V. E. Lyubovitskij, Phys.Rev. **D78**, 114004 (2008), 0808.0705.

[157] X. Liu and H. W. Ke, Phys. Rev. D **80**, 034009 (2009), 0907.1349.

[158] T. Branz, T. Gutsche, and V. E. Lyubovitskij, Phys. Rev. **D80**, 054019 (2009), 0903.5424.

[159] N. Mahajan, Phys.Lett. **B679**, 228 (2009), 0903.3107.

[160] R. Albuquerque and M. Nielsen, Nucl. Phys. **A815**, 53 (2009), 0804.4817.

[161] R. M. Albuquerque, J. M. Dias, and M. Nielsen, Phys. Lett. **B690**, 141 (2010), 1001.3092.

[162] Z. X. L. X. Liu, X., Phys. Rev. **D72**, 054023 (2005).

[163] P. W. C. Z. Yuan and X. H. Mo, Phys.Lett. **B634**, 399 (2006), hep-ph/0511107.

[164] G. J. Ding, Phys.Rev. **D79**, 014001 (2009), 0809.4818.

[165] F. K. Guo, C. Hanhart, and U. G. Meissner, Phys.Lett. **B665**, 26 (2008), 0803.1392.

[166] F.-K. Guo, C. Hanhart, and U.-G. Meissner, Phys.Rev.Lett. **102**, 242004 (2009), 0904.3338.

[167] F.-K. Guo, J. Haidenbauer, C. Hanhart, and U.-G. Meissner, (2010), 1005.2055.

[168] C. Meng and K.-T. Chao, (2007), 0708.4222.

[169] S. H. Lee, A. Mihara, F. S. Navarra, and M. Nielsen, Phys.Lett. **B661**, 28 (2008), 0710.1029.

[170] X. Liu, Y.-R. Liu, W.-Z. Deng, and S.-L. Zhu, Phys.Rev. **D77**, 034003 (2008), 0711.0494.

[171] X. Liu, Y.-R. Liu, W.-Z. Deng, and S.-L. Zhu, Phys.Rev. **D77**, 094015 (2008), 0803.1295.

[172] G.-J. Ding, W. Huang, J.-F. Liu, and M.-L. Yan, Phys.Rev. **D79**, 034026 (2009), 0805.3822.

[173] S. Godfrey, (2009), 0910.3409.

[174] CLQCD Collaboration, G.-Z. Meng *et al.*, Phys.Rev. **D80**, 034503 (2009), 0905.0752.

[175] X. Liu, X.-Q. Zeng, and X.-Q. Li, Phys.Rev. **D72**, 054023 (2005), hep-ph/0507177.

[176] G. J. Ding, Phys. Rev. D **80**, 034005 (2009), 0905.1188.

[177] A. Bondar, A. Garmash, A. Milstein, R. Mizuk, and M. Voloshin, (2011), 1105.4473.

[178] D.-Y. Chen, X. Liu, and S.-L. Zhu, (2011), 1105.5193.

[179] J.-R. Zhang, M. Zhong, and M.-Q. Huang, (2011), 1105.5472.

[180] M. Voloshin, (2011), 1105.5829.

[181] Y. Yang, J. Ping, C. Deng, and H.-S. Zong, (2011), 1105.5935.

[182] J. Nieves and M. Valderrama, (2011), 1106.0600.

[183] H.-W. Ke and X.-Q. Li, (2011), 1107.0443.

[184] F. Navarra, M. Nielsen, and J.-M. Richard, (2011), 1108.1230.

[185] Z.-F. Sun, J. He, X. Liu, Z.-G. Luo, and S.-L. Zhu, Phys.Rev. **D84**, 054002 (2011), 1106.2968.

[186] R. L. Jaffe and K. Johnson, Phys. Lett. **B60**, 201 (1976).

[187] A. I. Vainshtein and L. B. Okun, Yad. Fiz. **23**, 1347 (1976).

[188] T. Barnes, F. Close, and E. Swanson, Phys.Rev. **D52**, 5242 (1995), hep-ph/9501405.

[189] T. Barnes and F. E. Close, Phys. Lett. **B116**, 365 (1982).

[190] T. Barnes, F. E. Close, F. de Viron, and J. Weyers, Nucl. Phys. **B224**, 241 (1983).

[191] P. Hasenfratz, R. R. Horgan, J. Kuti, and J. M. Richard, Phys. Lett. **B95**, 299 (1980).

[192] Y. S. Kalashnikova and D. S. Kuzmenko, Phys. Atom. Nucl. **66**, 955 (2003), hep-ph/0203128.

[193] D. Horn and J. Mandula, Phys. Rev. **D17**, 898 (1978).

[194] M. Tanimoto, Phys. Lett. **B116**, 198 (1982).

[195] M. Tanimoto, Phys. Rev. **D27**, 2648 (1983).

[196] F. Iddir *et al.*, Phys. Lett. **B205**, 564 (1988).

[197] S. Ishida, H. Sawazaki, M. Oda, and K. Yamada, Phys. Rev. **D47**, 179 (1993).

[198] S. Ishida, M. Oda, H. Sawazaki, and K. Yamada, Prog. Theor. Phys. **82**, 119 (1989).

[199] S. Perantonis and C. Michael, Nucl. Phys. **B347**, 854 (1990).

[200] F. E. Close and P. R. Page, Nucl. Phys. **B443**, 233 (1995), hep-ph/9411301.

[201] F. Close and P. Page, Phys.Lett. **B628**, 215 (2005).

[202] S. L. Zhu, Phys.Lett. **B625**, 212 (2005).

[203] E. Kou and O. Pene, Phys.Lett. **B631**, 164 (2005).

[204] K. Juge, J. Kuti, and C. Morningstar, Phys.Rev.Lett. **82**, 4400 (1999), hep-ph/9902336.

[205] G. S. Bali, Eur.Phys.J. **A19**, 1 (2004), hep-lat/0308015.

[206] A. N. Yu.S. Kalashnikova, Phys.Rev. **D77**, 054025 (2008).

[207] R. Kokoski and N. Isgur, Phys.Rev. **D35**, 907 (1987).

[208] Belle Collaboration, G. Pakhlova *et al.*, Phys.Rev.Lett. **100**, 062001 (2008).

[209] Belle Collaboration, G. Pakhlova *et al.*, Phys. Rev. **D80**, 091101 (2009).

[210] Z.-G. Wang, Eur.Phys.J. **C63**, 115 (2009), 0903.5200.

[211] F. Close, (2007), 0706.2709.

[212] M. Chanowitz and S. Sharpe, Nucl. Phys. **B222**, 211 (1983).

[213] J. Merlin and J. Paton, Phys.Rev. **D35**, 1668 (1987).

[214] S. Dubynskiy and M. B. Voloshin, Phys. Lett. **B666**, 344 (2008), 0803.2224.

[215] S. Dubynskiy, A. Gorsky, and M. B. Voloshin, Phys. Lett. **B671**, 82 (2009), 0804.2244.

[216] G. 't Hooft, (2004), hep-th/0408148.

[217] LEPS Collaboration, T. Nakano *et al.*, Phys.Rev.Lett. **91**, 012002 (2003), hep-ex/0301020.

[218] R. L. Jaffe and F. Wilczek, Phys.Rev.Lett. **91**, 232003 (2003), hep-ph/0307341.

[219] G. 't Hooft, G. Isidori, L. Maiani, A. Polosa, and V. Riquer, Phys.Lett. **B662**, 424 (2008), 0801.2288.

[220] R. L. Jaffe, K. Johnson, and Z. Ryzak, Ann. Phys. **168**, 344 (1986).

[221] R. Jaffe, Phys.Rept. **409**, 1 (2005), hep-ph/0409065.

[222] M. G. Alford and R. Jaffe, Nucl.Phys. **B578**, 367 (2000), hep-lat/0001023.

[223] N. Mathur *et al.*, Phys.Rev. **D76**, 114505 (2007), hep-ph/0607110.

[224] S. Prelovsek and D. Mohler, Phys.Rev. **D79**, 014503 (2009), 0810.1759.

[225] H. Suganuma, K. Tsumura, N. Ishii, and F. Okiharu, Prog.Theor.Phys.Suppl. **168**, 168 (2007), 0707.3309.

[226] M. Loan, Z.-H. Luo, and Y.-Y. Lam, Eur.Phys.J. **C57**, 579 (2008), 0907.3609.

[227] S. Prelovsek *et al.*, PoS **LAT2009**, 103 (2009), 0910.2749.

[228] C. Alexandrou, P. de Forcrand, and B. Lucini, Phys.Rev.Lett. **97**, 222002 (2006), hep-lat/0609004.

[229] L. Maiani, F. Piccinini, A. Polosa, and V. Riquer, Phys.Rev. **D71**, 014028 (2005), hep-ph/0412098.

[230] L. Maiani, V. Riquer, F. Piccinini, and A. Polosa, Phys.Rev. **D72**, 031502 (2005), hep-ph/0507062.

[231] L. Maiani, A. Polosa, and V. Riquer, Phys.Rev.Lett. **99**, 182003 (2007), 0707.3354.

[232] L. Maiani, A. Polosa, and V. Riquer, New J.Phys. **10**, 073004 (2008).

[233] N. Drenska, R. Faccini, and A. Polosa, Phys.Rev. **D79**, 077502 (2009), 0902.2803.

[234] TWQCD Collaboration, T.-W. Chiu and T.-H. Hsieh, Phys.Rev. **D73**, 094510 (2006), hep-lat/0512029.

[235] TWQCD Collaboration, T.-W. Chiu and T.-H. Hsieh, Phys.Rev. **D73**, 111503 (2006), hep-lat/0604008.

[236] TWQCD Collaboration, T.-W. Chiu and T.-H. Hsieh, Phys.Lett. **B646**, 95 (2007), hep-ph/0603207.

[237] A. Ali, C. Hambrock, I. Ahmed, and M. Aslam, Phys.Lett. **B684**, 28 (2010), 0911.2787.

[238] K. Terasaki, Prog.Theor.Phys. **122**, 1285 (2010), 0904.3368.

[239] F. Stancu, J.Phys.G **G37**, 075017 (2010), 0906.2485.

[240] Y. Cui, X.-L. Chen, W.-Z. Deng, and S.-L. Zhu, High Energy Phys. Nucl. Phys. **31**, 7 (2007), hep-ph/0607226.

[241] M. Abud, F. Buccella, and F. Tramontano, Phys.Rev. **D81**, 074018 (2010), 0912.4299.

[242] L. Maiani, A. Polosa, and V. Riquer, (2007), 0708.3997.

[243] S. Gershtein, A. Likhoded, and G. a. Pronko, (2007), 0709.2058.

[244] M. Bracco, S. Lee, M. Nielsen, and R. Rodrigues da Silva, Phys.Lett. **B671**, 240 (2009), 0807.3275.

[245] N. Drenska, R. Faccini, and A. Polosa, Phys.Lett. **B669**, 160 (2008), 0807.0593.

[246] F. Wilczek, p. 322 (2004), hep-ph/0409168.

[247] A. Selem and F. Wilczek, p. 337 (2006), hep-ph/0602128.

[248] S. Gershtein, A. Likhoded, and A. a. Luchinsky, Phys.Atom.Nucl. **70**, 759 (2007).

[249] L. Solovev, Phys.Rev. **D61**, 015009 (2000), hep-ph/9907486.

[250] F. Brau, Phys.Rev. **D62**, 014005 (2000), hep-ph/0412170.

[251] Particle Data Group, C. Amsler *et al.*, Phys.Lett. **B667**, 1 (2008).

[252] BABAR Collaboration, P. del Amo Sanchez *et al.*, Phys.Rev. **D82**, 111102 (2010), 1004.0175.

[253] T. Barnes and S. Godfrey, Phys.Rev. **D69**, 054008 (2004), hep-ph/0311162.

[254] L. Fulcher, Phys.Rev. **D44**, 2079 (1991).

[255] J. J. Dudek, (2007), 0711.1600.

[256] Belle, K. Abe *et al.*, (2005), hep-ex/0505037.

[257] M. Suzuki, Phys. Rev. **D72**, 114013 (2005), hep-ph/0508258.

[258] P. L. Cho and M. B. Wise, Phys. Rev. **D51**, 3352 (1995), hep-ph/9410214.

[259] E. J. Eichten, K. Lane, and C. Quigg, Phys. Rev. Lett. **89**, 162002 (2002), hep-ph/0206018.

[260] Y. Jia, W.-L. Sang, and J. Xu, (2010), 1007.4541.

[261] N. Brambilla, Y. Jia, and A. Vairo, Phys. Rev. **D73**, 054005 (2006), hep-ph/0512369.

[262] V. Bhardwaj, (2010), http://conferences.fnal.gov/QWG2010/.

[263] BABAR, B. Aubert *et al.*, Phys. Rev. Lett. **102**, 132001 (2009), 0809.0042.

[264] E. J. Eichten, K. Lane, and C. Quigg, Phys. Rev. **D69**, 094019 (2004), hep-ph/0401210.

[265] L. Maiani, F. Piccinini, A. Polosa, and V. Riquer, Phys.Rev.Lett. **93**, 212002 (2004), hep-ph/0407017.

[266] S. Godfrey and S. Olsen, Ann.Rev.Nucl.Part.Sci. **58**, 51 (2008), 0801.3867.

[267] D. Ebert, R. Faustov, and V. Galkin, Eur.Phys.J. **C58**, 399 (2008), 0808.3912.

[268] A. Ali, C. Hambrock, and M. Aslam, Phys.Rev.Lett. **104**, 162001 (2010), 0912.5016.

[269] A. Ali, C. Hambrock, and S. Mishima, Phys.Rev.Lett. **106**, 092002 (2011), 1011.4856.

[270] R. Feynman, F. Morinigo, W. Wagner, and B. Hatfield, *Feynman lectures on gravitation* (Addison-Wesley, 1995).

[271] J. Sakurai, *Currents and Mesons* (Chicago University Press, 1969).

[272] G. Corcella *et al.*, JHEP **0101**, 010 (2001), hep-ph/0011363.

[273] T. Sjostrand *et al.*, Comput.Phys.Commun. **135**, 238 (2001), hep-ph/0010017.

[274] CDF, (2004), http://www-cdf.fnal.gov/physics/new/bottom/051020.blessed-X3872/XLife/xlonglivedWWW.ps.

[275] CDF Collaboration, T. Aaltonen *et al.*, Phys.Rev. **D80**, 031103 (2009), 0905.1982.

[276] E. C. Titchmarsh, *The theory of functions* (Oxford University Press, 2nd ed., 1939).

[277] CDF, (2006), http://www-cdf.fnal.gov/physics/new/bottom/060921.blessed-double-charm-corr/.

[278] M. L. Mangano, M. Moretti, F. Piccinini, R. Pittau, and A. D. Polosa, JHEP **0307**, 001 (2003), hep-ph/0206293.

[279] P. Artoisenet and E. Braaten, Phys.Rev. **D81**, 114018 (2010), 0911.2016.

[280] K. M. Watson, Phys.Rev. **88**, 1163 (1952).

[281] P. L. Cho and M. B. Wise, Phys.Rev. **D51**, 3352 (1995), hep-ph/9410214.

[282] J. Engels, F. Karsch, H. Satz, and I. Montvay, Phys.Lett. **B101**, 89 (1981).

[283] J. D. Bjorken, Phys. Rev. **D27**, 140 (1983).

[284] NA50, B. Alessandro *et al.*, Eur. Phys. J. **C39**, 335 (2005), hep-ex/0412036.

[285] NA50, M. C. Abreu *et al.*, Phys. Lett. **B530**, 33 (2002).

[286] PHENIX, S. S. Adler *et al.*, Phys. Rev. **C76**, 034903 (2007), 0704.2894.

[287] ALICE Collaboration, E. Alessandro, G *et al.*, J.Phys.G **G32**, 1295 (2006).

[288] Atlas Collaboration, G. Aad *et al.*, Phys.Rev.Lett. **105**, 252303 (2010), 1011.6182.

[289] Atlas Collaboration, G. Aad *et al.*, Phys.Lett. **B697**, 294 (2011), 1012.5419.

[290] C. Blume, Eur.Phys.J. **C34**, S287 (2004).

[291] L. McLerran, Prog.Theor.Phys.Suppl. **187**, 17 (2011), 1011.3204.

[292] J. Rafelski and R. Hagedorn, *From Hadrons Gas to Quark Matter II.* (, 1980).

[293] J. Rafelski and B. Muller, Phys.Rev.Lett. **48**, 1066 (1982).

[294] J. Letessier and J. Rafelski, *Hadrons and quark - gluon plasma* (Cambridge University Press, 2002).

[295] H. Satz, Nucl.Phys. **A418**, 447C (1984).

[296] T. Matsui and H. Satz, Phys.Lett. **B178**, 416 (1986).

[297] NA50 Collaboration, M. Abreu *et al.*, Phys.Lett. **B477**, 28 (2000).

[298] A. Faessler, C. Fuchs, M. Krivoruchenko, and B. Martemyanov, Phys.Rev.Lett. **93**, 052301 (2004), nucl-th/0212064.

[299] C. Fuchs, B. V. Martemyanov, A. Faessler, and M. I. Krivoruchenko, Phys. Rev. **C73**, 035204 (2006), nucl-th/0410065.

[300] L. Tolos, A. Ramos, and T. Mizutani, (2007), 0710.3323.

[301] L. Tolos, A. Ramos, and T. Mizutani, Phys.Rev. **C77**, 015207 (2008), 0710.2684.

[302] F. O. Gottfried and S. P. Klevansky, Phys.Lett. **B286**, 221 (1992).

[303] A. Hayashigaki, Phys.Lett. **B487**, 96 (2000), nucl-th/0001051.

[304] A. Kumar and A. Mishra, (2009), 0912.2477.

[305] A. Kumar and A. Mishra, Phys.Rev. **C81**, 065204 (2010), 1005.5018.

[306] A. Kumar and A. Mishra, (2010), 1010.0403.

[307] L. Maiani, F. Piccinini, A. Polosa, and V. Riquer, Nucl.Phys. **A741**, 273 (2004), hep-ph/0402275.

[308] L. Maiani, F. Piccinini, A. D. Polosa, and V. Riquer, Nucl. Phys. **A748**, 209 (2005), hep-ph/0408150.

[309] C.-Y. Wong, E. Swanson, and T. Barnes, Phys.Rev. **C62**, 045201 (2000), hep-ph/9912431.

[310] C.-Y. Wong, E. Swanson, and T. Barnes, Phys.Rev. **C65**, 014903 (2002), nucl-th/0106067.

[311] N. Armesto and A. Capella, Phys. Lett. **B430**, 23 (1998), hep-ph/9705275.

[312] N. Armesto, A. Capella, and E. G. Ferreiro, Phys. Rev. **C59**, 395 (1999), hep-ph/9807258.

[313] A. Capella and E. G. Ferreiro, Eur. Phys. J. **C42**, 419 (2005), hep-ph/0505032.

[314] K. Yokokawa, S. Sasaki, T. Hatsuda, and A. Hayashigaki, Phys.Rev. **D74**, 034504 (2006), hep-lat/0605009.

[315] A. Sibirtsev, K. Tsushima, K. Saito, and A. W. Thomas, Phys.Lett. **B484**, 23 (2000), nucl-th/9904015.

[316] G. R. G. Burau, D. B. Blaschke, and Y. L. Kalinovsky, Phys. Lett. **B506**, 297 (2001), nucl-th/0012030.

[317] D. Blaschke, G. Burau, Y. Kalinovsky, and T. Barnes, Eur.Phys.J. **A18**, 547 (2003), nucl-th/0211058.

[318] C.-Y. Wong, Phys.Rev. **C65**, 034902 (2002), nucl-th/0110004.

[319] X.-M. Xu, C.-Y. Wong, and T. Barnes, Phys.Rev. **C67**, 014907 (2003), nucl-th/0207018.

[320] K. Morita and S. H. Lee, (2010), 1012.3110.

[321] PHENIX, A. Adare *et al.*, Phys. Rev. Lett. **98**, 232301 (2007), nucl-ex/0611020.

[322] A. Capella *et al.*, Eur. Phys. J. **C58**, 437 (2008), 0712.4331.

[323] Z.-w. Lin and C. Ko, Phys.Rev. **C62**, 034903 (2000), nucl-th/9912046.

[324] J. Kapusta, *Finite-temperature field theory*, 2 edition ed. (Cambridge University Press, 2006).

[325] R. Thews and M. Mangano, Phys.Rev. **C73**, 014904 (2006), nucl-th/0505055.

[326] N. Armesto *et al.*, J.Phys.G **G35**, 054001 (2008), 0711.0974.

[327] NA50, M. C. Abreu *et al.*, Phys. Lett. **B450**, 456 (1999).

[328] V.-N. Tram and F. Arleo, Eur. Phys. J. **C61**, 847 (2009), 0907.0043.

[329] NA50, P. Cortese *et al.*, Nucl. Phys. **A715**, 679 (2003).

[330] NA50, M. C. Abreu *et al.*, Phys. Lett. **B410**, 337 (1997).

[331] NA50, M. C. Abreu *et al.*, Phys. Lett. **B410**, 327 (1997).

[332] J. Cleymans and D. Worku, (2011), 1103.1463.

[333] F. Becattini, L. Maiani, F. Piccinini, A. Polosa, and V. Riquer, Phys.Lett. **B632**, 233 (2006), hep-ph/0508188.

[334] CLEO, R. Balest *et al.*, Phys. Rev. **D52**, 2661 (1995).

[335] CLEO, M. S. Alam *et al.*, Phys. Rev. **D50**, 43 (1994), hep-ph/9403295.

[336] CLEO, S. Anderson *et al.*, Phys. Rev. Lett. **89**, 282001 (2002).

[337] Particle Data Group, D. E. Groom *et al.*, Eur.Phys.J. **C15**, 1 (2000).

[338] Belle, K. Abe *et al.*, Phys. Rev. Lett. **87**, 161601 (2001), hep-ex/0105014.

[339] CLEO Collaboration, S. Richichi *et al.*, Phys.Rev. **D63**, 031103 (2001), hep-ex/0010036.

[340] M. Beneke, G. A. Schuler, and S. Wolf, Phys. Rev. **D62**, 034004 (2000), hep-ph/0001062.

[341] BABAR, B. Aubert *et al.*, Phys. Rev. **D67**, 032002 (2003), hep-ex/0207097.

[342] S. J. Brodsky and F. S. Navarra, Phys. Lett. **B411**, 152 (1997), hep-ph/9704348.

[343] C.-H. V. Chang and W.-S. Hou, Phys. Rev. **D64**, 071501 (2001), hep-ph/0101162.

[344] G. Eilam, M. Ladisa, and Y.-D. Yang, Phys. Rev. **D65**, 037504 (2002), hep-ph/0107043.

[345] F. E. Close and J. J. Dudek, Phys. Rev. Lett. **91**, 142001 (2003), hep-ph/0304243.

[346] F. E. Close and J. J. Dudek, Phys. Rev. **D69**, 034010 (2004), hep-ph/0308098.

[347] C.-K. Chua, W.-S. Hou, and G.-G. Wong, Phys. Rev. **D68**, 054012 (2003), hep-ph/0305180.

[348] Belle, H. Guler *et al.*, Phys. Rev. **D83**, 032005 (2011), 1009.5256.

[349] I. Bigi, L. Maiani, F. Piccinini, A. Polosa, and V. Riquer, Phys.Rev. **D72**, 114016 (2005), hep-ph/0510307.

[350] http://hfag.phys.ntu.edu.tw/b2charm/index.html.

[351] G. T. Bodwin, E. Braaten, and G. Lepage, Phys.Rev. **D51**, 1125 (1995), hep-ph/9407339.

[352] I. Z. Rothstein, p. hf8/010 (1999), hep-ph/9911276.

[353] G. Altarelli, N. Cabibbo, G. Corbo, L. Maiani, and G. Martinelli, Nucl.Phys. **B208**, 365 (1982).

[354] M. Maggiore, *A Modern introduction to quantum field theory* (Oxford University Press, 2005).

[355] H. Georgi, *Lie Algebras in particle physics. From Isospin to unified theories*, 2 ed. (Westview Press - Frontier in Physics, 1999).

[356] B. De Wit and J. Smith, *Field Theory in Particle Physics* (North-Holland, Amsterdam, 1986).